
This item was submitted to [Loughborough's Research Repository](#) by the author.
Items in Figshare are protected by copyright, with all rights reserved, unless otherwise indicated.

The mechanics of the curved approach in high jumping

PLEASE CITE THE PUBLISHED VERSION

PUBLISHER

© John Cher Chay Tan

LICENCE

CC BY-NC-ND 4.0

REPOSITORY RECORD

Tan, John C.C.. 2019. "The Mechanics of the Curved Approach in High Jumping". figshare.
<https://hdl.handle.net/2134/10489>.

This item was submitted to Loughborough University as a PhD thesis by the author and is made available in the Institutional Repository (<https://dspace.lboro.ac.uk/>) under the following Creative Commons Licence conditions.



For the full text of this licence, please go to:
<http://creativecommons.org/licenses/by-nc-nd/2.5/>

Pilkington Library

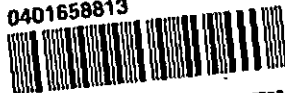
Author/Filing Title TAN, J.C.C.

Accession/Copy No. 040165881

Vol. No.	Class Mark
---------------	------------------

LOAN COPY	
-----------	--

0401658813



**THE MECHANICS OF
THE CURVED APPROACH IN HIGH JUMPING**


BY

JOHN CHER CHAY TAN

**A Doctoral thesis
Submitted in partial fulfilment of the requirements for
the award of Doctor of Philosophy
of Loughborough University**

**Supervisors: Dr M.R. Yeadon
Dr D.G. Kerwin**

© by John Cher Chay Tan

 Loughborough University	
Date	Jul 98
Class	
Acc No.	040165881

K063 0907

ABSTRACT

THE MECHANICS OF THE CURVED APPROACH IN HIGH JUMPING

by John Cher Chay Tan

Loughborough University, September 1997

In high jumping, the Fosbury Flop technique is currently used by all elite high jumpers throughout the world. The technique involves an acrobatic bar clearance at the end of a curved approach run. Initially the curved approach was considered to be no more than an idiosyncrasy of Dick Fosbury. However, the curved approach remains the preferred approach among elite jumpers, and therefore can be expected to be advantageous in high jumping. Speculations on the possible advantages of the curved approach have been made, but most are not based on experimental data and all lack convincing mechanical explanations.

In order to understand the contribution of the curved approach to high jumping technique, the characteristics of the approach needed to be examined. Analysis of the 15 m approach phase of the high jump posed a challenge in terms of obtaining the appropriate size of image and field of view. A number of image analysis systems were evaluated before one with the appropriate accuracy was selected. A total of 15 jumps performed by two elite high jumpers in two competitions were analysed.

It was found that the curve through the foot placements tightened towards the end of the approach. Concurrently the inward body tilt towards the centre of the curve decreased resulting in an angular velocity about the frontal axis of the body. This suggested that the curved approach was used to provide the somersault rotation over the bar.

In order to test this hypothesis a computer simulation model of the approach phase was developed and evaluated using the data from the image analyses. The model was used to explain the mechanics underlying the curved approach in the Fosbury Flop. It was found that tightening of the foot placement curve towards the end of the approach generated somersault rotation and also contributed to twist rotation at takeoff.

ACKNOWLEDGEMENTS

I wish to express my thanks to:

My supervisors Dr. Yeadon and Dr. Kerwin for their advice and continued encouragement,

M. Brewin, M. King, M. Hiley, M. Greig, J. Prescott, S. Dixon and L. Griffin for their assistance and support,

Brendan Reilly and Steve Smith for performing the jumps,

and the Nanyang Technological University, Singapore for making this study financially possible.

DEDICATION

To Jenny and Jaime

TABLE OF CONTENTS

	PAGE
ABSTRACT	i
STATEMENT OF RESPONSIBILITY	ii
ACKNOWLEDGEMENTS	iii
DEDICATION	iv
TABLE OF CONTENTS	v
LIST OF TABLES	viii
LIST OF FIGURES	x
Chapter 1 INTRODUCTION	1
OVERVIEW	1
QUESTIONS FOR INVESTIGATION	4
CHAPTER ORGANISATION	6
Chapter 2 REVIEW OF LITERATURE	
HISTORICAL PERSPECTIVE AND GENERAL DESCRIPTION	8
<i>Approach phase</i>	10
<i>Takeoff phase</i>	13
<i>Flight phase</i>	17
INVESTIGATIONS OF HIGH JUMPING	18
<i>Observational studies</i>	18
<i>Experimental studies</i>	26
<i>Theoretical studies</i>	30
<i>Combination method</i>	33
<i>Summary of investigations of high jumping</i>	34
TECHNIQUES OF INVESTIGATION	35
<i>Image analysis methods</i>	35
<i>Segment inertia parameters</i>	42
<i>Simulation models</i>	45
Chapter 3 IMAGE ANALYSIS PROCEDURES	47
INTRODUCTION	47
SELECTION OF IMAGE MEASUREMENT SYSTEM	47
<i>Systems evaluated</i>	49
<i>Procedure for evaluation of digitising systems</i>	50
<i>Optimisation of the Apex Target video digitising system</i>	53

<i>Lens distortion</i>	54
<i>Image recording for Fosbury Flop</i>	58
<i>Data collection procedure</i>	59
<i>Data processing procedure</i>	64
SUMMARY	69
Chapter 4 DEVELOPMENT OF THE SIMULATION MODEL	70
INTRODUCTION	70
POINT MASS MODEL	71
<i>Equation of motion</i>	71
SIMULATION PROGRAM PMASS	72
<i>Input data</i>	73
<i>Output data</i>	73
<i>Calculation of input data</i>	73
<i>Limitations of PMASS</i>	74
APPROACH MODEL	74
<i>The moving point of foot curve</i>	74
<i>Reference frame</i>	75
<i>The body orientation of approach</i>	76
<i>Velocities</i>	77
<i>Torque about fixed foot</i>	78
<i>Angular momentum equation</i>	79
<i>Equation for ground phase</i>	81
<i>Aerial phase</i>	83
<i>Numerical integration</i>	87
<i>Input parameters</i>	88
<i>Output data</i>	89
<i>Tilt angles</i>	89
<i>Tilt angular velocity</i>	93
<i>The distance h</i>	93
<i>Inertia values</i>	93
<i>Angular momentum about the horizontal axis i</i>	94
<i>Calculation of s</i>	94
<i>Calculation of twist velocity $\dot{\psi}$ and foot radius R</i>	95
<i>Calculation of the distances r, d and f</i>	97
<i>Preliminary attempt to quantify twist using hip angle</i>	99
<i>Foot direction for quantifying twist</i>	100
<i>Ratio of inertias for quantifying twist</i>	101
Chapter 5 EVALUATION OF IMAGE ANALYSIS AND MODEL	102
INTRODUCTION	102
IMAGE ANALYSIS	102
<i>Lens distortion correction</i>	102

<i>Picture resolution</i>	103	
<i>Measurement resolution of digitising systems</i>	104	
<i>Optional digitising features of the Apex Target system</i>	107	
<i>Summary</i>	110	
<i>Evaluation of high jumping data</i>	111	
<i>Evaluation of the pressure insole</i>	120	
EVALUATION OF THE MODEL	122	
<i>Foot curve</i>	122	
<i>Tilt angle</i>	123	
<i>Angular momentum about the mass centre</i>	125	
<i>Sensitivity analyses</i>	127	
<i>Summary</i>	131	
CONCLUSION	132	
Chapter 6 THE CURVED APPROACH OF FOSBURY FLOP	134	
INTRODUCTION	134	
IMAGE ANALYSIS	134	
<i>Radius of the curved approach</i>	134	
<i>Tilt angle</i>	137	
<i>Image analysis of the curved approach</i>	138	
MODEL	138	
<i>Radius of the foot curve</i>	138	
<i>Experiments</i>	140	
MECHANICS UNDERLYING THE CURVED APPROACH	142	
<i>Terms in the tilt angular acceleration equation</i>	142	
TWIST CONTRIBUTION	148	
SUMMARY OF FINDINGS	150	
<i>Future direction</i>	150	
REFERENCES	151	
APPENDIX A:	Listing of the program APPROACH	163
APPENDIX B:	A sample input file for a simulation	188
APPENDIX C:	Sample output files for a simulation	190
APPENDIX D:	Anthropometric measurements of the subjects	211
APPENDIX E:	Record of competition performances	214
APPENDIX F:	Centre of pressure patterns for curve running	216

LIST OF TABLES

	PAGE
 CHAPTER 3	
Table 3.1. Image analysis systems to be evaluated	49
Table 3.2. Digitising configurations for optimisation of Apex Target system	54
Table 3.3. Errors of measurement of a video system	55
Table 3.4. Physical and performance characteristics of jumpers	59
 CHAPTER 4	
Table 4.1. Locations of COP at midstance	91
 CHAPTER 5	
Table 5.1. Root mean square errors of 2D reconstruction [mm]	102
Table 5.2. Root mean square errors of 3D reconstruction [mm]	103
Table 5.3. Accuracy and precision of video recording format systems [mm]	104
Table 5.4. Accuracy and precision of video digitising format systems [mm]	104
Table 5.5. Accuracy and precision of film and video digitising formats systems [mm]	105
Table 5.6. Optimising digitising features of the Apex Target system	107
Table 5.7. Optimised video and 16 mm film image measurements	110
Table 5.8. Digitising precision of the high jumping recordings	111
Table 5.9. Reconstruction errors of the calibration points	112
Table 5.10. Reconstruction errors of the body landmarks	113
Table 5.11. Standard deviation of calculated segment lengths [mm]	113
Table 5.12. Precision estimates of foot placement locations	115
Table 5.13. Precision of mass centre estimates	115
Table 5.14. Precision of approach speed, distance h, and tilt angle θ	120
Table 5.15. Tilt angles (in degrees) from video data and the model (B. Reilly)	123
Table 5.16. Tilt angles (in degrees) from video data and the model (S. Smith)	124
Table 5.17. Angular momentum values from video and model (B. Reilly)	126
Table 5.18. Angular momentum values from video and model (S. Smith)	126
Table 5.19. The sensitivity of the model to the initial tilt angle	127

Table 5.20 The sensitivity of the model to the initial tilt velocity	128
Table 5.21. The sensitivity of the model to the time interval for numerical integration	129
Table 5.22. The sensitivity of the model to approach speed	130
Table 5.23. Sensitivity of the model to the small changes in mass centre distance h	131

CHAPTER 6

Table 6.1. The effect of changing radius of the foot curve	140
Table 6.2. The effect of the foot approach speeds on rotation	141
Table 6.3. The effect of using different anthropometric data	142
Table 6.4. The mean values [in rad.s^{-2}] of the terms in $\ddot{\theta}$ equation (for B01)	143
Table 6.5. The mean values [in rad.s^{-2}] of the terms in $\ddot{\theta}$ equation (for B02)	143
Table 6.6. The mean values [in rad.s^{-2}] of the terms in $\ddot{\theta}$ equation (for S01)	144
Table 6.7. The mean values [in rad.s^{-2}] of the terms in $\ddot{\theta}$ equation (for S02)	144
Table 6.8. The contribution of the approach to the twist velocity at takeoff	149

LIST OF FIGURES

CHAPTER 1	PAGE
Figure 1.1 The Fosbury Flop (adapted from Doherty, 1985).	2
Figure 1.2. The rotational components of the twisting somersault Fosbury Flop (adapted from Dick, 1993).	3
Figure 1.3. The curved approach (plan view).	4
 CHAPTER 2	
Figure 2.1 Techniques of high jumping (adapted from Hay, 1985 and Doherty, 1985).	9
Figure 2.2. J-shaped approach run in Fosbury Flop.	10
Figure 2.3. Inward body tilt (adapted from Dick, 1993).	12
Figure 2.4. Backward body lean (adapted from Dick, 1993).	14
Figure 2.5. Forward pike clearance (adapted from Hay, 1973).	33
 CHAPTER 3	
Figure 3.1. Locations of markers and cameras (plan view).	50
Figure 3.2. Markers on poles.	51
Figure 3.3. Camera positions relative to the high jump area (for B. Reilly).	60
Figure 3.4. Camera positions relative to the high jump area (for S. Smith).	60
Figure 3.5. Positions of calibration poles in the high jump area (for B. Reilly).	61
Figure 3.6. Position of calibration poles in the high jump area (for S. Smith).	61
Figure 3.7. The digitising protocol for references frames (for B. Reilly).	62
Figure 3.8. Digitising protocol for references frames (for S. Smith).	63
Figure 3.9. The lean angle ϕ .	67
Figure 3.10. The tilt angle θ .	67
 CHAPTER 4	
Figure 4.1. When the wheel turns more into the curve, the cyclist will "straighten-up" (adapted from Konopka, 1989).	70
Figure 4.2. Point mass model.	71
Figure 4.3. Foot curve of the moving point.	75

Figure 4.4. The moving reference frame $[i, j, k]$.	75
Figure 4.5. Foot (F) and mass centre (G) locations of approach phase (plan view).	76
Figure 4.6. Velocities when mass centre is 'alongside' the foot contact.	77
Figure 4.7. Three-dimensional geometry of the vector \mathbf{FG} .	78
Figure 4.8. Torque at G about F.	79
Figure 4.9. Axes of the body and the moving reference frames.	79
Figure 4.10. Axes of the inertial and the body reference frames.	84
Figure 4.11. Foot and mass centre locations relative to v_h and v_t (plan view).	89
Figure 4.12. Projections on planes normal to v_t and v_h .	89
Figure 4.13. The rear view of θ and the outside shoe.	90
Figure 4.14. The rear view of θ and the inside shoe.	92
Figure 4.15. Partitioning the 'mean' gradient.	96
Figure 4.16. Foot contact at F.	97
Figure 4.17. Hipline at C3 - C2 (jump S04).	99
Figure 4.18. Foot location at touchdown and takeoff of the approach (jump S07).	100
Figure 4.19. Foot direction at C5 and C4 (jump S07).	100

CHAPTER 5

Figure 5.1. Accuracy estimates for digitising static markers.	106
Figure 5.2. Precision estimates for digitising static markers.	106
Figure 5.3. Precision estimates for digitising points on a moving body.	106
Figure 5.4. Precision comparison for Apex Target digitising features.	108
Figure 5.5. Accuracy comparison of Apex Target digitising features.	109
Figure 5.6. Centre of pressure patterns from force plate and pressure insole (trial 1).	121
Figure 5.7. Centre of pressure patterns from force plate and pressure insole (trial 2).	121
Figure 5.8. Foot curves of the approach.	122
Figure 5.9. The tilt angles of the approach in jump B02.	124
Figure 5.10. The tilt angles of the approach in jump S01.	125

CHAPTER 6

Figure 6.1. Foot and mass centre paths.	135
Figure 6.2. Radii of curves through the foot placements and mass centre positions.	136
Figure 6.3. Mean inward tilt angles.	137
Figure 6.4. Radii of the foot curve from the model.	139
Figure 6.5. Computer graphics sequences of the curved approach and somersault rotation of B. Reilly (jump B04).	146
Figure 6.6. Computer graphics sequences of the curved approach and somersault rotation of S. Smith (jump S05).	147

Chapter 1

INTRODUCTION

In high jumping, for a jump to be successful, a high jumper needs to propel his or her body over the cross-bar. Although one needs to clear the greatest bar height in the competition to win, the aim of the high jump is not just jumping as high as possible. High jumpers need to avoid the displacement of the cross-bar while rotating their bodies over it. Therefore for high jumping, rotating over the bar is an important technique of the jump. The rules do not restrict the technique or style used in clearing the bar as long as the jumper takes off from one foot. There are no less than six recognised techniques used by jumpers to rotate over the bar. The latest of this long line of techniques is the Fosbury Flop.

Prior to the 1960 Olympics, the landing area of the high jump consisted of a sand pit. This constrained the technique of high jumping because jumpers had to consider a technique which would provide a safe landing. Techniques such as the Western Roll or the Straddle which facilitate the foot landing ahead of the rest of the body were popular then. However with the introduction of foam mats in the landing area, this safety constraint of landing had less influence on deciding the technique of the jump.

Dick Fosbury introduced the world to the 'Fosbury Flop' at the 1968 Olympic Games in Mexico. By winning the gold medal in that Olympics, Dick Fosbury also showed that this new technique is not only an attractive acrobatic stunt but is also an effective technique for high jumping. The current world recorder holder in the high jump (Javier Sotomayer) also endorses the Flop technique with a 2.45m bar clearance. This technique has withstood the test of time and has remained as the preferred choice of clearing the bar among elite high jumpers throughout the world.

Although the Fosbury Flop is an invention of Dick Fosbury, he has admitted that he discovered the technique by accident. Dick recalled that during one competition while attempting the Scissors Kick technique, he accidentally turned his left shoulder into the bar as he jumped and leaned back to avoid dislodging the bar (Tansley, 1980). This bar clearance inadvertently went on to revolutionize high jumping. However with this accidental discovery, the mechanics of this revolutionized technique are far from obvious.

Yeadon (1984) commented that without understanding the mechanics of a technique, coaches have no foundation upon which to base their advice to their charges. He also added that if poor advice is given, it will not only aggravate the problem but may place the performer in a dangerous situation. Thus the practical need for an understanding of the mechanics of Fosbury Flop is obvious. In order to understand the mechanics of this interesting and complex technique, a variety of investigations is required on the different phases of the jump.

The Fosbury Flop is made up of three phases, namely; the approach phase, the take-off phase and the flight phase. The approach phase consists of a straight run-up followed by a curved section during the last four to five steps prior to take-off. This approach is often described as the J-shaped approach. The approach run delivers the jumper to the take-off phase which occurs during the last foot-ground contact. At the end of the take-off phase, the flight phase begins. It is during this flight phase that the high jumper clears the bar. However, many of the characteristics of the flight phase are determined by the approach phase.

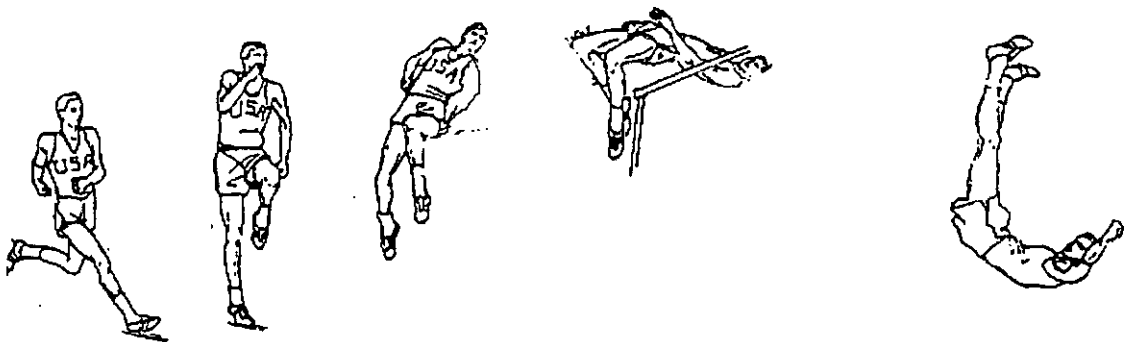


Figure 1.1 The Fosbury Flop (adapted from Doherty,1985).

The bar clearance in the Fosbury Flop may be described as performing a twisting somersault rotation over the bar as shown in Figure 1.1. This twisting somersault rotation consists of forward somersault, side somersault and twisting components (as shown in Figure 1.2). The forward somersault is the rotation about the lateral axis perpendicular to the final direction of approach. The side somersault component is the rotation about the frontal axis in line with the final direction of the approach. The twist component is the

rotation about the longitudinal axis of the jumper. The summation of these rotations will produce the twisting somersault in the Fosbury Flop technique.

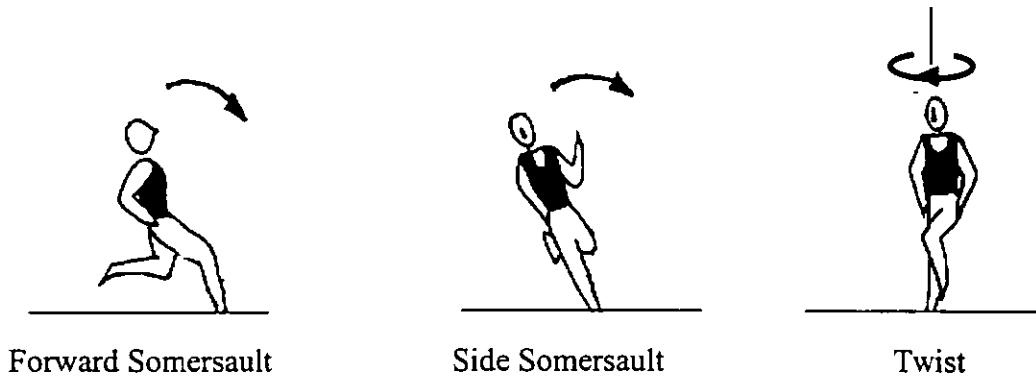


Figure 1.2. The rotational components of the twisting somersault Fosbury Flop (adapted from Dick, 1993).

The Fosbury Flop has attracted a lot of attention from both coaches and researchers. Many have speculated on the reasons for its success and popularity among athletes (Vitorri, 1972; Heinz, 1974; Ecker, 1976; Beulke, 1977; Hay, 1985; Doherty, 1985; Wagner, 1985). Some compared the Flop with the straddle technique (Carr, 1974; Fix, 1974; Ecker 1976, van Gheluwe and van Donnick, 1978; Ross, 1979; Martin, 1982). Others were concerned about projecting the mass centre to the maximum height (Ae et al., 1986; Dapena and Chung, 1988; Alexander, 1990). Few researchers, however, have considered the mechanics of the rotation techniques in the Fosbury Flop.

Most of the conclusions drawn from the few investigations on rotation in the Fosbury Flop consisted of opinions or were poorly supported. The views asserted in the literature do raise a number of questions which may be presented as follows:

There were speculations that the characteristic curved approach of the Fosbury Flop might be of some assistance in generating rotation (Beulke, 1977; Ecker, 1971; Wagner, 1985). There were no experimental data, however, to support these theories. Dapena (1980b) on the other hand, found that the angular momentum for somersault rotation was not generated prior to the take-off phase. He concluded that the curved approach has little or no contribution to the generation of the somersault rotation. If this is indeed the case, then the curved approach would be of little benefit. However, the fact that the curved approach has remained the preferred technique among elite jumpers for almost three decades suggests that the curved approach must have a mechanical basis.

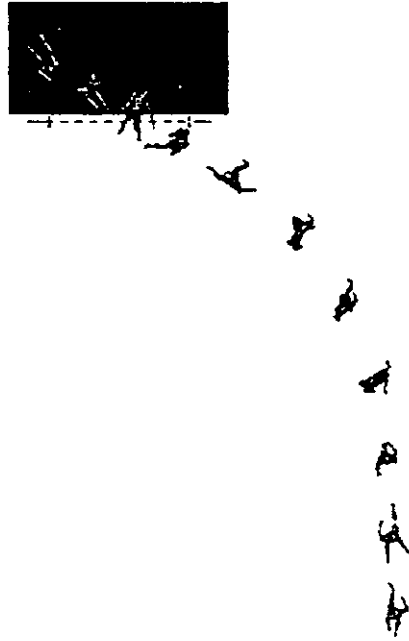


Figure 1.3. The curved approach (plan view).

Ecker (1976) claimed that the curved approach facilitates an appropriate body position for bar clearance. Heinz (1974) suggested that the inherent inward tilt of the curved approach provides a lower mass centre for a longer vertical projection. Jacoby (1987) also suggested that the process of the body straightening up from the inward tilt during the final part the curved approach may impart rotation about the jumper's frontal axis. Dapena (1980b) also observed that jumpers using the straight approach had to resort to tilting into the bar at take-off to attain the somersault rotation whereas the jumpers using the curved approach could attain the required somersault rotation without tilting into the bar. This prompts the following question:

Question 1

To what extent does the curved approach contribute to the somersault rotation?

In the Fosbury Flop, twist rotation is required to turn the back of the athlete towards the bar (Dapena, 1995). Fix (1974) suggested that while negotiating the curved approach, the twist rotation may be generated. However, Dapena (1980b) claimed that the curved approach assists only slightly in the twist rotation.

Question 2

To what extent does the curved approach contribute to the twist rotation?

In order to answer the above questions, the characteristics of the curved approach need to be examined so that the mechanics involved in the contribution of the curved approach can be understood. Hence, the following question needs to be addressed:

Question 3

What are the mechanics underlying the use of a curved approach?

To answer these questions regarding the curved approach, image analysis of this phase is required. With a variety of image recordings and digitising systems available, there is a need to determine which image analysis system would be most appropriate for this study. Studies have shown that image analysis data obtained from video were of lower accuracy than that from 16 mm film systems (Shapiro et al., 1987; Kennedy et al. 1989; Angulo and Dapena, 1992). However no study has yet shown why a video system should produce data of lower accuracy than that of a film 16 mm film. Angulo and Dapena (1992) speculated that the lower accuracy could be due to the image quality and resolution of the video system. The effects of these limitations in video have so far received little attention. Since video systems have advantages such as ease of use, immediate availability of recordings and relative low cost compare to the 16 mm film systems, it is worth considering the following questions:

Question 4

What are the features of a video digitising system that affect the accuracy of image analysis?

If these features can be identified and improved, then the following question must be considered before determining which the system should be used in this study.

Question 5

Can a high resolution video digitising system produce accuracy comparable to that of a 16 mm film system?

The approach phase of the high jump covering about 20 metres poses another challenge in terms of obtaining the appropriate size of image and field of view. Although panning cameras may be used, this procedure requires the use of markers throughout the panning field of view (Yeadon, 1989). In the high jump competition area, even if permission can be obtained for the placement of these markers, the displacement or occlusion of these markers are problems to be expected. Therefore, the use of fixed cameras is preferred. However, the use of fixed cameras does pose the following question:

Question 6

What configuration of camera placement is required in order to span over 20 metre field of view?

A computer simulation model of the curved approach will be developed using personalised inertia data obtained from the subject. This computer simulation model will be used in conjunction with the kinematic data obtained from image analysis to explain the mechanics underlying the use of the curved approach in the Fosbury Flop.

CHAPTER ORGANISATION

Chapter 2 reviews the coaching literature on the development and general description of high jumping techniques, particularly with Fosbury Flop. The results of the previous studies on the Fosbury Flop are also critically examined. A review of investigative techniques that have or can be used in the study of the Fosbury Flop is also included to provide the framework for the following chapters.

Chapter 3 describes the methodology used in evaluating the features of various image analysis systems. The details of image analysis procedure required for obtaining the necessary kinematic data of the high jumps also are described in this chapter.

Chapter 4 presents the development and the description of the simulation model.

Chapter 5 provides the evaluation of the image analysis systems. In the process of this evaluation the effect of the different features of the image analysis systems are investigated. The accuracy of the high jumping data is also evaluated in this chapter. This chapter also provides the evaluation of the computer simulation model. The simulations are evaluated with the data obtained from the image analysis.

Chapter 6 investigates the contributions of the curved approach in the Fosbury Flop using the image analysis and the simulation model. A summary of the results obtained is also provided at the end of this chapter.

Chapter 2

REVIEW OF LITERATURE

HISTORICAL PERSPECTIVE AND GENERAL DESCRIPTION

High jumping has been a known physical pursuit for such a long time that no-one knows its origins. Matthews (1986) claimed that as early as 3300 BC, children were jumping over linked arms of other children. It was not till the early 1820s, in the professional Lowland Games of Scotland when the heights of 1.6 to 1.7 m were recorded for high jumping. However, it was only in 1876, when M.C. Brooks of Oxford cleared 1.83m, that the first record in high jumping was established. This was simply because prior to 1876, there was no formalised record of agreed rules in high jumping (McNab, 1980). Rules in high jumping have changed considerably over the years. For example, prior to 1938, diving over the bar (leading with the head) was considered to be an illegal jump.

With the evolution of rules and technological development (particularly with the introduction of foam landing mats), different techniques of high jumping were experimented with throughout the history of competitive high jumping. There are no less than six known techniques used by jumpers to clear the bar (Hay, 1985). The well known ones are; Scissors, Back layout, Eastern cutoff, Western Roll, Straddle and Fosbury Flop (as shown in Figure 2.1).

The latest of this long line of techniques is the Fosbury Flop. It is currently used by all elite high jumpers in major track and field competitions. This technique was introduced by Dick Fosbury in 1968 Mexico Olympics where he won the gold medal in the high jump event. His performance at the Olympics provided quite a task for many reporters to describe to the rest of the world who were not there to witness the technique used. Jon Hendershott reporting for the Track and Field News then, described it as “unorthodox backward Flop”. Melvyn Watman from the Athletic Weekly described the whole performance as “ . . . an Eastern cutoff type of approach run and then rotated the opposite way to that expected in diving backwards over the bar.” Later Tom McNab (1980), however gave a clearer picture when he summed it all up as “linking the curved run of the Eastern cut-off with the back lay-out technique.” However Jacoby (1987) distinguished the Fosbury Flop from the back lay-out technique by describing the jump as

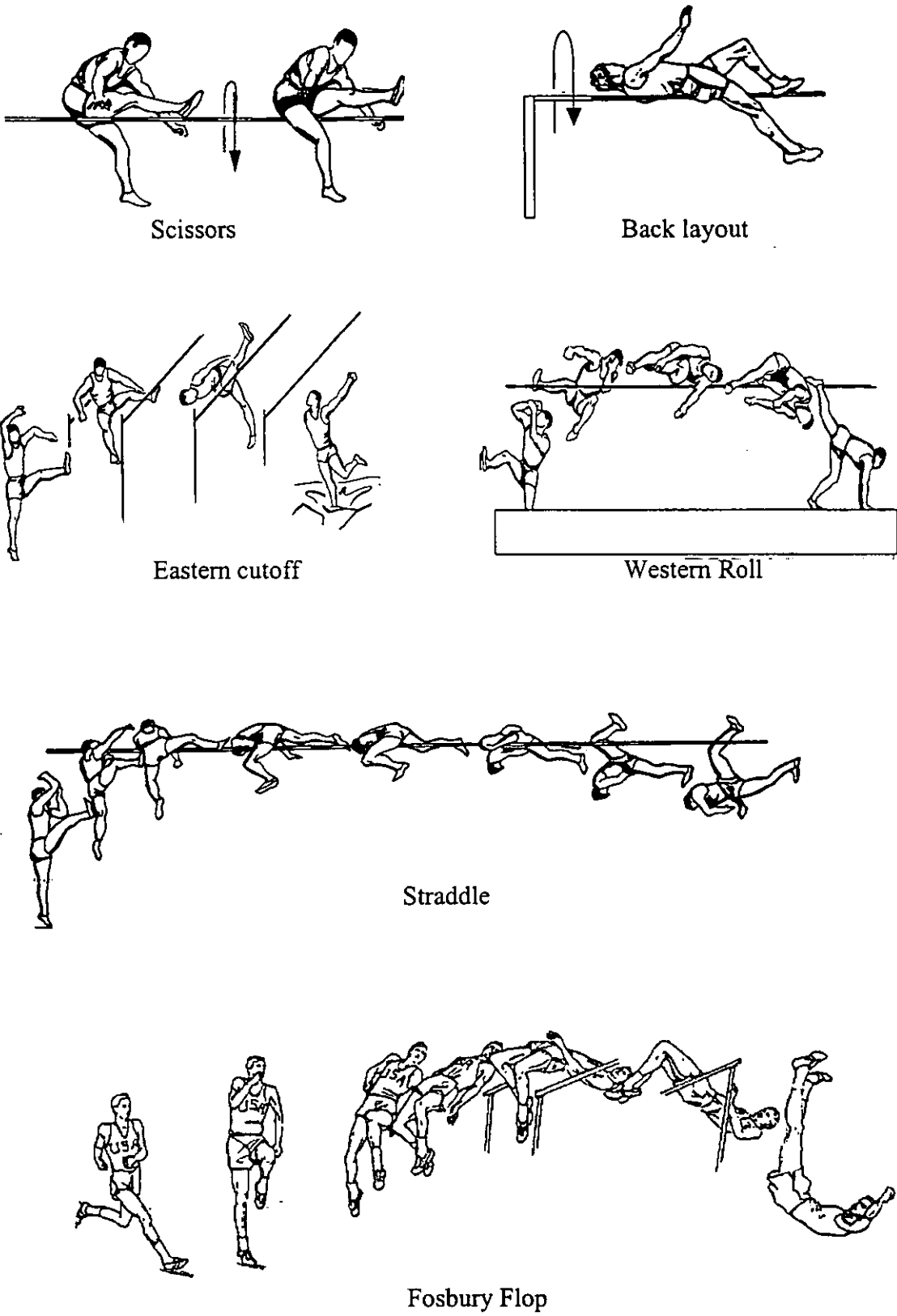


Figure 2.1. Techniques of high jumping (adapted from Hay, 1985 and Doherty, 1985).

a “twisting backward somersault.” This term suggested that a backward somersault is involved in the Flop. However, most jumpers do not take off with their back facing the bar and it is the twist rotation that causes the turning of their back towards the bar. Hence the flight phase of the Fosbury Flop should be described as a “twisting somersault”.

The Fosbury Flop consists of three distinct and closely related phases:

- (i) The approach phase
- (ii) The take-off phase
- (iii) The flight phase.

It will provide a clearer picture if the description of high jump is systematically reviewed from each of the distinct phases.

Approach phase

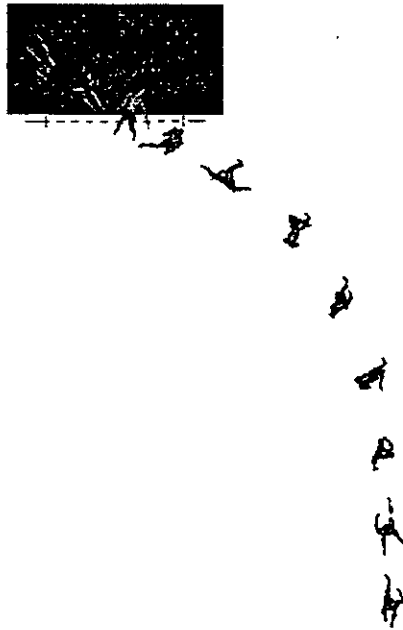


Figure 2.2. J-shaped approach run in Fosbury Flop.

The Fosbury Flop differs from the previous dominant technique, the Straddle, not only with the jump which involves a twisting somersault but also with the characteristic curved approach. Although floppers have experimented with various types of curved run ranging from pure circular to parabolic curved runs, the J-shaped approach run (Figure

2.2) still brought about the most success (Payne and Payne, 1981). There were some speculations that Dick Fosbury used a parabolic curve similar to one Mike Sweeney used for his Eastern cutoff technique in 1895! However, according to Fosbury's coach Berny Wagner, Fosbury used a J-shaped approach. This was also confirmed by Kerksenbrock (1974) who based his findings on film analysis of Fosbury's jump.

Straight portion of the approach

The initial straight portion of the J-shaped approach allows the jumper to achieve more horizontal velocity and attain a more consistent stride pattern than is possible with completely curved runs. (Martin, 1982; Wagner 1985). It may be common sense that one can run faster in a straight line than in a curve. In fact in an experiment, it was found that a runner who could manage 10 m/s in a straight run was unable to go faster than 5.1 m/s when running in a circle of 3.7 m radius (Alexander, 1992). Killing (1994) has shown that elite high jumpers were not very consistent in their stride patterns. For a particular world-class jumper, there were variations of up to 30 cm even in the take-off stride. This may indicate that a consistent stride pattern may not be an important factor in high jumping.

Curved portion of the approach

Initially it was thought that the curved portion of the approach was nothing more than an idiosyncrasy of Dick Fosbury. Efforts have been made to substitute the curved approach with the straight approach in the Flop but with little or no success. Then some coaches begin to consider whether the curved approach may be an advantage after all. There was even a suggestion that the curved approach should be used for the straddle technique (Heinz, 1974). But what are the advantages of the curved portion of the approach? Wagner (1985) suggested that the curved portion puts the jumper in the needed position at take-off so that more thrust is used for achieving upward velocity. He did not, however, explain what is this 'needed position' or how was the position attained. He has also not explained how more thrust can be used to achieve an upward velocity.

Dapena (1988) maintained that the curved approach enabled jumpers to tilt away from the bar. He also observed that a jumper with a greater inward body tilt angle (Figure 2.3) at the start of take-off phase usually jumps higher. With more tilt angle toward the

inside of the curve, the jumper would have more time to rock up from the heel to the toe and hence more time to apply more force to the ground to get more vertical lift (Wagner 1985). Jacoby (1986) endorsed this theory with the use of the concept of impulse.

$$\text{Force} \times \text{Time} = \text{Impulse}$$

He noted that the inward tilt will increase the time to apply force so that a greater impulse can be created. Dapena however contradicted this with his observations that the smaller the change in this tilt angle at take-off, the higher was the jump. He also added that this occurred even if the trunk does not quite reach the vertical. Dapena himself admitted that he was unable to account for this observation.

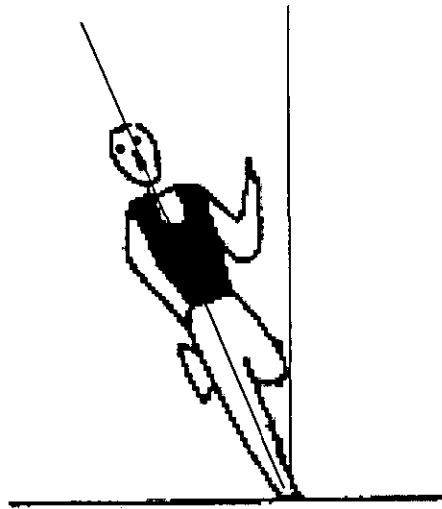


Figure 2.3. Inward body tilt (adapted from Dick, 1993).

Rotation

Ecker (1976) suggested that the curved portion of the approach is also to facilitate an appropriate body position for bar clearance. To achieve the appropriate body position for the bar clearance, the athlete needs to perform rotations about his longitudinal, frontal and lateral axes. The process of the body straightening up from the inward tilt during the latter part of the curve, may have imparted angular momentum about the jumper's frontal axis (Jacoby, 1986).

Dapena (1980b) claimed that the curved approach could not contribute much to the somersault rotations (rotations about the jumper's frontal and lateral axes) because little or none of the angular momentum necessary for these rotations was generated prior to the initial phase of take-off. This conclusion seems unwarranted since the curved approach might affect the ability to generate angular momentum during take-off. Dapena

did, however, find that some angular momentum necessary for the twist was generated prior to take-off.

Summary of the approach

The straight portion of the approach may be used to achieve more horizontal speed. There is no evidence that the straight portion can assist in maintaining a consistent stride pattern. Even some world class jumpers were found to be quite inconsistent with their stride lengths or foot placements. The curved portion of the approach run 'delivers' the inward tilt of the body to the take-off phase. The curved approach may also assist in the straightening up of the body at take-off. The process of straightening up also provides angular momentum for rotation about the jumper's frontal axis. However, the mechanics of how the body straightens up remains unanswered. The curved approach is also thought to be responsible for generating some angular momentum for rotation about the jumper's longitudinal axis.

The take-off phase

Description

The take-off phase begins at the last foot placement of the approach run. It starts when the take-off foot touches the ground (touchdown) and ends when it leaves the ground (take-off). The term "touchdown", also known as the plant, is referred to as the start of the take-off phase. At touchdown, the foot usually contacts the ground heel first then it rocks up to the toes for the take-off. This usually takes about 0.12 to 0.17 seconds (Tidow 1993).

There seems to be agreement among coaches that the take-off foot should be placed at a point directly in front of the near upright (about 1m away from the bar) to ensure clearance of the bar at its lowest point and provide a landing on the mats (Doherty 1985). There is a wide variation in regard to the line of placement of the take-off foot. Wagner (1985) recommended that the angle of the foot should be about 15 degrees to the plane of the uprights whereas Tidow (1993) suggested that it should be about 30 degrees. However Doherty (1985) pointed out that most effective line of placement of the foot should be a balance between the curve of the final stride and the facilitation of rotation during the take-off.

The take-off foot is also placed well ahead of the rest of the body. This implies that there is a backward body lean at touchdown (Figure 2.4).

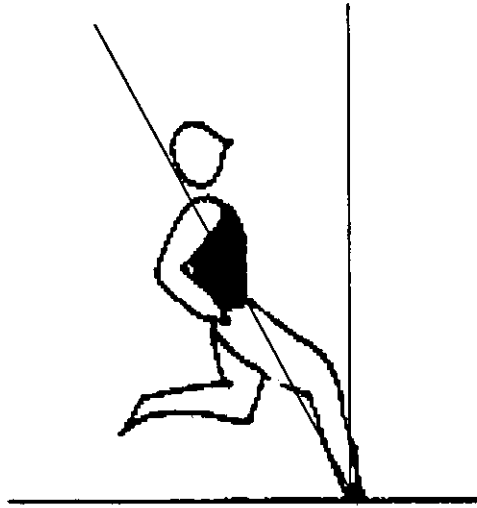


Figure 2.4. Backward body lean (adapted from Dick, 1993).

Tidow (1993) estimated that the backward lean angle of the body is about 10 to 15 degrees. At take-off the body will straighten up to almost vertical. The knee of the take-off leg will flex as the heel is planted, although the jumper should resist this motion (Wagner, 1985). This knee flexion probably helps to cushion the impact of the foot plant and also pre-tense for subsequent extension. Ritzdorf and Conrad (1987) observed that the knee angle at the plant was around 160 degrees and would decrease till 150 degrees before going into full extension.

There are variations of the arm swings during this phase. However they can be classified broadly as single arm and double arms swings. The single arm swing is like a natural running action swing. The double arm swing occurs when both arms are pulled back at the plant position and swung forward and upwards at take-off (Wagner, 1985). During this phase, the lead leg or sometimes known as the free leg is driven upwards till the thigh is about parallel to the ground (Wagner, 1985). The knee of this leg could be semi-bent or straightened.

Vertical velocity

The vertical velocity at the end of the take-off phase is of crucial importance for the height of the jump. This velocity is dependent on the action of the athlete during the take-off phase. Dapena (1988) suggested that at the end of a fast approach, the take-off leg should be planted ahead of the body so that the knee could be forced to flex. This flexion stretches the knee extensor muscles which could in turn forcefully extend the take-off leg to attain the needed vertical velocity. This implies that horizontal velocity can be converted into vertical velocity. However the limit to this technique of conversion is that a large flexion at the joint could result in greater absorption of the approach speed.

Dapena (1987) also suggested that to attain a large vertical velocity at take-off, the vertical force exerted must not only be large but it should also be exerted for as long as possible. This can be achieved if the initial height of the mass centre could be lower so that the ground reaction force would have a longer duration. Heinz (1974) suggested that increasing the vertical range of motion or lowering the initial height of the mass centre can be achieved by maintaining a greater inward tilt. However to maintain a lower mass centre height during the take-off phase and the penultimate step requires great muscular strength and neuromotor coordination (Dapena, 1987).

At the beginning of the take-off phase, if the mass centre is moving towards the ground then energy is needed to reverse this direction and so there will be less energy to generate the vertical velocity for the jump. However, if the mass centre is on its way up (vertically away from the ground), the final vertical velocity will be greater. A long penultimate step with a short final step may be the strategy to use to limit the downward velocity of the mass centre at the plant. This would however contradict the effort of maintaining a lower mass centre height for maximising the vertical range for application of ground reaction force.

At take-off, with an arm swing (especially a double arm swing) greater reaction force can be developed. This would increase the vertical velocity of the mass centre and hence improve the jump height. This take-off phase is therefore considered to be the most important part of the jump (Dapena, 1992). Hence the purpose of the take-off phase is to attain maximum vertical velocity to maximise the height jumped. Jarver (1981) also suggested that another aim of the take-off phase is to create sufficient body rotation for an efficient lay-out for the bar clearance.

Rotation

Dapena (1988) found that during the take-off phase, greater forward somersault rotation was generated with larger changes in trunk lean angle from backwards to forwards. He also found that the double arm swing and lead leg actions at take-off would reduce this forward rotation. Ecker (1976) claimed that the checking of the linear motion at the start of the take-off phase may generate the forward rotation. This implies that the forward movement of the lower body is blocked when the jumper plants his take-off foot while the upper body continues forward imparting a forward rotation about the lateral axis. However no experimental data has been given to verify these speculations.

Dapena (1988) pointed out that the curved approach facilitated the inward tilt of the body towards the centre of the curve. He also stated that a larger change in this tilt angle towards the vertical will result in the generation of greater side somersault momentum. He did not explain how the change of tilt angle is brought about. Hence the generation of side somersault rotation has yet to be understood.

Ecker (1976) also observed that the lead leg swing during the take-off phase could have assisted in the rotation about the longitudinal axis. Dapena (1980) claimed that the angular momentum for this twist rotation at take-off was twice more than at the plant. He also added that at take-off, if the 'single arm swing' is used, the twist rotation could be retarded. Dapena basically implied that the twist rotation is generated mainly at the take-off phase. However he did not explain how the twist momentum was achieved.

Summary of the take-off phase

The take-off phase is a short and yet very important part of the high jump. The objectives of this phase are to maximise the production of vertical velocity of the mass centre and to create sufficient body rotation for bar clearance. To enable jumpers to improve on their performance, not only the optimum conditions for maximising the vertical velocity need to be determined, but the mechanics of how rotation is generated also needs to be understood.

The flight phase

There are variations in the ways in which jumpers move their bodies across the bar. However, in the Fosbury Flop, the jumper's body would have to roughly undergo a 'twisting somersault' in the air to clear the bar. Killling (1993) stated that the important features of the flight phase are mainly:

- i) The over extension of the hip and back in the initial stage.
- ii) The lowering of the hips and the lifting of the legs in the later stage.

He has however omitted the twist portion at the initial stage of the flight. This may be because the twist portion is not quite conspicuous in flight.

The parabolic path of the mass centre is determined once the body loses contact with the ground. There is nothing that the jumper can do to change it. However, this does not mean that the paths of all the body parts are determined. In short the jumper could raise the hips in flight by lowering his head and legs. The rotation of the body depends on the angular momentum of the body about that axis. Angular momentum about the mass centre cannot be altered once the athlete leaves the ground. However, Dapena (1995) pointed out that some alterations of rotation are still possible. This is done by slowing down the rotation of certain parts of the body, while the other parts of the body will speed up as compensation. This is also known as "counter-rotation" or "catting". Yeadon (1993) has shown that in a somersault, twist also can be produced by inducing tilt using asymmetrical movement of the arms, chest or hips about the sagittal plane. This implies that by using counter-rotation and asymmetrical body configuration manipulations, rotations may be induced in flight. However the question asked in high jumping is: "Could rotations required by the jumper for effective bar clearance be initiated or altered during the flight stage?" Dyson (1986) argued that this was not possible because the time the jumper spent in flight was too short. He has however no experimental data to show that this was not possible. Dapena (1995) stated that the twist rotation may be affected by the proportion of the angular momentum of the side and front somersault rotation. This may give rise to a situation in which a jumper finds that he has too little or too much twist while in flight and hence needs to make adjustments for effective bar clearance. Santos (1978) presented a number of movements which the jumper could use to vary the speed of rotation and the position of different body parts so as to avoid dislodging the bar. Hence

the question on whether rotation can be generated or varied in the flight phase of the Fosbury Flop technique remains to be examined. However since this study is primarily concern with the contributions of the curved approach, the question on whether rotation can be generated in the flight phase is beyond the scope of this study.

Summary of the flight phase

The flight phase of the Fosbury Flop requires the jumper to perform a twisting somersault. Many coaches and researchers have speculated on how this twisting somersault rotation can be varied or generated in the flight phase. However, Dyson (1986) argued that time spent in flight was too short for the generation of rotation.

INVESTIGATIONS OF HIGH JUMPING

The technique of high jumping has been investigated through observational, experimental and theoretical studies. Observational studies in high jumping consist of kinematic and kinetic analyses. Experimental studies involve analyses through planned intervention in the technique and observation of the effects of such intervention. Theoretical studies involve analyses which employ a theoretical representation of the activity, usually in the form of mathematical equations.

In the following sections, studies conducted in an attempt to understand the mechanical principles behind the high jump are reviewed. Although most of the studies reviewed here are far from conclusive, the intent of this review is to enlighten as well as to raise questions to prompt and guide further investigations so that a clearer understanding of the mechanics of the Fosbury Flop can be achieved.

Observational studies

Kinematic analysis often involves the use of image analysis techniques. Cinematography as well as videography could provide the opportunity to capture complex movement sequences so that a detailed analysis can be performed. At a subjective level of analysis, the recorded movement from film or video may be sufficient to allow general comments to be made on the observed characteristics but without a quantitative mechanical analysis the conclusions that can be drawn are limited. At the objective or

quantitative level of analysis it is not sufficient to just record and observe the movement. Detailed measurements must be taken so that inferences drawn with reference to the movement can be accurate. The sampling rate of the camera also need to be considered.

Kinetic analysis implies the direct measurement of external force. This usually involves using a force platform. Force platforms are capable of measuring the three orthogonal components of the resultant ground contact force (F_x , F_y , and F_z). The point of resultant force application (A_x , A_z) with reference to the centre of the platform, a position often referred to as the centre of pressure can also be obtained. The force platform can also provide the calculations of the moment about the axis perpendicular to the plane of the platform and the frictional torque. However, force platforms are required to be bolted to a base plate which is set in concrete and hence it is difficult to use them outside the laboratory settings.

Force platforms provide the centre of pressure position relative to the centre of the force platform. However, if information about the distribution of the pressure under the foot is required, the use of pressure pads is to be preferred. A pressure pad consists of a set of force transducers recording force at discrete points on the contact surface. These pads have been constructed as insoles which may be placed in the shoes to monitor pressure under the foot.

Image analysis technique

Since Dick Fosbury introduced his Fosbury Flop in 1968, there have been a number of image analyses made on the technique. Initially, photosequences of high jumping (Ecker, 1969; Hay, 1974) was a common method of studying the jump. Such studies do not produce kinematic data and hence merely provide a qualitative description of the activity. Some quantitative studies on the Fosbury Flop have been based on two-dimensional analyses of the motion (Adachi et al., 1973; Nigg, 1974). The major limitation of such studies is that the Fosbury Flop is essentially a three-dimensional movement. Kerssenbrock (1974) analysed the original approach of Dick Fosbury's Flop technique using cinematographic film analysis. He was able to obtain certain kinematic data of Fosbury's run-up (such as approach speed and stride lengths). No mechanical explanation or theory was advanced from his investigation, however. Thus his study only provides a quantitative description of the historical jump.

Curved approach

Kerssenbrock (1974) found that Fosbury's approach run consisted of eight steps of which the last three were run on the curve. He also found that the radius of this curve was about 13 m and was shortening as Fosbury approached the bar. He did not, however, explore the effect of shortening the radius of the curved approach.

In order to determine the radius of the curved approach, Dapena et al. (1997) fitted an arc of a circle through the foot-print locations of the curved approach. They had to omit the penultimate foot location (prior to take-off) because many of their jumpers placed that foot outside the general curve. Since there are many jumpers in their study placing this penultimate step of the approach outside the general curve, it is surprising that they have not investigated or questioned these occurrences. From such an observation one would have thought that placing the penultimate step outside the curve might be an integral part of the technique. If this is indeed part of the technique then what effect does this have?

Kerssenbrock also found that Fosbury's take-off stride was about 2.23 m which is about 0.08 m longer than his previous stride. Dapena (1980a) also used film analysis to investigate the Fosbury Flop technique. He found that the frequency of athletes using a shorter last step following the penultimate step were higher. But there were variations between trials even with an individual athlete. Killing (1995) reported that the step length of the approach could vary up to 30 cm among world class high jumpers. The variations could even occur for an individual athlete within the same competition. With these findings, Killing suggested that curved approach is not sensitive to variations in stride length. The reasons for this effect have yet to be explored.

Dapena (1980b) used data generated from three-dimensional film analysis to calculate the angular momentum required for the side somersault rotation. He found that the angular momentum was not generated prior to the take-off phase. Hence he concluded that the curved approach does not produce side somersault rotation but favours its production during take-off. However, it has yet to be explained how the curved approach could favour the production of side somersault during take-off.

Take-off

For optimum performance in high jumping, a high jumper must impart maximum vertical velocity to the mass centre and to acquire sufficient body rotation to permit a flat back layout at take-off (Martin, 1982). Several researchers have presented theories on how the vertical velocity can be maximised. Some suggested that a fast horizontal velocity at the beginning of take-off may enhance the vertical force and hence maximise the vertical velocity (Dapena, 1987; Ozolin, 1973). Others suggested that a low position of mass centre at the beginning of the take-off also assists in the maximising of the vertical velocity (Dapena & Chung, 1988; Dyatchkov, 1968). There were also suggestions that the ways in which the arms are swung during the take-off may affect the generation of the vertical velocity (Dapena & Chung, 1988; Dyatchkov, 1968). These theories have prompted many investigators to use image analysis (either with video or film) to examine the characteristics of these performance variables at take-off (e.g. Ilboshi et al., 1994; Brüggemann & Loch, 1992; Ae et al., 1986). However, establishing relationships between performance variables should be considered cautiously. Nigg et al. (1974) found that peak height of the jump increased as the height of the mass centre at the beginning of take-off decreased (Hay, 1985). It would be too simplistic to establish such a relationship in high jumping without considering other variables such as approach velocity or angle of projection. Besides these variables, limiting factors such as the strength of the jumper's take-off leg should also be considered (Dapena, 1990). These considerations imply that the optimum solution for maximising the vertical velocity at take-off cannot be found by using image analysis technique alone.

Unlike the numerous studies on the generation of vertical velocity, there are only two studies (Dapena, 1980b; Dapena, 1988) on the acquisition of rotation at take-off in the Fosbury Flop. In both of the studies, the angular momenta for the twist and the two somersault rotations required for the jump were quantified. An extended version of the procedure designed by Hay et al. (1977) was used to calculate these angular momenta in the earlier study (Dapena, 1980b). This procedure required knowledge of the three-dimensional coordinates of the endpoints of 14 segments (in which the body was considered to be divided). These coordinates were obtained from film analysis. In this study he found that only a little of the angular momentum for the twist rotation was produced prior to the take-off phase. While as much as two thirds of the angular

momentum for the twist was generated during take-off. He also found that practically all the angular momentum for both somersault rotations were produced during take-off.

He attributed 'the swing' of the lead leg to be mainly responsible for the production of the twisting angular momentum at take-off. He implied that the angular momentum for the forward somersault rotation was 'produced by checking of linear motion'. Although this theory is quite widely accepted (Ecker, 1971; Santos, 1976; Wagner, 1985; Dyson, 1976) it has yet to be verified with any quantitative data.

In the second study (Dapena, 1988), he postulated that the angular momentum for side somersault was produced during take-off by the generation of a ground reaction force that could rotate the jumper over the bar. This ground reaction force must be acting in a direction between the mass centre of the jumper and the centre of the curve (of the approach). However, the question of how such a ground reaction force was generated during take-off has yet to be answered. In short, the mechanics of how side somersault rotation was produced needs further investigation.

Flight phase

The difference between the bar height and the peak height of the mass centre attained by the jumper of a successful clearance is a measure of the effectiveness of bar clearance (Dapena, 1980a). The smaller the difference is, the more effective is the bar clearance. This depends on the athlete's body position at the peak of the jump and the movements that he makes in crossing the bar (Hay, 1985). Theoretically, it is possible for the jumper to pass over the bar while his mass centre passes under the bar (Dyson, 1986). However this has yet to be demonstrated by any high jumper although Dapena (1980a) claimed that one of the subjects in his study was observed to have cleared the bar successfully with his mass centre attaining the same height as the bar.

From film and video analyses (Santos, 1978; Tidow, 1993; Dapena 1988), jumpers were noted to have made a number of body movements during the flight phase such as flexion of the knees and extension of the hips. On the other hand, Wagner (1985) claimed that Fosbury and the majority of successful male jumpers used a passive bar clearance. Dyson (1986) argued that all rotation had to be initiated while the jumper was still in contact with the ground because the time the jumper spent in flight was too short to cause rotation. This implied that any attempt to make adjustments during the flight phase were

indeed superfluous. Dyson argued that the amount of angular momentum generated prior to the flight phase was sufficient to perform the twisting somersault rotation required for a successful bar clearance.

Dapena (1995), however, claimed that the movements or adjustments made during the flight phase could indeed cause alterations of the rotation. This can be done by either counter-rotation or by altering the moment of inertia. He also claimed that the difference in the proportion of the forward and side somersault rotation could also affect the amount of twisting momentum required. Therefore, he argued that the angular momentum generated prior to the flight phase may at times be insufficient or excessive for proper bar clearance. He concluded that adjustments made during the flight phase were necessary to ensure appropriate rotation for effective bar clearance. Hay (1985) on the other hand, implied that these movements in flight were reactive reflexes of the jumper, simply moving the particular body segment to avoid dislodging the bar. This implied that a passive body in flight is incapable of effective bar clearance.

However these theories derived from observational studies have yet to be verified. This raises the question on whether the adjustments made by the jumpers during flight were indeed necessary for successful or efficient bar clearance. Since the aim of the present study is focused on the curved approach, the direct attempt to answer the question on whether the adjustments made by the jumpers during flight phase will not be made. However if the contribution of curved approach in the twist rotation in high jumping is known, an indication of whether adjustment in the flight phase is necessary may be inferred.

Force platform

Many high jump studies have involved the use of a force platform (Hay, 1968; Kuhlow, 1973; Pedotti and Rodano, 1981; Dessureault and Lafortune, 1981; Aura and Viitasalo, 1987; Deporte and van Gheluwe, 1989). A force platform is designed to measure reaction forces and moments as well as the point of application of the resultant vertical reaction. In addition, the force platform also records the time at which the forces were applied. Some of these studies (Hay 1968; Kuhlow, 1973) were involved in examining the impulse at take-off. The vertical impulse exerted at take-off is of great

importance in determining how high a jumper jumps (Hay, 1973). Impulse can be defined as the product of force exerted and the time of exertion. Therefore, by integrating the vertical ground reaction force with respect to time, the vertical impulse can be obtained. Hay (1968) found that the vertical impulse for the Western Roll technique was in fact higher than for the Straddle for the same height cleared. He concluded that the Western Roll technique was more effective in generating a higher impulse and therefore provides a more effective take-off. However, he also found that jumpers using the Straddle technique were capable of clearing a greater height, although the vertical impulses generated were much lower. Basically, he could not understand why jumpers using the Western roll technique could not clear a greater height although this technique imparts greater vertical impulse. It may be that the Western Roll technique was indeed more effective in generating a higher impulse, projecting the jumpers' mass centres to greater heights but the technique itself was poor in efficiency in bar clearance compared with the Straddle. Kuhlow (1973) also found that the Straddle yielded a higher vertical impulse than the Flop technique for jumpers clearing the same height. Perhaps, in the same way, the Straddle technique predisposes jumpers to generate a higher vertical impulse than the Fosbury Flop but not a more efficient bar clearance. Hay (1985) developed an efficiency index (H_3) from observation as well as theoretical analysis to rate techniques in their effectiveness in clearing the bar. This efficiency index depicts the difference between the bar height and the peak height of the jumper's mass centre. He ranked the Flop technique ahead of the Straddle and the Straddle ahead of the Western Roll. Since the Fosbury Flop emerged as the preferred technique among elite high jumper, it may imply that raising the mass centre is secondary to a more effective bar clearance.

Although force platforms are quite commonly used for studying the ground reaction forces during take-off in jumping activities, a standardised methodology of data collection has yet to be defined. Further, in most studies, the methodology of data collection are often not clearly reported. This certainly makes data comparison and interpretation difficult. Variations in the results of such studies are quite common. For example, Aura and Viitasalo (1987) found that the peak ground reaction force at take-off for the Fosbury Flop to be about 9 bodyweights whereas Dessureault and Lafortune (1981) found it to be only 3.4 bodyweights. Neither study reported the conditions in

which the kinetic data were collected. The large discrepancy prompts the speculation that the methodologies of data collection were different.

Miller and Nissinen (1987) reported that the placement of a mat over the force platform surface markedly reduced the peak ground reaction force recorded for take-offs of somersaults. Nigg et al. (1981) also reported that for jumping take-offs, the use of spiked or hard soled shoes inevitably increased the peak ground reaction force. In some studies (Sung and Shin, 1989; McMahon and Greene, 1979) kinetic data were collected with a synthetic track surface (like tartan) placed on top of the force platform. This would permit jumpers to use spiked shoes for jumping. However, in such a condition, the calibration of the force platform can be difficult especially for the horizontal forces. In some studies (such as Taguchi et al., 1983) jumpers were instructed to jump with sneakers (or soft soled training shoes). It can be expected that the results can be quite different with these different conditions of kinetic data collection.

To ensure ecological validity (the extent to which the real activity is emulated in the study) data must be collected during competition or at least in conditions similar to competition. For example, in analysing the technique of high jumping, if data are collected during a training session, the heights cleared by the jumper should be similar to those cleared in competition. Deporte and van Gheluwe (1989) claimed to have recorded a vertical impact force varying between 8.4 to 8.9 bodyweights and horizontal impact forces between 5.6 to 6.5 bodyweights from an indoor competition. However, they have not reported on how they recovered the data from the competition. During competition, kinetic data must be collected with the appropriate synthetic track surface placed on top of the force platform and subjects inevitably wear spiked shoes to jump. Although Nigg and Yeadon (1987) claimed that the transferred forces collected from this condition may be affected only slightly, mathematical equations can be developed such that the actual values can be recovered from the ones obtained.

Moreover, in order for kinetic data to be collected during competition, the facilities in which a force plate can be placed under the take-off area of the high jump must be available. There are only a few high jump competition arenas in the world that have such facilities. The opportunities of collecting kinetic data from high jump competitions are indeed rather remote.

The above studies may have placed too much emphasis on peak ground reaction force during take-off. It is the net vertical impulse exerted during take-off that determines how high a jumper jumps. It should be noted that having a larger peak force during take-off is not synonymous with having a greater vertical impulse.

Pressure Pads

Unlike force platform, pressure pads do not place extensive demand on the testing area. Pads that are constructed as insoles could simply be placed in shoes to monitor pressure. The pressure sensed by these pads during a movement can be downloaded onto a computer and displayed graphically relative to the shape of the insole. The pressure insole of the Parotec system was even noted to be able to measure vertical force exerted. However, with a discrete number of pads covering about 60% of the insole, the amount of force measured may only be a percentage of the total force. The accuracy of the centre of pressure measurement may also be affected by the placement of these pads in the insoles (Bartlett, 1997). Since the pressure insole is relatively new in its development, it may be prudent to evaluate the measurements obtained for accuracy. This can be done by comparing the measurements obtained from the pressure insoles with the data obtained from a force platform. Pressure insole requires cabling and a control unit or a data storing pack to be worn by the subject which to a certain extent may affect performance. It may not be practical for data collection in high jump competitions.

Although there were no reports of the use of pressure insoles to study high jumping performance, Milani and Hennig (1994) taped 10 pressure sensors onto the plantar surface of the foot to study pressure distribution in high jumping. They found high peak pressure values in the heel and lateral midfoot region during take-off. They were able to relate their findings to excessive pronation and the high incident of navicular stress fractures.

Experimental studies

An experimental study is more than observing the effect of implemented intervention. It is necessary to ascertain that it is only the particular intervention applied that caused the effect. This requires a measure of control over the experiment. In an experiment, direct intervention in the activity may meet some understandable resistance

from the subjects, for fear of injuries. However, Yeadon and Challis (1994) pointed out that some experiments are 'invisible' to the subjects and are purely dependent on the way in which data are selected. By obtaining movement data, it is possible to relate some elements of technique to the performance. Such an experiment lacks the rigor of control and hence may be considered less valid. However, a rigidly controlled experiment may render the movement totally void of ecological validity.

Hence caution must be exercised when establishing the relation of cause and effect from an experimental study.

Straddle versus Flop

From 1973 to 1982, world records in the men's high jump event have been held with jumping techniques toggling between the Flop and the Straddle techniques. This raised the question as to which of these jumping techniques is more efficient. Many investigators were prompted to compare the strengths and weaknesses of the two techniques (Fix, 1974; Carr, 1974; Ecker, 1976; Zacharias, 1976; Daniel, 1978; Castello, 1979; Ross, 1979). The conclusions derived from these studies were contradictory. Ecker claimed that the Fosbury Flop was a better technique because it was easier to be taught or learned. He also stated that the Fosbury Flop technique was more efficient in both bar clearance and creating vertical lift at take-off. Ross (1979), however argued that generating body rotation from the effect of the curve was indeed a complicated kinesthetic act to master. Daniel (1978) claimed that the Straddle technique was more efficient than the Flop in bar clearance. However, the conclusions drawn from most of these investigations were not based on quantitative data.

On the other hand, quantitative analyses revealed that the time recorded for take-off was found to be longer for the Straddle (Vittori, 1972; Kuhlowl, 1973; Dessureault and Lafortune, 1981). Data from force platforms showed that jumpers using the Straddle technique had higher vertical impulses for the same height cleared (Kuhlowl, 1973; Dessureault and Lafortune, 1981). With higher vertical impulses, it would be expected that the projection of the mass centre is higher. Therefore, a higher vertical impulse is required to clear the same height may imply that the Straddle is a less effective technique for bar clearance. Hay (1975) reported that theoretically it was possible to achieve a better bar clearance with the Straddle technique but in practice, the Fosbury Flop was

observed to be more efficient. Beulke (1977), however, claimed that the Straddle technique requires a larger portion of the vertical impulse to generate the required rotation. Thus, for the same height jumped, the Straddle technique would require a higher vertical impulse.

Dessureault and Lafortune (1981) also found that the characteristics of the vertical and horizontal force-time curves produced by jumpers using the Flop technique were rather similar and hence suggested that lower stresses were placed upon the knees of the take-off legs. This could be indeed responsible for the increasing popularity of the technique. Martin (1982) also pointed out that knee injuries have tormented many elite straddle jumpers among whom were Belischmidt and Yashchenko. Tidow (1995) suggested that the demise of the straddle technique could simply be that the technique placed a higher load on the body and hence predisposed jumpers to injuries. On the other hand, Krahl and Knebel (1978) reported that navicular stress fractures resulting from the extreme pronation movement of the foot during the take-off in Fosbury Flop has disabled many elite high jumpers.

The studies comparing the efficiency of the two techniques have so far been inconclusive. With the 'extinction' of the Straddle technique, the question regarding the efficiency of the two techniques may be difficult to answer.

Approach run

The curved approach was used in high jumping about one hundred years ago. It was recorded that, as early as 1895, Mike Sweeney approached the jump with a curved run up (Doherty, 1985). However it was not until 1968, when Dick Fosbury re-introduced the curved approach into high jumping, that many coaches and researchers began to speculate on the purpose of the curved approach. Dapena (1980a, 1980b) conducted an experimental study to ascertain the purpose of the curved approach. He recorded and analysed the jumps of six experienced high jumpers. Of these six jumpers, two used a straight approach run while the other four used a curved approach. He found that the curved approach causes an inherent body tilt away from the bar which favours the production of the angular momentum for somersault rotation and also facilitates a more vertical take-off. He also found that the angular momentum required for the somersault rotation was not produced prior to the take-off phase. In short, he suggested that the

curved approach merely facilitates an appropriate position for the production of rotation and a more vertical take-off. Therefore the question on how rotation or a more vertical take-off position was achieved were not answered. Hence the contributions of the curved approach to the Fosbury Flop was inadequately explained.

Take-off

In competition, an elite high jumper will perform close to optimum on every jump. Therefore the ranges of kinematic variables such as approach speed and plant angle are small. A wider range is required if relationships between these variables and peak height of the mass centre (attained by the jumper) are to be established. Hence, a training environment where direct intervention can be applied by the investigator would be a more appropriate site for data collection. Greig et al. (1996) managed to collect kinematic data of jumps with varying speeds and lengths of the approach from a training session. They were not only able to obtain a wider range of approach speeds but also of knee and leg plant angles at the beginning of take-off. They found that at touchdown the optimum approach speed for their subject was 7.12 ms^{-1} and the leg plant angle was about 36.5° . (The leg plant angle was defined as the angle between the vertical and a line from the foot to the hip.) They also found that the jump height increased with the knee angle at the touchdown. However, their subject was not observed to have a straight leg plant and this was speculated to be related to injury prevention.

Although the optimum values of the approach speed and body plant angles were within the athlete's competition range, the variables were not independently controlled. Therefore the extraneous variance effect (the variation arising from variables not accounted for the study) and interaction effect (the variation arising from the interaction of other variables) were not controlled. Hence the optimum values and the relationships established must be accepted with caution.

On the other hand Ae et al. (1986) identified five high jumpers with varying degrees of knee flexion of the take-off leg. Kinematic data of the jumps made by these jumpers from a competition were then recorded and analysed. They found that jumpers with deep knee flexion at take-off have longer support times and hence were able to afford a larger take-off motion such as a wider double arm swing. However, the loss of the approach velocity was noted to be quite considerable. They also found that with

lesser knee flexion at take-off, the support time was shorter and hence they did not facilitate a large range of movement during take-off. However, the loss of approach velocity was small. They concluded that the two techniques have their respective advantages and disadvantages; therefore a jumper needs to compromise in deciding which motion needs to be emphasized. With such an experiment, the effects of the two extreme knee flexion conditions could be observed. However, it was not possible to quantify the effect of the varying knee flexion on the jump height. Hence, an optimum knee angle for an individual jumper could not be found from this study.

Theoretical studies

High jumping has also been investigated by another method known as the theoretical approach. This takes the form of an idealization of the activity using a theoretical model (Yeadon and Challis, 1994). The advantage of such an approach is that selected variables of the experiment can be isolated or effectively controlled. Athletes are saved from performing under experimental conditions which could be rather hazardous. The potential for predicting optimal performance could also easily be realised. It would also save a lot of time and expenses compared with other approaches.

However, the use of theoretical studies do have their fair share of limitations. The most important drawback of the theoretical approach is the difficulty of validation and the fact that incorrect models would prejudice the results (Vaughan, 1984). Hence, caution has to be used in interpreting the results obtained from such mathematical models.

There are only a few simulation models developed and used in the study of high jumping. Most of the theoretical studies in high jumping use inverse dynamic models to calculate energy or angular momentum. The results obtained from these inverse dynamic approaches are often questionable and hence the conclusions derived from such studies may be considered as speculations rather than established facts.

Approach

Beulke (1977) calculated the kinetic energy from the take-off impulse of the Fosbury Flop and the required rotational energy from an inertia model of a jumper. He used the subtraction of the rotational energy from the kinetic energy to predict the height elevated. Noting the “straightening up” or the rotation about the frontal axis (of the

jumper) during the last but one step, he concluded that some rotational energy must be produced by the curved approach in Fosbury Flop. The production of this rotational energy would imply that more of the kinetic energy derived from the take-off impulse could be used for height elevation. He did not explain, however, how the curved approach could produce rotational energy.

Dapena (1980b) used a theoretical method (Dapena, 1978) to compute the angular momentum of jumpers about three orthogonal axes (relative to the position of the upright posts) at the beginning and also at the end of take-off. He found that little or no angular momentum was generated prior to the beginning of take-off. Hence he concluded that contrary to the Beulke's hypothesis, the curved approach did not contribute to the production of rotational energy but merely "favours" the production during take-off.

Take-off

Alexander (1990) developed a simple two segment model that consisted of a thigh and shank with a knee extensor muscle to study high and long jumping. From this theoretical study he was able to establish that there is indeed an optimum approach velocity and knee angle at take-off for high jumping.

Townend (1984) used the Newtonian Laws of Motion equations and a 'nine hinged rods plus a disc' model of an athlete to predict the maximum height that the mass centre would be raised for a given height of the athlete. Using a vertical velocity at take-off (5 ms^{-1}) and the height of the mass centre at take-off (1.32 m), his model predicts the maximum height that could be cleared was 2.60 m, which is well beyond the present world record holder. Perhaps, his model was a little too simplistic to represent the biomechanical system of an athlete. Based on the typical body positions of an athlete clearing the bar, he also found that for a given height cleared (2.13m), a jumper using the Flop technique needs only about 94% of the vertical impulse required using the straddle technique. The results compared favourably with the vertical impulses recorded directly from the force platform by Kuhlow (1973). However this calculation was based on an unsubstantiated assumption that with the straddle technique, the best clearance possible was when the mass centre height is equal to the bar height.

Van Gheluwe and van Donnick (1978) calculated the propulsion forces during the upward motion at take-off of both the Straddle and the Flop techniques by using the

kinematic data (namely; the vertical take-off velocity and time) obtained from film analysis. They found that the propulsion forces for Straddle and for Flop were 4.0 and 4.8 bodyweights respectively.

Sung (1990) calculated the maximum vertical ground reaction force from the vertical acceleration of the mass centre to be between 6.3 to 7.6 bodyweights. The maximum vertical ground reaction calculated was a little lower than the 8 to 9 bodyweights recorded by the force platforms of Deporte & van Gheluwe (1989) and Aura & Viitasalo (1987) respectively.

Flight

Hubbard and Trinkle (1985) modelled high jumper as a rigid rod. They were able to find an optimal trajectory which consisted of two brushes with the bar from their theoretical approach. In the Fosbury flop, the body of the high jumper is far from being straight during the bar clearance, so their rigid rod model may be an over-simplification. It might be more realistic to model the jumper as a bent rod. The assumption that a specified amount of energy may be distributed between linear and rotational movements is unsubstantiated (Yeadon and Challis, 1994). However, this study may have demonstrated that a passive body configuration in flight is possible for the Fosbury Flop technique in high jump.

Dapena (1981) developed a procedure to analyze the flight phase of a jump and then simulate the modified motion by prescribing different initial conditions or different segmental movements. Using his simulation model, he found that by altering the limb movements of a jumper who failed to clear the bar at 2.08 m, the jumper could clear the bar set at 2.14 m. This would imply that by modifying body configuration in flight, a jumper indeed could clear a greater height. However, his simulation model is not without error. It was found that between 0.6 to 0.8 seconds, the somersault error was about 12° and the twist error was about 20°. Another limitation is that his model does not take into account whether the perturbed joint angles would require joint torques beyond the subject's capabilities.

Hay (1973) theorized an ultimate technique in the high jump that involved a frontal approach with a bent knee action take-off and a forward piked bar clearance (as shown in Figure 2.5). The forward pike position or the 'jackknife-position' can be

considered as the optimal position of the limbs with respect to the mass centre and the bar. However, Preiss (1985) using computer simulation found that in reaching and leaving this pike position the athlete's body must pass through lesser than optimal positions relative to the bar. In short, the athlete is likely to dislodge the bar either before or after the mass center had attained the peak height. Besides, it was also found that the landings for jumps with vertical take-off velocities below 3.5 ms^{-1} appeared to be very hazardous. These findings may have deterred jumpers from adopting this technique.

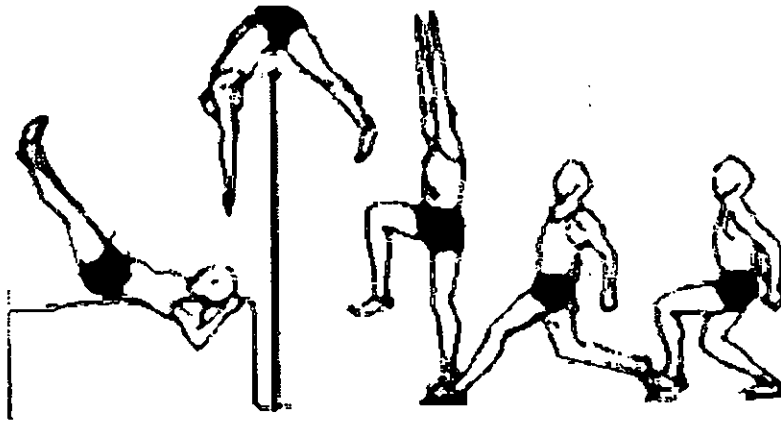


Figure 2.5. Forward pike clearance (adapted from Hay, 1973).

Combination method

Different methods of analysis have been used in the study of high jumping, but each method has its weaknesses. A combination of the different techniques is therefore required if a realistic understanding of the Fosbury Flop is to be achieved. An observational study could provide the necessary description of the activity so that a theoretical model can be developed. With a theoretical model, optimum technique can be predicted. The conditions of the predicted optimum technique can then be used to set up an experimental study. The comparison of the experimental and theoretical outcomes can then be used to evaluate the theoretical model (Yeadon and Challis, 1994).

Summary of investigations of high jumping

Video or cinematographical investigation without an accompanying quantitative mechanical analysis is incapable of providing a comprehensive understanding of the technique. Some such studies simply provide a quantitative description of the jump. Some “conclusions” from these studies are drawn from the reflections of the investigators’ own opinions. Such conclusions may indeed be true, but without proper verification they should not be accepted as so. Although none of the video and cinematographical investigations in high jumping can be considered conclusive, it does appear that the angular momentum for rotation in high jumping is generated during take-off. However, the contribution of the curved approach still remains unclear.

The use of force platforms to investigate the forces exerted during take-off have so far yielded a wide variation in results. It is speculated that this is caused by the use of different methodologies in data collection. However, the highest recorded maximum vertical and anterior-posterior ground reactions are about 8.9 and 6.5 bodyweights respectively. The opportunity for collecting kinetic data from high jump competitions is rather remote. This is because there are too few athletic arenas that have facilities in which a force platform can be placed under the high jump take-off area.

The use of the ‘invisible’ experiment may be criticised for the lack of effective controls and on the other hand an effectively controlled experiment renders the activity out of realism. Therefore, conclusions derived from experimental studies may have to be treated with a little scepticism. However experimental studies in high jump seem to suggest that certain performance variables such as approach speed, knee and leg plant angles at the beginning of take-off have some influence on the height jumped.

Theoretical modelling requires the validation of the represented system. However, most of the theoretical studies in high jumping have either failed to evaluate their models or fared poorly when compared with the real life system. Despite this limitation, theoretical studies seem to suggest that a specific sequence of limb movements during flight may optimise bar clearance in the high jump. However there is the question of whether the required perturbed movements are within the capability of the jumper.

Since each of the approaches used in the study of high jumping has its weaknesses, a combination of the different approaches is therefore required before proper conclusions can be drawn.

TECHNIQUES OF INVESTIGATION

Image analysis methods

The study of human movement often requires the recording of motion using either film or video. In sports biomechanics, the most common means of obtaining data has been the manual digitising of these recordings using a digitising system (Yeadon and Challis, 1994). The process of digitising involves placing a cursor over of the desired landmarks in the recorded image so that Cartesian coordinates can be obtained. These coordinates are then transformed from the image reference frame into a reference frame in the activity or movement space for analysis (Yeadon and Challis, 1994).

Video vs. cinematographic recording system

There are many different sizes of cinematographic film format available, for example; 8 mm, 16 mm, and 35 mm. According to Winter (1990), the image size of the 8 mm is somewhat small for accurate measurement while the 35 mm format is too expensive to buy and operate, therefore the 16 mm format is considered as a reasonable compromise for the study of human movement. The type of film required usually depends on the lighting and the speed of movements involved in the particular activity studied. A reversal film with the ASA rating of 400 is commonly used in sport biomechanics research.

With the introduction of video technology, there has been a trend to replace cinematography with video for motion analysis. This is because video offers many advantages such as: the low cost of video tapes, the ease of use and the immediate availability of the recordings. However, before embarking on the use of video for motion analysis, one must consider the negative features in the video system such as: its low sampling rate (50 Hz), inferior quality of the image and most of all, the accuracy of the data.

Sampling rates

Most video cameras sample at the rate of 50 or 60 Hz. High speed video cameras (in excess of 1000 Hz) are available but are presently incompatible with the standard

video equipment such as the monitor and the cassette recorder. In addition the current price may be considered to be extravagant for most research institutions. The recording rate of 50 or 60 Hz may cause the problem of blurred images especially when the activity recorded involves high speed movements. This can be resolved by reducing the exposure time. Another more serious problem associated with low sampling rate is aliasing error which results in the generation of false frequencies (Winter, 1990). In short, too low a sampling rate will cause distortions due to missing vital movement characteristics. The relevant question to be raised is whether the sampling rate of video (which is 50 Hz for the PAL television system) is sufficient for studying high jumping.

Lees (1980) suggested that the sampling frequency must be high enough to define movement and will depend on the type of movement analysed. Although the basic (Nyquist) sampling theorem dictates that sampling must occur at the rate of at least twice that of the maximum frequency of interest, Lees pointed out that in practice, a sampling rate used is often four to five times higher than the maximum frequency of the interest. He recommended the sampling rate need not exceed 50 Hz in analysing various forms of human motion. This is because the highest frequency found in most of the voluntary repetitive human movement from film analysis appears to be about 4 to 5 Hz (Winter et al., 1974; Smith, 1972). However, Lees also noted that higher frequencies may appear in impact situations and the trajectories of the ankles and toes of high speed running.

Winter (1990) claimed that in repetitive movements, the frequencies present will be multiples (harmonics) of the fundamental frequency (stride frequency). He cited the example of walking at 120 steps per minute. In this case the stride frequency is 1 Hz and therefore the harmonics are at 2Hz, 3Hz, 4Hz and so on. The highest harmonics were found to be the trajectories of the toes and heels and it was found that 99.7% of the signal power was contained in the lower seven harmonics or 6 Hz. In high jumping the maximum approach speed is about 8 m/s at take-off. The average step length prior to take-off is about two metres. This would give rise to a stride frequency of the high jump approach at about 2 Hz. The intricate details of the movements of ankles and toes are not that vital in the study of the technique of rotation in high jumping. Hence, sampling at the rate of 50 Hz should be more than adequate for analysis of the high jump.

Resolution

Although many studies have reported that the accuracy of 16mm film technique is better than video (Shapiro, 1987; Kennedy et al., 1989; Angulo and Dapena, 1992), none has explained why this is so. Angulo and Dapena (1992), however, speculated that it could be due to the quality of image, lens distortion or the resolution of the digitising system.

The quality of image is in part dependent on the picture resolution which is determined by the image resolution of camera, video tape format, video cassette recorder (VCR), image capture board and monitor. Standard video is constrained by the television broadcasting system like the Phase Alternating Line (PAL) or National Television Systems Committee (NTSC). In the PAL system (used by most European countries), the number of horizontal scanning lines is fixed at 625 of which only 576 lines are visible on the screen. This implies that standard video equipment (using the PAL system) have a maximum of 576 horizontal visible lines. The resolution of the image capture board is however not constrained by this standard.

The number of vertical lines varies with different video equipment. For example, the sVHS tape format has 400 lines while the Sony PQ1444 monitor has 600 lines. In a television monitor screen, each intersection of the horizontal and vertical lines can be considered as a picture elements (pixel). It is the number of these pixels that define the picture resolution. That is, a picture with higher resolution will have more pixels (or lines). The picture resolution displayed on the screen to be digitised is equivalent to the component of the video system with the worst picture resolution. In most cases, the video tape has the worst picture resolution in the system. For the PAL system the images of the VHS and Hi-8 tapes, are defined by 240 x 288 and 400 x 288 lines per field respectively. The picture resolution of 16mm is about 40 lines per mm or 420 x 305 lines. In short the picture resolution of the 16mm film is better than any video system.

Although the resolution of film is better, the perceived sharpness of a video image is about equal, if not better than 16mm film (Inglis, 1993). It is difficult to compare the quality of video and film images because of their inherent differences in the processing of the images. It is impossible to duplicate precisely the appearance of film images with a video system or vice versa. The image quality is also dependent on many other factors such as its quality of colour, the brightness, contrast of the images and the magnitude of

the lens distortion. Hence it is inconclusive to consider the image quality of 16mm film to be better than that of videos. However, it is possible to conclude from the previous studies (Shapiro, 1987; Kennedy et al., 1989; Angulo and Dapena, 1992) that the reconstruction accuracy is inferior for the video systems. This may be due to the differences in the inherent celluloid and electronic processes of images of film and video. The question is whether, with improved picture resolution or image quality of the video system, the accuracy of the video digitising system would attain that of the film digitising system.

Lens Distortion

Angulo and Dapena (1992) suggested that lens distortion in video systems may be accountable for the lower accuracy data obtained. Poliner et al. (1994) also pointed out that one of the errors inherent in video system is lens distortion. He also showed that accuracy varies with images recorded with different video lenses. Antonsson and Mann (1989) mapped a video image plane using 12,000 points and found from the isoradial and isocircumferential error contour plot that the lenses of the video cameras are far from radial. However no study has shown that lens distortion in video images is accountable for the lower accuracy of the data obtained.

More importantly, if lens distortion in video can be corrected so that more accurate results can be obtained then video analysis would be a more valid replacement of 16mm film techniques in motion analysis. Hence the effect of lens distortion correction for video images must be investigated.

According to Marzan and Karara (1975), the basic theoretical concept used in photogrammetry is that the image being a perfect plane is a central projection of the object space. However, lens distortion, the result of imperfect lenses in cameras, deforms the image and therefore invalidates this assumption. There are mainly two types of lens distortion; symmetrical and asymmetrical distortion. Symmetrical distortion causes the displacement of an image relative to the optical axis of the camera. An outward displacement of image results in 'pin-cushion' distortion while an inward displacement results in the 'barrel' distortion (Challis, 1991). Asymmetrical distortion is caused by the imperfect centering of lenses and accounts for the selection of a point other than that of symmetry as reference (Allard et al., 1995).

There are different ways in which the effects of lens distortion have been alleviated. Marzan and Karara (1975) incorporated a lens distortion correction into their modified DLT formulation. They increased the number of parameters to 16, correcting both the symmetrical and asymmetrical lens distortion. They used three terms for the symmetrical correction and two terms for the asymmetrical correction. Challis (1991) evaluated the accuracy of a number of lens distortion models with the use of varying numbers of terms of symmetrical and asymmetrical lens distortion on static and dynamic data. He found little improvement in reconstruction accuracy for static data and no increase in accuracy for dynamic data. Miller et al. (1980) used the lens distortion model of Marzan and Karara (1975) and found no improvement in accuracy when compared with the data obtained from the standard 11 DLT parameter model. Wood and Marshall (1986) also found little reduction in accuracy of point reconstruction when they used the model with one term of symmetrical lens distortion correction. Hatze (1988) examined his modified DLT with the lens distortion model of Marzan and Karara (1975) and found that accuracy only improves when 30 or more control points were used.

From the results of these studies, it is not surprising that lens distortion correction was seldom incorporated in the reduction of data in motion analysis. However, the reason for the little or no improvement in reconstruction accuracy may be due to the fact that the image recorded had little or no lens distortion due to the good quality of 16 mm film camera lenses used. The quality of lenses of the video cameras may not be comparable to the 16 mm or 35 mm motion cameras and the magnitude of lens distortion in video have a more drastic effect on reconstruction accuracy.

Bennett (1996) copied a 16mm film recording of 30 markers placements on ten surveying poles (as described in Chapter 3) onto a VHS format using 'the flying scanner method'. She evaluated the accuracy of the location of the markers obtained from the digitised data of the copied VHS version with the measurement obtained from surveying technique. She found that the accuracy obtained from the copied version was comparable to digitised data obtained from the direct video recording (VHS format) of the 30 markers. She also applied lens distortion correction on the copied version and found that the accuracy improved in the same magnitude as the direct video recording version. This implied that the image distortion may not be caused by the lenses of the video camera but by the entire video digitising system.

Chen et al. (1994) reconstructed a rectangular frame from the digitised data of the video images using the standard 11 DLT. They found symmetrical distortions and the errors were also related to the distances between the digitised points and the calibration centre. They used a quadratic function to correct this distortion. With this modification they were able to improve their reconstruction accuracy by about 20 to 40 percent.

Hence, it may be useful to develop a procedure for lens distortion correction and explore the effect of lens distortion on the accuracy of video analysis.

Digitising Systems

Challis and Yeadon (1994) suggested that this lower accuracy is not the consequence of the poorer image but arises because the video digitiser coordinates are limited to the integral pixel values. In video digitising systems, the cursor is overlaid onto the image capture board. The cursor resolution is constrained by the pixels of the video image capture board and therefore the digitiser coordinates are limited to the number of pixels of the image capture board. This is what Angulo and Dapena (1992) referred to "pixel size limit resolution". However, Challis and Yeadon (1994), claimed that this constraint can be overcome by allowing the cursor to move across the captured images in fractions of a pixel (using anti-aliasing techniques) or by using a standard high resolution film digitiser tablet in conjunction with a video projector. This implies that with one of these modifications, video techniques could possibly yield data as accurate as film data. Hence, the effect of these modifications are certainly worth exploring.

Tsirakos and Bartlett (1995), compared the accuracy of data obtained from projecting 16 mm film and video onto TDS HR48 digitiser tablet. They found that the 16mm film was more accurate than the video projection. This implies that with same system measuring resolution, the quality of image accounts for the difference in accuracy.

Kerwin (1995) developed a better image quality and high measuring resolution video digitising system based upon 24 bit colour Millipede Apex image capture. This digitising system not only enables separate luminance and chrominance video components to be captured giving an improved colour separation and boundary delineation, it also allows sub-pixel measurement. It would be worthwhile to investigate

if such a digitising system could provide accuracy comparable to that of a 16mm film digitising system.

Camera Placements

Abdel-Aziz (1974) examined the accuracy of the object space reconstruction in a two camera condition. He showed that if the cameras were assumed to be positioned symmetrically, the accuracy is dependent on the distance between the cameras, the angle of optical axes of the cameras and the distance between the midpoint of the cameras to the intersection of the optical axes. He also found that if the distance between the midpoint of the cameras to the intersection of the optical axes is kept constant, an angle of 80 degrees convergence between the optical axes yielded the best accuracy.

Wood and Marshall (1986) examined DLT accuracy with different angles of convergence of the camera optical axes. They expressed the angle of convergence as the ratio of the distance between the midpoint of cameras to the point of convergence and the distance between the two cameras. Two ratios were examined: 1:1 and 1:2 ratios. Assuming that the optical axes of the cameras intersected at the object, the 1:2 ratio would be equivalent to an angle of convergence of 90° while the 1:1 ratio would be equivalent to an angle of 53° . They found that reconstruction accuracy of the 1:2 ratio (90° convergence) was significantly better than the 1:1 ratio (53° convergence) in the horizontal (x) and the depth (z) axes.

According to the unpublished work of both Putnam (1979) and Neal (1983) camera position and orientation are not a critical factor in achieving reconstruction accuracy. Chow (1994) analysed 1,134 camera combination views and found that there is no definite direct relationship between reconstruction accuracy and the camera angle of convergence. However, he found that the camera set-up relative to the orientation of the object space to be an important consideration in addition to the angle of convergence in attaining reconstruction accuracy.

The above literature seems to indicate that the position of cameras can affect reconstruction accuracy and ideally the cameras should converge at almost a right angle. However the camera set-up must also reflect the need for a clear view of the control points or the body landmarks to be digitised. Hence to attain reconstruction accuracy, the activity or the orientation of the activity must also be taken into consideration.

Segment inertia parameters

Quantitative biomechanical analyses of human movement require accurate values for inertia parameters of the body segments. There are different methods of determining these parameters. Some researchers have categorized the methods as experimental and theoretical methods (Nigg, 1994). Others have classified methods as cadaver studies, techniques with living subjects and mathematical models (e.g. Miller and Nelson, 1973). Yeadon (1984) reviewed the different methods as experimental, cadaver and linear regression analyses, and mathematical inertial models. Pearsall and Reid (1994), on the other hand, presented the methods according to three developmental periods namely; 1850 to 1950, 1951 to 1975 and 1976 to 1993. This section presents a selection of the different methods used to enlighten as well as to reflect the choice of the method selected for this study.

Borelli's balance technique to evaluate mass distribution properties of the human body was probably the first method to be introduced (Pearsall and Reid, 1994). This 17th Century method consists of balancing a person on a board with a fulcrum. The mass centre is assumed to be at the fulcrum point. This method has been adopted and extended by other researchers through the centuries, to investigate the mass distribution characteristic of the body. The reaction-board method described in Hay (1985) is probably a sophisticated extension of Borelli's balance technique. This reaction board method consists of placing a board on a fixed base at one end and a weighing scale at the other. After scale readings have been taken, a subject is placed on the board and the scale reading is taken again. If the weight of the subject is known, principle of moments can be employed to calculate the mass centre location. Hay also noted that this method could be further extended with the use of a larger board supported with two or more scales. This method uses the premise that the algebraic sum of the moments produced about the fulcrum is zero so it cannot alone estimate mass centre location unless one of the weight is known or vice versa.

Pearsall and Reid (1994) also claimed that Harless in 1860 was the first to use cadaver dissection to predict the segmental inertia parameters. They reported that Harless also used geometrical modelling of the human trunk and water displacement measures of the head. His methods were also refined by other investigators over the years. Dempster (1955), Clauser et al. (1969) and Chandler et al. (1975) extended Harless's cadaver

segmentation studies to give some valuable segmental inertia parameters. However, inertia values obtained from cadavers should be viewed with caution, since the age and the former health of the individuals in the cadaver samples makes extrapolation to live athlete population questionable (Yeadon and Challis, 1994). Geometrical models devised by Kulwicksi et al. (1962), Whitsett (1962), and Hanavan (1964) to calculate segmental inertia parameters can also be considered extensions of Harless's work. Dempster (1955), Drillis and Contini (1966) also made refinements of Harless's water displacement methods.

Some of the more recent methods of determining segmental inertia parameters are: quick release method, relaxed oscillation method, photogrammetric methods, gamma-scanner method, computerized axial tomography (CT) and magnetic resonance imaging (MRI) methods.

The quick release method requires the subject's limb to exert a constant force against a device which is then suddenly released (Nigg, 1994). The moment of inertia of the limb can then be calculated from the angular acceleration, the force exerted and the distance between the point of force application and the pivot point. The oscillation method demonstrated by Hatze (1975) calculates the segment inertia from the oscillation time of the limb. Although quick release and oscillation as well as other experimental methods can produce reasonably accurate and precise data, the experiments, however, can be rather tedious and time consuming. In addition none can provide estimates of inertia parameters of central segments such as the pelvis.

The photogrammetric method calculates segment inertial parameters by using data obtained from digitising photographs of subjects in a prone position. The segment average densities are taken from published references. Jensen (1978) found that the errors in the estimation of the body masses of three children were less than 2%. Although it takes about ten minutes per subject to have the reference points marked and photographed, the process of manual digitising requires about two hours (Pearsall and Reid, 1994).

The gamma scanner method calculates the density of the segment from the intensity reduction of a gamma ray that has been passed through the segment. The difference between the estimation of the total mass of the legs of a lamb from this method and from the value obtained from weight was less than 1% (Brooks and Jacobs, 1975).

CT can measure the density of the segment from the digitised data of the three-dimensional x-ray of the segment and calculate segment inertia parameter. Rodrigue and Gagnon (1984) found that the cadaver and the CT measures in segmental inertia parameters compared favourably. Ackland et al. (1988) found little variation in mass and density between the photogrammetry and CT measures of the legs of cadavers and living subjects. Both gamma scanner and CT have produced valuable segmental inertia data, but they have not been widely adopted because of the potential hazard of exposure to radiation. Accurate segmental inertia data can also be calculated from the MRI of cross-sectional images of the segment. The MRI method also do not pose any radioactive risk. Although MRI gives accurate results with no known risk, the limited number of MRI units and the high associated cost has currently reduced its practicality for biomechanics research.

With the limitations in the techniques reviewed, it is understandable that Reid and Jensen (1990) recommended the use of mathematical models such as Hatze's (1980) or Yeadon's (1990) that were based to a smaller extent on cadaver studies. In addition, in sport biomechanics research, the subjects are usually elite athletes to whom access is often restricted or limited to a short period of time. However the need for individual segmental parameters remains (Yeadon and Challis, 1994). Hence, the use of Yeadon's (1990) geometrical model method that needs relatively fewer anthropometric measurements would be preferred in determining the segmental inertia for this study.

Summary of the determination of inertia parameters

Segmental inertia parameters can be determined experimentally by a number of methods for living subjects. However the techniques involved are either time consuming, expensive or even hazardous to health. With most of the techniques, obtaining a full set of inertia parameters is a problem. Cadaver studies could provide a complete set of segmental inertia parameters and these values could be personalised to some extent by the use of regression equations or scaling techniques. The accuracy of such values applied outside the particular cadaver sample is dubious. On this account, Reid and Jensen (1990) recommended the use of mathematical models based to a smaller extent on cadaver studies for segmental inertia parameter determination. In sport biomechanics research, access to the subjects is often restricted or limited to a short period of time. Yeadon's

(1990) geometrical model needs relatively few anthropometric measurements and would be a preferred choice to determine segmental inertias.

Simulation models

A descriptive study can record what happens but is incapable of providing an explanation for the results. A well-controlled experimental study can provide an explanation for the results obtained but with human movement, complete control is not possible. Yeadon (1986) recommended a theoretical approach, such as using simulation models to overcome these problems. In addition a simulation model also could answer the “what if” questions. Pike (1980) used a five-segment model to show that it is possible to produce a full twist in a dive using asymmetrical arm movements. With the use of such a simulation model, it is certain that the results obtained are due to the interventions introduced and not others. Experimentation with real divers cannot produce such certainty because they may themselves make additional changes to those requested.

For a valid representation of human movement the model must have sufficient detail but as the complexity increases, the ease of use decreases (Yeadon, 1984). Alexander (1992) also raised the concern that some biomechanicists are inclined to devise complicated models because the human body is complex. This inclination disregards the observation by Hubbard (1993) that the most fundamental understanding often comes from the simplest models. Hatze (1981) developed a 17 segment model which required 46 muscle groups to be specified as input parameters. Since the input parameters cannot be obtained directly, he had to guess the values and then make adjustments until the simulated trajectory agreed with that of the film.

However a simple model may be too restrictive in its application, or omit important features which affect the accuracy of the model. For example, the simple two segment model developed by Alexander (1990) was sufficient to account for the relative low approach velocities required for optimum high jump take-off. However, this model may be too simple to be used in the analysis of competitive performance (Yeadon and Challis, 1994). Hence the complexity of the model must reflect the purpose or application of the model.

It is possible that in the process of developing a model, errors are made in the programming or mechanics formulations. Wilson (1977) correctly identified the errors in

mechanics formulations of Page's (1974) model of a diver. Therefore, accuracy of the model must be evaluated before the results obtained from the simulation can be accepted.

In order to evaluate a model, the output parameters must be compared with the values obtained from the actual performances in the situations in which the model is used (Panjabi, 1979). Van Gheluwe (1981) demonstrated how this can be done when he evaluated his six segment model using film data input. He found that the differences between the simulated twisting backward somersault and the film records were less than 5% for somersault angles and 10% for twist angles.

Dapena (1979) developed a 15 segment model to simulate the airborne motion in the Fosbury Flop. He noted that data from film may not be sufficient to determine rotations of the limbs about the longitudinal axes and so he assumed that their moments of inertia were zero instead of the angular velocities about the longitudinal axes. This procedure does ensure that the momenta arising from such rotation is zero, but it also introduces errors in the calculated momenta due to other rotations since the inertia values are not correct. Yeadon (1984) pointed out that when Dapena validated his model with a double somersault with 180° of twist rotation, an error of 140° was incurred.

Hence, to analyse the contribution of the curved approach in the Fosbury Flop, it would be necessary to adopt a theoretical approach by using a computer simulation model. The simulation model used must be simple enough to explain the contribution and yet complex enough to adequately represent the curved approach. The model must also be evaluated with the image recordings of the movement in order to ascertain accuracy of the representation.

Summary of the simulation model technique

Among the many advantages of a simulation model used as a research tool, the greatest is probably that it can answer the "what if" questions (Vaughan, 1984). However before the results obtained from such models are accepted, the complexity of the models must reflect the activities modelled. The model must also be validated using actual performances.

Chapter 3

IMAGE ANALYSIS PROCEDURES

INTRODUCTION

In order to address the questions raised in Chapter 1 regarding the contribution of the curved approach in high jumping, information is needed on the last five steps of the approach, the take-off, and the flight over the bar. The distance covered by the athlete during these phases is in excess of 15 m and this poses a problem for the collection of image data. Under these circumstances, to obtain a sufficiently large image for digitisation, panning cameras may be used but this procedure requires that markers be placed throughout the panning field of view (Yeadon, 1989). This requirement can pose a considerable difficulty in the competitive environment and so an alternative solution was sought using fixed cameras. However, to cover such a large movement space with fixed cameras the image size of the athlete will be small. The image measurement system is likely, therefore, to be close to its limit of accurate operation and so it will be important to use a system with high accuracy.

SELECTION OF IMAGE MEASUREMENT SYSTEM

Kerwin and Templeton (1991) noted that the performance of a digitising system is dependent on the combination of the specific equipment used. This implies that the quality of the data obtained will be different if, for example, a different video or film format was used for recording or a different digitising tablet was used for digitising. In order to determine which system or combination of equipment is more suitable for analysing high jumping, a variety of recording and digitising systems need to be evaluated. The evaluation of these systems would not only assist in selection of an appropriate system but would also ascertain the quality of data collected.

A measuring system can be evaluated on the basis of its resolution, precision and accuracy. The resolution of a measurement system is the least discernible change that the system can measure (Yeadon and Challis, 1994). Precision is the repeatability of the measured values, that is the consistency of the data when measured more than once under the same condition. Accuracy is the comparison between the measured values and the true values. Precision and accuracy are dependent on the measurement

resolution. Good precision might be obtained with low measuring resolution but this would give low accuracy. With poor precision, however, accuracy will also suffer.

Video offers an attractive alternative to 16 mm film digitising systems with advantages such as ease of use, immediate availability of recording and its relatively low cost. However studies have shown that data obtained from video have been of lower accuracy than that from film systems (Shapiro et al., 1987; Kennedy et al., 1989; Angulo and Dapena, 1992). No study has yet shown why video system should produce data of lower accuracy than that of a 16 mm film system. Angulo and Dapena (1992), however, speculated that this could be due to lens distortion, image quality and resolution of the video system. The effects of these limitations in video have so far received little attention.

Although there have been studies on the lens distortion in a 16 mm film system, (e.g. Challis, 1991) little has been published on the magnitude and the effect of lens distortion correction on the accuracy of the digitised data for video systems.

Image quality is often associated with accurate and precise measurement in image analysis. It is often thought that the quality of video images is inferior to that of film images and this might account for the lower accuracy of video systems. However, due to the inherent differences in their respective celluloid and electronic image processes, comparing the image quality of video and film is problematic. With the recent development of video technology, improved picture resolution video formats such as Hi-8, sVHS and even digital tapes are now available. The effect of digitising using these improved picture resolution video formats has also received little attention.

With the development of the Apex Target video digitising system capable of sub-pixel measurement (Kerwin, 1995), the effect of increasing the digitising resolution on the precision and accuracy of measurement of video systems can be examined. The Apex Target also provides optional features such as image magnification (up to about four times the normal size), video line interpolation (for a more refined picture) and a variety of different digitising cursors. It would be useful to know the effect of using the different digitising features on the accuracy and precision of the data. Most of all, it would be beneficial to examine if this newly developed Apex Target video digitising system can provide data of quality comparable to that of a 16 mm film system.

The main objective of this section is to describe the methodology used to evaluate the various recording and digitising systems in order to determine which system would be most appropriate for image analysis of high jumping. In the process of this evaluation, the effect of lens distortion, image quality and measuring resolution on accuracy and precision of image measurements are investigated. The effect of using the different optional features of the newly developed Apex Target video digitising system are also explored in this section. Hence, when the most appropriate image analysis system is determined, a procedure for data collection on high jumping will then be developed.

Systems evaluated

The recording systems that will be evaluated in this study are the VHS, the Hi-8 video systems and the 16 mm cine film system. The digitising systems that will be evaluated will be the Millipede Prisma III, Apex Target video digitising systems, and the HR48 TDS film digitising system. In order to evaluate the video recording systems, measurements obtained from the VHS and the Hi-8 recording formats digitised using the Prisma system are compared. The measurements obtained from the Hi-8 recording format digitised using the Prisma and Apex systems are compared in the evaluation of the two video digitising systems. The combination of video recording and digitising system that produced the most precise and accurate data are then compared with the data obtained from the 16 mm film HR48 TDS system. A summary of the systems to be evaluated are shown in Table 3.1.

Table 3.1. Image analysis systems to be evaluated

Systems	Recording formats	Digitising systems
1.	VHS	Prisma Millipede III
2.	Hi-8	Prisma Millipede III
3.	VHS	Apex Target
4.	Hi-8	Apex Target
5.	16 mm	HR48 TDS

Procedure for evaluation of digitising systems

Data Collection

A static and movement image settings were filmed and video recorded. The static setting consisted of ten poles located relative to the cameras as shown in Figure 3.1. Each pole had three markers affixed at vertical intervals of one metre. The poles were in an upright position and were one metre apart as shown in Figure 3.2. The positions of markers on the poles was also determined by surveying technique to provide the true criterion coordinates for in the accuracy test. After the static setting had been recorded and surveyed, the movement setting was then arranged. The movement setting consisted of a human subject running at the speed of 8 ms^{-1} through the previous location of the row of ten poles. The cameras were not moved throughout the recordings in the two settings. The video cameras used for the recordings were 50 Hz Panasonic MS2 and Sony HAD. The Panasonic and the Sony cameras recordings were in the VHS and Hi-8 tape formats respectively. The 16 mm film recordings were obtained with the Locam camera set at 50 Hz.

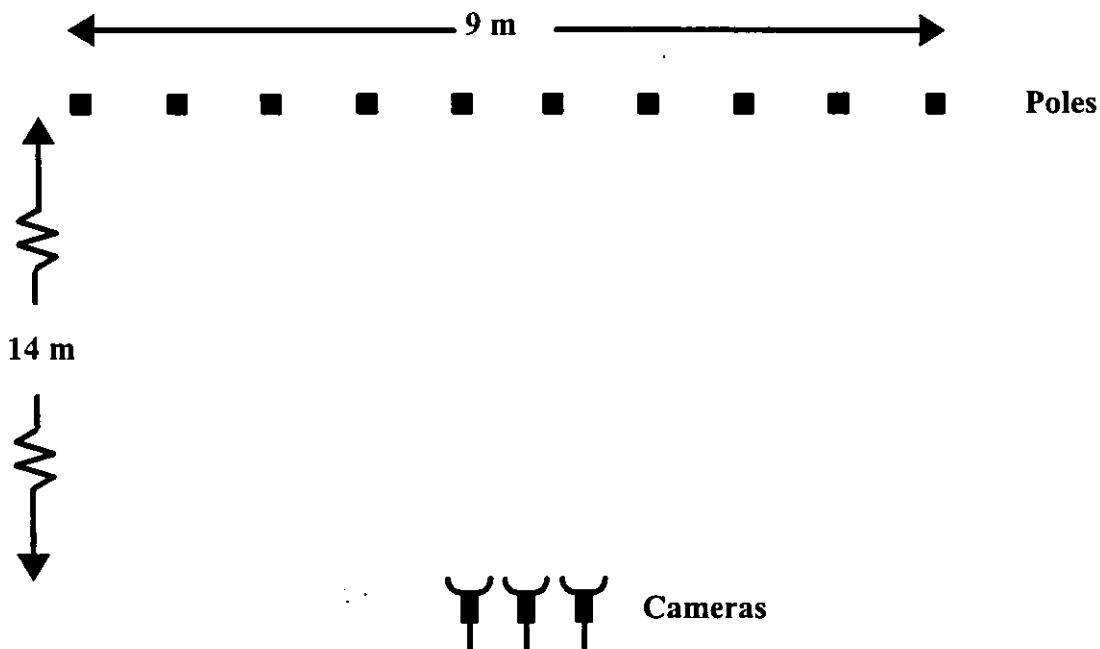


Figure 3.1. Locations of markers and cameras (plan view).

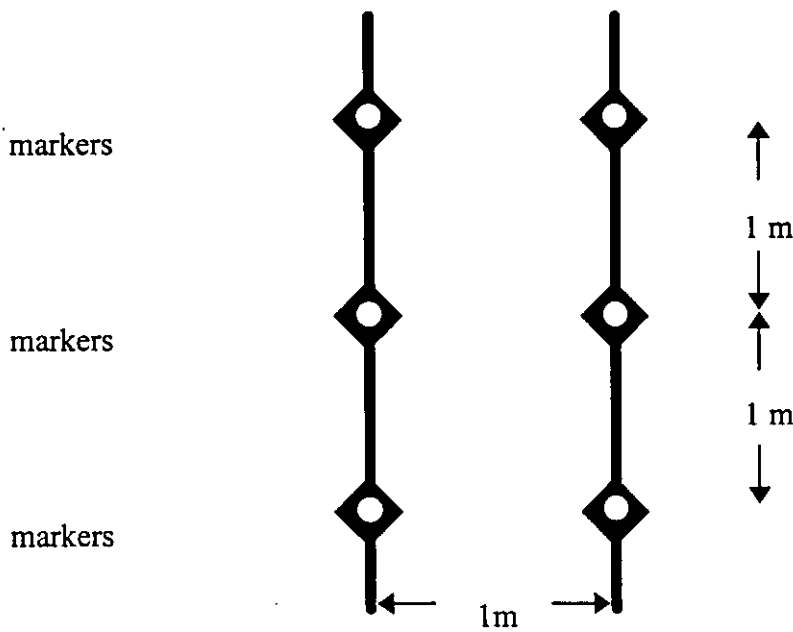


Figure 3.2. Markers on poles.

Data Processing

The video recordings from both the Panasonic and Sony cameras were copied into sVHS format and digitised using the Apex Target as well as the Millipede Prisma III system. The Millipede Prisma system (Kerwin, 1993) is based upon an 8-bit colour Millipede Prisma III image capture board. Unlike the Apex Target system, with its sub-pixel cursor movement, the Prisma system allows cursor movement only in pixel increments. With the image magnified twice the normal size, the Prisma digitising system has a measuring resolution of 1536 by 1150 whereas the Apex Target system resolution is 6144 by 4608. The video recordings were digitised with image magnification twice the normal size. This is equivalent to the size of the projected 16 mm film image (595 x 390 mm) used for digitising. The 16 mm film was digitised by projecting it onto a HR48 TDS digitising tablet using a NAC analysis projector (DF16C). For the static setting a total of 10 fields were digitised on each system. For the movement setting, a total of ten sets of the first step (comprising 13 fields) were digitised on each system.

Data Analysis

Precision measurement

From the digitised data of each system, the mean coordinates (\bar{x}_i, \bar{z}_i) of each marker or landmark digitised (x_i, z_i) , were computed. The deviations from these mean coordinates was used as the measurement of precision for the digitised data. The root mean square deviations of each marker or landmark digitised $(\text{rms}_p dx_i, \text{rms}_p dz_i)$ were calculated using the following formulae:

$$\text{rms}_p dx_i = \frac{\left[\sum_{j=1}^m (x_{ij} - \bar{x}_i)^2 \right]^{1/2}}{(m-1)}, \quad \text{rms}_p dz_i = \frac{\left[\sum_{j=1}^m (z_{ij} - \bar{z}_i)^2 \right]^{1/2}}{(m-1)}$$

where m was the number of sets digitised.

The root mean square deviations $(\text{rms}_p dx, \text{rms}_p dz)$ of all the digitised coordinates of each system were calculated using the following formulae:

$$\text{rms}_p dx = [1/(n) \sum_{i=1}^n (\text{rms}_p dx_i)^2]^{1/2}, \quad \text{rms}_p dz = [1/(n) \sum_{i=1}^n (\text{rms}_p dz_i)^2]^{1/2},$$

where n was the number of markers or landmarks digitised in each set.

The deviations were converted from digitising units to millimetres by using a conversion scale established from the mean coordinates of the digitised marker data and the measurements from the setting.

Since the deviations were obtained from each of the digitised coordinates and their mean coordinates, the x and z deviations are expected to be normally distributed about the mean, zero. Hence to assess whether the precisions of the digitised data obtained from two systems were significantly different, the homogeneity test of the variance of the x and z deviations was used.

Accuracy Measurement

The spatial coordinates of the markers obtained from the surveying technique measurements were used as criterion reference values to evaluate accuracy measurements of the digitising systems. For each system, the mean digitised data set was reconstructed to spatial coordinates using the Direct Linear Transformation (DLT) technique (Abdel-Aziz and Karara, 1971). The root mean square deviations $(\text{rms}_s dx,$

rms_a dz) between the reconstructed coordinates and the criterion reference coordinates were calculated. The following formulae were used:

$$\text{rms}_a dx = \frac{\left[\sum_{i=1}^n (\bar{x}d_i - xr_i)^2 \right]^{1/2}}{(n - c)}, \quad \text{rms}_a dz = \frac{\left[\sum_{i=1}^n (\bar{z}d_i - zr_i)^2 \right]^{1/2}}{(n - c)}$$

where n was the number of markers in a set; c is the constraint of the degrees of freedom; $\bar{x}d_i$, $\bar{z}d_i$ were the reconstructed coordinates and xr_i , zr_i were the criterion reference coordinates of the i^{th} markers.

For a two-dimensional DLT reconstruction, eight unknown parameters are needed to be obtained from at least eight transformation equations. The transformation equations require the use of digitised coordinates and the spatial coordinates of four markers. Thus the number of degrees freedom is reduced by four and $c = 4$.

However when one term of symmetrical lens correction was applied in the reconstruction of the digitised data, an additional unknown parameter is required. This further reduced the number of degrees of freedom and therefore c became 4.5.

The deviations obtained from the reconstructed coordinates and the reference criterion coordinates of each system, may be expected to normally distributed about a mean that is quite close to zero. Therefore to examine the differences between the accuracy of the digitised data from two different systems, the homogeneity of the variances of the x and z deviations were tested.

Accuracy was not evaluated for the movement setting (a human subject running at a speed of about 8 ms⁻¹) because of the absence of a true criterion reference.

Optimisation of the Apex Target video digitising system.

The evaluation of the video recording and digitising systems (presented in Chapter 5) revealed that the use of Hi-8 video recording format digitised using the Apex Target digitising system produced data with the best accuracy and precision. The Apex Target system also provides a variety of optional digitising features such as image magnification (up to about four times the normal size), video line interpolation (for a more refined picture) and a variety of different digitising cursors (Kerwin, 1995). In order to examine the effect of using the optional digitising features, four fields of the video recordings from the Sony camera were digitised using the Apex Target system










default features. The default digitising features consist of using a size 10,  cursor type, and no line or 'coarse' interpolation. An image magnification of twice the normal size (2x) was also selected. This default system was used as the initial configuration. The precision and accuracy measurements were assessed as each selected optional feature was introduced as an intervention. The different configurations used in the investigation of the effect of the different digitising options are shown in Table 3.2 .

Table 3.2. Digitising configurations for optimisation of Apex Target system

Configurations	Line interpolation	Cursor Type	Cursor Size	Zoom
Initial	coarse		10	2x
Smooth interpolation	smooth		10	2x
Cursor Type 1	smooth		10	2x
Cursor Type 2	smooth		10	2x
Cursor Size 1	smooth		4	2x
Cursor Size 2	smooth		16	2x
Zoom 1x	smooth		16	1x
Zoom 4x	smooth		16	4x

Lens Distortion

The errors in accuracy measurement of markers using the VHS recordings digitised on Prisma system are presented in Table 3.3. The effect of excluding the six markers of the extreme left and right poles did not reduce the z (vertical) errors but significantly reduced x (horizontal) errors ($p < 0.05$). This suggests that there is considerable amount of lens distortion in this video system. The exclusion of the markers on the extreme poles, however, did not reduce significantly ($p < 0.05$) the x and y errors for the film system. This implies that there is little or almost no lens distortion in the film system.

Table 3.3. Errors of measurement of a video system

VHS camera format, digitising on Prisma System	x [mm]	z [mm]
10 poles (30 markers)	15.1	7.4
8 poles (24 markers)	10.0	6.4
<hr/>		
16 mm film, digitising on HR48 TDS System	x [mm]	z [mm]
10 poles (30 markers)	2.8	2.4
8 poles (24 markers)	2.6	2.1

According to Marzan and Karara (1975), the basic theoretical concept used in photogrammetry is that the image, being a perfect plane, is a central projection of the object space. However, lens distortion is the result of imperfect lenses which deform the image and therefore invalidates this assumption. There are mainly two types of lens distortion: symmetrical and asymmetrical distortion. Symmetrical distortion causes the displacement of image points radially to or from the centre of the image field. An outward displacement is referred to as a 'pincushion' distortion while an inward displacement is known as a 'barrel' distortion. Asymmetrical distortion is caused by the imperfect 'centering' of lenses which causes the displacement of image points tangentially (normal to the radial lines) as well as radially (Challis, 1991).

There are different ways in which lens distortion has been alleviated. Marzan and Karara (1975) incorporated lens distortion correction into their modified DLT formulation. They increased the number of parameters to 16, correcting both symmetrical and asymmetrical lens distortion. They used three terms for the symmetrical correction and two terms for the asymmetrical correction. Challis (1991) evaluated the effects of a number of lens distortion correction models. He found little or no improvement in accuracy when he applied a varying number of symmetrical as well as asymmetrical lens distortion correction terms to his 16 mm film recordings. Wood and Marshall (1986) also found little or no reduction in accuracy of point reconstruction when they used the model with one term of symmetrical lens distortion correction.

As above studies show little or no increase in reconstruction accuracy with lens distortion correction, it is no surprise that it was seldom incorporated in the reduction

of data in motion analysis. However, the reason for the small improvement in reconstruction accuracy may be due to the fact that there was little lens distortion due to the good quality of camera lenses used. The quality of lenses of video system may not be comparable to those of film system so that the magnitude of lens distortion may be much higher and this may explain why video produces lower measurement accuracy. If indeed the problem of lower accuracy arises from lens distortion, then with lens distortion correction video systems should be able to produce measurement accuracy comparable to that of 16 mm film. In order to investigate this possibility, a procedure of lens distortion correction needs to be developed.

Procedure for correction of lens distortion

The most common method of reconstructing three-dimensional coordinates of body landmarks from digitised information obtained from two or more camera views is the DLT method developed by Abdel-Aziz and Karara (1971). The method produces a direct linear relation between the digitised coordinates and the spatial coordinates of that point under the condition that the point in space, the centre of the lens and the image point are collinear. This linear transformation can be defined by 11 parameters which are functions of camera location and orientation and characteristics of digitising system.

With the known locations of at least six digitised control points, 12 equations or more can be derived to solve this set of 11 parameters for each camera. For each control point and its digitised coordinates (U, V) two DLT equations can be written as:

$$U = (L_1X + L_2Y + L_3Z + L_4) / (L_9X + L_{10}Y + L_{11}Z + 1)$$

$$V = (L_5X + L_6Y + L_7Z + L_8) / (L_9X + L_{10}Y + L_{11}Z + 1)$$

where X, Y, Z, are the spatial coordinates of the control point and $L_1 \dots L_{11}$ are the 11 transformation parameters of the camera.

These basic DLT equations do not involve any image refinement parameters (Karara, 1980). Karara and Abdel-Aziz (1974) suggested that only one term of symmetrical distortion correction needs to be taken for modelling lens distortion for all practical purposes. They found no significant improvement when additional terms of symmetrical or asymmetrical correction were incorporated. In this study, one term of

symmetrical distortion correction will be applied to examine the effect of the lens distortion in video images.

If U and V are the undistorted digitised coordinates and u, v are the distorted digitised coordinates then $U = u + \Delta u$ and $V = v + \Delta v$ where Δu and Δv are the corrections for the symmetrical distortions. Karara (1980) suggested that corrections Δu and Δv for the symmetrical distortion can also be expressed as:

$$\Delta u = (u - u_0)r^2L_{12}, \text{ and } \Delta v = (v - v_0)r^2L_{12}$$

where L_{12} is the lens distortion parameter, r is the distance between the digitised point and the principal point (u_0, v_0) which should be close to the centre of the video image. If the digitiser origin is at the centre of the video frame we may assume $u_0 = v_0 = 0$. Therefore the undistorted digitised coordinates U, V can be written as:

$$U = u + u r^2 L_{12}, \quad V = v + v r^2 L_{12}.$$

Hence, DLT equations can be expanded into :

$$L_1X + L_2Y + L_3Z + L_4 - UL_9X - UL_{10}Y - UL_{11}Z - ur^2L_{12} = u$$

$$L_5X + L_6Y + L_7Z + L_8 - VL_9X - VL_{10}Y - VL_{11}Z - vr^2L_{12} = v.$$

By substituting u for U and v for V , initial estimates of L_1 to L_{12} were obtained by using a least squares technique. This process was repeated with U and V continuously updated using the previously obtained L_{12} . The iterations continued until the estimates of L_1 to L_{12} varied little from the estimates of the previous iteration. (It was found that the estimates of L_1 to L_{12} stabilised within five iterations.)

For two-dimensional DLT reconstruction, the procedure can be modified to obtain the transformation parameters. For example, if (X, Z) are the spatial coordinates of the digitised point (U, V) , Y is assumed to be 0 in the DLT equations. Therefore the DLT equations can be written as:

$$U = (L_1X + L_3Z + L_4) / (L_9X + L_{11}Z + 1)$$

$$V = (L_5X + L_7Z + L_8) / (L_9X + L_{11}Z + 1).$$

Incorporating the lens distortion correction, the DLT equations can be expanded as:

$$L_1X + L_3Z + L_4 - UL_9X - UL_{11}Z - ur^2L_{12} = u$$

$$L_5X + L_7Z + L_8 - VL_9X - VL_{11}Z - vr^2L_{12} = v$$

Therefore, instead of solving for 12 parameters (L_1 to L_{12}), only nine parameters ($L_1, L_3, L_4, L_5, L_7, L_9, L_{11}, L_{12}$) need to be obtained from the least squares technique. This process is also repeated (with the U and V modified from the previous calculation) until the parameters stabilise.

Hence, the known locations of at least five digitised control points are required to derive 10 equations to solve this set of 9 transformation parameters. The digitised data also need to be transformed such that the coordinate origin coincides with the centre of the video frame. The transformed data then can be reconstructed into spatial data using the calculated DLT parameters.

The accuracy of this DLT with lens distortion correction procedure for the reconstruction of 2D and 3D spatial data was assessed using the data obtained from the surveying measurements. This accuracy was also compared with the accuracy of the data reconstructed using the basic DLT procedure.

Image recording of Fosbury Flop

The results in Chapter 5 also showed that the use of the different digitising options in the Apex Target system have only a slight effect of the measurement of the system. However it was found that the combination of 'smooth' line interpolation, 2x image zoom and 'the circle with a dot' size 16 cursor produced data with the best accuracy and precision. The image settings used in the evaluation of the digitising system were conceived from the requirements of high jump recordings. Therefore, from the results of the evaluation of the digitising systems, it was decided that high jumps should be recorded on the video recording format of Hi8 or sVHS. (sVHS has picture resolution equivalent to that of the Hi-8.) The high jumping recordings should also be digitised on the Apex Target video system using the digitising features that provided the best precision and accuracy.

Data collection procedure

It was decided that the high jumps should be recorded from competition. Although the location of cameras is somewhat restricted in competition, the jumps are considered to be a better representation of the techniques involved than those used in training sessions. Prior to the competition, permission for recording and for the placement of cameras was also obtained from the competition director.

Two Panasonic MS2 video cameras were used to record all the jumps attempted by two elite male high jumpers in two competitions. The cameras were not genlocked. The physical and performance characteristics are presented in Table 3.4. The jumps were recorded in the sVHS video format. The athletes were consulted prior to the competition so that the locations of their foot placements of their approach run of the jumps were obtained. These locations were used to assist in the positioning of cameras and the calibration poles.

Table 3.4. Physical and performance characteristics of the jumpers

Subjects	Height	Weight	Personal Record	Direction of approach
B. Reilly (B)	1.96 m	79 kg	2.26 m	left to right
S. Smith (S)	1.86 m	73 kg	2.37 m	right to left

Camera set-up

The cameras were positioned beyond the perimeter of the track, approximately 45 metres from the centre of the bar and with optical axes of the cameras intersecting at approximately 45 degrees as shown in Figures 3.3 and 3.4. The field of view of each camera was set to include the last five steps of the approach run and the entire flight phase. The recordings of the jumps were carried out at 50 fields per second with a shutter speed of 1/250.

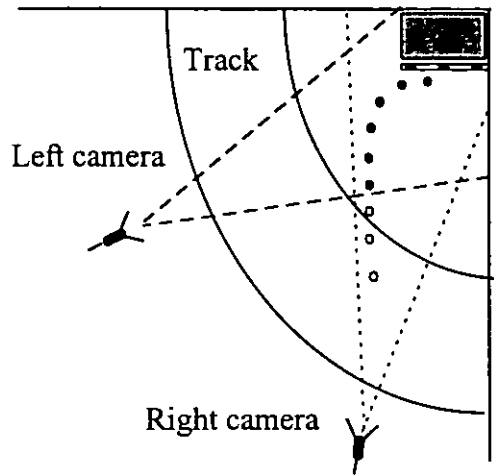


Figure 3.3. Camera positions relative to the high jump area (for B. Reilly).

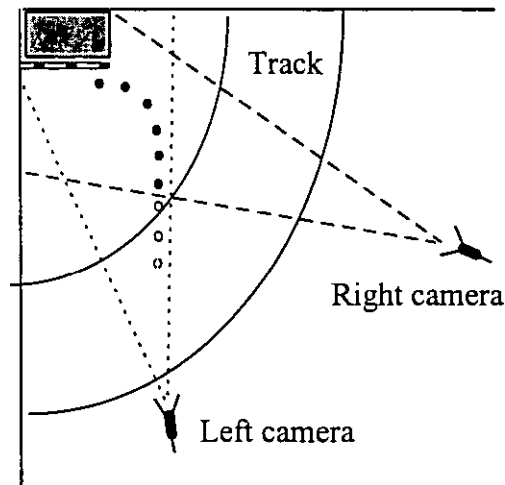


Figure 3.4. Camera positions relative to the high jump area (for S. Smith).

Calibration

For calibration purposes, calibration poles were placed in the approach run area at precisely measured locations as shown in Figure 3.5 and 3.6. Two markers were also placed on each of the high jump uprights and poles. The exact placements of markers and the set-up of the poles were carried out with great care. The quality of the three-dimensional coordinates reproduced by the modified DLT technique (described in the earlier section on *Procedure for correction of lens distortion*) depended on the accuracy of the placements of the markers. The calibration set-up was video recorded by the two cameras prior to the competition.

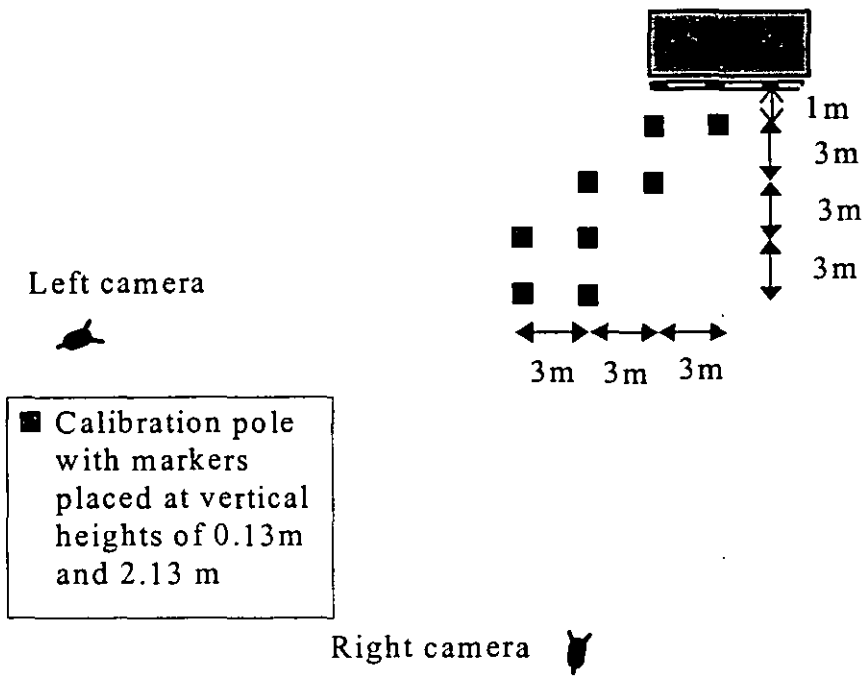


Figure 3.5. Positions of calibration poles in the high jump area (for B. Reilly).

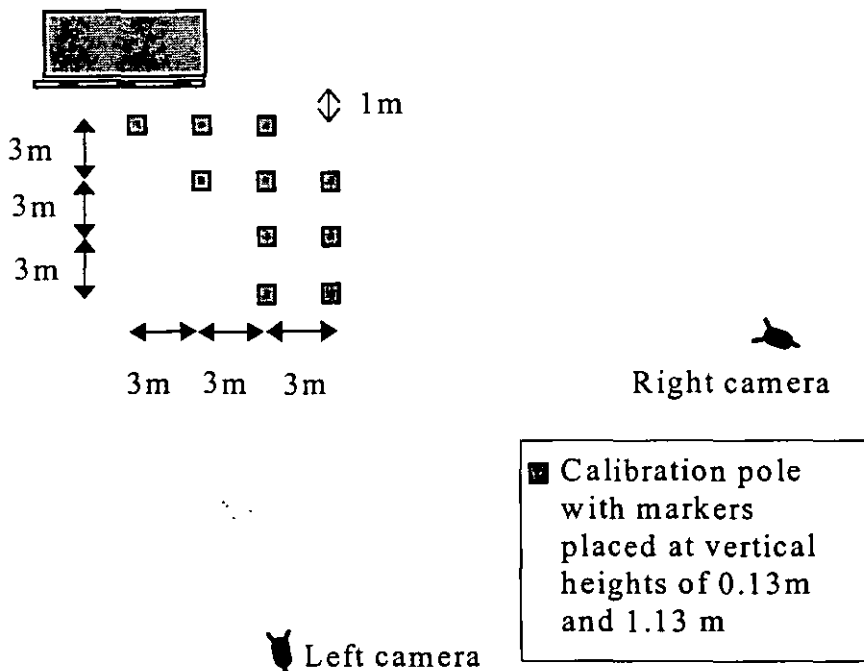


Figure 3.6. Position of calibration poles in the high jump area (for S. Smith).

Digitising Procedure

The video recordings of both cameras were played back using a high quality video recorder (Panasonic AG-7350) and displayed on the video monitor (Sony Trinitron PQV 1444) to ensure that the image sequence of the jumps were of sufficient quality for analysis. The video images were then digitally time-coded so that an automated image capture process (Target) could be used for the digitising process. The digital time coded signal was passed through a time-code translator (IMP Electronics) to enable the necessary fields to be detected for display on the video monitor. The timings (from the time-coding) and the field numbers of the touch-down and take-off of the six foot placements prior to the flight phase were noted for each camera recording. These timings and field numbers were used for synchronising the sequences of the jumps from the two camera recordings.

The equipment for digitising (i.e. the video recorder, image capture board and monitor) were linked to a personal computer (Archimedes model 410/1). The mouse facility was used to control the digitising cursor.

Reference Files

For each field, markers on the calibration poles and on the uprights (as shown in Figures 3.7 and 3.8) were digitised as the reference frame. This was needed for camera calibration in order to reconstruct spatial coordinates from the digitised coordinates. This digitising process was repeated for five consecutive fields for both camera recordings. The repeated digitisation was to ensure that more precise digitised data were used for calculating the camera calibration parameters.

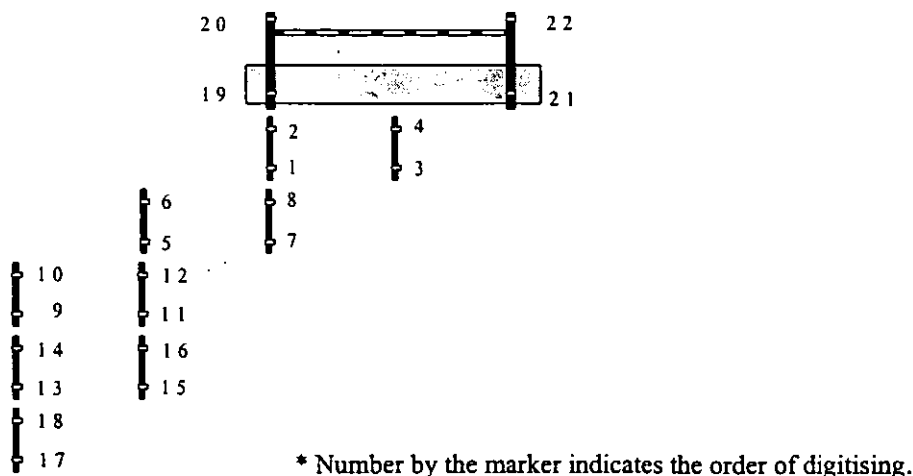
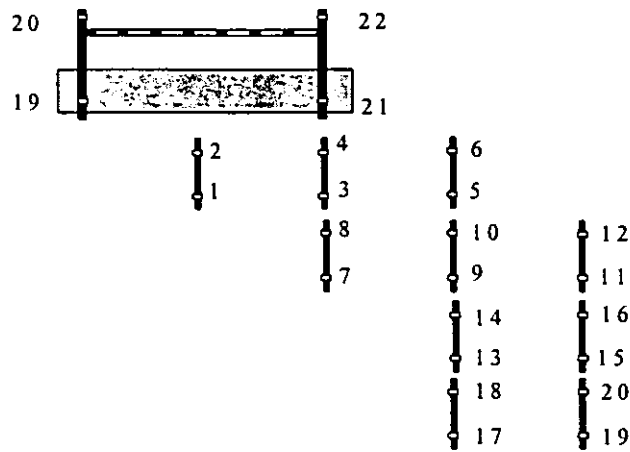


Figure 3.7. The digitising protocol for references frames (for B. Reilly).



*Number by the marker indicates the order of digitising.

Figure 3.8. Digitising protocol for references frames (for S. Smith).

Movement files

a) Reference fields

Two consecutive reference fields were digitised to check for camera movements that may have occurred between jumps. In each of the reference fields, four markers on the uprights and the end points of the high jump bar were digitised. This procedure was done for both the camera recordings. If the camera had moved, the 'displaced' coordinates of the markers and the end points of the bar could be used to correct the movement data.

b) Movement fields

Fifteen body landmarks were digitised in the movement fields. The fifteen body landmarks were wrists, elbows, shoulders, hips, knees, ankles, toes of the left and right sides and the centre of the head. The digitising procedure for both camera recordings began with five fields prior to the foot contact of the last five steps of the approach and ended when the athlete landed on the mats. In short, the curved approach, take-off phase and the flight phase were digitised.

Anthropometric Measurement

Anthropometric measurements were taken directly from the athletes in order to facilitate the calculation of the segment and body inertial properties and mass centre locations. Details of the calculations were presented by Yeadon (1990). With one of the subjects (B. Reilly) a complete set of the 95 anthropometric measurements was

taken. For the other subject (S. Smith), a smaller set of measurements was taken and expanded using regression equations for the necessary analyses (Yeadon et al., 1994). Measurements are presented in the Appendix D.

Data processing procedures

Synchronisation

Since both cameras were triggered manually, the digitised data needed to be synchronised. Since the digitisation of both camera views began at a fixed number of frames before the required movement and both cameras were operating at 50 Hz, the respective digitised frames of each camera view may differ by less than 0.02 s. To correct for this difference, the frame number of 13 identifiable instants such as touchdown and take-off of the approach run and the instant of landing on the foam mat were noted from each camera view. If there were no differences in the frame numbers for the two digitised views on the 13 identifiable instants then the two sets of data were taken to be synchronised. However, if there were differences in the frame numbers, the proportion of the number of discrepant frames was used to determine the difference in the synchronisation of the two camera views.

Image Analysis Program

The digitised and the anthropometric data were fed as input into FILM software program developed by Yeadon (1984) to obtain the necessary kinematic data. The FILM program was modified to obtain the distance between the mass centre and the mid-foot position, the tilt and lean angle of the body.

Splining of data

Prior to splining, the data were transformed into coordinates in metres of the projections of the landmarks on a vertical plane which is normal to the optical axis of the camera and which passes through the origin of the reference frame as described in Yeadon (1984). In the FILM program the displacement data were fitted with quintic splines (as described in Wood and Jennings, 1979). In order to fit quintic splines to the displacement data, it is necessary to have estimates of the errors in the data values. Since the data were only digitised once, estimates of the errors were obtained by

generating an estimated set of data using the mean value of the coordinates from one field before and one field after such as:

$$x'_i = \frac{[x_{(i-1)} + x_{(i+1)}]}{2}$$

where x'_i is the x coordinate of the estimated set at field i. The first and last values of the estimated set is taken to be the same as the digitised values. With the estimated data set generated, the local (V_L) and global (V_G) variance estimates can be calculated as:

$$V_L = \frac{2}{3} (x_i - x'_i)^2$$

and

$$V_G = V_L/n$$

where the $i = 1, n$ and n is the number of fields.

Assuming that each x_1, x_2, x_3 of a landmark in field 1, 2 and 3 of the digitised data set has equal variance σ^2 , and the method in which the estimated data sets were obtained where x'_2 the x coordinate of the same landmark in field 2 of the estimated set is: $\frac{x_1 + x_3}{2}$, the variance $\text{var}(x'_2)$ of x'_2 can be expressed as:

$$\text{var}(x'_2) = \frac{\text{var}(x_1) + \text{var}(x_3)}{4} = \frac{\sigma^2 + \sigma^2}{4} = \frac{\sigma^2}{2}$$

Then the variance in the difference d between between the digitised and the estimated set, $\text{var}(d)$ can be written as:

$$\begin{aligned} \text{var}(d) &= \text{var}(x(i) - x'(i)) \\ &= \text{var}(x(i)) + \text{var}(x'(i)) \\ &= \sigma^2 + \frac{\sigma^2}{2} = \frac{3\sigma^2}{2} \end{aligned}$$

and hence

$$\sigma^2 = \left(\frac{2 \text{var}(d)}{3} \right)^2$$

Hence the constant $2/3$ in the calculation of the local variance V_L is required to account for the reduction in the variance between the digitised and the estimated set as

compared with two independent data sets. The calculation of the local and the global error variance enable the calculation of the standard error estimates.

The standard error estimates ∂_x for the digitised movement data was calculated as 75% local error and 25% global error such that:

$$\partial_x = (kV_L + (1-k)V_G)^{1/2} \text{ where } k = 0.75.$$

The k value of 0.75 was chosen as it was expected that there were large errors in the data to be smoothed and the 25% global error was used to prevent the error estimate at any points from being too small. For the subsequent splining of the data of the orientation angles, the k values were chosen to be 0.50. Since the displacement data that was used to calculate the orientation angles has been smoothed considerably, the k value chosen at 0.5 for the orientation angle is a compromise solution to prevent the error estimates from being smaller than 70% of the global error. The smoothing parameter S that controls the extent of smoothing of the spline was set at $1.0n$ (where n is the number of fields) for the displacement and orientation angle data (Wood and Jennings, 1979).

Mass centre locations

The location of the mass centre was calculated in a subroutine of the FILM program using the measured anthropometric data and the digitised data. The subroutine of the program used the mass and location of the mass centre of each segment relative to its length from the anthropometric data and locations of the joint centres provided by the digitised data to calculate the mass centre location of the whole body in each field by using the segmentation method (described in Hay, 1985).

Lean angle

The lean angle of the body is defined as the backward lean of the body in the plane of the approach. In order to calculate this lean angle ϕ , the straight line joining the mid-foot F and the mass centre G was projected onto a vertical plane parallel to the horizontal velocity vector v_h of the mass centre (as shown in Figure 3.9). The lean angle ϕ was calculated as the angle between the projected FG (FG') and the vertical (FE).

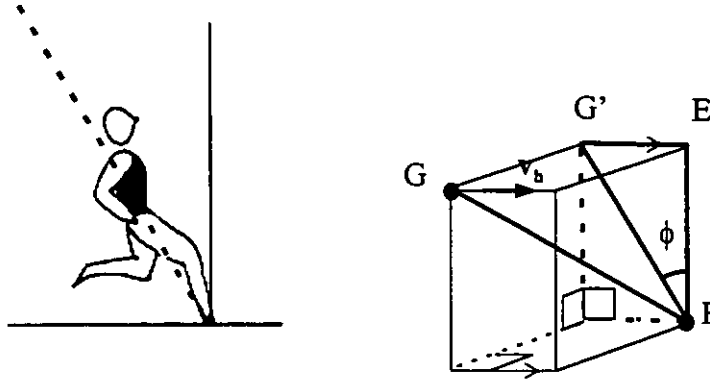


Figure 3.9. The lean angle ϕ .

Tilt angle

The tilt angle of the body was defined as the tilt towards the centre of the curved approach. In order to calculate this tilt angle θ , the straight line joining the mid-foot F (the mid-point between the ankle and the toe) and the mass centre G is projected through G onto a vertical plane normal to the horizontal velocity vector v_h of the mass centre (as shown in Figure 3.10). The tilt angle θ was calculated as the angle between the projected FG (ZG) and the vertical axis DZ. The tilt angles were obtained by projection on to the vertical plane normal to the horizontal velocity because they were needed for the simulation model and the simulation model assumes that the mass centre is always 'alongside' the foot. In short, the model only allows for tilting and not leaning.

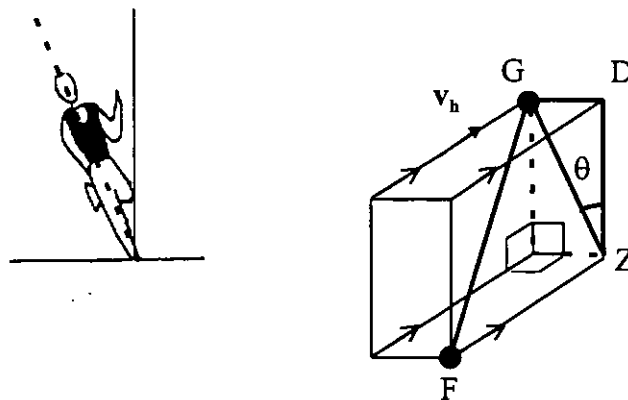


Figure 3.10. The tilt angle θ .

Foot contact

In order to describe the curve traversed by the foot, the coordinates of the mid-foot positions when the foot is in contact with the ground were identified. It was assumed that when the lean angle is zero the mass centre will be 'alongside' or in the vertical plane through the radius of the foot curve. Therefore, these foot placements coordinates were identified at the times when the lean angle were zero. Throughout this study, the term midstance refers to the instant during foot contact when the lean angle is zero.

Moment of inertia and angular momentum

The whole body moment of inertia and the angular momentum values about the mass centre were obtained from the software program SIMU developed by Yeadon, (1984) using the spline coefficients of the orientation angles. In this study the SIMU program was modified to allow for independent leg movement. The moment of inertia about the frontal axis during touchdown, midstance and take-off during the approach phase were identified and used as input values for the simulation model APPROACH (which will be described in Chapter 4). The mean moment of inertia about the longitudinal, lateral and frontal axes were computed when the athlete was in the aerial phase of the approach. These values were also required as input for the APPROACH model. The values of the moment of inertia about the longitudinal axis were also used to estimate the relative amount of twist in the aerial and the ground phase of the approach (described in the section on *Ratio of inertia approach* in Chapter 4) for the APPROACH model.

The angular momentum about three principal orthogonal inertia axes x , y , z , were computed by the modified SIMU program throughout the approach and the flight phase of the jump. The values of the angular momentum about the horizontal (lateral) axis i were required as an input for the APPROACH model. The angular momentum about the x and y axes during the approach were used to calculate the angular momentum about the axis i of the athlete (as described in Chapter 4). The mean angular momenta about the y and the z axes during the flight phase of the jump were required for evaluating the APPROACH model in chapter 5.

Centre of pressure

The locations of the centre of pressure relative to the foot during the midstance was required to give a better estimate of the tilt angle (as described in the section on *Tilt angles* in Chapter 4). In order to identify the location of the centre of pressure, Parotec pressure insoles were used. However, since the Parotec pressure insoles are relatively new in development, it was necessary to evaluate the accuracy of the obtained measurements.

In the evaluation of the measurement accuracy of the pressure insoles, a pressure insole was taped over a force platform (Kistler 9281B12) with the longitudinal and lateral axis of the insole aligned with the horizontal x and y axes of the force platform. By walking over the taped pressure insole, the pattern of the centre of pressure for that movement was simultaneously acquired by both the force plate and the pressure insole. The patterns of the centre of pressure obtained from the pressure insole and the force plate were compared. The comparison of the centre of pressure patterns obtained from the pressure insole and the force plate are presented in the section on the *Evaluation of pressure insole* in Chapter 5.

In order to identify the centre of pressure during the midstance of the foot contact in the approach phase, the pressure insoles were inserted into the jumping spike shoes of a high jumper before the high jumper ran a curved approach. The data from the pressure insoles were then downloaded into a portable computer. Data from three trials were collected and the centre of pressure locations at midstance for the last four foot contacts of the approach were calculated relative to the mid-line of the insole. The results are presented in the section on *Tilt angles* in Chapter 4.

SUMMARY

A procedure has been developed to evaluate the image analysis systems. The evaluation of the image analysis systems is undertaken in Chapter 5. A methodology of data collection and analysis has also been developed for high jumping. With high jumping data collected and processed, a simulation model of the approach can be developed and evaluated in order to be used in explaining the underlying mechanics of the curved approach in high jumping. The development of the model is undertaken in Chapter 4 and the evaluation of the model is detailed in Chapter 5.

Chapter 4

DEVELOPMENT OF THE SIMULATION MODEL

INTRODUCTION

The image analysis of high jumping (reported in Chapter 6) reveals that as the athlete approaches the bar, his inward tilt angle is reduced to almost zero at take-off. The curve that describes the athlete's foot contacts was also observed to be 'tightening'. This implies that the radius of this curve becomes smaller as the athlete approaches the bar. The tightening of the curve and the concurrent reduction of the tilt angle may not just be a mere coincidence. The tightening of the foot contact curve may induce the athlete to rotate towards the bar and in the process reduce the tilt angle to almost zero at take-off. This also implies that the tightening of the foot curve may provide the momentum for the side somersault rotation for the bar clearance. In short, running a curve is quite similar to cycling around a corner. By turning the front wheel a little more into the corner (tightening the radius), the cyclist would 'straighten up' or rotate away from the curve (as shown in the Figure 4.1). This is analogous to tightening the foot placement curve in the high jump approach to provide the momentum for the somersault rotation.

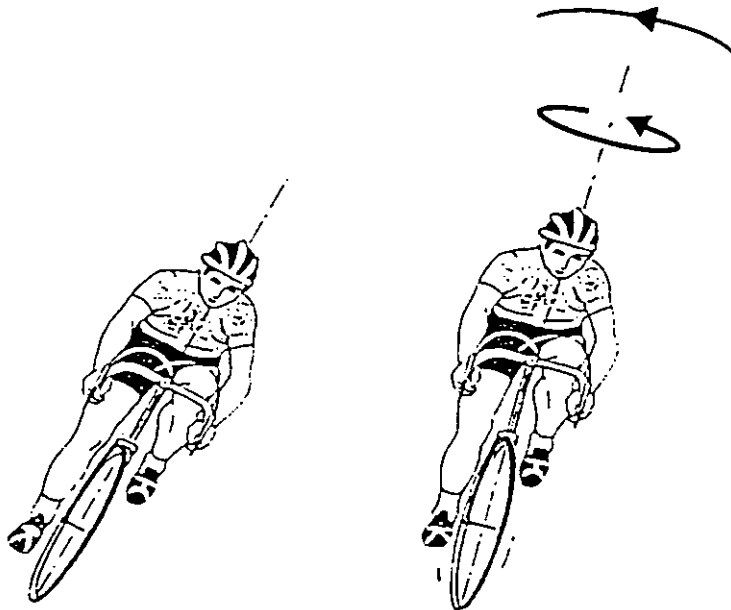


Figure 4.1. When the wheel turns more into the curve, the cyclist will "straighten-up" (adapted from Konopka, 1989).

POINT MASS MODEL

A simple mathematical point mass model can be used to demonstrate how the tightening of the curve could produce this rotation or 'straightening-up' process. This model consists of a point mass with a link length h to the ground, inclined at θ from the vertical, traversing in a circular path radius r about a vertical axis (as shown in Figure 4.2). The model is free to rotate about an axis through the foot F parallel to the velocity of F . This model simulates the approach with the foot F sliding on a curve with variable radius of curvature R .

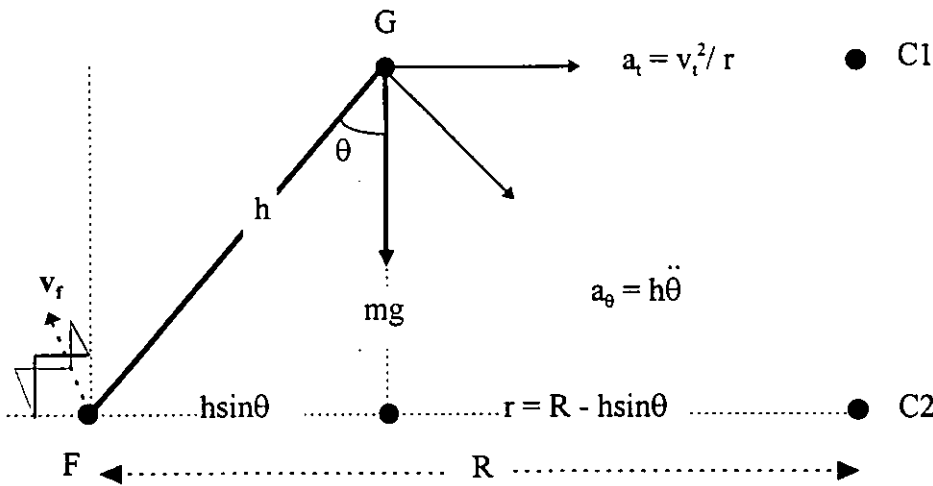


Figure 4.2. Point mass model.

Equation of motion

The torque about a point is the product of the force and the perpendicular distance from the point to the line of action of the force. Therefore, the torque T acting about F is:

$$T = mg h \sin \theta \quad (1)$$

in the direction parallel to the velocity of F .

The angular momentum about a point is the product of the linear momentum and the perpendicular distance from the point to the velocity vector. The angular momentum L about F has a horizontal component $mv_t h \cos \theta$ where v_t is the horizontal velocity of the mass centre parallel to the foot velocity v_f and a component $mv_\theta h$ parallel to v_f where v_θ is the velocity due to rotation about v_f .

Therefore the rate change of angular momentum was:

$$\frac{dL}{dt} = m a_0 h + m a_t h \cos \theta \quad (2)$$

about the axis v_p , where $a_0 = \ddot{v}_0$ and $a_t = \ddot{v}_t$

However, torque is also equal to rate of change of angular momentum.

Therefore from equation (1) and (2):

$$mgh \sin \theta = m a_0 h + m a_t h \cos \theta .$$

Since $a_0 = h\ddot{\theta}$ and $a_t = v_t^2/r$,

$$mg h \sin \theta = m h^2 \ddot{\theta} + (m v_t^2 h \cos \theta) / r .$$

Then substituting $r = R - h \sin \theta$ into equation (4) gives;

$$m g h \sin \theta = m h^2 \ddot{\theta} + (m v_t^2 h \cos \theta) / (R - h \sin \theta) .$$

The equation can be rearranged as:

$$h\ddot{\theta} = g \sin \theta - (v_t^2 \cos \theta) / (R - h \sin \theta) . \quad (3)$$

In equation (3), it can be noted that if the value of R is reduced (as the curve tightens) then the term on the left side will be more negative. This implies that if the radius of the foot contact curve is sufficiently reduced, the point G will rotate over F ('straighten up' and side somersault over F).

SIMULATION PROGRAM PMASS

PMASS is a simulation program based on equation (3) in which the time history of the tilt angle and angular velocity of the approach phase were calculated. The simulation procedure comprises the numerical integration of the equation (3) using a modified Euler procedure. In this modified Euler procedure, the initial angular acceleration $\ddot{\theta}_0$ is calculated from equation (3) using the initial values of the tilt angle θ_0 , R and v_t . The solution is then advanced by a small time Δt (0.01 seconds) from the initial tilt angle θ_0 and angular velocity $\dot{\theta}_0$ to obtain a new tilt angle θ_1 and angular velocity $\dot{\theta}_1$ using the equations for constant acceleration:

$$\theta_1 = \theta_0 + \dot{\theta}_0 \Delta t + \frac{1}{2} \ddot{\theta}_0 \Delta t^2$$

and

$$\dot{\theta}_1 = \dot{\theta}_0 + \ddot{\theta}_0 \Delta t$$

With this new tilt angle θ_1 and the next R and v_f values, a new angular acceleration $\ddot{\theta}_1$ was calculated using the equation (3) again. Finally the average angular acceleration α (of $\ddot{\theta}_1$ and $\ddot{\theta}_0$) is used as an estimate of $\ddot{\theta}$ over the time interval to recalculate θ_1 and $\dot{\theta}_1$ as:

$$\theta_1 = \theta_0 + \dot{\theta}_0 \Delta t + \frac{1}{2} \alpha \Delta t^2$$

and

$$\dot{\theta}_1 = \dot{\theta}_0 + \alpha \Delta t$$

At the end of each integration the distance of the approach curve s is incremented by the product of the velocity of the foot v_f and the time interval Δt . The numerical integration is continued until the s distance reaches the value at take-off.

Input data

To run a simulation, the initial conditions and characteristics of the approach curve must be provided. The initial conditions of a simulation comprise the initial tilt angle θ_0 , and the angular velocity $\dot{\theta}_0$. The distance h between the foot and the mass centre and the radius and the arc distance of the curve through each foot contact must also be provided for the simulation. The times of the foot contacts were also required in order to define the velocity of the foot through the curved approach.

Output data

The output data comprises the time history of the tilt angle and the tilt angular velocity. The units used for the angle is degrees while the angular velocity is reported in radians per second. The output values are calculated at intervals of 0.01s.

Calculation of input data

The initial tilt angle θ_0 was calculated from the video data using a projection of the mass centre and the foot onto the plane normal to the horizontal mass centre velocity (as described in Chapter 3). The initial tilt angular velocity $\dot{\theta}_0$ was calculated by using the tilt angles θ of the six foot contacts and their associated times identified from the video data. (Details of the calculations are to be found in the latter section of this Chapter on *Tilt angular velocity*).

The distance h was also obtained using the video data of the mass centre and the coordinates of the moving foot of the foot curve (as described in the section on *The distance h* of this chapter). The coordinates of the foot placements from the video data were used in calculating the arc distance and the radius of the foot contact curve (as described in the section in this chapter on *Calculation of s*). The horizontal velocity of the mass centre v_t was calculated from the foot velocity v_f which is described in the section on *Velocities*.

Limitations of PMASS

This program may be effective in demonstrating the mechanics of how side somersault rotation is generated in high jumping. However, modelling the body of the athlete as a point mass and simulating the approach as simply sliding on a curve may not provide enough accuracy for a quantitative study of such a complex movement. Although the athlete's foot placements do describe a curve, the foot does not slide along a curve in continuous contact with the ground. In fact, the athlete will spend a portion of each stride in the air as he runs up to the bar. In order to model this approach to the bar more accurately, a more complex model needs to be developed.

APPROACH MODEL

This section details the development of the APPROACH model which simulates more realistically the inward tilt motion of the athlete during the approach phase of the high jump. The athlete is modelled as a single segment with a variable mass centre height and variable moment of inertia. This model uses the initial conditions and the curve that describes the foot-ground contact during the approach to calculate the time history of the inward tilt angle and its angular velocity.

The evaluation of this program is undertaken in Chapter 5 where the output of this model is compared with the data obtained from the image analysis of Chapter 3.

The moving point of foot curve

Although there are a number of discrete foot placements, it will be convenient to consider a point that moves along a curve through the foot placements (Figure 4.3) at an appropriate velocity. As this moving point reaches each of the foot placements, the mass

centre G will be 'alongside' or in the vertical plane through the radius of the foot curve. The values of the foot placement coordinates used in the simulation were obtained from the video analysis as described in Chapter 3 and the distance s traversed by this moving foot was calculated (as detailed in the section on *Calculation of s*). The x distance of CO is used in the program as the terminating point of the simulation.

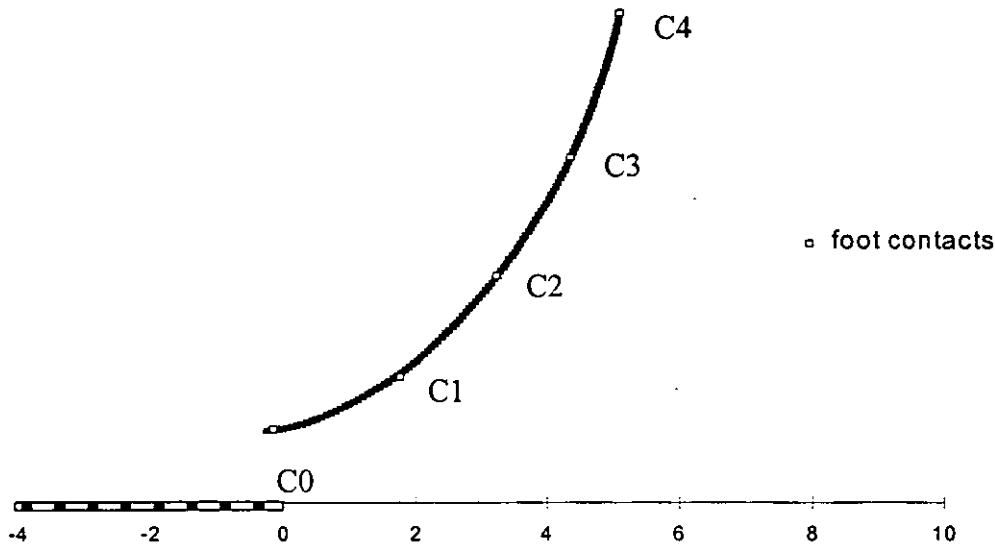


Figure 4.3. Foot curve of the moving point.

Reference frame

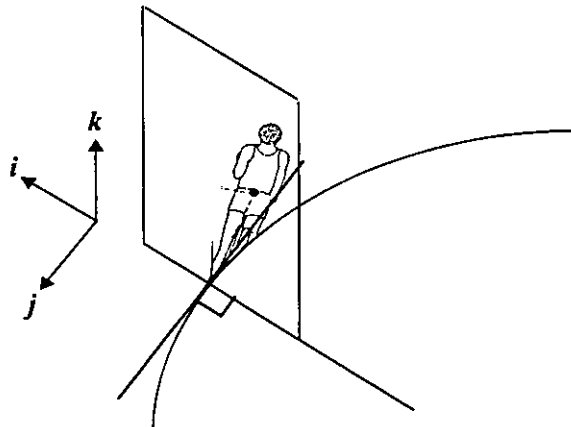


Figure 4.4. The moving reference frame $[i, j, k]$.

In order to describe the position and the movement of the athlete, a moving reference frame $[i, j, k]$ is adopted (as shown in Figure 4.4). In this frame, i horizontal indicates the right to left direction perpendicular to the direction of the curve through the foot contacts, j horizontal is defined as the anterior-posterior direction that is parallel to

the curve through the foot contacts, and k refers to the axis pointing vertically upwards. The orientation of the moving reference frame $[i, j, k]$ is defined by a rotation through $-\psi$ about k from an initial orientation with an inertial frame $[x, y, z]$. The body axes relative to the moving reference frame are defined as f_1, f_2, f_3 such that initially f_1, f_2, f_3 are aligned with i, j , and k and then a rotation through θ about $-j$ brings the body into its final orientation.

The body orientation of the approach

The body of the athlete will twist about a vertical axis during the curved approach so that he is always facing forward tangentially to the curve that describes the foot placement. The tangent of the foot placement curve makes an angle of ψ with a fixed line, parallel to the y horizontal (as shown in Figure 4.5). Since the tangent is in the direction of j of the moving reference, the rate of this twist rotation will be $d\psi/dt$.

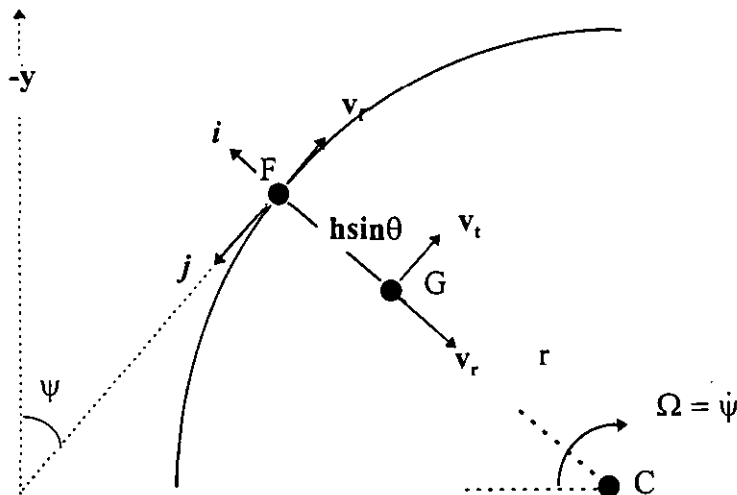


Figure 4.5. Foot (F) and mass centre (G) locations of approach phase (plan view).

Unlike a bicycle where the wheels maintain a continuous rolling contact with the ground, the high jumper's foot makes intermittent contacts. The path of the mass centre of the high jumper (from a plan view) follows a curve during these intermittent ground contacts and a straight line when there is no foot-ground contact. During the aerial phase, however, the body continues to twist and this affects the next foot placement. In the model, therefore, the path of the moving point (passing through the foot contacts) which

defines the body orientation maintains a curved path throughout both ground and aerial phases.

Velocities

This section provides the expressions of certain velocity terms so that they can be substituted in the equations used in the following sections.

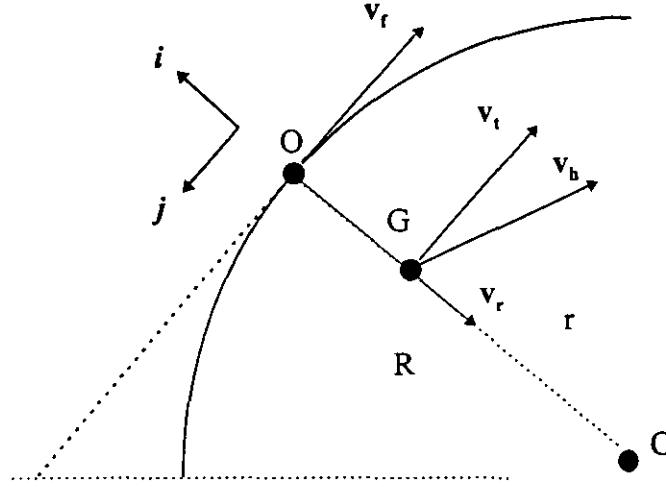


Figure 4.6. Velocities when mass centre is 'alongside' the foot contact.

If the moving point of the foot curve is at O such that OG is perpendicular to the curve (as shown in Figure 4.6), the horizontal velocity v_h may be resolved into a tangential component, v_t and a radial component v_r , such that:

$$v_h = v_t + v_r. \quad (4)$$

Therefore v_t and v_r are parallel and perpendicular to the curve at O respectively. The magnitude of v_h may be calculated as:

$$v_h = (v_r^2 + v_t^2)^{1/2}.$$

Since v_t at G is also parallel to the velocity v_f of the foot at O, v_t can be expressed in terms of v_f as:

$$\frac{v_t}{r} = \frac{v_f}{R}$$

or

$$v_t = \frac{v_f}{R} r \quad (5)$$

where R and r are the radius of the foot contact and the mass centre curves respectively.

Since the distance s for six contacts has been calculated and the time t (when the mass centre were 'alongside' the foot) can be identified from the video data, a quadratic curve can be fitted through these six pairs of distances and times (s,t) . Therefore, v_f can be obtained by differentiating this quadratic function:

$$v_f = \frac{ds}{dt} \quad (6)$$

If the times of the touchdown and take-off of the foot contacts are identified, their associated s distance can be interpolated from this quadratic function.

Since the radius of a curve R can be defined as

$$R = \frac{ds}{d\psi} \quad (7)$$

therefore

$$\frac{d\psi}{ds} = \frac{1}{R}$$

and so

$$\frac{d\psi}{dt} = \frac{ds}{dt} \frac{1}{R}$$

Therefore, by substituting equation (6), the twist velocity $\dot{\psi}$ can be written as:

$$\dot{\psi} = \frac{v_f}{R} \quad (8)$$

Torque about fixed foot

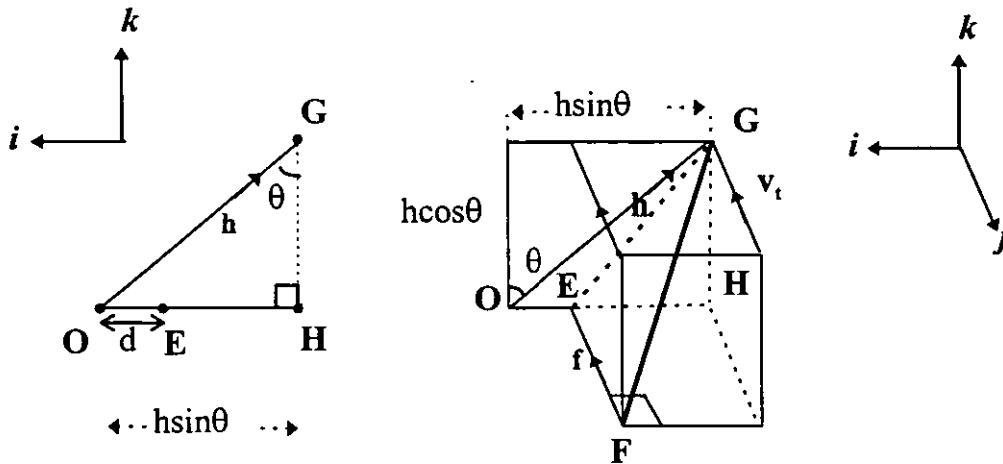


Figure 4.7. Three-dimensional geometry of the vector FG .

If \mathbf{f} is a horizontal vector that is parallel to \mathbf{v}_t such that

$$\begin{aligned}\mathbf{FG} &= \mathbf{FE} + \mathbf{EH} + \mathbf{HG} \\ &= \mathbf{FE} + (\mathbf{OH} - \mathbf{OE}) + \mathbf{HG} \\ &= -f\mathbf{j} - (h\sin\theta - d)\mathbf{i} + h\cos\theta\mathbf{k}\end{aligned}\quad (9)$$

\mathbf{h} will be the projection of \mathbf{FG} on a vertical plane through G perpendicular to \mathbf{v}_t .

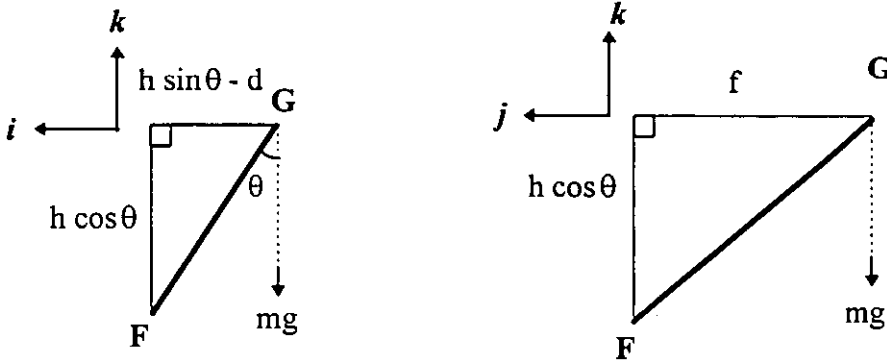


Figure 4.8. Torque at G about F .

Taking moments about F , the torque \mathbf{T} (as shown in Figure 4.8) can be expressed as;

$$\mathbf{T} = \mathbf{FG} \times (-m\mathbf{g}\mathbf{k})$$

where :

m is the mass of the jumper

g is the gravitational acceleration.

Since $\mathbf{FG} = -f\mathbf{j} - (h\sin\theta - d)\mathbf{i} + h\cos\theta\mathbf{k}$ from equation (9)

and therefore

$$\mathbf{T} = mgf\mathbf{i} - mg(h\sin\theta - d)\mathbf{j}. \quad (10)$$

The component of torque $-mg(h\sin\theta - d)\mathbf{j}$ will affect the tilt acceleration $\ddot{\theta}$.

Angular momentum equation

This section explains how angular momentum L_F about the foot can be calculated.

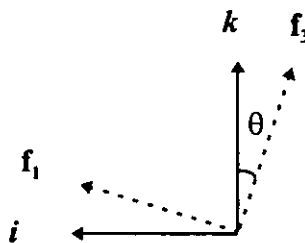


Figure 4.9. Axes of the body and the moving reference frames.

L_F can be expressed as the sum of the angular momentum L_m about the foot due to the motion of the mass centre and the angular momentum L_g about the mass centre as:

$$L_F = L_m + L_g$$

The angular velocity ω of the body is:

$$\omega = -\dot{\theta}j - \dot{\psi}k$$

Since the body of the athlete is inclined at angle of θ from the vertical, the body axes can be defined as:

$$f_1 = i \cos \theta + k \sin \theta \quad (11)$$

$$f_2 = j \quad (12)$$

$$f_3 = -i \sin \theta + k \cos \theta \quad (13)$$

Therefore the angular velocity ω can be expressed as

$$\begin{aligned} \omega &= -\dot{\psi} \sin \theta f_1 - \dot{\psi} \cos \theta f_3 - \dot{\theta} f_2 \\ &= -\dot{\psi} \sin \theta f_1 - \dot{\theta} f_2 - \dot{\psi} \cos \theta f_3 \end{aligned} \quad (14)$$

Although the model does not permit rotation about f_1 there will be some angular momentum L_1 about this axis due to the rotations of the limbs during running. Therefore, the angular momentum L_g about G will be;

$$L_g = (L_1 - I_1 \dot{\psi} \sin \theta) f_1 - I_2 \dot{\theta} f_2 - I_3 \dot{\psi} \cos \theta f_3 \quad (15)$$

where:

I_1 is the moment of inertia about the transverse axis f_1

I_2 is the moment of inertia about the frontal axis f_2

I_3 is the moment of inertia about the longitudinal axis f_3 .

Substituting (11)-(13) in equation (15), the angular momentum L_g about G can be written

$$\begin{aligned} \text{as: } & (L_1 - I_1 \dot{\psi} \sin \theta)(i \cos \theta + k \sin \theta) - I_2 \dot{\theta} j - I_3 \dot{\psi} \cos \theta (-i \sin \theta + k \cos \theta) \\ &= [L_1 \cos \theta - (I_1 - I_3) \dot{\psi} \sin \theta \cos \theta] i \\ &\quad - [I_2 \dot{\theta}] j \\ &\quad [L_1 \sin \theta - \dot{\psi} (I_3 \cos^2 \theta + I_1 \sin^2 \theta)] k. \end{aligned} \quad (16)$$

The angular momentum about F due to the motion of mass centre is:

$$\begin{aligned}\mathbf{L}_m &= \mathbf{FG} \times m \mathbf{v} \\ &= [-(h \sin \theta - d) \mathbf{i} - f \mathbf{j} + h \cos \theta \mathbf{k}] \times m [\mathbf{v}_t + \mathbf{v}_\theta] \\ &= [-(h \sin \theta - d) \mathbf{i} - f \mathbf{j} + h \cos \theta \mathbf{k}] \times m [-v_t \mathbf{j} - h \dot{\theta} \cos \theta \mathbf{i} - h \dot{\theta} \sin \theta \mathbf{k}]\end{aligned}$$

Since \mathbf{f} and \mathbf{v}_t are parallel,

$$\begin{aligned}&= m[(h \sin \theta - d)v_t \mathbf{k} - (h \sin \theta - d)h \dot{\theta} \sin \theta \mathbf{j}] + m[-f h \dot{\theta} \cos \theta \mathbf{k} + f h \dot{\theta} \sin \theta \mathbf{i}] \\ &\quad + m[h \cos \theta v_t \mathbf{i} - h^2 \dot{\theta} \cos^2 \theta \mathbf{j}] \\ &= [m v_t h \cos \theta + m f h \dot{\theta} \sin \theta] \mathbf{i} - [-m h^2 \dot{\theta} + m h \dot{\theta} d \sin \theta] \mathbf{j} \\ &\quad + [m v_t (h \sin \theta - d) - m f h \dot{\theta} \cos \theta] \mathbf{k}\end{aligned}\tag{17}$$

by substituting;

$$\begin{aligned}\mathbf{h} &= (h \cos \theta \mathbf{k} - h \sin \theta \mathbf{i}) \\ \mathbf{v}_\theta &= (-\dot{\theta} h \cos \theta \mathbf{i} - \dot{\theta} h \sin \theta \mathbf{k})\end{aligned}$$

and using the relations;

$$\begin{aligned}\mathbf{j} \times \mathbf{i} &= -\mathbf{k} \\ \mathbf{j} \times \mathbf{k} &= \mathbf{i} \\ \mathbf{k} \times \mathbf{j} &= -\mathbf{i} \\ \mathbf{i} \times \mathbf{j} &= \mathbf{k} \\ \mathbf{k} \times \mathbf{i} &= \mathbf{j} \\ \mathbf{i} \times \mathbf{k} &= -\mathbf{j} \\ \mathbf{i} \times \mathbf{i} &= \mathbf{k} \times \mathbf{k} = 0.\end{aligned}$$

Using equations (16) and (17) the total angular momentum about F becomes:

$$\begin{aligned}\mathbf{L}_F &= \mathbf{L}_m + \mathbf{L}_g \\ &= [m v_t h \cos \theta + m f h \dot{\theta} \sin \theta + L_1 \cos \theta - (I_1 - I_3) \dot{\psi} \sin \theta \cos \theta] \mathbf{i} \\ &\quad - [(I_2 + m h^2 - m h d \sin \theta) \dot{\theta}] \mathbf{j} \\ &\quad + [m v_t (h \sin \theta - d) - m f h \dot{\theta} \cos \theta + L_1 \sin \theta - \dot{\psi} (I_1 \sin^2 \theta + I_3 \cos^2 \theta)] \mathbf{k}.\end{aligned}\tag{18}$$

Equation for ground phase

However torque equals the rate of change of angular momentum:

$$\mathbf{T} = \frac{d \mathbf{L}_F}{dt}$$

The rate of change of angular momentum in an inertial frame $[x, y, z]$ is the sum of the apparent rate of change in a rotating frame $[i, j, k]$ and a second term that is the cross-product of the rotation rate of the moving frame and the angular momentum vector.

Therefore,

$$\frac{d\mathbf{L}_F}{dt} = [\dot{\mathbf{L}}_F]_m + \boldsymbol{\Omega} \times \mathbf{L}_F$$

and hence

$$\mathbf{T} = [\dot{\mathbf{L}}_F]_m + \boldsymbol{\Omega} \times \mathbf{L}_F \quad (19)$$

where $[\dot{\mathbf{L}}_F]_m$ is the rate of change of \mathbf{L}_F in the moving frame $[i, j, k]$

and $\boldsymbol{\Omega} = -\dot{\psi} \mathbf{k}$ is the angular velocity of $[i, j, k]$.

From equation (10)

$$\mathbf{T} \cdot \mathbf{j} = -m g h \sin \theta \quad (20)$$

From equation (18):

$$[\dot{\mathbf{L}}_F] \cdot \mathbf{j} = -[I_2 + mh(h-d\sin\theta)]\ddot{\theta} - [2mh\dot{h}\dot{\theta} - m\dot{h}d\sin\theta - mh\dot{d}\sin\theta - mh\dot{\theta}d\cos\theta]\dot{\theta} - \dot{I}_2\dot{\theta} \quad (21)$$

$$\begin{aligned} \boldsymbol{\Omega} \times \mathbf{L}_F \cdot \mathbf{j} &= (-\dot{\psi} \mathbf{k} \times \mathbf{L}_F) \cdot \mathbf{j} \\ &= -\dot{\psi} m v_i h \cos \theta - \dot{\psi} m f h \dot{\theta} \sin \theta - \dot{\psi} L_1 \cos \theta + \dot{\psi}^2 (I_1 - I_3) \sin \theta \cos \theta \end{aligned} \quad (22)$$

where :

\dot{I}_2 is the change of the moment of inertia about the frontal axis I_2 with time,

\dot{h} is the change in length of h with time $\frac{dh}{dt}$,

$\ddot{\theta}$ is the tilt angular acceleration.

Using equations (19)-(22) the equation of motion becomes:

$$\begin{aligned} -mg(h\sin\theta - d) &= -[I_2 + mh(h-d\sin\theta)]\ddot{\theta} - [2mh\dot{h}\dot{\theta} - m\dot{h}d\sin\theta - mh\dot{d}\sin\theta - mh\dot{\theta}d\cos\theta]\dot{\theta} \\ &\quad - \dot{I}_2\dot{\theta} - \dot{\psi} m v_i h \cos \theta - \dot{\psi} m f h \dot{\theta} \sin \theta - \dot{\psi} L_1 \cos \theta \\ &\quad + \dot{\psi}^2 (I_1 - I_3) \sin \theta \cos \theta \end{aligned}$$

This can be arranged as:

$$\begin{aligned}
 mg(h\sin\theta - d) = (I_2 + mh(h-d\sin\theta))\ddot{\theta} + [2mh\dot{h}\dot{\theta} - m\dot{h}d\sin\theta - mh\dot{d}\sin\theta - mh\dot{\theta}d\cos\theta]\dot{\theta} \\
 + \dot{I}_2\dot{\theta} + \dot{\psi}(mv_t h\cos\theta) + \dot{\psi}mfh\dot{\theta}\sin\theta \\
 + \dot{\psi}[L_1\cos\theta - \dot{\psi}(I_1 - I_3)\sin\theta\cos\theta]
 \end{aligned} \quad (23)$$

From equation (16) the angular momentum L_i about the horizontal axis i can be expressed as:

$$L_i = L_1\cos\theta - \dot{\psi}(I_1 - I_3)\sin\theta\cos\theta$$

and therefore equation (23) can be written as:

$$\begin{aligned}
 mg(h\sin\theta - d) = (I_2 + mh(h-d\sin\theta))\ddot{\theta} + [2mh\dot{h}\dot{\theta} - m\dot{h}d\sin\theta - mh\dot{d}\sin\theta - mh\dot{\theta}d\cos\theta]\dot{\theta} \\
 + \dot{I}_2\dot{\theta} + \dot{\psi}(mv_t h\cos\theta) + \dot{\psi}mfh\dot{\theta}\sin\theta + L_i\dot{\psi}
 \end{aligned}$$

By substituting (5) and (8) where $v_t = \frac{v_f}{R}r$ and $\dot{\psi} = \frac{v_f}{R}$, this equation may be written as:

$$\begin{aligned}
 mg(h\sin\theta - d) = (I_2 + mh(h-d\sin\theta))\ddot{\theta} + [2mh\dot{h}\dot{\theta} - m\dot{h}d\sin\theta - mh\dot{d}\sin\theta - mh\dot{\theta}d\cos\theta]\dot{\theta} \\
 + \dot{I}_2\dot{\theta} + (mv_f^2 r h\cos\theta)/R^2 + mfhv_f\dot{\theta}\sin\theta/R + L_i v_f/R
 \end{aligned}$$

Hence the tilt angular acceleration for the ground contact can be expressed as:

$$\begin{aligned}
 \ddot{\theta} = & mg(h\sin\theta - d)/(I_2 + mh(h-d\sin\theta)) \\
 & - [2mh\dot{h}\dot{\theta} - m\dot{h}d\sin\theta - mh\dot{d}\sin\theta - mh\dot{\theta}d\cos\theta]\dot{\theta}/(I_2 + mh(h-d\sin\theta)) \\
 & - (\dot{I}_2\dot{\theta})/(I_2 + mh(h-d\sin\theta)) - (mv_f^2 r h\cos\theta)/R^2(I_2 + mh(h-d\sin\theta)) \\
 & - (mfh v_f\dot{\theta}\sin\theta)/R(I_2 + mh(h-d\sin\theta)) - (L_i v_f)/R(I_2 + mh(h-d\sin\theta)) \quad (24)
 \end{aligned}$$

Aerial phase

In high jumping, during the run up to the bar, the athlete spends part of each stride in the air. Therefore to make the model more realistic, the flight phase of each stride must be taken into consideration. The body reference frame $[f_1, f_2, f_3]$ is brought from its initial orientation with an inertial frame $[x, y, z]$ into its final orientation by successive rotations through $-\psi$ about f_3 (bringing f_2 into alignment with f) and through $-\theta$ about f_2 (as shown in Figure 4.10). At the beginning of the aerial phase $\psi = \psi_0$, $\dot{\psi} = \dot{\psi}_0$, $\theta = \theta_0$, $\dot{\theta} = \dot{\theta}_0$.

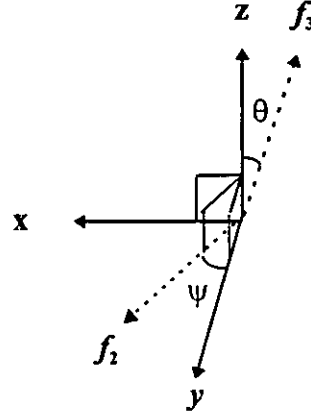


Figure 4.10. Axes of the inertial and the body reference frames.

The angular velocity may be written as:

$$\begin{aligned}
 \omega &= -\dot{\psi} \mathbf{z} - \dot{\theta} \mathbf{f}_2. \\
 &= -\dot{\psi} (f_1 \sin \theta + f_3 \cos \theta) - \dot{\theta} \mathbf{f}_2. && \text{substituting } \mathbf{z} = f_1 \sin \theta + f_3 \cos \theta \\
 &= -\dot{\psi} \sin \theta \mathbf{f}_1 - \dot{\theta} \mathbf{f}_2 - \dot{\psi} \cos \theta \mathbf{f}_3
 \end{aligned} \tag{25}$$

If I_1, I_2, I_3 are the principal moments of inertia about axes f_1, f_2, f_3 the angular momentum will be:

$$\mathbf{L}_g = -I_1 \dot{\psi} \sin \theta \mathbf{f}_1 - I_2 \dot{\theta} \mathbf{f}_2 - I_3 \dot{\psi} \cos \theta \mathbf{f}_3 \tag{26}$$

The angular momentum vector \mathbf{L}_g will have constant components in the frame $[\mathbf{x}, \mathbf{y}, \mathbf{z}]$:

$$\mathbf{L}_g = L_x + L_y + L_z$$

The components of \mathbf{L} in the body reference frame $[f_1, f_2, f_3]$ may be obtained from L_x, L_y, L_z using the transformation matrix $S_{if} = R_2(-\theta).R_3(-\psi)$

$$\text{where } R_2(-\theta) = \begin{bmatrix} \cos \theta & 0 & \sin \theta \\ 0 & 1 & 0 \\ -\sin \theta & 0 & \cos \theta \end{bmatrix} \quad \text{and } R_3(-\psi) = \begin{bmatrix} \cos \psi & -\sin \psi & 0 \\ \sin \psi & \cos \psi & 0 \\ 0 & 0 & 1 \end{bmatrix}$$

Thus:

$$[\mathbf{L}]_f = S_{if}[\mathbf{L}]_i = R_2(-\theta).R_3(-\psi) \begin{bmatrix} L_x \\ L_y \\ L_z \end{bmatrix}$$

$$= \begin{bmatrix} \cos\theta & 0 & \sin\theta \\ 0 & 1 & 0 \\ -\sin\theta & 0 & \cos\theta \end{bmatrix} \begin{bmatrix} \cos\psi & -\sin\psi & 0 \\ \sin\psi & \cos\psi & 0 \\ 0 & 0 & 1 \end{bmatrix} \begin{bmatrix} L_x \\ L_y \\ L_z \end{bmatrix}$$

$$= \begin{bmatrix} \cos\theta & 0 & \sin\theta \\ 0 & 1 & 0 \\ -\sin\theta & 0 & \cos\theta \end{bmatrix} \begin{bmatrix} L_x \cos\psi - L_y \sin\psi \\ L_x \sin\psi + L_y \cos\psi \\ L_z \end{bmatrix}$$

$$= \begin{bmatrix} L_x \cos\psi \cos\theta - L_y \sin\psi \cos\theta + L_z \sin\theta \\ L_x \sin\psi + L_y \cos\psi \\ -L_x \cos\psi \sin\theta + L_y \sin\psi \sin\theta + L_z \cos\theta \end{bmatrix}$$

Using the equation (26) for L_g in the $[f_1, f_2, f_3]$ frame:

$$\begin{bmatrix} I_1 \dot{\psi} \sin\theta \\ -I_2 \dot{\theta} \\ I_3 \dot{\psi} \cos\theta \end{bmatrix} = \begin{bmatrix} L_x \cos\psi \cos\theta - L_y \sin\psi \cos\theta + L_z \sin\theta \\ L_x \sin\psi + L_y \cos\psi \\ -L_x \cos\psi \sin\theta + L_y \sin\psi \sin\theta + L_z \cos\theta \end{bmatrix}$$

(27)

ψ and $\dot{\psi}$ may be approximated from the spline function (as described in the section on *Calculations of $\dot{\psi}$ and R*) used to express $\psi = \psi(s)$.

The second component of the angular momentum equation (27) yields:

$$-I_2 \dot{\theta} = L_x \sin\psi + L_y \cos\psi \quad (28)$$

The constant angular momentum components L_x and L_y may be obtained by transforming;

$$[L]_i = R_3(\psi) R_2(\theta) [L]_f$$

$$\begin{bmatrix} L_x \\ L_y \\ L_z \end{bmatrix} = \begin{bmatrix} \cos\psi & \sin\psi & 0 \\ -\sin\psi & \cos\psi & 0 \\ 0 & 0 & 1 \end{bmatrix} \begin{bmatrix} \cos\theta & 0 & -\sin\theta \\ 0 & 1 & 0 \\ \sin\theta & 0 & \cos\theta \end{bmatrix} \begin{bmatrix} I_1 \dot{\psi} \sin\theta \\ -I_2 \dot{\theta} \\ I_3 \dot{\psi} \cos\theta \end{bmatrix}$$

$$= \begin{bmatrix} \cos \psi & \sin \psi & 0 \\ -\sin \psi & \cos \psi & 0 \\ 0 & 0 & 1 \end{bmatrix} \begin{bmatrix} (I_1 - I_3) \dot{\psi} \sin \theta \cos \theta \\ -I_2 \dot{\theta} \\ (I_1 \sin^2 \theta + I_3 \cos^2 \theta) \dot{\psi} \end{bmatrix}$$

$$= \begin{bmatrix} (I_1 - I_3) \dot{\psi} \sin \theta \cos \theta \cos \psi - I_2 \dot{\theta} \sin \psi \\ -(I_1 - I_3) \dot{\psi} \sin \theta \cos \theta \sin \psi - I_2 \dot{\theta} \cos \psi \\ (I_1 \sin^2 \theta + I_3 \cos^2 \theta) \dot{\psi} \end{bmatrix}$$

Therefore, initially:

$$L_x = (I_1 - I_3) \dot{\psi}_0 \sin \theta_0 \cos \theta_0 \cos \psi_0 - I_2 \dot{\theta}_0 \sin \psi_0 \quad (29)$$

$$L_y = -(I_1 - I_3) \dot{\psi}_0 \sin \theta_0 \cos \theta_0 \sin \psi_0 - I_2 \dot{\theta}_0 \cos \psi_0 \quad (30)$$

Equation (28):

$$-I_2 \dot{\theta} = L_x \sin \psi + L_y \cos \psi$$

gives

$$\dot{\theta} = -\frac{L_x}{I_2} \sin \psi - \frac{L_y}{I_2} \cos \psi \quad (31)$$

$$\begin{aligned} &= -\frac{(I_1 - I_3)}{I_2} \dot{\psi}_0 \sin \theta_0 \cos \theta_0 \cos \psi_0 \sin \psi + \dot{\theta}_0 \sin \psi_0 \sin \psi \\ &\quad + \frac{(I_1 - I_3)}{I_2} \dot{\psi}_0 \sin \theta_0 \cos \theta_0 \sin \psi_0 \cos \psi + \dot{\theta}_0 \cos \psi_0 \cos \psi \\ &= -\frac{(I_1 - I_3)}{I_2} \dot{\psi}_0 \sin \theta_0 \cos \theta_0 \sin(\psi - \psi_0) + \dot{\theta}_0 \cos(\psi - \psi_0) \end{aligned} \quad (32)$$

using the equations (29), (30) and the expressions:

$$\sin(\psi - \psi_0) = \sin \psi \cos \psi_0 - \cos \psi \sin \psi_0$$

and

$$\cos(\psi - \psi_0) = \sin \psi \sin \psi_0 + \cos \psi \cos \psi_0.$$

This equation (32) may be used to advance the solution for θ in the aerial phase by using numerical integration midpoint method (as described in Press et al., 1988). For example, using equation (32) the new tilt angular velocity $\dot{\theta}_1$ can be calculated as:

$$\dot{\theta}_1 = -\frac{(I_1 - I_3)}{I_2} \dot{\psi}_0 \sin \theta_0 \cos \theta_0 \sin(\psi_1 - \psi_0) + \dot{\theta}_0 \cos(\psi_1 - \psi_0)$$

where ψ_1 is the twist angle after time Δt .

Therefore the average angular velocity $\dot{\theta}_{av}$ during the time interval Δt may be estimated as:

$$\dot{\theta}_{av} = \frac{1}{2} (\dot{\theta}_0 + \dot{\theta}_1)$$

Hence the new tilt angle θ_1 can be advanced from the initial angle and the average angular velocity $\dot{\theta}_{av}$ by:

$$\theta_1 = \theta_0 + \dot{\theta}_{av} \Delta t.$$

Numerical integration

The simulation procedure comprises the numerical integration of the equations (24) and (32) until the final distance s (the stride distance at take-off) is reached. For each ground contact phase, initially the angular acceleration $\ddot{\theta}_0$ is taken as the initial tilt angular acceleration then a modified Euler procedure is used to obtain a better estimate of angular acceleration to recalculate θ_1 and $\dot{\theta}_1$.

In this modified Euler procedure, the initial angular acceleration $\ddot{\theta}_0$ is calculated using equation (24) with the initial values of the tilt angle θ_0 , R and v_f . The solution is then advanced by a small time Δt (0.01 seconds) from the initial tilt angle θ_0 and angular velocity $\dot{\theta}_0$ to obtain a new tilt angle θ_1 and angular velocity $\dot{\theta}_1$ using the equations for constant acceleration as:

$$\theta_1 = \theta_0 + \dot{\theta}_0 \Delta t + \frac{1}{2} \ddot{\theta}_0 \Delta t^2$$

and

$$\dot{\theta}_1 = \dot{\theta}_0 + \ddot{\theta}_0 \Delta t$$

With this new tilt angle θ_1 and the advanced R and v_h values, a new angular acceleration $\ddot{\theta}_1$ is calculated using equation (24) again. The average angular acceleration α (of $\ddot{\theta}_1$ and $\ddot{\theta}_0$) is used to recalculate θ_1 and $\dot{\theta}_1$:

$$\theta_1 = \theta_0 + \dot{\theta}_0 \Delta t + \frac{1}{2} \alpha \Delta t^2$$

and

$$\dot{\theta}_1 = \dot{\theta}_0 + \alpha \Delta t$$

The distance of the approach curve s is also advanced by the product of the velocity of the foot v_f and Δt .

$$s_1 = s_0 + v_f \Delta t \quad (33)$$

The numerical integration of each ground contact begins when s reaches the touchdown value and continues until s reaches a toecoff value. When s reaches a toecoff value the solution is advanced using the aerial integration equations. In short, the ground and the aerial numerical integrations alternate until the final s distance is reached.

Input parameters

In order to run a simulation, the initial conditions must be furnished along with the characteristics of the foot contact curve and the inertia data of the athlete. The initial conditions of the simulation consist of the initial tilt angle and initial tilt angular velocity. The coordinates of each foot contact of the approach are also required as input into the simulation. These coordinates are used in calculating the radius and the arc distance of the foot contact curve (as described in the latter sections on *Calculation of s* and *Calculations of ψ and R* of this Chapter). In order to identify the aerial and ground phases, the touchdown and toecoff times were required. The time when the mass centre lies on the plane of the radius of the foot contact curve is also known as 'time at midstance'. These times are taken when the lean angle of the body ϕ is zero (as described in Chapter 3). The time interval Δt for the numerical integration must also be specified. Since the video data (that are used as input values to the model) are collected at 50 Hz (0.02s), setting the time interval for numerical integration at 0.01 seconds would be appropriate.

Starting point of simulation

This simulation program permits a simulation to begin at a particular foot contact. Therefore the input would require an indication on the starting point of the simulation. However, to enable the model to simulate the tilt angle moving through the maximum angle, the model begins simulation at C3 for both S. Smith and B. Reilly.

Output data

The output data comprises the time history of the tilt angle, tilt angular velocity, the twist angle, foot curve distance, radius and velocity. The units used for the angles are in degrees and the tilt angular velocity is reported in radians per second. The unit used for the foot curve distance and radius are in metres. The foot velocity is given in metres per second. The output values are calculated at intervals of 0.01s.

Tilt angles

The tilt angle θ_v is calculated from the video data using a projection onto the plane normal to the horizontal mass centre velocity v_h . This is done during foot contact when the mass centre is 'alongside' the foot. The tilt angle θ determined from the simulation model is based on the projection onto the plane normal to tangential velocity v_t (which is parallel to the velocity of the moving foot on the foot curve).

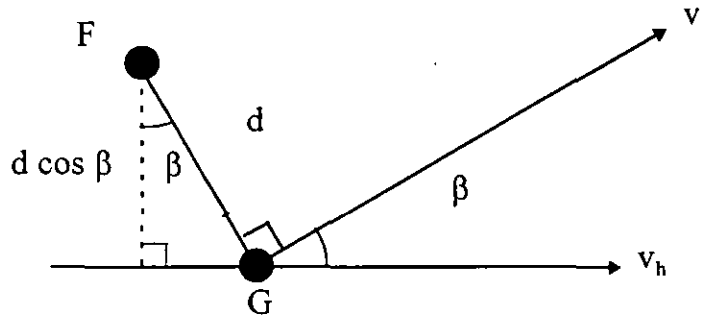


Figure 4.11. Foot and mass centre locations relative to v_h and v_t (plan view).

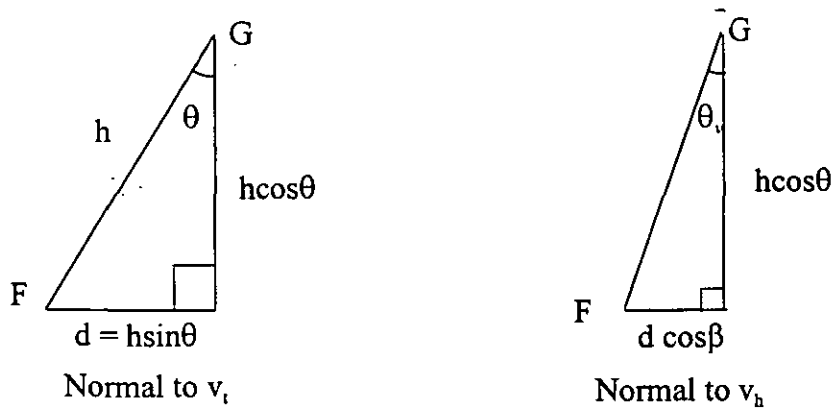


Figure 4.12. Projections on planes normal to v_t and v_h .

Therefore the θ_v estimated from the video will be smaller than the θ determined in the simulation model. From Figure 4.12,

$$\tan \theta_v = d \cos \beta / h \cos \theta$$

where β is the angle between v_t and v_h .

Since $d = h \sin \theta$,

$$\tan \theta_v = (h \sin \theta \cos \beta) / h \cos \theta$$

$$= \tan \theta \cos \beta$$

$$\tan \theta = \tan \theta_v / \cos \beta \quad (34)$$

The tangential velocity v_t is determined by the foot placements and its direction is given by ψ . The horizontal velocity v_h is calculated from the FILM program and its direction is given by the approach angle ψ_v . Therefore angle β can be estimated as;

$$\beta = |\psi - \psi_v|$$

and the discrete values of θ_v at each foot contact can be corrected using equation (34). Thus with these corrections, the tilt angle θ from video and simulation will be made equitable for comparison.

Asymmetrical differences

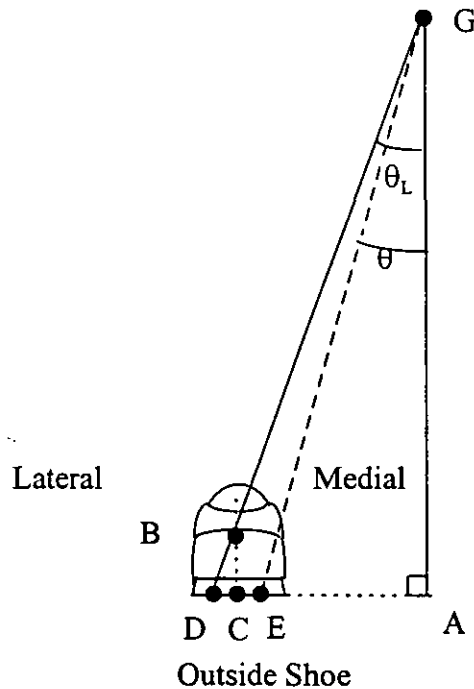


Figure 4.13 The rear view of θ and the outside shoe.

The tilt angle is measured between the line joining the mass centre G to the midfoot B and the vertical (as shown in Figure 4.13). With such a measurement, the centre of pressure of the contact is assumed to be a point lateral to the mid-line of the 'outside' foot or shoe at about D (as shown in the Figure 4.13). Although Hamill et al. (1987) observed that with curve running both the inside and the outside foot were pronated during midstance, the positions of centre of pressure relative to the mid-line of the shoe or foot were not reported.

Therefore, an experiment was conducted to determine the location of the centre of pressure relative to the mid-line of the shoe or foot (as described in Chapter 3). The patterns of the centre of pressure during the foot contacts of the curved approach are presented in Appendix F. The locations of the centre of pressure at midstance for three trials of the curved approach are presented in Table 4.1.

Table 4.1. Locations of COP at midstance

	Distance (in mm) medial to the mid-line of the foot		
	Trial 1	Trial 2	Trial 3
Outer foot contacts	10	13	12
Inner foot contacts	2	1	1

It was found that at midstance the centre of pressure E of the outside foot was about 12 mm medial to the mid-line of the foot. Since the centre pressure is not on the lateral side of the shoe at D (as shown in Figure 4.13) the measured tilt angle would be a little larger than it should be ($\theta_L > \theta$). The vertical height of the midfoot is the mid-distance between the ankle and the toe, and the ankle is about 6 cm vertically above the toe when the foot is flat on the ground; the vertical height BC of the midfoot can assumed to be 30 mm above the ground. If the measured tilt angle is 30° and CD is about 17 mm ($CD = BC \tan 30^\circ$) then DE will be about 29 mm. If the vertical height of the mass centre GA is about 1050 mm then:

$$\tan \theta = AE / 1050$$

and $AE = AD - DE$ where AD is about 600 mm ($GA \tan 30^\circ$)

therefore,

$$\tan \theta = 571 / 1050$$

$$\theta = 28.5^\circ$$

Hence, when the foot contact is made with the outside foot, the tilt angle θ needs to be adjusted to about 1.5° smaller.

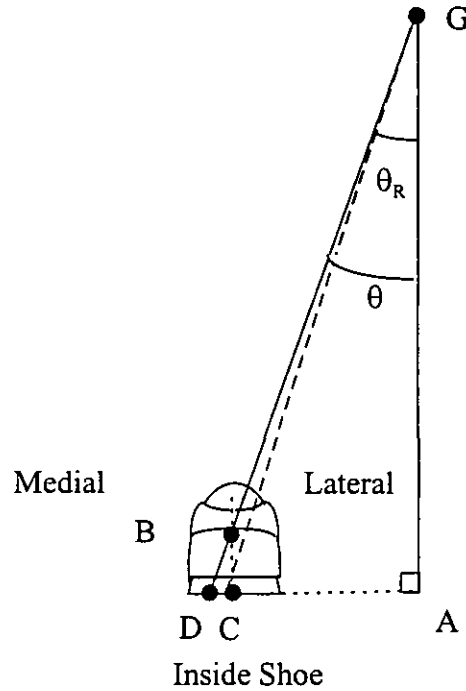


Figure 4.14. The rear view of θ and the inside shoe.

From the result of the experiment (Table 4.1), it was also found that at midstance the centre of pressure of the inside foot was about 1 mm medial to the mid-line C of the foot (as shown in Figure 4.14). If the measured tilt angle is 30° and CD is about 17 mm ($CD = BC \tan 30^\circ$) then the distance between the centre of pressure and A will be about 584 mm (600-16 mm). Therefore,

$$\tan \theta = 584 / 1050$$

$$\theta = 29^\circ$$

Hence, when the foot contact is made with the outside foot, the tilt angle θ calculated from video needs to be adjusted to about 1° smaller.

Tilt angular velocity

The tilt angles θ of the five foot contacts (C5-C1) were expressed as a fourth degree polynomial function with their associated times. The initial tilt angular velocity $\dot{\theta}$ (that is required as an input to the simulation program) was calculated by obtaining the first derivative of the polynomial function at the corresponding time, as:

$$\dot{\theta} = \frac{d\theta}{dt}$$

The distance h

Since the distance h and its rate of change during the ground contact were required, h values at touchdown, midstance and take-off were provided as input for the simulation. The distance h between the mass centre and the foot was calculated as: $DZ/\cos\theta$ where DZ is the vertical height of the mass centre and θ is the tilt angle. The vertical height of the mass centre DZ was obtained from the video data. The tilt angle θ was obtained using the (x, y) coordinates of the mass centre (from the video data) and the position moving foot of the foot curve at the corresponding time.

In the simulation program at each foot contact these h values were expressed as a quadratic function of their associated s distances. The rate of change \dot{h} was obtained by multiplying the first derivative of the quadratic function with the moving point velocity v_f as:

$$\begin{aligned}\dot{h} &= \frac{dh}{dt} \\ &= \frac{dh}{ds} \cdot \frac{ds}{dt}\end{aligned}$$

using equation (6) where $v_f = \frac{ds}{dt}$

$$\dot{h} = \frac{dh \cdot v_s}{ds}$$

Inertia values

The mass and the moment of inertia values (I_1, I_2, I_3) about the principal axes of the athlete are also required for a simulation. The mass of each athlete was obtained at the same time the anthropometric measurements were taken from the two athletes involved.

The moment of inertia data for each jump were obtained from the software program SIMU (detailed in Chapter 3). For the moment of inertia values about lateral and the longitudinal axes (I_1 , I_3), the average values of the ground contact phases are used as input. However the simulation model requires the inertia values (I_2) about the frontal axis and the rate of change (\dot{I}_2) during ground contact.

The values of I_2 at touchdown, midstance and take-off of each contact were provided as inputs. In the simulation program at each foot contact these I_2 were expressed as a quadratic function of their associated s distances. The rate of change \dot{I}_2 was obtained by multiplying the first derivative of the quadratic function with the moving point velocity v_f as:

$$\begin{aligned}\dot{I}_2 &= \frac{dI_2}{dt} \\ &= \frac{dI_2}{ds} \cdot \frac{ds}{dt} \\ &= \frac{dI_2}{ds} \cdot v_f\end{aligned}$$

$$\text{since } \frac{ds}{dt} = v_f$$

Angular momentum about the horizontal axis i

The values of angular momenta L_x and L_y about the x and y horizontal axes can be obtained from the SIMU program (as detailed in Chapter 3). Since the values of the angular momentum L_i about i were required for the simulation, the values of L_x and L_y were resolved into L_i as:

$$L_i = L_x \cos \psi + L_y \sin \psi$$

The average values of L_i at each ground contact were provided as input to the simulation program.

Calculation of s

The curve distance c between two foot contacts (e.g. C5 and C4) was calculated by using the difference of the two ψ angles and the radius R at 'mid-way' between the two foot contacts, as: $c = R(\psi_4 - \psi_5)$ where ψ_4 is the ψ angle at C4 and ψ_5 is the ψ angle at C5.

By summing the calculated curve distances between the foot contacts, the distance s traversed by the foot is obtained.

The distance s was initially calculated by summing the length of the straight lines joining the various foot contacts to obtain the radius R 'mid-way' between two foot contacts. The mean twist angle ψ_m was estimated as the angle between the line through two consecutive foot contacts and the y horizontal. This twist angle is associated with the point on the foot path that lies 'mid-way' between the two foot contacts. This point can be described by s_m , the s distance travelled along the foot curve. With six foot contacts (C5 to C0), five ψ angles and their five associated s distances can be found. These five pairs of angles and distances (ψ_m, s_m) were fitted with a fourth degree polynomial curve. The radius R , of the foot contact curve at each s_m distance was obtained from this polynomial function using the equation (7) :

$$R = 1 / \left(\frac{d\psi}{ds} \right)$$

where $\frac{d\psi}{ds}$ is the gradient of the polynomial curve.

With the radius in between foot contacts calculated, s distance is recalculated to take into the consideration that this foot path is more of a curve than a straight line through the foot contacts. Since the s distance at the various foot contacts can be obtained, the ψ angles can also be estimated from the polynomial function by interpolation or extrapolation.

Calculations of twist velocity $\dot{\psi}$ and foot radius R

During the aerial phase of the approach, the moment of inertia about the longitudinal axis was found to be markedly larger than in the ground phase. This implies that the jumper will twist more in the ground contact phase and less in the aerial phase. Therefore the model must allow ψ to vary between contact and aerial phases to ensure that the orientation of the body is realistic throughout the simulation. The $\dot{\psi}$ of the aerial and the ground phase will need to be adjusted from the average value according to the inverse proportion of their moment of inertia values. If the five pairs of (ψ_m, s_m) values are plotted on a graph, the gradient of two consecutive points would represent the mean rate of

change in ψ angle with respect to s during two foot contacts. These gradient values need to be partitioned to represent the change of ψ during the aerial and ground phase.

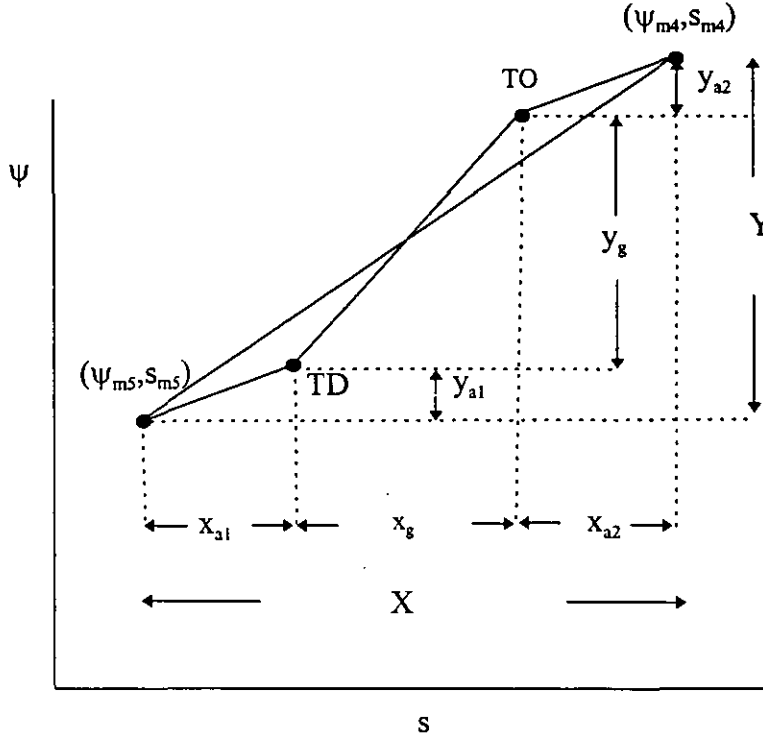


Figure 4.15. Partitioning the 'mean' gradient.

If the 'mean' gradient is Y/X (as in Figure 4.15) then

$$Y / X = (y_g + y_a) / (x_g + x_a) \quad (35)$$

where $x_a = x_{a1} + x_{a2}$ and $y_a = y_{a1} + y_{a2}$

If the ratio of the moment of inertia values about vertical axis of the aerial phase and the ground phase is I_r then

$$y_g/x_g = I_r(y_a/x_a)$$

and $(y_a/x_a) = y_g/(I_r x_g)$.

If M_a is the gradient or the change in ψ angle of the aerial phase, then

$$y_a = M_a \cdot x_a \quad (36)$$

and

$$y_g = M_a \cdot I_r x_g \quad (37)$$

Substituting equation (36) and (37) into the equation (35)

$$Y/X = (M_a \cdot I_r x_g + M_a \cdot x_a) / (x_g + x_a)$$

Therefore

$$M_a = Y / (I_r x_g + x_a)$$

If the gradient of the aerial phase can be obtained then the corresponding gradient or the change of angle for the ground phase M_g can be estimated as:

$$M_g = I_r \cdot M_a$$

The ψ angles of take-off and touchdown can be estimated from the respective aerial and ground gradients. For example, the ψ angle at the C4 touchdown ψ_{td4} can be calculated by using the straight line equation as:

$$\psi_{td4} = \psi_{m5} + M_{a4} (s_{td4} - s_{m5})$$

where M_{a4} is the rate of change of ψ during the aerial phase between s_{m4} and s_{m5} , s_{td4} is the s distance at C4 touchdown.

The ψ values of the touchdown and take-off for all the six foot contacts were fitted with an interpolating cubic spline. Hence the radius throughout the foot curve can be obtained from this spline as in equation (7);

$$R = 1 / \left(\frac{d\psi}{ds} \right)$$

where $\left(\frac{d\psi}{ds} \right)$ is the first derivative of the spline at the associated s distances.

Calculations of the distances r , d and f

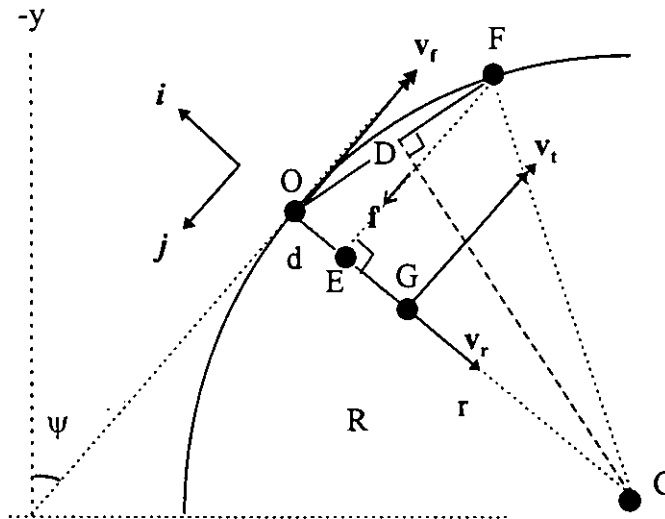


Figure 4.16. Foot contact at F.

The distance r between the mass centre (G) to the centre of rotation (C) can be expressed as:

$$r = R - OG \text{ where } OG = h \sin \theta .$$

The distance d or OE can be expressed as:

$d = OF \sin \hat{OFE}$ and \hat{OFE} can be calculated from the coordinates of O and F together with ψ .

In order to calculate \dot{d} rate of change of d , certain approximations will be made. In Figure 4.16, F is the position on foot curve when the mass centre is 'alongside'. If O is the moving point on the foot curve and D is the mid-point of OF , then DC will be perpendicular to OF (as shown in Figure 4.16). Hence $\triangle COD$ is congruent to $\triangle CDF$ (assuming that the radius R is not changing). Therefore,

$$\hat{FOE} = \frac{1}{2} \pi - \frac{1}{2} \hat{OCF} \text{ (since } \hat{OCD} = \hat{DCF})$$

and

$$\hat{OFE} = \frac{1}{2} \hat{OCF} \text{ (FE is perpendicular to OC) .}$$

$$\text{Hence, } \hat{OFE} = \frac{1}{2} |\psi_O - \psi_F|$$

where ψ_O is the value of ψ at O

and ψ_F is the value of ψ at F .

But $d = OF \sin \hat{OFE}$ and since $\hat{OFE} = \frac{1}{2} |\psi_O - \psi_F|$, so d can be approximated as:

$$d = OF \sin\left(\frac{1}{2} |\psi_O - \psi_F|\right).$$

In order to calculate \dot{d} rate of change of d , OF was assumed to be approximated by the curved distance s_d between the distance s traversed by the moving point and the s distance denoting the fixed foot. Therefore,

$$d = s_d \left(\frac{1}{2} |\psi_O - \psi_F|\right)$$

and \dot{d} rate of change of d can be expressed as:

$$\begin{aligned} \dot{d} &= \frac{1}{2} \dot{s}_d (\psi_O - \psi_F) + \frac{1}{2} s_d \dot{\psi}_O \\ &= \frac{1}{2} v_f (\psi_O - \psi_F) + \frac{1}{2} s_d \dot{\psi}_O \end{aligned}$$

The distance FE or f can be expressed as $(R - d) \tan (\psi_O - \psi_F)$.

Preliminary attempt to quantify twist using hip angle

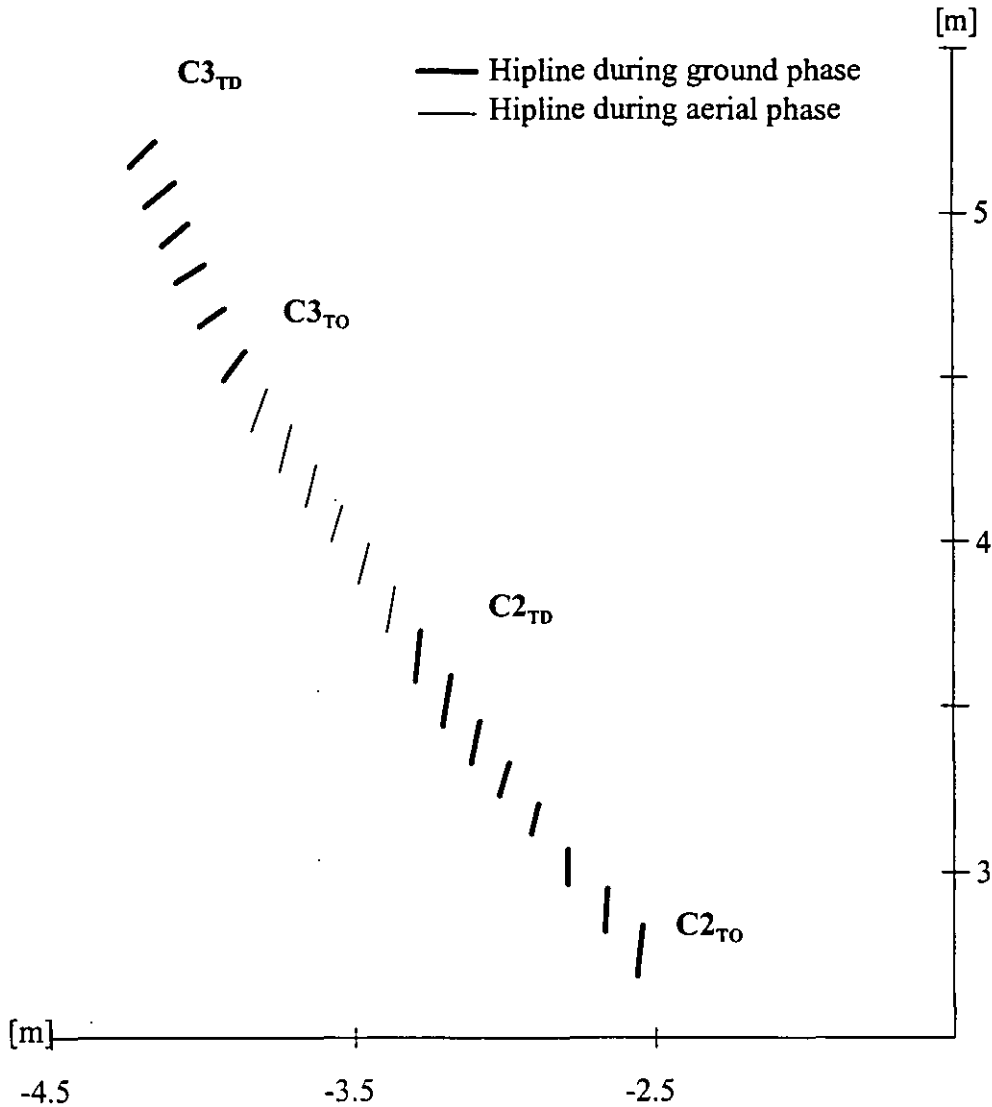


Figure 4.17 Hipline at C3 - C2 (jump S04).

An earlier attempt to quantify the twist angle was with the use of the hip angle ψ_h which was calculated as the twist of the hips relative to the longitudinal axis f_3 . The hip twist angles ψ_h obtained from the digitised video data were used to compute the ratio of twist rotation between the aerial and the ground phase. The digitised data of hips were not sufficiently accurate. This was because in the video image the athlete's shorts did not provide a clear landmark for digitising the hip joints. Repeated digitisation was required to improve the accuracy of the data. However, the ψ_h angle was also observed to twist clockwise and anti-clockwise corresponding to the left and right leg swing instead of reflecting the orientation of the body due the running of the curve (see Figure 4.17). The

shoulder twist angle ψ_s (the angle between the shoulder line and the y horizontal) obtained from the video data was also used to filter out the systematic oscillation of the ψ_h angle. This is done by averaging the values of the ψ_s and ψ_h in each field. The attempt to use ψ_h to determine the ratio of the twist rotation between the aerial and ground phase was aborted because there was still too much noise in the data even after much filtering and smoothing.

Foot direction for quantifying twist

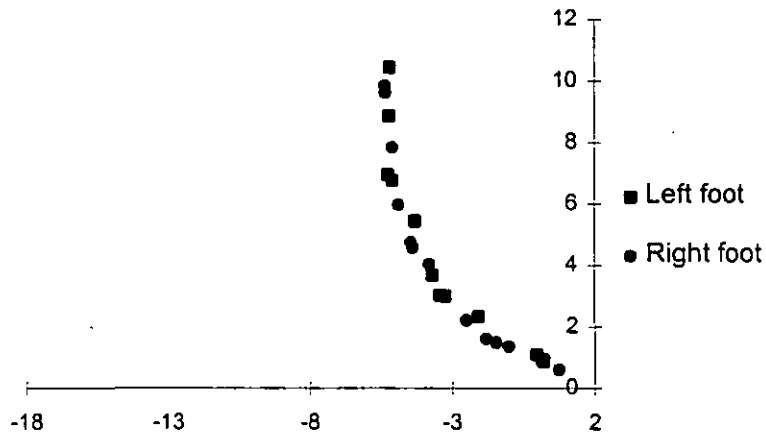


Figure 4.18. Foot location at touchdown and take-off of the approach (jump S07).

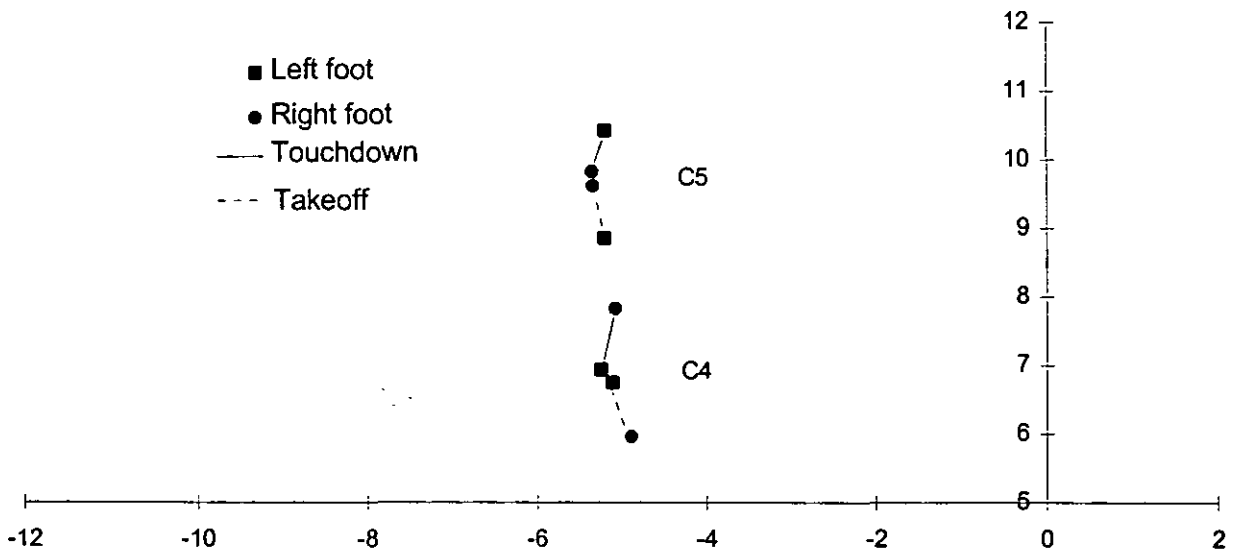


Figure 4.19. Foot direction at C5 and C4 (jump S07).

An attempt was also made to use the foot directions to determine the ratio of the twist rotation for the aerial and the ground phase. The x and y horizontal coordinates of the left and right ankles at touchdown and toecoff were plotted (Figure 4.18). No meaningful data could be derived from this exercise. The noise due to asymmetrical differences arising from the bipedal mode of movement seem to dominate the data (as shown in Figure 4.19).

Ratio of inertias for quantifying twist

For a given angular momentum, the rate of rotation can be determined from the moment of inertia. This prompted the use of the moment of inertia as a means to define the ratio of the amount of twist rotation between the aerial phase and the ground phase. The angular velocity about the longitudinal axis f_3 is $-\dot{\psi} \cos \theta$ and so the angular momentum about f_3 is $L_3 = -I_3 \dot{\psi} \cos \theta$. As $I_3 \cos \theta$ changes $\dot{\psi}$ will change in inverse proportion. The mean ratio of $\dot{\psi}$ between the ground and aerial phases can be estimated from the mean ratio of $I_3 \cos \theta$ in these two phases.

The moment of inertia about the longitudinal axis I_3 during high jumping performances can be obtained from the video data using the software program SIMU (as described in Chapter 3). The values of the tilt angle θ throughout the approach can be obtained by interpolating the polynomial function of the tilt angle and the time (as described in the earlier section on *Tilt velocity* in this chapter). Therefore the moment of inertia about the vertical axis $I_3 \cos \theta$ can be obtained.

For each jumper, a mean ratio of $I_3 \cos \theta$ between the ground and aerial phases of the approach was calculated from ratio of each step. The mean ratio of $I_3 \cos \theta$ for each jumper was used to partition the aerial and ground twist from the ψ_m values (as described in the earlier section of this chapter on the *Calculation of $\dot{\psi}$ and R*). This method of obtaining the ratio of twist rotation from the moment of inertia about the longitudinal axis was found to be quite satisfactory as the ψ angles obtained were capable of defining a foot curve passing through or near all the foot contacts of the approach.

Chapter 5

EVALUATION OF IMAGE ANALYSIS AND MODEL

INTRODUCTION

This chapter presents the results of the evaluation of the image analysis systems and the models developed for the high jump approach. The effect of using lens distortion correction, recording formats, and the digitising systems are presented in the following sections. Accuracy and precision estimates are also presented for the data obtained from video. The accuracy of the simulation models are assessed by comparing with the video data.

IMAGE ANALYSIS

Lens Distortion Correction

The results show that by using the procedure developed for lens distortion correction (9 or 12 DLT parameters), the accuracy of data obtained from the video recordings improved by quite a large margin for both the two-dimensional (2D) and three-dimensional (3D) reconstructions (Tables 5.1 and 5.2). For the 3D reconstruction, although the distortion correction made a large improvement in the accuracy, the errors in the direction markers to cameras (y) remained rather large (11.3 mm). This may have been caused by the placement of the two cameras. The cameras may have been placed too close to each other for accurate 3D reconstruction in this direction.

Table 5 1. Root mean square errors of 2D reconstruction [mm]

	x	x	z	z
DLT parameters	8	9	8	9
Panasonic VHS / Prisma	15.1	7.0	7.4	4.5
Sony HAD Hi8 / Apex	14.1	2.3	5.9	2.8
Locam 16mm / TDS	2.8	2.9	2.4	2.4

Table 5.2 Root mean square errors of 3D reconstruction [mm]

	x	x	y	y	z	z
DLT parameters	11	12	11	12	11	12
	15.0	2.8	39.8	11.3	6.0	2.3

Note: The Sony PROHi8 and Panasonic F15 cameras were used with the Apex system.

The results showed that the accuracy obtained from the use of 16 mm film did not improve with lens distortion correction. These results agreed with those of previous studies (e.g. Challis, 1991). This implies that lens distortion in 16 mm film images is minimal. The results obtained for video indicate that there is considerable lens distortion on video images. However, with lens distortion correction, the accuracy obtained from Hi-8 video images is comparable with that of 16 mm film.

Even after lens distortion correction, the measurement accuracy of VHS video system is still inferior to that of the 16mm film system. Perhaps, other factors such as the picture resolution or digitising resolution may also have affected accuracy.

Picture Resolution

In order to examine the effect of picture resolution on accuracy and precision measurements, digitised data obtained from the use of VHS (240 vertical lines) and Hi-8 (400 vertical lines) were compared. The accuracy and precision of the different video recording formats are presented in Table 5.3. The results indicated that when the Hi 8 recording format was used for digitising, the errors in the x and z directions were significantly reduced ($p < 0.05$). This is a result of the higher picture resolution recording format.

When Hi-8 recordings were used, the precision of both the static and the movement settings also improved significantly ($p < 0.05$). The better results in accuracy and precision with the use of higher picture resolution format can be attributed to the fact that better image quality enables more accurate and consistent digitising.

The magnitude of the measures of accuracy and precision in this study are not comparable because the estimates of accuracy were obtained by using the mean of ten sets of digitisations to reconstruct the three-dimensional coordinates and then

comparing with the survey measurements while the precision estimates were the measures of the variation among the ten sets of digitisations.

Table 5.3. Accuracy and precision of video recording format systems [mm]

	Static points Accuracy		Static points Precision		Movement Precision	
	x	z	x	z	x	z
VHS Camera format (Prisma system)	7.0	4.5	8.8	13.9	20.1	20.2
Hi-8 Camera format (Prisma system)	2.8	3.0	5.4	9.8	17.5	19.1

Measurement Resolution of Digitising Systems

When the Hi-8 recordings were digitised with the Apex system (sub-pixel measurement resolution) instead of the Prisma system, the errors were further reduced (Table 5.4). The errors in the x direction were significantly reduced (at $p < 0.05$). These differences in accuracy can be accounted for by the fact that Apex system has a considerably higher measuring resolution.

Table 5.4. Accuracy and precision of video digitising format systems [mm]

	Static points Accuracy		Static points Precision		Movement Precision	
	x	z	x	z	x	z
Prisma video digitising system (Hi-8 format)	2.8	3.0	5.4	9.8	17.5	19.1
Apex video digitising system (Hi-8 format)	2.3	2.8	4.5	4.0	13.7	12.6

The precision estimates obtained from the Apex system were significantly smaller than those from the Prisma for both static and movement points. The Apex system can display up to 16 million different colours whereas the Prisma system can only display up to 256 colours. This superior feature of the Apex system may enable the production of a more distinctive image for more consistent identification and digitisation of the image markers or landmarks.

TDS 16 mm film

Although 16 mm film is noted for its fine image resolution and the TDS system for its high measurement resolution, the accuracy measurement obtained from this combined system was not significantly different ($p < 0.05$) from the Apex Hi-8 video system when lens distortion was corrected. The precision measurements using the TDS 16 mm film system were, however, significantly worse ($p < 0.05$) than that of the video system (as shown in Table 5.5).

Accuracy of a measuring system may be constrained by different factors such as the process of measuring and the inherent nature of the system. Theoretically, accuracy should improve with an increased number of repeated measures. However after a number of repeated measures the degree of accuracy may reach a saturation point, that is with further repeated measurements the improvements in accuracy may be negligible. It is possible that the Apex Hi-8 system may reach the limit of accuracy with fewer repeated digitisations than the TDS 16 mm system. The high precision of the Apex Hi-8 system did not further improve the accuracy. Although the use of the TDS 16 mm film system did not produce good precision, the accuracy is comparable to the Apex Hi-8 system.

Table 5.5. Accuracy and precision of film and video digitising formats systems [mm]

	Static points Accuracy		Static points Precision		Movement Precision	
	x	z	x	z	x	z
HR48 TDS (16mm film)	2.8	2.3	10.0	7.9	17.5	15.1
Apex video digitising system (Hi-8 format)	2.3	2.8	4.5	4.0	13.7	12.6

Mean x and z errors of the different image systems

The accuracy measurements of the different image analysis systems is illustrated with the mean of the horizontal (x) and the vertical (z) errors in Figure 5.1. The accuracy measurements obtained from the use of Hi-8 recording formats and the Apex digitising system are not only better than the other video combination systems but are also comparable to those of the 16 mm film TDS system.

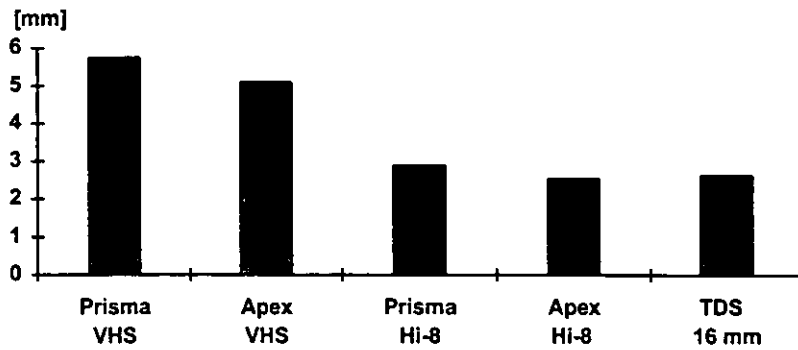


Figure 5.1. Accuracy estimates for digitising static markers.

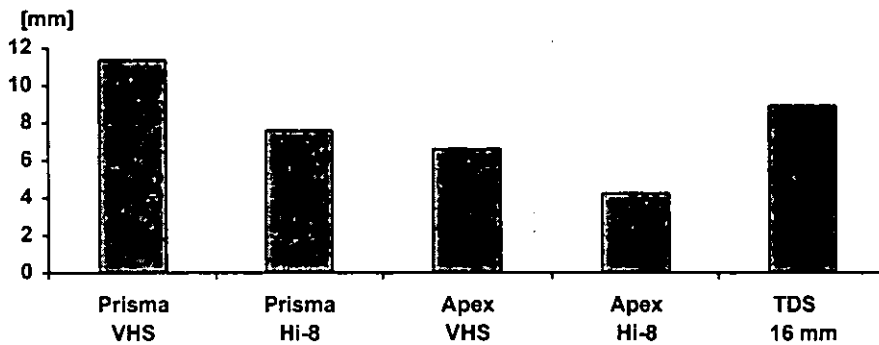


Figure 5.2. Precision estimates for digitising static markers.

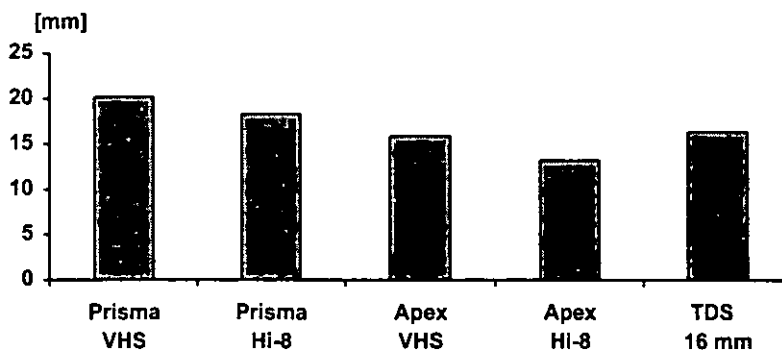


Figure 5.3. Precision estimates for digitising points on a moving body.

The precision of the different recording formats and digitising systems can be illustrated by the mean of the x and z precision estimates (Figure 5.2 and 5.3). The precision estimate for the Apex Hi-8 was the best of the different systems. Since the Apex Hi-8 system was also capable of producing data with a high level of accuracy it should be used as the image analysis system in the study on high jumping.

Optional digitising features of the Apex Target system




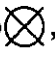

To investigate the effect of the optional features of the Apex digitising system, a set of default features of the digitising system were used as the initial configuration to digitise the Hi-8 recordings of the static markers. The initial configuration consisted of using the size 10,  cursor type, and no line or 'coarse' interpolation. An image magnification of twice the normal size (2x) was also selected. The precision and accuracy measurements were assessed as each selected optional feature was introduced as an intervention. For each configuration four fields of the video recordings were digitised. The results are presented in Table 5.6.

Table 5.6. Optimising digitising features of the Apex Target system

Configurations	Static points		Static points	
	Precision		Accuracy	
	x	z	x	z
Initial configuration	4.8	4.3	2.8	3.2
Smooth interpolation effect	4.1	3.8	2.4	3.1
Cursor type 	4.1	3.8	2.3	3.1
Cursor type 	4.1	2.9	2.7	2.4
Cursor Size 4	3.6	3.3	2.5	2.7
Cursor Size 16	3.9	2.6	2.6	2.1
Zoom 1x	3.9	3.3	2.9	2.7
Zoom 4x	4.0	3.7	2.7	3.0

Precision Measurement

There were improvements in precision estimates when smooth line interpolation was used, although the reductions were not significant. When the cursor type was changed to , the precision estimates were not reduced. However, when the cursor type  was used in digitising, the precision estimates in the vertical direction

(z) were significantly reduced ($p < 0.05$). The precision was not significantly improved with the use of cursor sizes 4 and 16. However, the size 16 cursor did give the smallest mean values of x and z. The precision did not improve with 4x or 1x image zoom. The precision in the z direction was significantly better ($p < 0.05$) for the 2x zoom compared with the 4x and 1x zoom.

Although digitising in the 'smooth' interpolation, size 16 cursor, \odot type and 2x zoom configuration yielded the best precision, the mean x and z estimates was only significantly different ($p < 0.05$) from the initial configuration and not from the other configurations. The precision of the different configurations can be illustrated by the mean of the x and y root mean square (rms) deviations as shown in Figure 5.4.

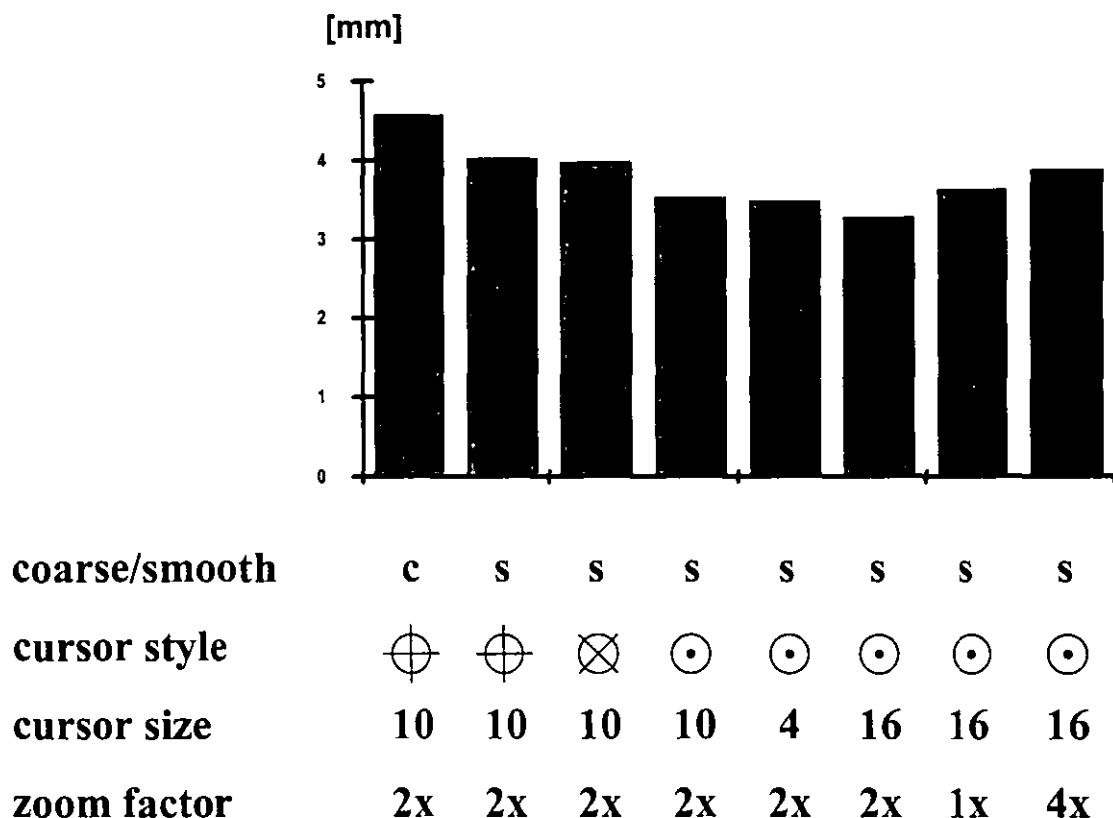


Figure 5.4. Precision comparison for Apex Target digitising features.

Accuracy Measurement

The errors for the 'smooth' line interpolation were not significantly lower than for the coarse interpolation. Among the three cursor types, the \odot type yielded the lowest z errors. When the cursor size 10 was replaced with size 4 or size 16, the errors were not significantly reduced ($p < 0.05$). However, the cursor size 16 produced the

smallest mean error of x and z. The use of 1x and 4x zoom produced significantly larger ($p < 0.05$) errors in the z direction than the 2x zoom. The configuration that gave the best precision result, also yielded the best accuracy, however the differences in errors among the different configurations were not significant. The accuracy performance of the different digitising configurations is illustrated by comparing the mean of the x and z errors as shown in Figure 5.5.

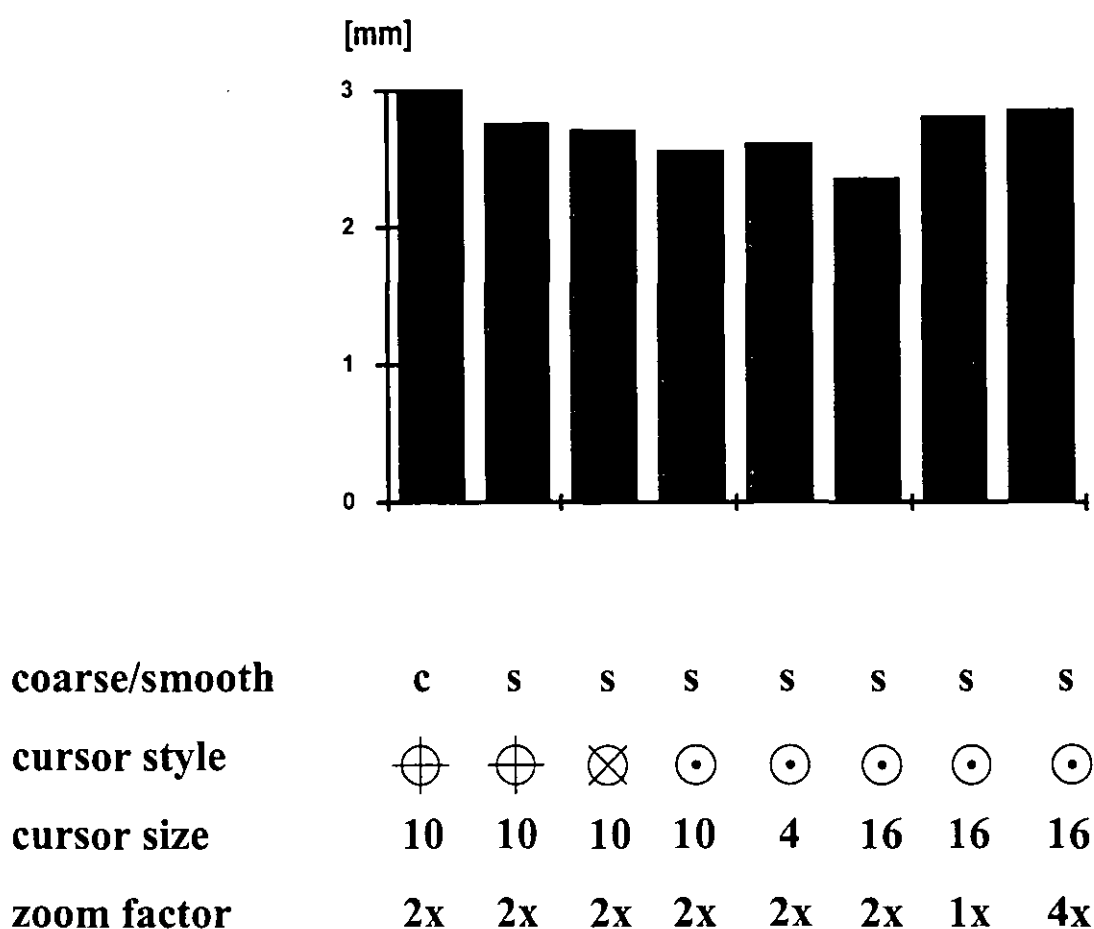


Figure 5.5. Accuracy comparison of Apex Target digitising features.

The accuracy results of the Hi-8 recordings digitised with the best digitising configuration of the Apex Target system were not significantly different from those of the 16mm film digitised on the HR48 TDS system as shown in Table 5.7. However the precision estimates for the Apex Target system were shown to be significantly

smaller ($p < 0.05$) than for the 16 mm film system for both the static and movement landmarks.

Table 5.7. Optimised video and 16 mm film image measurements

	Static points		Static points		Movement	
	Accuracy		Precision		Precision	
	x	z	x	z	x	z
Optimised video system	2.6	2.1	3.9	2.6	11.4	12.0
16mm film	3.5	2.7	6.3	6.0	15.5	13.3

*Note that the above results were based on four sets of digitisations.

Summary

This image analysis study shows that there is a considerable amount of radial distortion in video analysis systems. However, using the radial distortion correction with the DLT reconstruction procedure (described in Chapter 3), errors in accuracy were shown to be reduced significantly. Precision and accuracy in image measurement has also been demonstrated to improve with the use of higher picture resolution images. The Apex Target digitising system with sub-pixel measuring resolution and high colour display has also shown to improve precision and accuracy of measurement.

Hence the accuracy of a video system was found to be comparable to that of the 16mm film TDS system when the image was recorded on Hi-8 format, digitised on the Apex Target system and corrected for radial image distortion. Since the precision measures in the Apex Hi-8 were better than the 16 mm system, the Apex Hi-8 should be the system used in the following study of high jumping.

In the Apex Target system, a combination of digitising features that produced the best result for accuracy and precision measurement was identified in this study. However the differences in precision and accuracy errors among the different digitising configurations were small. Therefore, the use of different combinations of optional digitising features in the Apex Target system would not markedly affect the precision or accuracy of the data obtained.

*Evaluation of high jumping data***Digitising precision**

The precision estimates are the “error” estimates of each landmark used in the quintic spline fitting of the data (as described in the section on *Splining of data* in Chapter 3). These estimates are given by the FILM program for each coordinate of the 15 landmarks. For each jump, an average precision estimate for each coordinate was calculated for the 15 landmarks. The mean of the estimates of the two cameras for each jump are presented on Table 5.8. The estimates ranging from 18 to 23 mm were larger than those obtained from the optimised video system test (11 and 12.4 mm) as reported in Table 5.4. In the optimised video system test, the field of view of the image recordings was smaller (10 m compared to 15 m in the high jump recordings) which means that the images to be digitised were larger and therefore higher precision was expected.

Table 5.8. Digitising precision of the high jumping recordings

Jump number	x [mm]	z [mm]
B01	20	23
B02	20	23
B03	21	21
B04	21	22
B05	20	20
Mean	20.4	21.8
Standard deviation	0.5	1.2
S01	20	21
S02	19	20
S03	19	20
S04	18	21
S05	20	21
S06	19	19
S07	20	20
S08	19	19
S09	20	20
S10	19	20
Mean	19.3	20.1
Standard deviation	0.6	0.7

Reconstruction accuracy

Markers on calibration poles

The reconstruction errors of the markers on the calibration poles for the two jumpers are presented in Table 5.9. These errors reflect the degree of accuracy in the reconstruction of the spatial coordinates from the digitised data. The accuracy of the reconstruction also depends on the accurate placement of the markers.

If the mean errors of these two calibrations are compared with the values obtained from the 12 DLT parameter test in Table 5.1, the error in the x direction is larger for the high jumping calibrations (8.25 vs. 2.8 mm). This can be accounted for by the wider field of view used in the recording of the high jump calibration (15 vs. 10 m) and the fact that the marker positions were not surveyed. The errors in the y direction are smaller for the high jump calibration (7.60 vs. 11.3 mm) and this is largely due to better camera placement during the high jump recordings where the camera axes intersected at about 45°. The errors in the z direction were about the same magnitude between these calibrations and the 12 DLT test recordings (2.7 vs. 2.3 mm).

Table 5.9. Reconstruction errors of the calibration points

	x [mm]	y [mm]	z [mm]	overall rms [mm]
B. Reilly	7.9	7.7	1.7	6.4
S. Smith	8.6	7.5	3.7	6.9
mean	8.25	7.60	2.70	6.65

Body landmarks

The root mean square (RMS) distances from the reconstructed body landmarks to the four planes defined by the four equations used in the DLT reconstruction range from 14 mm to 20 mm (Table 5.10). These values are similar to the digitising precision estimates in Table 5.8 but they are also representative of the errors in the three-dimensional data since the digitised data sets from each camera view are independent.

Table 5.10. Reconstruction errors of the body landmarks

Jump number	RMS distances [mm]
B01	18
B02	17
B03	20
B04	18
B05	20
Mean	18.6
Standard deviation	1.3
S01	16
S02	17
S03	17
S04	17
S05	17
S06	16
S07	17
S08	14
S09	18
S10	17
Mean	16.6
Standard deviation	1.1

Segment lengths

Since the RMS error from Table 5.10 are at most 20 mm in each coordinate, the error in the difference between the x- values of two landmarks will be $\sqrt{2}$ times or about 28 mm. Thus the error in the estimated segment length will be $\sqrt{3}$ times 28 mm or about 50 mm. The standard deviations of the segment length shown in Table 5.11 are similar to this value.

Table 5.11. Standard deviation of calculated segment lengths [mm]

	arm	forearm	thigh	calf
B. Reilly	52	65	50	43
S. Smith	37	55	54	46

Precision estimates of the foot placement locations

The precision estimates of the locations of the foot placement were calculated from the precision estimates of the ankle and toe positions in two fields where the lean angles were nearest to zero. During ground-foot contact, if x_1 and x_2 were the x coordinates of the toe in the two fields where the lean angles were closest to zero, the variance estimate σ_t^2 of the x coordinates of the toe can be calculated as:

$$\sigma_t^2 = \frac{(x_1 - \mu)^2 + (x_2 - \mu)^2}{(2-1)2} \quad \text{where } \mu = \frac{x_1 + x_2}{2} \text{ and therefore,}$$

$$\sigma_t = \frac{1}{2}(x_1 - x_2).$$

Similarly, if x_3 and x_4 were the x coordinates of the ankle in these two fields, the variance of the x coordinates of the ankle can be calculated as σ_a^2 where:

$$\sigma_a = \frac{1}{2}(x_3 - x_4).$$

Therefore the variance of the x coordinates of the midfoot can be calculated as:

$$\text{var} \frac{(t+a)}{2} = \frac{1}{4}(\sigma_t^2 + \sigma_a^2).$$

Hence the x coordinate error estimate for the foot placement σ_m was calculated as

$$\sigma_m = \frac{1}{2}(\sigma_t^2 + \sigma_a^2)^{1/2}$$

The mean precision estimates of the foot placements for each jump are presented in Table 5.10. The precision of the foot placements is better than the mean precision of digitising the 15 landmarks (presented in Table 5.8). At midstance when foot movement is limited, the toe and ankle landmarks are more distinctive landmarks in the body to digitise, precision of the foot placements are therefore expected to be better than the mean precision of the 15 landmarks throughout the jump. The precision is also better because the four estimates have been used in determining the location of each foot placement.

Since the foot placement coordinates are means of four estimates the variation will be around a half of the variation in one estimate. Using the value of 20 mm (from Table 5.10) for the error in one coordinate of a landmark, the corresponding foot coordinate would have an error of 10 mm. The precision estimates in Table 5.12 are about 6 mm which is somewhat lower than this estimated error. The reason for this

could be that a stationary foot can be digitised more accurately than a moving landmark.

Table 5.12. Precision estimates of foot placement locations

Trial no.	x [mm]	y [mm]
B01	3.2	6.5
B02	2.9	6.2
B03	4.2	5.4
B04	3.1	5.9
B05	4.3	4.5
Mean	3.5	5.7
S01	3.8	12.1
S02	3.7	8.6
S03	3.3	7.8
S04	2.1	7.6
S05	4.6	6.5
S06	2.9	8.6
S07	3.8	5.3
S08	3.7	9.9
S09	3.2	5.6
S10	5.1	9.7
Mean	3.6	8.2

Precision of mass centre estimates

Since the mass centre coordinates are weighted means of 15 landmark coordinates the error in each coordinate of the mass centre may be expected to be $1/\sqrt{15}$ times smaller than the errors in the corresponding landmark coordinate. Using the value 20 mm (the largest value from Table 5.10) the mass centre coordinate error should be smaller than 5 mm. The values presented in Table 5.13 are of this order.

Table 5.13. Precision of mass centre estimates [mm]

	x	y	z	overall rms
B. Reilly	2	2	3	2.4
S. Smith	2	1	3	2.2

Precision estimate of approach speed

The precision estimates of the approach speed of the foot were calculated for each step. The precision estimate of approach speed over a step is the precision estimate of the step length divided by the step time. Since the step length S between C4 and C5 can be expressed as:

$S^2 = (x_4 - x_5)^2 + (y_4 - y_5)^2$ where (x_4, y_4) and (x_5, y_5) are the foot placements coordinates of C4 and C5, or

$$S^2 = X^2 + Y^2 \quad \text{where } X = (x_4 - x_5) \text{ and } Y = (y_4 - y_5),$$

$$(S + E_s)^2 = (X + E_x)^2 + (Y + E_y)^2$$

where E_s is the error in S and E_x is the error in X and E_y is the error in Y .

The equation can also be expanded to :

$$\begin{aligned} (S + E_s)^2 &= X^2 + 2XE_x + (E_x)^2 + Y^2 + 2YE_y + (E_y)^2 \\ &= X^2 + Y^2 + 2(XE_x + YE_y) \quad \text{since } (E_x)^2 \text{ and } (E_y)^2 \text{ are small} \\ &= S^2 \left[1 + \frac{2(XE_x + YE_y)}{S^2} \right]. \end{aligned}$$

Therefore ,

$$\begin{aligned} (S + E_s) &= S \left[1 + \frac{2(XE_x + YE_y)}{S^2} \right]^{1/2} \\ &= S \left[1 + \frac{1}{2} \frac{2(XE_x + YE_y)}{S^2} + \dots \right] \quad \text{using the binomial expansion.} \end{aligned}$$

Since the third and successive terms of the expansion are small,

$$E_s = \left[\frac{(XE_x + YE_y)}{\sqrt{X^2 + Y^2}} \right].$$

E_x can be substituted as:

$$\sqrt{\text{var} \frac{(x_4 + x_5)}{2}} = \frac{1}{2} \sqrt{(\sigma_{x4})^2 + (\sigma_{x5})^2}$$

and E_y as $\frac{1}{2} \sqrt{(\sigma_{y4})^2 + (\sigma_{y5})^2}$ where σ_{x4}, σ_{x5} and σ_{y4}, σ_{y5} are the standard deviations of the errors in the x and y coordinates in C4 and C5 respectively.

Hence the precision of the approach speed for a step length E_v can be estimated as:

$$E_v = E_s / t \quad \text{where } t \text{ is the time taken for the step.}$$

The mean precision estimates of the foot approach speed for all the step lengths were found to be 0.04 ms^{-1} for B. Reilly as well as for S. Smith. From C5 to C0, the foot approach speeds calculated for B. Reilly and S. Smith ranged from 7 to 8 ms^{-1} . Therefore, the precision estimate is about 0.5% of the approach speed. This suggests that the measurement error in the approach speed may have little effect on the results of the model.

Precision estimate of the distance h

Since the distance h between the mass centre and the foot placement is calculated as:

$$h^2 = D^2 + Z^2$$

where D is the horizontal distance between the mass centre and the midfoot and Z is the vertical height of the mass centre. Therefore,

$$(h + E_h)^2 = (D + E_D)^2 + (Z + E_Z)^2$$

where E_h , E_D , E_Z are the error estimates in h, D and Z respectively.

The equation can also be expanded to :

$$\begin{aligned} (h + E_h)^2 &= D^2 + 2.D.E_D + (E_D)^2 + Z^2 + 2.Z.E_Z + (E_Z)^2 \\ &= D^2 + Z^2 + 2(D.E_D + Z.E_Z) \text{ since } (E_D)^2 \text{ and } (E_Z)^2 \text{ are small} \\ &= h^2 \left[1 + \frac{2(D.E_D + Z.E_Z)}{h^2} \right] \\ (h + E_h) &= h \left[1 + \frac{2(D.E_D + Z.E_Z)}{h^2} \right]^{1/2} \\ &= h \left[1 + \frac{1}{2} \frac{2(D.E_D + Z.E_Z)}{h^2} + \dots \right] \end{aligned}$$

and

$$E_h = \left[\frac{(D.E_D + Z.E_Z)}{\sqrt{D^2 + Z^2}} \right]$$

E_D can be expressed as:

$$E_D = \left[\frac{(x_g - x_f)E_x + (y_g - y_f)E_y}{\sqrt{(x_g - x_f)^2 + (y_g - y_f)^2}} \right]$$

where (x_g, y_g) (x_f, y_f) are the coordinates of the mass centre and the midfoot.

E_x is:

$$\sqrt{\text{var} \frac{(x_g + x_f)}{2}} = \frac{1}{2} \sqrt{(\sigma_{xg})^2 + (\sigma_{xf})^2}$$

and E_y is $\frac{1}{2} \sqrt{(\sigma_{yg})^2 + (\sigma_{yf})^2}$

where σ_{xg}, σ_{xf} and σ_{yg}, σ_{yf} are the standard deviations of the x and y coordinates of mass centre and the midfoot respectively.

E_z is the standard deviation of the z coordinate of the mass centre.

The variance of each mass centre coordinate was obtained using the same method in the calculation of local variance for digitised data before fitting a quintic spline. This method is described in Chapter 3: *Splining of data*.

The mean precision estimates of the distance of the mass centre to foot were found to be 4.4 mm for B. Reilly and 5.4 mm for S. Smith. The distance of the mass centre and the foot for B. Reilly and S. Smith ranged from 850 mm to 1400 mm. Therefore, the precision estimates represent 0.5% or less of the measured distance. The measurement errors of the mass centre to foot distance would therefore not expected to have a effect on the results of the model.

Precision estimate of the tilt angle

Since the tangent of the tilt angle θ can be expressed as: $\tan\theta = D/Z$ where D is the horizontal distance between the mass centre and the midfoot and Z is the vertical height of the mass centre,

$$\tan (\theta+E_{\theta}) = \frac{D+E_D}{Z+E_Z}$$

where E_{θ}, E_D, E_Z are the error estimates in θ, D and Z respectively.

This equation can be expanded into:

$$\tan (\theta+E_{\theta}) = \frac{D\left(1+\frac{E_D}{D}\right)}{Z\left(1+\frac{E_Z}{Z}\right)}$$

$$\begin{aligned}
&= \frac{D}{Z} \left(1 + \frac{E_D}{D}\right) \left(1 + \frac{E_Z}{Z}\right)^{-1} \\
&= \frac{D}{Z} \left(1 + \frac{E_D}{D}\right) \left(1 - \frac{E_Z}{Z}\right) \\
&= \frac{D}{Z} \left(1 + \frac{E_D}{D} - \frac{E_Z}{Z} - \frac{E_D}{D} \cdot \frac{E_Z}{Z}\right)
\end{aligned}$$

Since the term $\left(\frac{E_D}{D} \cdot \frac{E_Z}{Z}\right)$ is small, it can be neglected therefore

$$\begin{aligned}
\tan(\theta + E_\theta) &= \frac{D}{Z} \left(1 + \frac{E_D}{D} - \frac{E_Z}{Z}\right) \\
&= \tan\theta \left(1 + \frac{E_D}{D} - \frac{E_Z}{Z}\right) \quad \text{for } \tan\theta = \frac{D}{Z}.
\end{aligned}$$

However, using the Taylor series where $f(a+x) = f(a) + f'(a)x + \frac{f''(a)}{2!}x^2 + \dots$,

$$\tan(\theta + E_\theta) = \tan\theta + E_\theta \sec^2\theta + \dots$$

Therefore

$$E_\theta \sec^2\theta = \tan\theta \left(\frac{E_D}{D} - \frac{E_Z}{Z}\right)$$

Hence the precision estimate of the tilt angle E_θ can be calculated as:

$$\begin{aligned}
E_\theta &= \cos^2\theta \tan\theta \left(\frac{E_D}{D} - \frac{E_Z}{Z}\right) \\
&= \cos\theta \sin\theta \left(\frac{E_D}{D} - \frac{E_Z}{Z}\right).
\end{aligned}$$

The precision estimates of the tilt angle were found to be about 0.6° to 0.7° throughout the approach phase for B. Reilly and S. Smith. The mean precision estimates of the approach speed, mass centre to midfoot distance and the tilt angle for each jump are presented in Table 5.14. The mean values for each jumper are also included in the table.

Table 5.14. Precision of approach speed, distance h, and tilt angle θ

Jump	Approach speed [ms^{-1}]	Mass centre to foot distance h [mm]	Tilt angle
B01	0.03	4.2	0.5°
B02	0.04	3.9	0.6°
B03	0.05	4.2	0.5°
B04	0.04	4.1	0.6°
B05	0.03	5.7	0.6°
Mean	0.04	4.4	0.6°
S01	0.06	4.8	0.7°
S02	0.04	5.3	0.6°
S03	0.05	5.4	0.7°
S04	0.04	5.5	0.7°
S05	0.04	5.5	0.8°
S06	0.05	4.2	0.6°
S07	0.03	5.4	0.6°
S08	0.05	5.6	0.6°
S09	0.03	5.8	0.6°
S10	0.05	6.4	0.8°
Mean	0.04	5.4	0.7°

Evaluation of the pressure insole

In order to evaluate the pressure insole for calculating the centre of pressure (COP) locations, the distribution pattern of COP between the force plate and the pressure are compared. The distribution pattern of COP for walking over the pressure insole placed on the force plate of two trials are shown in Figure 5.6 and 5.7. In both trials the patterns of the COP obtained from the pressure insole showed good agreement with those obtained from the force plate.

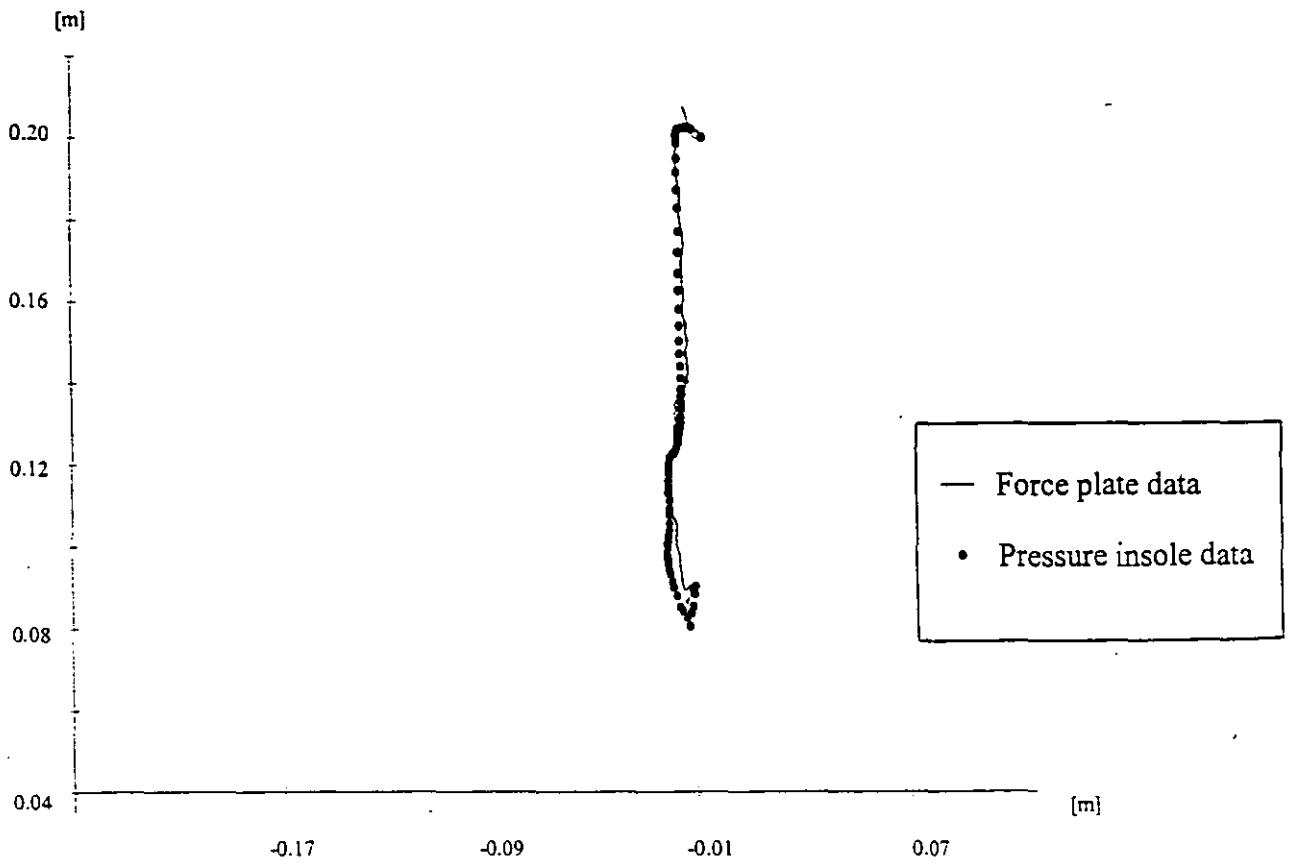


Figure 5.6. Centre of pressure patterns from force plate and pressure insole (trial 1).

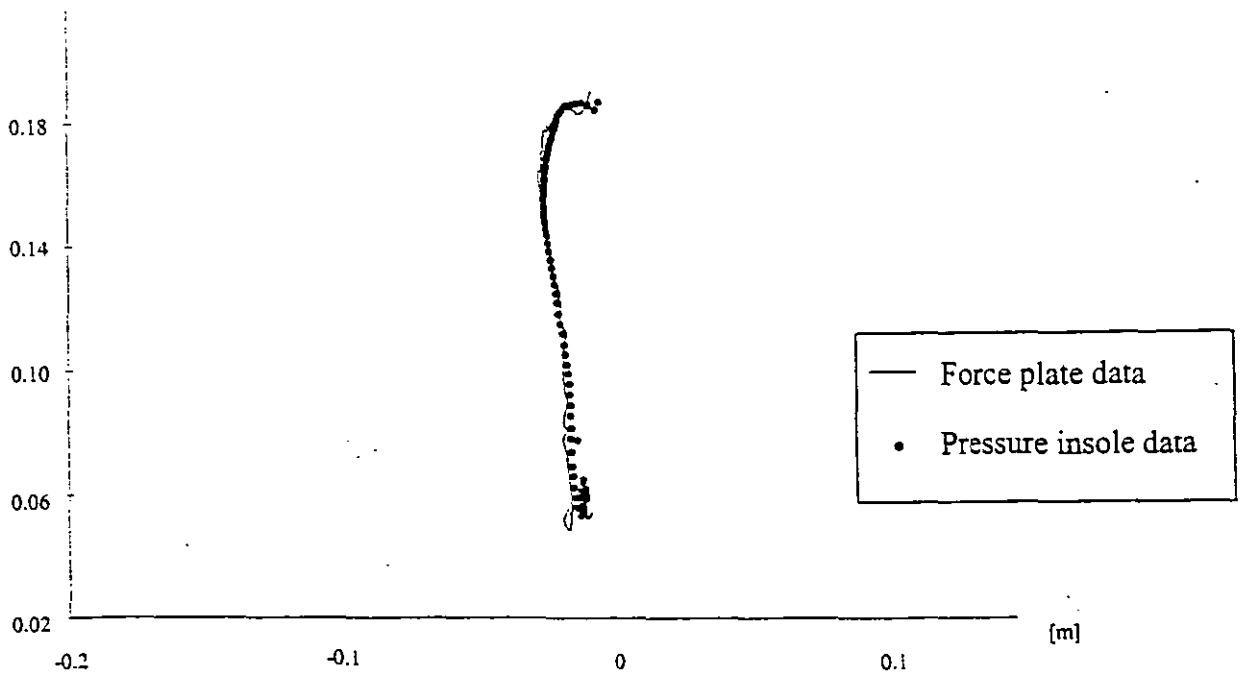
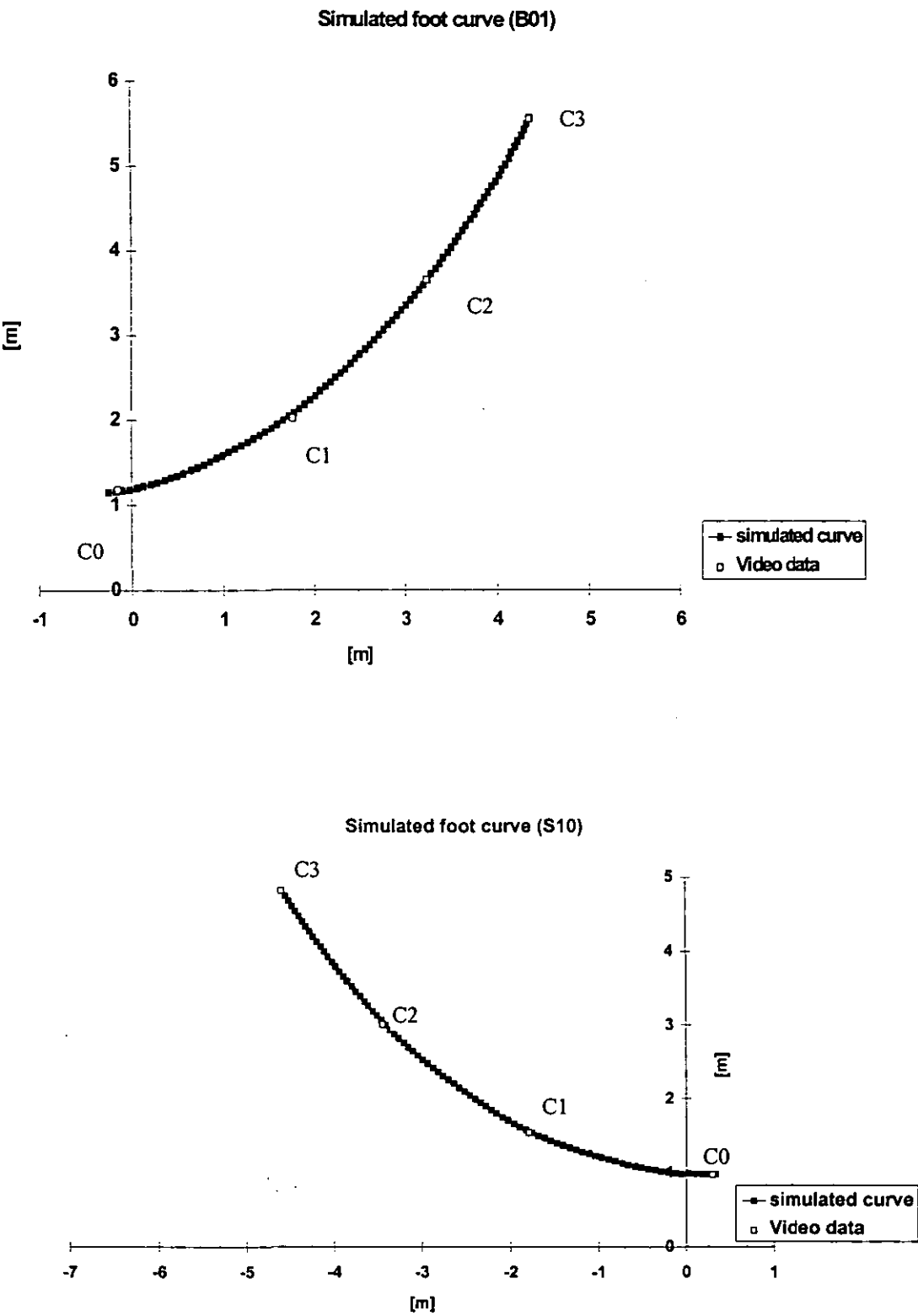


Figure 5.7. Centre of pressure patterns from force plate and pressure insole (trial 2)

EVALUATION OF THE MODEL

Foot curve



The curves traversed by the foot during the approach simulated by the APPROACH model for a typical jump for B. Reilly and S. Smith are shown in Figure 5.8. Figure 5.8 also shows that for both B. Reilly and S. Smith, the simulations commenced at C3. The foot placements (from C3 to C0) at midstance obtained from the video data are superimposed in Figure 5.8 for comparison. The simulated foot curves in all the jumps passed through or near the foot placement locations.

Tilt angle

The tilt angles obtained from the APPROACH model and the video data are presented in Tables 5.15 and 5.16. The deviations between the simulated angles and those obtained from the video data are also presented. The negative sign (-) next to the deviation values indicate that the simulated values are smaller, that is the lean is more into the cross bar. Since the model calculates the tilt angles based on the different projections of the mass centre velocity (v_i instead of v_h in video), tilt angles obtained from the video data were adjusted in order to be comparable with those obtained from the model. The tilt angles from the video data were also adjusted to take into consideration of the centre of pressure locations at midstance. These adjustments are described in the section on *Tilt angles* in Chapter 4.

Table 5.15. Tilt angles (in degrees) from video data and the model (B. Reilly)

	C2			C1			C0		
	simulated	video	deviation	simulated	video	deviation	simulated	video	deviation
B01	23.9	25.4	-1.5	18.8	25.4	-6.6	-4.2	-1.4	-2.8
B02	25.1	26.1	-1.0	20.6	25.5	-4.9	-0.8	-1.6	0.8
B03	25.3	26.6	-1.3	21.1	28.5	-7.4	-1.2	1.0	-2.2
B04	23.1	24.6	-1.5	18.7	26.2	-7.5	-9.4	-1.1	-8.3
B05	27.0	28.2	-1.2	24.2	29.2	-5.0	-2.0	-1.3	-0.7
Mean absolute deviation			1.3°			6.3°			3.0°

Table 5.16. Tilt angles (in degrees) from video data and the model (S. Smith)

	C2			C1			C0		
	simulated	video	deviation	simulated	video	deviation	simulated	video	deviation
S01	29.9	31.2	-1.3	24.6	27.1	-2.5	-5.1	-7.8	2.7
S02	30.2	31.6	-1.4	27.3	31.2	-3.9	-9.0	-4.8	-4.2
S03	30.0	32.3	-2.3	26.7	31.9	-5.2	-4.1	-6.0	1.9
S04	31.2	32.9	-1.7	26.6	27.9	-1.3	-4.3	-6.2	1.9
S05	28.6	30.5	-1.9	22.8	29.1	-6.3	-13.6	-5.0	-8.6
S06	30.3	32.7	-2.4	27.5	31.9	-4.4	-2.2	-6.4	4.2
S07	31.3	32.8	-1.5	26.1	30.2	-4.1	-7.5	-3.3	-4.2
S08	31.0	33.3	-2.3	28.0	32.5	-4.5	-1.1	-2.5	1.4
S09	30.4	31.9	-1.5	25.2	31.6	-6.4	-2.1	-1.3	-0.8
S10	29.2	31.1	-1.9	23.2	27.1	-3.9	-15.5	-7.0	-8.5
Mean absolute deviation	1.8°			4.3°			3.9°		

At C0, the tilt angles from the simulation and video have a mean absolute deviation of about 3.0° for B. Reilly and 3.9° for S. Smith. The time history of the simulated tilt angles during the approach phase are shown in Figures 5.9 and 5.10. The tilt angles obtained from the video are also included in Figures 5.9 and 5.10 for comparison.

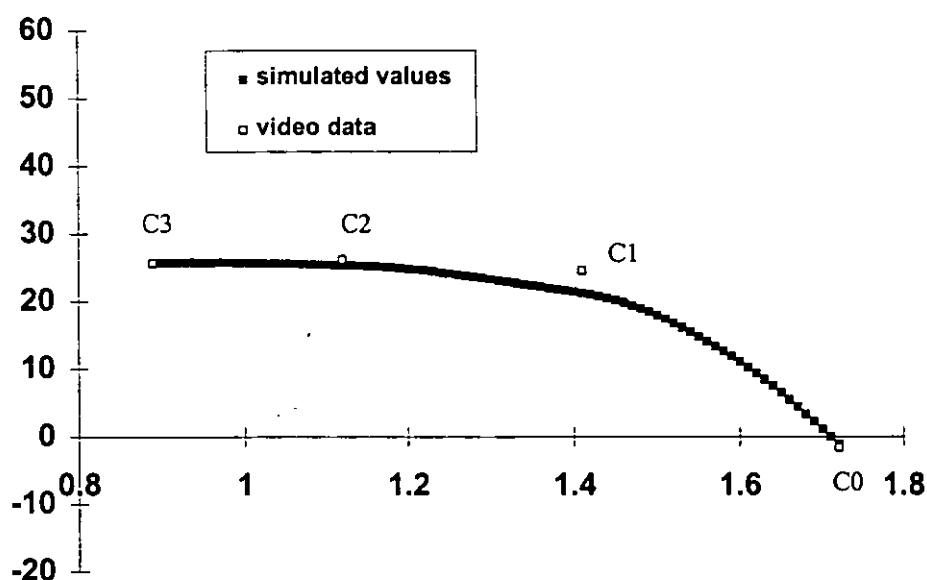


Figure 5.9. The tilt angles of the approach in jump B02.

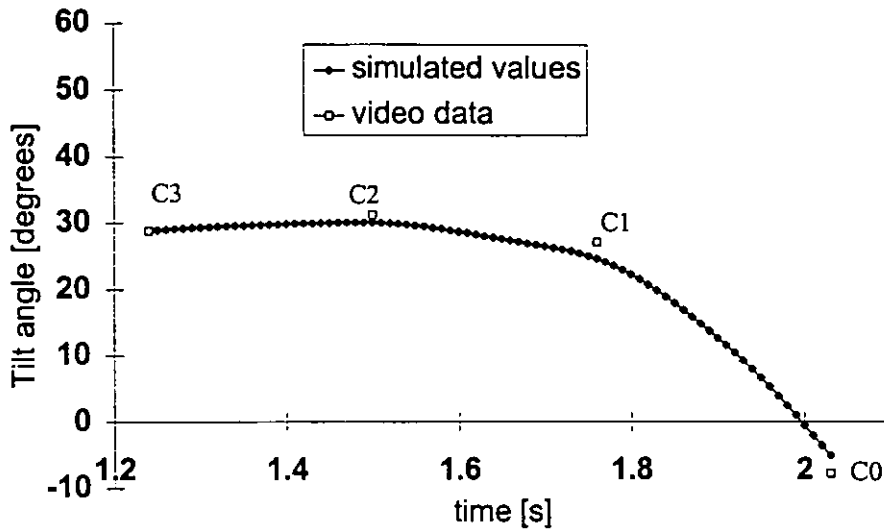


Figure 5.10. The tilt angles of the approach in jump S01.

Angular momentum about the mass centre

At the end of the approach phase, the angular momentum L_x of the mass centre about the horizontal axis x is:

$$L_x = L_i \cos \psi + L_j \sin \psi$$

where L_i and L_j are the angular momentum about the i and j axes of the moving frame $[i, j, k]$ and ψ is the twist angle about axis k . Since $\cos \psi$ is small because at the end of the approach phase ψ is about 90° and L_i also is small (for example, for B. Reilly, L_i at the end of approach phase ranges from 1.7 to 2.8 $\text{kgm}^2\text{s}^{-1}$). L_x at this point can be expressed as:

$$L_x = L_j \sin \psi.$$

But $L_j = I_2 \dot{\theta}$ where I_2 is the moment of inertia about the frontal axis of the body and $\dot{\theta}$ is the final tilt angular velocity of the approach phase, therefore

$$L_x = I_2 \dot{\theta} \sin \psi.$$

Since the angular momentum of the mass centre at the instant of toeoff and that during the flight phase are equal, the angular momentum L_{xF} of the mass centre about the horizontal x axis in the flight phase (which can be obtained from the video data using the software program SIMU) can be used to compare with L_x obtained from the model. In order to compare the values of L_x and L_{xF} between different jumpers, these values can be divided by I_2 to be normalised. The normalised values of L_x and L_{xF}

obtained from the model at the end of the approach phase and the flight phase are presented in Tables 5.17 and 5.18. There is a good agreement in the normalised values of the angular momentum about the x-axis for B. Reilly and S. Smith obtained from either the video or the model. However, the angular momentum about the x-axis obtained from the model was about 94% of the value obtained from the video data.

Table 5.17. Angular momentum values from video and model (B. Reilly)

	L_{xF} with std error [kgm ² s ⁻¹]	Normalised L_{xF} (nL_{xF}) [ms ⁻¹]	Normalised L_x (nL_x) [ms ⁻¹]	Proportion (nL_x / nL_{xF})
B01	46.3 ± 1.3	2.9	2.3	0.79
B02	46.7 ± 1.6	2.8	2.1	0.75
B03	41.4 ± 1.2	2.7	2.6	0.96
B04	41.2 ± 1.1	2.7	3.2	1.18
B05	46.7 ± 1.0	3	3.2	1.06
Mean	44.42	2.8	2.7	0.95

Table 5.18. Angular momentum values from video and model (S. Smith)

	L_{xF} with std error [kgm ² s ⁻¹]	Normalised L_{xF} (nL_{xF}) [ms ⁻¹]	Normalised L_x (nL_x) [ms ⁻¹]	Proportion (nL_x / nL_{xF})
S01	33.4 ± 1.1	3.0	2.7	0.90
S02	30.8 ± 1.9	2.9	3.1	1.06
S03	30.3 ± 1.6	2.9	2.6	0.89
S04	27.0 ± 1.6	2.5	2.4	0.86
S05	33.9 ± 1.6	3.2	3.2	0.99
S06	27.0 ± 1.5	2.5	2.7	1.08
S07	28.5 ± 0.9	2.8	2.7	0.96
S08	29.3 ± 1.6	2.8	2.4	0.85
S09	32.4 ± 1.2	3.0	2.3	0.75
S10	32.2 ± 1.2	2.9	2.9	0.99
Mean	30.5	2.9	2.7	0.93

Sensitivity analyses

The sensitivity of the model output is tested for changes in the initial tilt angle, initial tilt angular velocity, the different time interval for the simulation, the approach speed and the mass centre height at take-off.

Initial tilt angle

The model output was tested for sensitivity to changes in the initial tilt angles. The initial tilt angles of the approaches changed by amounts equivalent to the precision estimates (0.7°) of the tilt angles. The sensitivity of the model to changes in initial tilt angles of two typical approaches from each jumper are presented in Table 5.19.

Table 5.19. The sensitivity of the model to the initial tilt angle

	initial θ	final θ	final $-\dot{\theta}$ [rad.s ⁻¹]
Pretest (B01)	24.9°	-4.2°	2.30
Increased initial θ	25.6°	-2.5°	2.23
Decreased initial θ	24.2°	-5.8°	2.36
Pretest (B02)	25.6°	-0.8°	2.11
Increased initial θ	26.3°	0.9°	2.05
Decreased initial θ	24.9°	-2.4°	2.18
Pretest (S01)	28.8°	-5.1°	2.68
Increased initial θ	29.5°	-3.2°	2.60
Decreased initial θ	28.1°	-7.0°	2.75
Pretest (S02)	28.3°	-9.0°	3.13
Increased initial θ	29.0°	-7.0°	3.04
Decreased initial θ	27.6°	-11.0°	3.21

This test shows that an error of 0.7° in the initial tilt angle would cause a variation of about 2° in the final tilt angle and a change in the final tilt velocity of about 3%. From this test, the model is shown to be moderately sensitive to changes in

the initial tilt angle. This implies that measurement errors in the initial tilt angle would lead to larger errors in the final tilt angle.

Initial tilt velocity

The model was tested for sensitivity to changes in the initial tilt velocity $\dot{\theta}_0$. The $\dot{\theta}_0$ of the model is obtained by calculating the first derivative of the fourth degree polynomial function of tilt angles and their associated times (as described in section *Tilt angular velocity*, Chapter 4.). Therefore, to test for sensitivity to changes in $\dot{\theta}_0$, simulations were performed by using tilt velocities obtained using other polynomial functions. The results of the test using two approaches from each jumper simulated with $\dot{\theta}_0$ obtained using different polynomial functions are presented in Table 5.20.

Table 5.20 The sensitivity of the model to the initial tilt velocity

	$\dot{\theta}_0$ [rad.s ⁻¹]	final θ	final $-\dot{\theta}$ [rad.s ⁻¹]
Pretest (B01)	0.06	-4.2°	2.30
3 rd degree function for $\dot{\theta}_0$	0.05	-5.2°	2.34
Pretest (B05)	0.16	-2.0°	3.24
3 rd degree function for $\dot{\theta}_0$	0.15	-3.1°	3.30
Pretest (S01)	0.20	-5.1°	2.68
5 th degree function for $\dot{\theta}_0$	0.18	-6.6°	2.74
Pretest (S02)	0.22	-9.0°	3.13
5 th degree function for $\dot{\theta}_0$	0.20	-10.5°	3.17

The results shown that if the $\dot{\theta}_0$ is changed by about 0.01 rad.s⁻¹ the final tilt angle will vary by about 1° and the final tilt velocity will change by about 2%. From this test, the model is shown to be moderately sensitive to changes in the initial tilt angular velocity.

Time interval in simulation

The model was tested for sensitivity to changes in the time intervals for the numerical integration. Simulations were performed by altering the value of the time interval in the input data of the model. The results of two approaches from each jumper simulated with 0.005 and 0.001s time intervals are shown in Table 5.18.

The results show that with the time interval reduced to 0.005 and 0.001s the final tilt and tilt velocity did not change much ($< 1.1^\circ$ and $< 0.08 \text{ rad.s}^{-1}$). With the video data (that are used as input values of the model and the evaluation of the model) having been collected at 50 Hz or 0.02s interval, and with these time intervals sensitivity results, the use of a 0.01s time interval for numerical integration of the model was thought to be appropriate.

Table 5.21. The sensitivity of the model to the time interval for numerical integration

	time interval	final θ	final $-\dot{\theta} [\text{rad.s}^{-1}]$
B01	0.01	-4.2°	2.30
B01	0.005	-4.6°	2.32
B01	0.001	-4.9°	2.34
B02	0.01	-0.8°	2.11
B02	0.005	-1.1°	2.14
B02	0.001	-1.2°	2.15
S01	0.01	-5.1°	2.68
S01	0.005	-5.9°	2.72
S01	0.001	-6.2°	2.76
S02	0.01	-9.0°	3.13
S02	0.005	-9.8°	3.17
S02	0.001	-10.0°	3.20

Approach Speed

The model was tested for sensitivity to changes in approach speed. The approach speed can be represented by the foot velocity in the model. Therefore, to test

for sensitivity to changes in approach speed or foot velocity, simulations were performed by using the error estimates of foot velocity to vary the foot velocity at C0. Since the error estimates of foot velocity were small, in order to vary the foot velocity, the time interval of the simulation was set at 0.001s. The take-off time was changed in order to obtain the necessary change in foot velocity. The results of the test using two approaches from each jumper simulated with the different foot velocities are presented in Table 5.22.

Table 5.22. The sensitivity of the model to approach speed

	final foot velocity [ms^{-1}]	final θ	final $-\dot{\theta}$ [rads^{-1}]
Pretest (B01)	7.72	-4.9°	2.34
Reduced foot velocity	7.67	-4.9°	2.33
Increased foot velocity	7.76	-5.1°	2.36
Pretest (B02)	7.75	-1.2°	2.15
Reduced foot velocity	7.71	-1.0°	2.13
Increased foot velocity	7.79	-1.3°	2.17
Pretest (S01)	8.27	-6.2°	2.76
Reduced foot velocity	8.23	-5.7°	2.73
Increased foot velocity	8.32	-6.6°	2.78
Pretest (S02)	8.04	-10.0°	3.20
Reduced foot velocity	7.99	-9.4°	3.18
Increased foot velocity	8.09	-10.5°	3.24

The results indicate that the measurement errors in the foot velocity have little effect on the final tilt or tilt velocity of the simulation. In other words the model is not sensitive to small changes in the approach speed.

Mass centre height h

The model was tested for sensitivity to changes in mass centre height. This test was conducted with simulations performed using the error estimates of the h distances

(distance between the mass centre and the foot) to vary h at C0. The results of the test using two approaches from each jumper simulated with the different h distances are presented in Table 5.23.

Table 5.23. Sensitivity of the model to small changes in mass centre distance h

	h	final θ	final $-\dot{\theta}$ [rad.s ⁻¹]
Pretest (B01)	1.311	-4.2°	2.30
Increased h	1.316	-4.1°	2.29
Reduced h	1.306	-4.2°	2.30
Pretest (B02)	1.359	-0.8°	2.11
Increased h	1.364	-0.7°	2.10
Reduced h	1.354	-0.8°	2.12
Pretest (S01)	1.255	-5.1°	2.68
Increased h	1.260	-5.1°	2.66
Reduced h	1.250	-5.1°	2.69
Pretest (S02)	1.314	-9.0°	3.13
Increased h	1.319	-9.0°	3.11
Reduced h	1.309	-9.1°	3.15

The results show that the model is not sensitive to measurement errors in the mass centre height.

Summary

The mean precision estimates of digitising the 15 landmarks of the body range from 18 mm to 23 mm for the different jumps. The estimates of foot placement, foot approach speed and mass centre to foot distance had high precision values. The three-dimensional reconstruction accuracy errors had an overall rms value of 6.7 mm for markers on the calibration poles and 17.8 mm for the landmarks on the athletes .

The centre of pressure measurement of the pressure insole was in good agreement with the values obtained from the force plate.

The tilt angles at C0 obtained from the model and from the video data had an absolute mean deviation of 3.0° for B. Reilly and 3.9° for S. Smith. The angular momentum of the mass centre about the x-axis calculated from the model was 94% of that calculated from the video data. The model appeared to have simulated the approach with reasonable accuracy

The model was also found to be sensitive to measurement errors of the initial tilt angle and angular velocity. This implies that the errors in the results of the simulations may be largely due the errors in the input of the initial tilt angle and angular velocity to the model.

Conclusion

Image analysis systems

The questions raised in Chapter 1 on the image analysis system can be addressed with the findings presented in this chapter. The features of a video digitising system that affect the accuracy in image analysis are radial distortion, picture resolution and the measuring resolution. Therefore, accuracy in image analysis using a video digitising system can be improved with the following conditions:

1. Radial distortion correction (e.g. the procedure described in Chapter 3) for the video digitising system is used in the reconstruction of the digitised data.
2. High picture resolution recording format (e.g. the Hi-8 or sVHs format) is used in the recording of the movement to be analysed
3. A high resolution video digitising system (such as the Apex Target video digitising system) is used in digitising the required landmarks.

The results have shown that the Apex Target video digitising system using Hi-8 recording format and lens distortion correction produced accuracy comparable to a 16 mm film system.

In order to span the curved approach in high jumping, one camera was placed such that its optical axis is almost normal to the centre of the high jump cross bar. The second camera was placed such that the optical axis bisected the axes normal and

parallel to the high jump cross bar. The reconstruction accuracy of the reference frame and the digitising error estimates indicate that this configuration of camera placement would provide a reasonable accuracy for image analysis.

Model

The APPROACH model simulated the tilt angles with mean absolute deviation from the video data at C0 of about 3° to 4° and also estimated the angular momentum of the mass centre about the x axis to be about 94% of the value obtained from the video data. These results indicate that the model simulates the high jump approach with reasonable accuracy.

The model was also found to be sensitive to measurement errors of the initial tilt angle and angular velocity. This implies that the accuracy of the simulations is largely dependent on the accuracy of the input values of initial tilt angle and angular velocity to the model.

Chapter 6

THE CURVED APPROACH OF THE FOSBURY FLOP

INTRODUCTION

This chapter investigates the contribution of the curved approach in the Fosbury Flop using the image analysis and the simulation model. In addition, this chapter also presents the summary of findings for the entire study.

IMAGE ANALYSIS

Initially the curved approach was considered to be no more than an idiosyncrasy of Dick Fosbury. However, with the curved approach still remaining as the preferred approach among elite jumpers, it can be expected to be more advantageous than a straight approach in high jumping. In order to understand the contribution of the curved approach, the characteristics of the curved approach need to be examined.

Radius of the curved approach

The radii of the curves through the foot placement and mass centre positions at midfoot contact were calculated by fitting a circle through three consecutive points on each curve. (Note that the radii of these curves are not calculated in the same way as for the foot curve in the model). With six points on each curve, a total of four radii could be calculated. The changes in the radii of the curves were analysed using analysis of variance with repeated measures. If the changes were significant, post hoc Tukey tests were used to analyse the differences.

The mean foot placement and mass centre curves (Figure 6.1) indicate that the foot placement curve tightened to meet the mass centre curve at the end of the approach (C0). Figure 6.2 also shows that the corresponding radius of the mean foot placement curve was reduced from about 12 to 7 m for both the jumpers. The changes in radius of the foot placement curves were also found to be significant ($p < 0.01$) for both the jumpers. For B. Reilly, the radius of the foot placement curve at C1 was found to be significantly smaller ($p < 0.01$) than the other radii at C2, C3 and C4. For S. Smith, the radius at C3 of the foot placement curve was found to be significantly larger ($p < 0.01$) than the other radii of C4, C2 and C1. The radii of the foot placement curves at the different foot

contacts indicate that B. Reilly indeed tightened the foot placement curve at C1 while S. Smith tightened the curve at C2.

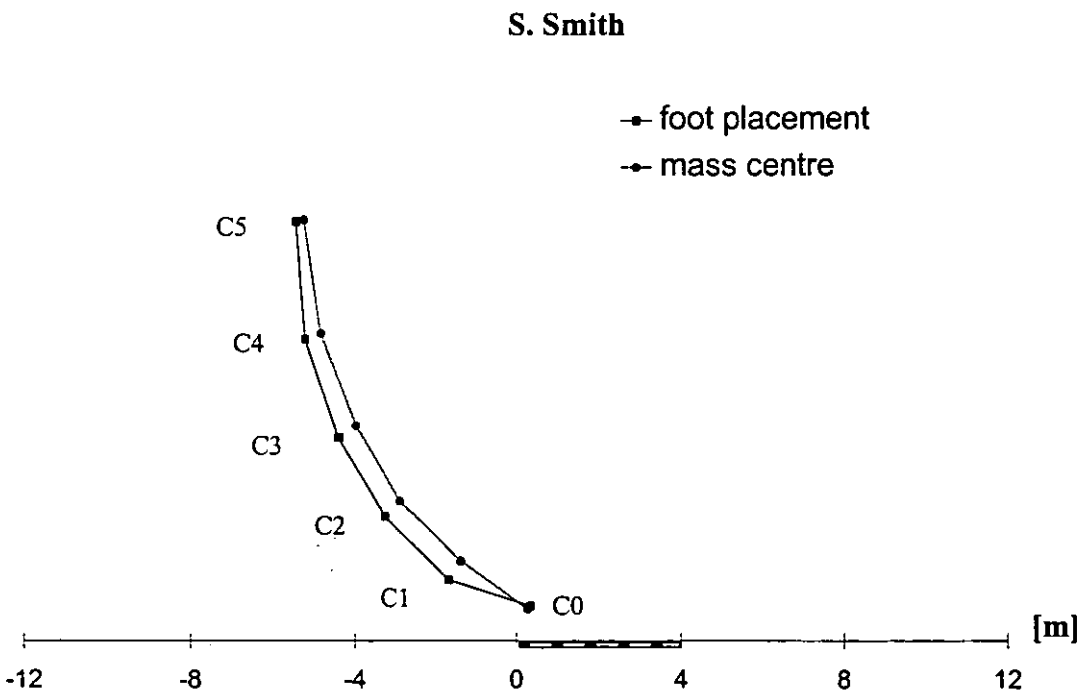
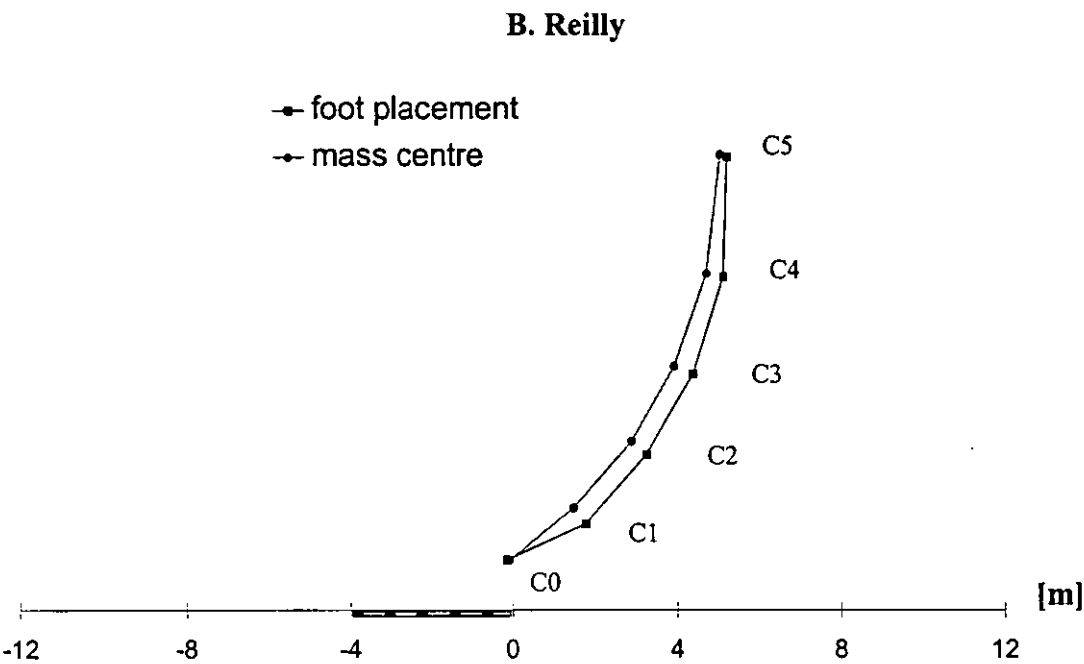


Figure 6.1. Foot and mass centre paths.

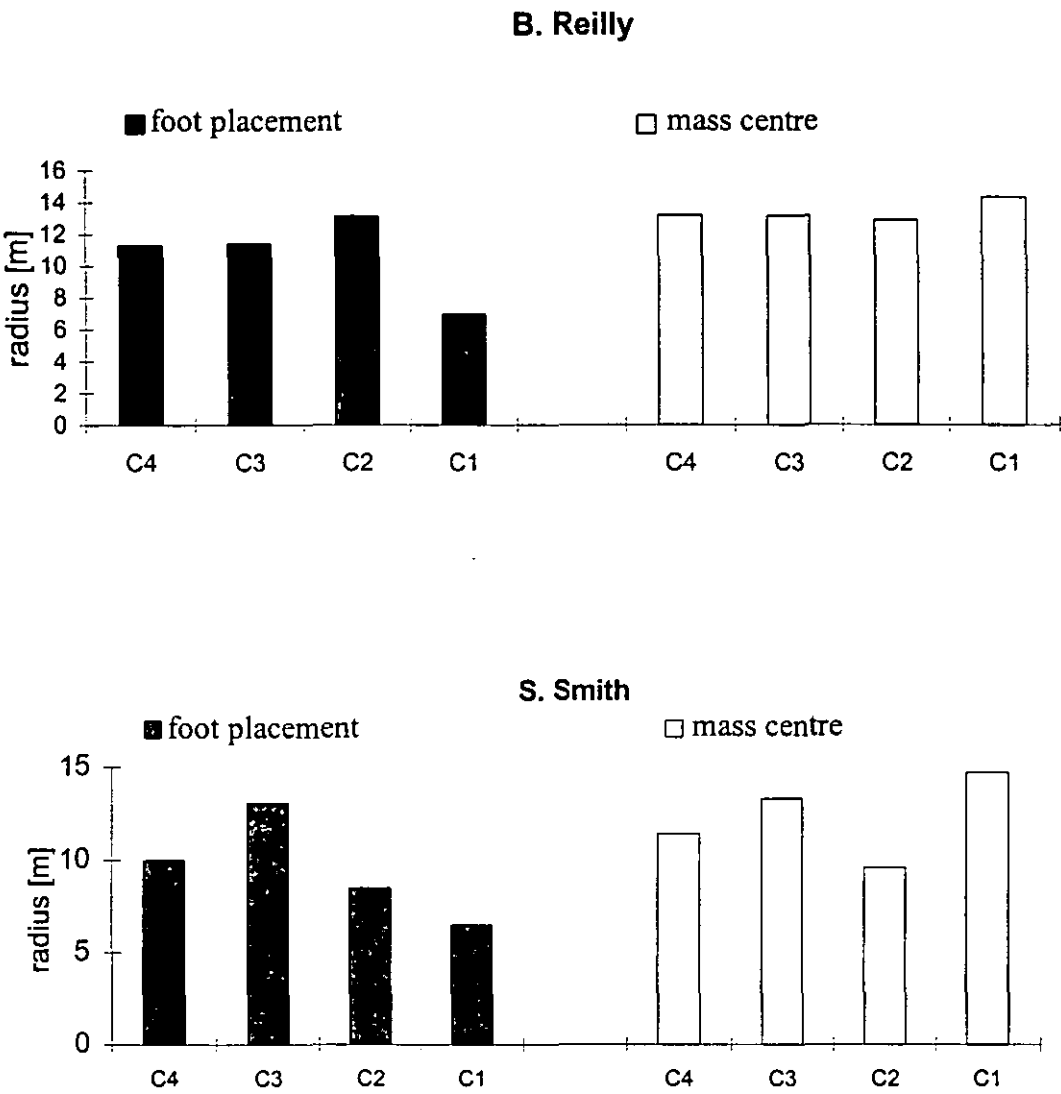


Figure 6.2. Radii of curves through the foot placements and mass centre positions.

For B. Reilly, the changes in the radius of the mass centre curves were found to be not significant. However, the changes in radius of the mass centre curves were found to be significantly different ($p < 0.01$) for S. Smith. This implies that from C4 to C1, the radius of the curve through the mass centre of B. Reilly was almost constant whilst the radius of the curve through the mass centre for S. Smith was changing at each foot contact. The radius of the mass centre is presumably a consequence of the different radius histories of the foot curves. Since S. Smith tends to approach his jump with a varied radius of the foot curve, it can be expected that there will be more variation in his radius of the mass centre curve than that of B. Reilly.

Tilt angle

The tilt angle for each foot contact of the approach is presented in Figure 6.3. The mean inward tilt angle in the approaches shown in Figure 6.3 shows an abrupt decrease between the penultimate foot contact and the last foot contact for both the jumpers. It should be noted that side somersault rotation occurs as the inward tilt angle is reduced during the take-off.

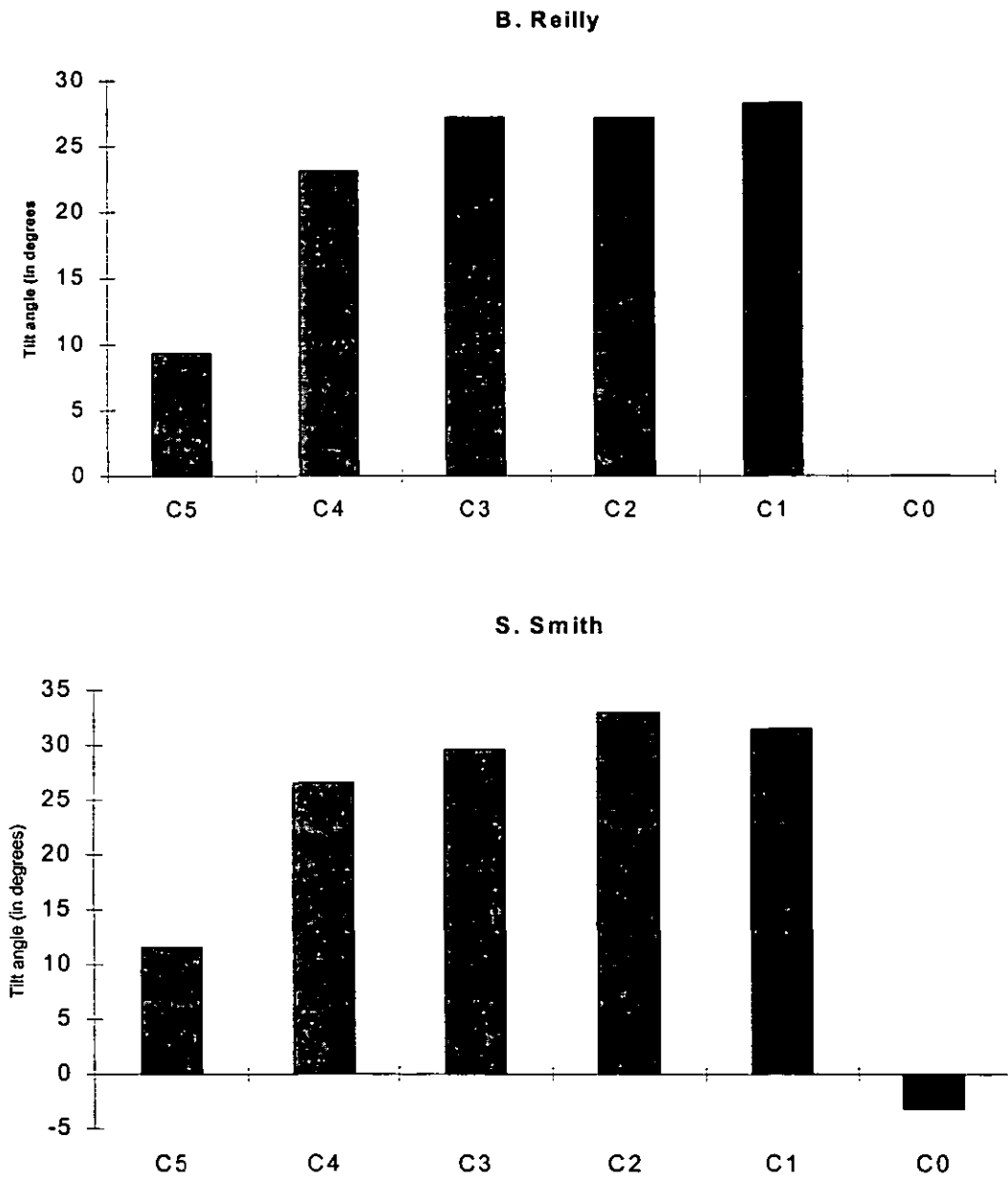


Figure 6.3. Mean inward tilt angles.

Image analysis of the curved approach

From the results of the image analysis, it can be concluded that towards the end of the approach the foot curve tightens and the inward tilt decreases so that the jumper attains a vertical take-off position and obtains the required somersault rotation for the bar clearance. The image analysis can not establish a causal connection between the tightening of the curved approach and the production of the somersault rotation. A simulation model of the curved approach is required to do this and to address the question raised in Chapter 1 on the contribution of the curved approach.

MODEL

Radius of the foot curve

In order to simulate the curved approach, the radius of the foot placement curve must be calculated at each foot ground contact. The method by which these radii of the foot curves were calculated for the model are described in the section on *Calculations of ψ and R* in Chapter 4. The mean values of the calculated radii of the foot curves at each contact are presented in Figure 6.4.

It should be noted that this method gives smaller radii during the contact phases than during the aerial phases and provides a radius at any point of the foot curve. The method used in the image analysis, however, makes no distinction between contact and aerial phases and only gives a value for the radius at four contacts (C4-C1).

The mean radius of the foot curves calculated for the model for the different trials of each athlete indicate that at C0 the radius is about 2 to 3 m. It can be seen that the radius of the foot curve calculated for the model decreases with each successive foot contact (C3 to C0) for S. Smith while the foot curves for B. Reilly decreases from C2 to C0. However for both jumpers, the foot curve radius was shown to be decreasing towards the end of the approach. The patterns of the change in the radius of the foot curve calculated for the model are similar to those found in the image analysis.

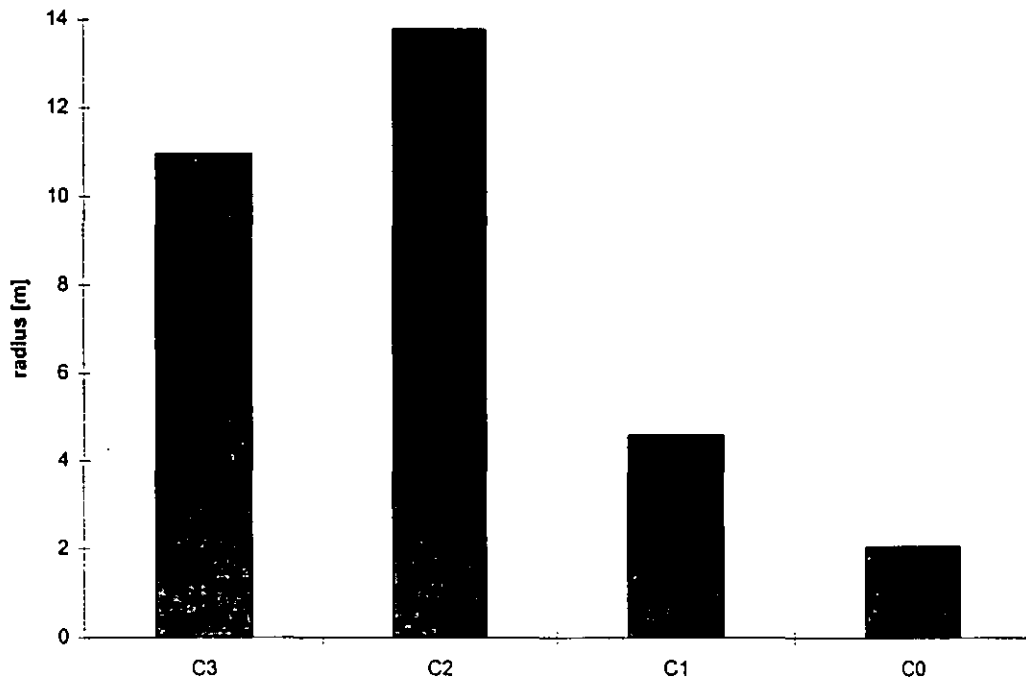
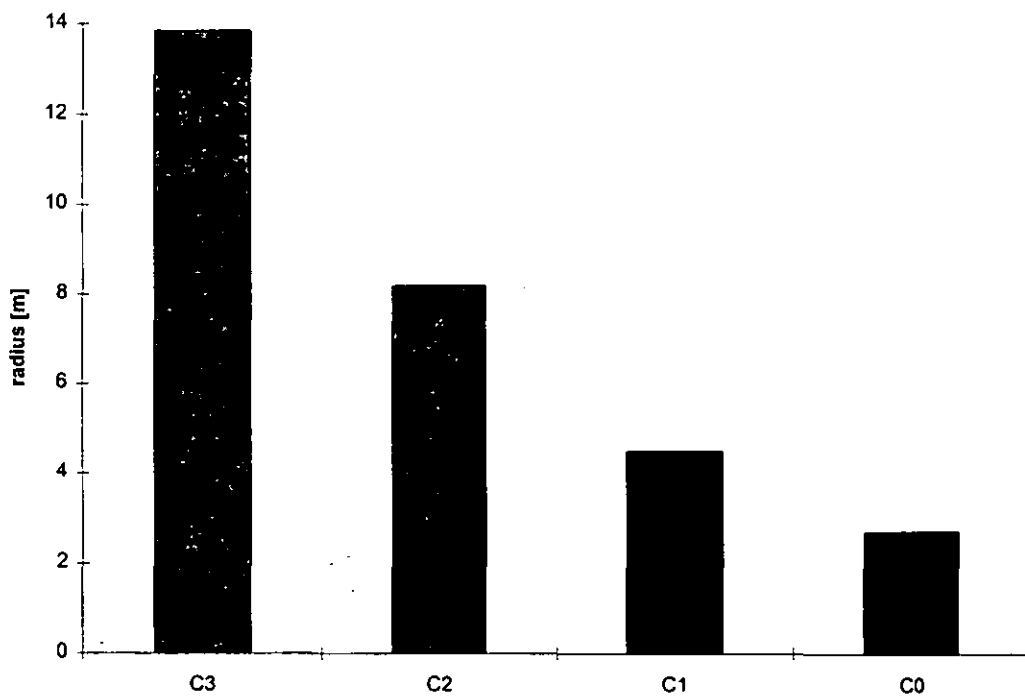
B. Reilly**S. Smith**

Figure 6.4. Radii of the foot curve from the model.

Experiments

Radius of the foot curve

The effect of tightening the foot curve can be demonstrated by using the following experiment with the model. Two curved approaches from each jumper were simulated and the results of the simulations were noted as pretest values. The same approaches were modified with the input values of foot placement coordinates at C0 increased by a small distance (7 cm) in the y horizontal direction so that the radii of the foot curves was decreased by about 10% at C0. The values of the final tilt angles and tilt angular velocities of these experimental simulations were compared with the pretest values to examine the effect of the ‘tightening’ of the foot curve.

Table 6.1. The effect of changing radius of the foot curve

	Radius [m]	final θ	final $-\dot{\theta}$ [rad.s ⁻¹]
Pretest (B01)	3.2	-4.2°	2.30
Reduced radius	2.8	-6.0°	2.54
Pretest (B02)	3.0	4.0°	2.11
Reduced radius (10%)	2.7	2.1°	2.40
Pretest (S01)	2.9	-5.1°	2.68
Reduced radius (10%)	2.6	-7.7°	2.99
Pretest (S02)	2.35	-9.0°	3.13
Reduced radius (10%)	2.15	-12.3°	3.58

The results of this experiment show that, when the radius at C0 is reduced by about 10%, the final tilt angle is reduced by about 2° to 3° and the magnitude of the final tilt angular velocity is increased by about 10%. Thus tightening the radius reduces the final tilt angle and the tilt angular velocity. This means that more somersault rotation can be generated by “stepping in” more towards the centre of the approach curve at the final foot placement.

Foot velocity

In addition to the radius of the foot placement, the approach speed during take-off may also affect rotation in high jumping. In order to examine the effect of approach speed during take-off the following experiment was performed with the model. The final tilt angle and tilt angular velocity of a simulated approach were noted. The simulation was performed again with the input value of the totoff time at C0 decreased such that the foot velocity would be increased by about 5%. The final tilt angle and tilt angular velocity of this modified input simulation were compared with the pretest values to examine the effect of increasing the foot velocity. This experiment was carried out with two approaches from each of the jumpers.

Table 6.2. The effect of the foot approach speeds on rotation

	foot speed [ms^{-1}]	final θ	final $-\dot{\theta}$ [rad.s^{-1}]
Pretest (B01)	7.72	-4.2°	2.30
Increased speed	8.14	-6.7°	2.57
Pretest (B02)	7.75	-0.8°	2.11
Increased speed	8.18	-4.3°	2.31
Pretest (S01)	8.27	-5.1°	2.68
Increased speed	8.59	-8.7°	2.78
Pretest (S02)	8.04	-9.8°	3.13
Increased speed	8.38	-13.2°	3.31

In the experimental simulation, when the foot velocity was increased by 5%, the tilt angle was reduced by about 3° to 4° and the magnitude of the tilt angular velocity increased by about 8%. These results indicate that an increased approach speed reduces the final tilt angle and tilt angular velocity. This means that more somersault rotation can be generated by increasing the approach speed towards the end of the approach.

Physical attributes of the jumpers

To assess the contribution of the physical characteristics between athletes in the curved approach, the following experiments were conducted. Two approaches performed

B. Reilly were simulated with the values for the moments of inertia, weight and mass centre to foot distance of S. Smith. The results were compared with the original simulation of B. Reilly's approach. Similarly, two approaches of S. Smith were simulated with the data of the physical characteristics of B. Reilly and the results were compared with the original simulation of S. Smith's approach.

The results show that using S. Smith's physical data in a typical approach of B. Reilly, produces more rotation into the bar. However, using the physical characteristics of B. Reilly to simulate an approach of S. Smith results in less rotation towards the bar. These results might be expected because the stature of S. Smith is smaller than that of B. Reilly. In short, athletes with a larger physical stature would require a smaller radius of approach especially at C0 in order to obtain the required rotation for bar clearance.

Table 6.3. The effect of using different anthropometric data

	final θ	final $-\dot{\theta}$ [rad.s ⁻¹]
Pretest (B01)	-4.2°	2.30
Using S. Smith's anthropometric data	-6.9°	2.41
Pretest (B02)	-0.8°	2.11
Using S. Smith's anthropometric data	-4.1°	3.36
Pretest (S01)	-5.1°	2.68
Using B. Reilly's anthropometric data	-1.2°	2.45
Pretest (S02)	-9.0°	3.13
Using B. Reilly's anthropometric data	-2.7°	2.93

MECHANICS UNDERLYING THE CURVED APPROACH

Terms in the tilt angular acceleration equation

The following equation is the tilt angular acceleration equation (24) of the model:

$$\begin{aligned}
 \ddot{\theta} = & mg(h\sin\theta - d)/(I_2 + mh(h-d\sin\theta)) \\
 & - [2mh\dot{h}\dot{\theta} - m\dot{h}d\sin\theta - mh\dot{d}\sin\theta - mh\dot{\theta}d\cos\theta]\dot{\theta}/(I_2 + mh(h-d\sin\theta)) \\
 & - (\dot{I}_2\dot{\theta})/(I_2 + mh(h-d\sin\theta)) - (m v_f^2 r h\cos\theta)/R^2(I_2 + mh(h-d\sin\theta)) \\
 & - (m f h v_f\dot{\theta}\sin\theta)/R(I_2 + mh(h-d\sin\theta)) - (L_f v_f)/R(I_2 + mh(h-d\sin\theta))
 \end{aligned}$$

The mean values of the different terms during each foot contact of a typical simulation are presented in Tables 6.4 to 6.7.

Table 6.4. The mean values [in rad.s^{-2}] of the terms in $\ddot{\theta}$ equation (for B01)

B01	C2	C1	C0
$mg(h\sin\theta - d)/(I_2 + mh(h-d\sin\theta))$	3.0	2.2	0.1
$-(m v_f^2 r h \cos\theta)/R^2(I_2 + mh(h-d\sin\theta))$	-5.2	-8.5	-11.7
$\frac{[2mh\dot{h}\dot{\theta} - m\dot{h}d\sin\theta - m\dot{h}d\sin\theta - mh\dot{\theta}d\cos\theta]\dot{\theta}}{(I_2 + mh(h-d\sin\theta))}$	0.1	-0.4	4.4
$-(\dot{I}_2 \dot{\theta})/(I_2 + mh(h-d\sin\theta))$	0.0	-0.1	0.1
$-(m f h v_f \dot{\theta} \sin\theta)/R(I_2 + mh(h-d\sin\theta))$	0.0	0.1	-0.2
$-(L_i v_f)/R(I_2 + mh(h-d\sin\theta))$	0.0	0.1	0.0
$\ddot{\theta}$	-2.3	-6.6	-7.3

Table 6.5. The mean values [in rad.s^{-2}] of the terms in $\ddot{\theta}$ equation (for B02)

B02	C2	C1	C0
$mg(h\sin\theta - d)/(I_2 + mh(h-d\sin\theta))$	3.1	2.4	0.6
$-(m v_f^2 r h \cos\theta)/R^2(I_2 + mh(h-d\sin\theta))$	-4.6	-8.3	-12.2
$\frac{[2mh\dot{h}\dot{\theta} - m\dot{h}d\sin\theta - m\dot{h}d\sin\theta - mh\dot{\theta}d\cos\theta]\dot{\theta}}{(I_2 + mh(h-d\sin\theta))}$	0.1	-0.7	5.5
$-(\dot{I}_2 \dot{\theta})/(I_2 + mh(h-d\sin\theta))$	0.0	-0.1	0.1
$-(m f h v_f \dot{\theta} \sin\theta)/R(I_2 + mh(h-d\sin\theta))$	0.0	0.1	-0.3
$-(L_i v_f)/R(I_2 + mh(h-d\sin\theta))$	0.0	0.0	0.0
$\ddot{\theta}$	-1.4	-6.6	-6.3

Table 6.6. The mean values [in rad.s⁻²] of the terms in $\ddot{\theta}$ equation (for S01)

S01	C2	C1	C0
$mg(h\sin\theta - d)/(I_2 + mh(h-d\sin\theta))$	4.1	3.1	0.2
$-(m v_f^2 r \hbar \cos\theta)/R^2(I_2 + mh(h-d\sin\theta))$	-7.3	-12.6	-16.8
$-\frac{[2mh\dot{h}\dot{\theta} - m\dot{h}d\sin\theta - m\dot{h}d\sin\theta - m\dot{h}\dot{\theta}d\cos\theta]\dot{\theta}}{(I_2 + mh(h-d\sin\theta))}$	0.1	-0.6	11.0
$-(\dot{I}_2 \dot{\theta})/(I_2 + mh(h-d\sin\theta))$	0.0	-0.3	0.1
$-(m f h v_f \dot{\theta} \sin\theta) / R(I_2 + mh(h-d\sin\theta))$	0.1	0.3	-0.4
$-(L_i v_f)/R(I_2 + mh(h-d\sin\theta))$	0.0	0.1	0.0
$\ddot{\theta}$	-3	-10	-5.9

Table 6.7. The mean values [in rad.s⁻²] of the terms in $\ddot{\theta}$ equation (for S02)

S02	C2	C1	C0
$mg(h\sin\theta - d)/(I_2 + mh(h-d\sin\theta))$	4.3	3.3	-0.2
$-(m v_f^2 r \hbar \cos\theta)/R^2(I_2 + mh(h-d\sin\theta))$	-6.3	-11.4	-19.1
$-\frac{[2mh\dot{h}\dot{\theta} - m\dot{h}d\sin\theta - m\dot{h}d\sin\theta - m\dot{h}\dot{\theta}d\cos\theta]\dot{\theta}}{(I_2 + mh(h-d\sin\theta))}$	0.1	-1.8	12.1
$-(\dot{I}_2 \dot{\theta})/(I_2 + mh(h-d\sin\theta))$	0.0	-0.2	0.2
$-(m f h v_f \dot{\theta} \sin\theta) / R(I_2 + mh(h-d\sin\theta))$	0.0	0.3	-0.6
$-(L_i v_f)/R(I_2 + mh(h-d\sin\theta))$	0.0	0.1	0.0
$\ddot{\theta}$	-1.9	-9.7	-7.6

The first term of the equation:

$$mg(h\sin\theta - d)/(I_2 + mh(h-d\sin\theta))$$

impedes the reduction of the inward tilt angle. This term has a value of about 4 rad.s⁻² for the both jumpers when the tilt angle is maximum. The value of this term is reduced to near zero (0.6 to -0.2) at the end of the approach phase when the jumpers are almost in the 'upright' position.

The second term of the equation:

$$-(m v_f^2 r \hbar \cos\theta)/R^2(I_2 + mh(h-d\sin\theta))$$

represents the main generator of tilt rotation. The value of this term is largely controlled by the radius R of foot curve and the foot velocity v_f . The mean value of this term was about -6 rad.s^{-2} when the tilt angle was maximum and at the end of the approach where the radius of the foot curve was smallest these values changed by about two or three times to about -15 rad.s^{-2} .

The other terms

$$\begin{aligned}
 & - [2mh \dot{h} \dot{\theta} - m \dot{h} d \sin \theta - mh \dot{d} \sin \theta - mh \dot{\theta} d \cos \theta] \dot{\theta} / (I_2 + mh(h-d \sin \theta)) \\
 & - (\ddot{I}_2 \dot{\theta}) / (I_2 + mh(h-d \sin \theta)) \\
 & - (m v_f^2 r h \cos \theta) / R^2 (I_2 + mh(h-d \sin \theta)) \\
 & - (m f h v_f \dot{\theta} \sin \theta) / R (I_2 + mh(h-d \sin \theta)) \\
 & - (L_i v_f) / R (I_2 + mh(h-d \sin \theta))
 \end{aligned}$$

have values close to zero throughout the simulation except for the third term: -

$$- [2mh \dot{h} \dot{\theta} - m \dot{h} d \sin \theta - mh \dot{d} \sin \theta - mh \dot{\theta} d \cos \theta] \dot{\theta} / (I_2 + mh(h-d \sin \theta)) ,$$

where the values at the end of the approach were the same magnitude as those of the second term but with the opposite sign. This implies that the second and the third terms of the $\ddot{\theta}$ equation would neutralise each other towards the end of final foot contact. The increase in the value of the third term towards the end of the approach is largely due to the increase in \dot{h} , the rate of the change of the projected distance between the mass centre and the foot during the final contact. This implies that the increase in the mass centre height has the effect of impeding the tilt rotation.

From the examination of the terms of the tilt angular acceleration, the main factors that affect the tilt or the somersault rotation are the foot velocity v_f , the mass centre height h and the radius R of the foot curve at C0. If a high jumper needs to alter the somersault rotation in order to have a successful jump, changing the radius of the approach at C0 would be a more practical approach than trying to change the mass centre height or the approach speed at take-off.

In short, running a curve is like cycling around a corner. By turning the front wheel into the curve, the cyclist rotates away from the centre of the curve (Figure 4.1). This is analogous to tightening the foot placement curve in the high jump approach which causes the somersault rotation (Figures 6.5 and 6.6).

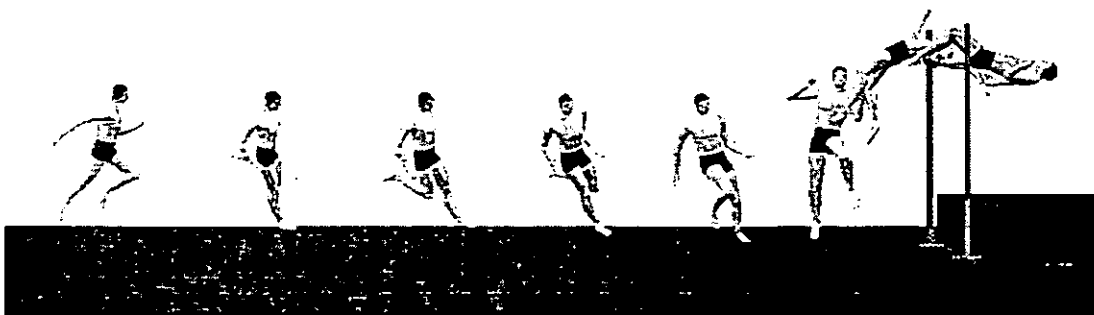
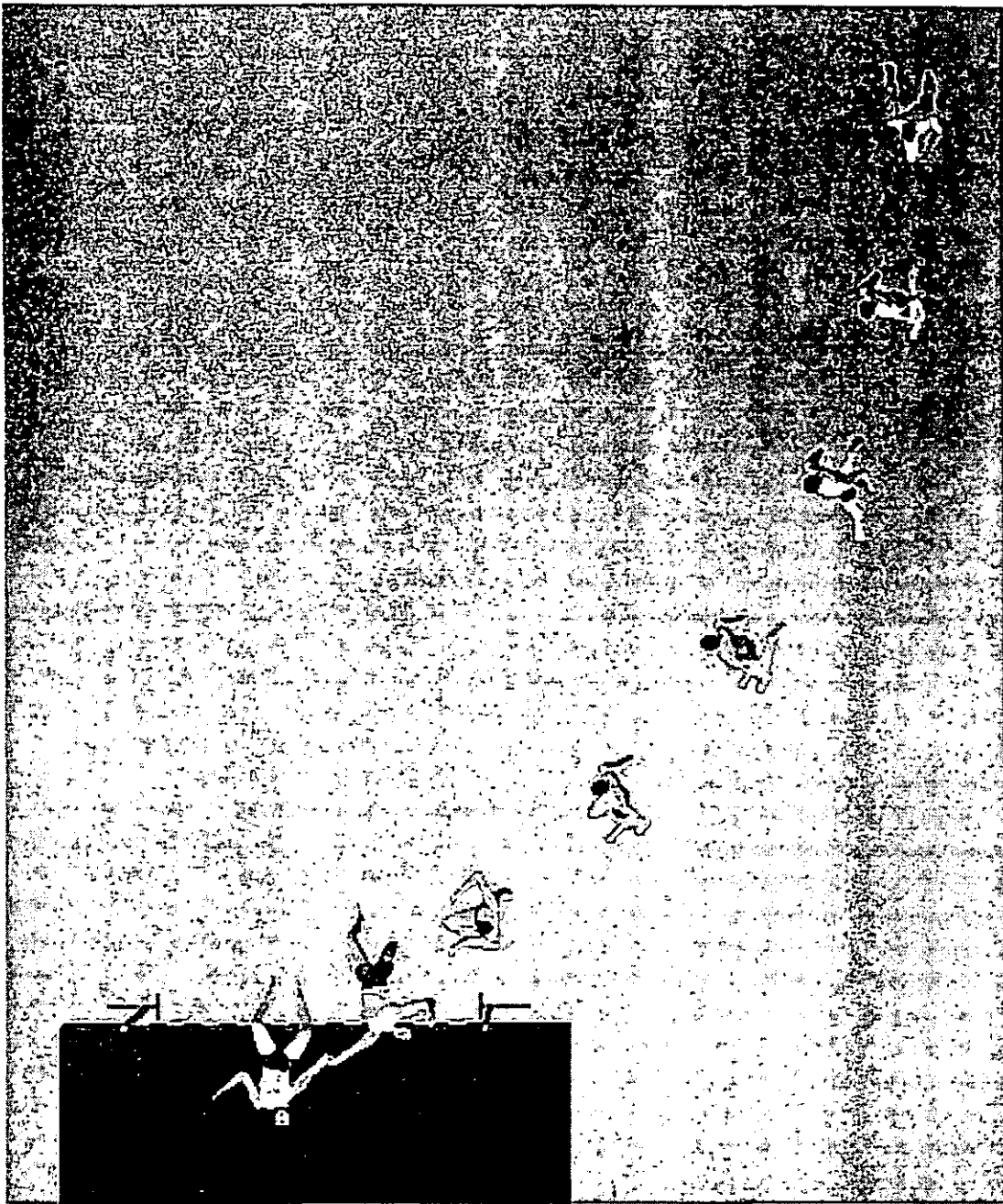


Figure 6.5. Computer graphics sequences of the curved approach and somersault rotation of B. Reilly (jump B04).

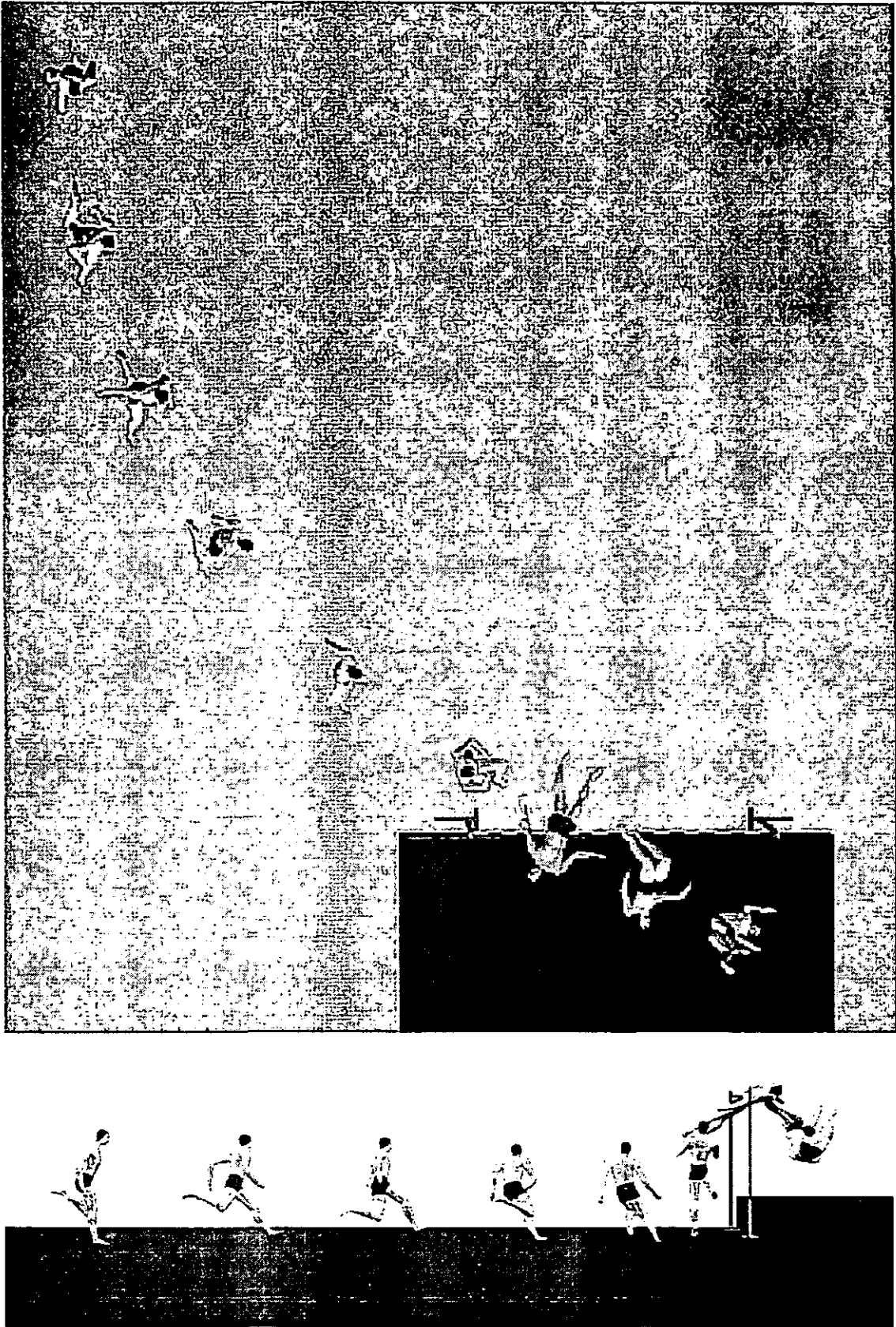


Figure 6.6. Computer graphics sequences of the curved approach and somersault rotation of S. Smith (jump S05).

TWIST CONTRIBUTION

The twist velocity $\dot{\psi}$ about a vertical axis at end of the approach phase can be obtained from the model. The angular momentum of the mass centre about a vertical axis through the mass centre can be calculated from the video data with the computer program SIMU. The angular momentum about the vertical axis is:

$$L_{ZF} = L_1 \sin \theta - \dot{\psi}_v (I_3 \cos^2 \theta + I_1 \sin^2 \theta) \quad \text{from equation (16)}$$

$$\approx -\dot{\psi}_v (I_3 \cos^2 \theta + I_1 \sin^2 \theta) \quad \text{since } \sin \theta \text{ is small at C0.}$$

Therefore

$$\dot{\psi}_v = \frac{-L_{ZF}}{I_z}$$

where $I_z = I_3 \cos^2 \theta + I_1 \sin^2 \theta$ is the moment of inertia about the vertical axis and $\dot{\psi}_v$ is the twist velocity at take-off.

Hence by comparing the value of the final $\dot{\psi}$ obtained from the model with the $\dot{\psi}_v$ value, the contribution of the curved approach to the twist velocity at take-off can be estimated.

The video data of the flight phase appeared to contain considerable noise. With the wide field of view (15 m) and the fact that flight phase occurred in the area furthest from the cameras, the image size of the jumper during this phase was rather small and this would have increased digitising errors. Errors in digitising may also have occurred as certain landmarks (e.g. the wrists, elbows and shoulders) were obscured by the trunk as the jumper rotated over the bar. In order to obtain reasonable angular momentum L_{ZF} values for the calculation of $\dot{\psi}_v$, the mean of the angular momentum values about the longitudinal axis for the last field of take-off and the first field in the flight phase was used. The values of $\dot{\psi}$ and $\dot{\psi}_v$ are presented in Table 6.8.

It should be noted that the twist velocity from the model only defines the rate of change in direction of the foot path of the approach. Since the movements undertaken by the jumper during take-off (e.g. the swing of the leading leg) cannot be considered as contributions of the approach, they were not included in the simulation model. These movements may indeed generate some twist rotation and so the approach may only provide part of the required twist rotation. By comparing the twist velocities from the video and simulation, the contribution of the approach to the twist rotation at take-off

amounted to about 60%. Therefore it may be concluded that the curved approach contributes more than half of the total twist rotation required. This proportion of twist rotation contribution is, however, subject to the errors of the video data and accuracy of the model. The results obtained from the model also indicate that curved approach can provide an angular velocity of about 3 radians per second for the twist rotation at take-off.

The twist velocity in the model is calculated as v_f/R . Therefore, the tightening of the foot curve will also contribute towards generating more twist rotation.

Table 6.8. The contribution of the approach to the twist velocity at take-off

	$\dot{\psi}$ [rad.s ⁻¹]	$\dot{\psi}_v$ [rad.s ⁻¹]	Proportion ($\dot{\psi} / \dot{\psi}_v$)
B01	2.5	5.8	0.43
B02	2.5	4.4	0.57
B03	3.2	4.5	0.71
B04	3.7	6.4	0.57
B05	4.2	5.2	0.80
Mean	3.2	5.3	0.62
S01	2.9	5.9	0.49
S02	3.4	4.3	0.79
S03	2.8	4.3	0.65
S04	2.5	4.0	0.63
S05	3.3	6.5	0.50
S06	3.3	9.1	0.37
S07	2.9	5.1	0.56
S08	2.7	3.7	0.73
S09	2.8	5.9	0.47
S10	2.7	5.0	0.54
Mean	2.9	5.4	0.57

SUMMARY OF FINDINGS

The curved approach contributes as much as 94% of the somersault rotation required for the clearance of the bar.

The curved approach can impart about 3 rad.s^{-1} of the initial twist angular velocity of the flight phase and this amounts to about 60% of the actual twist velocities attained at take-off.

The curves through the foot placements of the approach were found to be tightening towards the end of approach. Tightening of the foot curve towards the end of the high jump approach produces the somersault rotation and increases the twist rotation.

The findings of this study seem to contradict those of Dapena (1980b) who found that the curved approach did not contribute much to somersault or twist rotation. His conclusion was drawn from the result that there was little angular momentum at touchdown of the last step of the approach. Therefore, he has discounted the possibility of the curved approach generating angular momentum for somersault and twist rotation during the last foot contact.

Future Direction

There are three phases in the Fosbury Flop, namely: the approach phase, the take-off phase and the flight phase. Since this study investigated the contribution of the approach phase, studies on the take-off and flight phases should ensue in order to provide a better understanding of other aspects of the mechanics of high jumping.

REFERENCES

- Abdel-Aziz, Y.I. (1974). Expected accuracy of convergent photos. *Photogrammetric Engineering*, **40**, 1341-1346.
- Abdel-Aziz, Y.I. and Karara, H.M. (1971). Direct linear transformation from comparator coordinates into object space coordinates in close-range photogrammetry (ASP Symposium on Close-Range Photogrammetry). Falls Church, V.A.: American Society of Photogrammetry.
- Ackland, T.R., Henson, P.W. and Bailey, D.A. (1988). The uniform density assumption: its effect upon estimation of body segment inertial parameters. *International Journal of Sport Biomechanics*, **4**, 146-55.
- Adachi, N., Asami, T., Togari, H., Kikuchi, T. and Sano, Y. (1973). An analysis of movement in backward-roll style high jump. (In Japanese) In Proceedings of the Department of Physical Education University of Tokyo **7**, 69.
- Ae, M., Shibukawa, K., Tada S. and Hashihara, Y. (1983). A biomechanical analysis of the segmental contribution of the takeoff of the one leg running jump for height. In H. Matsui and K. Kobayashi (Eds.), *Biomechanics VIII-B* (pp. 737-745). Champaign, IL: Human Kinetic Publishers.
- Ae, M., Sakantani, Y., Yokoi, T., Hashihara, Y. and Shibukawa, K. (1986). Biomechanical analysis of the preparatory motion for takeoff in the Fosbury Flop. *International Journal of Sport Biomechanics*, **2**, 66-77.
- Alexander, R.M. (1990). Optimum takeoff technique for high and long jumps. *Philosophical Transactions of the Royal Society of London, B* **329**, 3-10.
- Alexander, R.M. (1992a). Simple models of walking and jumping. *Human Movement Science*, **11**, 3-9.
- Alexander, R.M. (1992b). *The human machine*. New York: Columbia University Press.
- Allard, P., Blanchi, J.-P., Aissaoui, R. (1995). Bases of three dimensional reconstruction. In P. Allard, I. Stokes, and J.-P. Blanchi (Eds.), *Three-Dimensional Analysis of Human Movement* (pp. 19-40). Champaign, IL: Human Kinetic Publishers.
- Angulo, R.M. and Dapena, J. (1992). Comparison of film and video techniques for estimating three-dimensional co-ordinates within a large field. *International Journal of Sport Biomechanics*, **8**, 145-151.

- Antonsson, E.K. and Mann, R.W. (1989). Automatic 6-D.O.F. kinematic trajectory acquisition and analysis. *Journal of Dynamic Systems, Measurement, and Control*, **111**, 31-39.
- Aura, O. and Viitasalo, J.T. (1987). An effective flop-style high jump take-off: a comparative study of two jumpers. In G. Droot, A.P. Hollander, P.A. Huijing and G.J. van Ingen Schenau (Eds.), *Biomechanics XI-B* (pp. 570-574). Amsterdam: Free University Press.
- Bennett, M. (1996). Digitisation accuracy of video copied cinefilm images. Unpublished MSc. Loughborough University.
- Beulke, H. (1977). The physical significance of the curved run-up in the Flosbury Flop. *Track and Field Quarterly Review*, **77**(3), 37-40.
- Bruggemann, G-P. and Loch, M. (1992). The High Jump. *New Studies in Athletics*, **7**(1), 67-72.
- Brooks, C.B. and Jacob, A.M. (1975). The gamma mass scanning technique for inertial anthropometric measurement. *Medicine and Science in Sports* **7**(4), 290-294.
- Carr, G.A. (1974). The flop for beginners. *Track Technique*, **58**, 1834-1836.
- Castello, F. (1979). Stylist Vladimir Yashchenko: 7' 8 $\frac{1}{2}$ ". Back in straddle again. *Scholastic Coach*, **48**(7), 22-23.
- Challis, J.H. (1991). Estimating individual muscle forces in human movement. Unpublished doctoral dissertation, Loughborough University.
- Chandler, R.F, Clauser, C.E., McConville, J.T., Reynolds, H.M., Young, J.W. (1975). Investigation of inertial properties of the human body. AMRL Technical Report, 74-137, Dayton, OH: Wright-Patterson Air Force Base.
- Chen, L., Armstrong, C.W. and Raftopoulos, D.D. (1994). An investigation on the accuracy of three dimensional space reconstruction using the direct linear transformation technique. *Journal of Biomechanics*, **27**, 4, 493-500.
- Chow, J.W. (1994). The optimal camera setup for a technique of three-dimensional cinematography. *Journal of Human Movement Studies*, **26**, 131-152.
- Clauser, C.E., McConville, J.T., Young, J.W. (1969). Weight, volume and centre of mass of segments of the human body. AMRL Technical Report, 74-137. Dayton, OH: Wright-Patterson Air Force Base.

- Dapena, J. (1978). A method to determine the angular momentum of a human body about three orthogonal axes passing through its centre of gravity. *Journal of Biomechanics*, **11**, 251-256.
- Dapena, J. (1979). A simulation method for predicting the effects of modifications in human airborne movements. Unpublished doctoral dissertation. University of Iowa.
- Dapena, J. (1980a). Mechanics of translation in the Fosbury Flop. *Medicine and Science in Sport and Exercise* **12**(1), 37-44.
- Dapena, J. (1980b). Mechanics of rotation in the Fosbury Flop. *Medicine and Science in Sport and Exercise* **12**(1), 45-53.
- Dapena, J. (1981). Simulation of modified human airborne movements. *Journal of Biomechanics*, **14**, 81-89.
- Dapena, J. (1987). Basic and applied research in Biomechanics of high jumping. In van Gheluwe B., and Atha, J (Eds.), *Current Research in Sports Biomechanics. Medicine and Sport Science* **25**, (pp. 19-33). Karger : Basel.
- Dapena, J. (1988). Biomechanics analysis of the Fosbury Flop. *Track Technique*, **104**, 3307-3317.
- Dapena, J. (1995). The rotation over the bar in the Fosbury-flop high jump. *Track Coach*, **132**, 4201-4210.
- Dapena, J., Ae, M. and Iiboshi, A. (1997). A closer look at the shape of the high jump run-up. *Track Coach*, **138**, 4406-4411.
- Dapena, J. and Chung, C.S. (1988). Vertical and radial motions of the body during the take-off phase of high jumping. *Medicine and Science in Sport and Exercise* **20**(8), 290-302.
- Dapena, J., McDonald, C. and Cappaert J. (1990). A regression analysis of high jumping technique. *International Journal of Sport Biomechanics* **6**(3), 246-261.
- Daniel, A. (1978). Yaschenko and the straddle. *Track Technique*, **72**, 2304-2305.
- Dempster, W.T. (1955). Space requirement of the seated operator. WADC Technical Report, 55-158, Dayton. OH: Wright-Patterson Air Force Base.
- Deporte, E. and van Gheluwe, B. (1989). Ground reaction forces in elite high jumping. In R. Gregor, R. Zernicke and W. Whiting (Eds.), *Congress Proceedings XII International Congress of Biomechanics* (pp. 202). Los Angeles: UCLA Press.

- Dessureault, J. and Lafortune, M.A. (1981). Biomechanical features of two styles of high jumping. In A. Morecki, K. Fidelus, K. Kedzior and A. Wilt (Eds.), *Biomechanics VII-B* (pp. 264-267. Warschau: Pwn-Polish Kinetics Publishers.
- Dick, F. W. (1993). *High jump* (Ninth edition). Birmingham: British Athletic Federation.
- Doherty, K. (1985). *Track and Field Omnibook* (Fourth edition). Los Altos, California: Tafnews.
- Drillis, R., Contini, R. and Bluestein, M. (1966). *Body segment parameters*. Technical Report No. 1166.03, PB 174945, School of Engineering and Science. New York University.
- Dyatchkov, V. M. (1968). The high jump. *Track Technique*, **34**, 1059-1075.
- Dyson, G.H. (1986). *Mechanics of athletics* (Eighth edition) revised by B. D. Wood and P.R. Hodder. London: Stoughton Ltd.
- Ecker, T. (1969). The Fosbury Flop. *Athletic Journal* **49**(8), 66.
- Ecker, T. (1971). *Track and field dynamics*. Los Altos, California: Tafnews Press.
- Ecker, T. (1976). *Track and Field - technique through dynamics*. Los Altos, California: Tafnews Press.
- Ecker, T. (1985). *Basic track and field biomechanics*. Los Altos, California: Tafnews Press.
- Fix, D. (1974). Why the flop is better? *Track Technique* **58**, 1834-1836.
- Greig, M., Yeadon, M.R. and Kerwin, D.G. (1996). The influence of approach parameters on high jumping performance. In J. Watkins (Ed.), *Proceedings of the Biomechanics Section of the British Association of Sport and Exercise Sciences Easter Meeting* (pp. 25-28). Loughborough: BASES.
- Hamill, J., Murphy, M., and Sussman, D. (1987). The effects of track turns on lower extremity function. *International Journal of Sport Biomechanics* **3**, 276-286.
- Hanavan, E.P. (1964). A mathematical model of the human body. AMRL Technical Report, 64-102. Dayton, OH: Wright-Patterson Air Force Base.
- Hatze, H. (1975). A new method for the simultaneous measurement of the moment of inertial, the damping coefficient and the location of the centre of mass of a body segment in situ. *European Journal of Applied Physiology* **34**, 217-226.

- Hatze, H. (1980). A mathematical model for the computational determination of parameter values of anthropomorphic segments. *Journal of Biomechanics* **13**, 833-843.
- Hatze, H. (1981). A comprehensive model for human motion simulation and its applications to the takeoff phase of the long jump. *Journal of Sports Science*, **1**, 3-12.
- Hatze, H. (1988). High precision three-dimensional photogrammetric calibration and object space reconstruction using a modified DLT approach. *Journal of Biomechanics*, **21**, 533-538.
- Hay, J.G. (1968). An investigation of take-off impulses in two styles of high jumping. *Research Quarterly*, **39**(4), 983-992.
- Hay, J.G. (1973). The Hay technique - ultimate in high jump styles? *Athletic Journal* **53**(7), 46-48.
- Hay, J.G. (1974). Characteristics of the Flop. *Athletic Journal* **54**(7), 10, 92-93.
- Hay, J.G. (1985). *The Biomechanics of sports techniques* (Third edition). California: Prentice-Hall.
- Hay, J., Dapena, J., and Wilson, B. (1977). A computational technique to determine the angular momentum of a human body. *Journal of Biomechanics*, **10**, 269-277.
- Heinz, S. (1974). A curved run-up in straddle? *Modern Athlete and Coach*, **12**(4), 28-29.
- Hubbard, M. and Trinkle, J.C. (1985). Optimal Fosbury-flop high jumping. In D.A. Winter, R.W. Norman, R.P. Wells, K.C. Hayes and A.E. Patla (Eds.), *Biomechanics IX-B* (pp. 448-453). Champaign, IL: Human Kinetic Publishers.
- Hubbard, M. (1993). Computer simulation in sport and industry. *Journal of Biomechanics*, **26**, 53-61.
- Iiboshi, A., Ae, M., Takanmatsu, J., Nagasawa, M., Tang, H.P. and Yuuki, M. (1994). Techniques of elite high jumpers at the 3rd IAAF world championships in athletics. In *Abstracts of the XIVth International Society for Biomechanics Congress 1993*, (pp.608-609). Paris: Societe de Biomecanique.
- Inglis, A.F. (1993). *Video Engineering*. New York: McGraw-Hill.
- Jacoby, E. (1986). High Jump - A technique evaluation. *Track Technique*, **97**, 3089-3093.

- Jacoby, E. (1987). A guide to the flop high jump approach, *Track and Field Quarterly Review*, **87**(4), 39-45.
- Jarver, J. (1981). The high jump in a nutshell. In J. Jarver (Ed.), *The Jump* (pp. 28-31). Los Altos, California: Tafnews.
- Jensen, R.K. (1978). Estimation of the biomechanical properties of three body types using a photogrammetric method. *Journal of Biomechanics*, **11**, 349-358.
- Karara, H.M. (1980). Non-metric cameras. In K.B. Atkinson (Ed.), *Developments in close range photogrammetry -1* (pp. 63-80). London: Applied Science Publishers.
- Karara, H.M. and Abdel-Aziz, Y.I. (1974). Accuracy aspects of non-metric imageries. *Photogrammetric Engineering*, **40**(9), 1107-1117.
- Kennedy, P.W., Wright, D.L. and Smith, G.A. (1989). Comparison of film and video techniques for three-dimensional DLT repredictions. *International Journal of Sport Biomechanics*, **5**, 457-460.
- Kerssenbrock, K. (1972). High jump technique. In F. Wilt (Ed.), *The Jumps. Contemporary theory technique and training* (pp. 13-15). Tafnews Press. Los Altos, California.
- Kerssenbrock, K. (1974). Fosbury's run-up. *Modern Athlete and Coach*, **12**(1), 18.
- Kerwin, D.G. (1993). High resolution video digitisation. In M.R. Yeadon (Ed.), *Proceedings of The Sports Biomechanics Section of BASS 18* (pp. 25-28.) Manchester Metropolitan University: BASS
- Kerwin, D.G. (1995). Apex/Target high resolution video digitising system. In J. Watkins (Ed.), *Proceedings of The Sports Biomechanics Section of BASES 20* (pp. 1-4.) Leeds Metropolitan University: BASES
- Kerwin, D.G. and Templeton, N. (1991). Cine-film and video: An assessment of digitisation accuracy. *Journal of Sports Science* **9**(4), 402.
- Killing, W. (1994) . The run-up control of top class high jumpers. *Modern Athlete and Coach*, **32**(4), 27,28.
- Killing, W. (1995) . The run-up of elite high jumpers. *Track Coach*, **134**, 4289-4290.
- Krahl, H. and Knebel, K.P. (1978). Medizinische und trainings methodische. Aspekte der Absprungphase beim Flop. *Leistungssport* **8**(6): 501-506.

- Kuhlow, A. (1973). A comparative analysis of dynamic takeoff features of Flop and Straddle. In S. Cerquiglini, A. Venerando, and J. Wartenweiler (Eds.), *Biomechanics III* (pp. 403-408). Karger: Basel.
- Kulwicki, P.V. Schlei, E.J. and Vergamini, P.L. (1962). Weightless man: self rotation techniques. AMRL Technical Report, 62-129. Dayton, OH: Wright-Patterson Air Force Base.
- Lees, A. (1980). An optimized film analysis method based on finite different techniques. *Journal of Human Movement Studies*, 6 165-180.
- Martin, D.E. (1982). The Flop - Technical perspectives. In D.E. Martin, D. Stones, G. Joy and J.Wszola. (Eds.), *The high jump book* (pp. 103-132). Los Altos, California: Tafnews Press.
- Marzan, G.T. and Karara, H.M. (1975). A computer program for the direct linear transformation solution of the collinearity condition and some applications of it *Close-Range Photogrammetric systems* (pp. 420-476). Falls Church, VA: American Society of Photogrammetry.
- Matthews, P. (1986). *Track and field athletics: The record*. Enfield, Middlesex: Guinness Superlatives Ltd.
- McMahon, T.A. and Greene, P.R. (1979). The influence of track compliance on running. *Journal of Biomechanics*, 12, 893-904.
- McNab, T. (1980). *The completed book of athletics*. London: Ward Lock Ltd.
- Milani, T.L. and Hennig, E.M. (1994). Pressure distribution under the foot at the take-off in volleyball jumps and Fosbury Flop high jumps. In *Abstracts of the XIVth International Society for Biomechanics Congress 1993, Paris*. *Journal of Biomechanics*, 27, 6, 677.
- Miller, D.I. and Nelson, R.C.. (1973). *Biomechanics of sport - A research approach*. Philadelphia: Lea and Febiger.
- Miller, D.I. and Nissinen, M.A. (1987). Critical examination of ground reaction force in running forward somersault. *International Journal of Sport Biomechanics*, 3, 189-206.
- Miller, N.R., Shapiro, R. and McLaughlin, T.M. (1980). A technique for obtaining spatial kinematic parameters of segments of biomechanical systems from cinetographic data. *Journal of Biomechanics*, 13, 535-547.

- Muraki, Y., Sakamoto, T., Saito, S., Ae, M., and Shibukawa, K. (1983). A 3-dimensional cinematographical analysis of foot deformations during the takeoff phase of the Fosbury Flop. In H. Matsui and K. Kobayashi (Eds.), *Biomechanics VIII-B* (pp. 762- 770). Champaign, IL: Human Kinetic Publishers.
- Neal, R. (1983). Three dimensional analysis of the golf swing. Unpublished Master's dissertation, University of Queensland, Brisbane, Australia.
- Nigg, B.M. (1974). Hochsprung. In B.M. Nigg (Ed.), *Sprung Springen Sprunge* (pp.75-132). Zurich: Juris Verlag.
- Nigg, B.M. (1994). Inertial properties of the human or animal body. In B.M. Nigg and W. Herzog (Eds.), *Biomechanics of the musculo-skeletal system* (pp.337-364). Chichester: John Wiley and Sons.
- Nigg, B.M., Denoth, J. and Neukomm, P.A. (1981). Quantifying the load on the human body: Problems and some solutions. In A. Morecki, K. Fidelus, K. Kedzior and A. Wilt (Eds.), *Biomechanics VII-B* (pp. 88-99). Baltimore: University Park Press.
- Nigg, B.M. and Yeadon, M.R. (1987). Biomechanical aspects of playing surfaces. *Journal of Sports Sciences*, **5**, 117-145.
- Ozolin, N. (1973). The high jump takeoff mechanism. *Track Technique*, **52**, 1668.
- Page, R. L. (1974). The mechanics of toppling techniques in diving. *Research Quarterly*, **45**, 185-192.
- Panjabi, M. (1979). Validation of mathematical models. *Journal of biomechanics*, **12**(3), 239.
- Payne, H. and Payne, R. (1981). *High Jump. The Science of Track and Field*. London: Pelham Books.
- Pearsall, D.J. and Reid, G.J. (1994). The study of the human body segment. *Sports Medicine*, **18**(2), 126-140.
- Pedotti, A. and Rodano, R. (1981). Dynamic characteristics of the high jump takeoffs and some training exercises. In A. Morecki, K. Fidelus, K. Kedzior and A. Wilt (Eds.), *Biomechanics VII-B* (pp. 249-256). Baltimore: University Park Press.
- Pike, N.L. (1980). Computer simulation forward full twisting dive in a layout position. Unpublished doctoral dissertation. Pennsylvania State University.

- Preiss, R.H. (1985). Investigation of the Hay technique of the high jump by computer simulation. In E. Schneider (Ed.), *Current Interdisciplinary Research* (pp. 693-698). Martinus: Dordrecht.
- Press, W.H., Flannery, B.P., Teukolsky S.A. and Vetterling, W.T. (1988). *Numerical recipes. The art of scientific computing*. Cambridge: Cambridge University Press.
- Putnam, C. (1979). DLT method of three dimensional cinematography: Instruction manual. Unpublished report, University of Iowa.
- Ritzdorf, W. and Conrad, A. (1987). Biomechnaical analysis of the high jump. In *International Athletic Foundation Scientific Report on the 2nd World Championships in athletics Rome 1987*, 2, F1-50.
- Rodrigue, D. and Gagnon, M. (1984). Validation of Weinbach's and Hanavan's models for computation of physical properties of the forearm. *Research Quarterly Exercise Sports*, 55(3), 272-277.
- Ross, R.W. (1979). Flop or straddle? *Scholastic Coach* 48(9), 40-42.
- Santos, J. (1978). The high jump. In F. Wilt, T. Ecker and J. Hay (Eds), *Championship Track and Field for Women*. Parker Publishing Co., New York.
- Shapiro, R., Blow, C. and Rash, G. (1987). Video digitizing analysis system. *International Journal of Sport Biomechanics*, 2, 80-86.
- Smith, A.J. (1972). A study of the force on the body in athletic activities with particular reference to jumping. Unpublished doctoral dissertation. Leeds University.
- Sung, R.-J. and Shin, I.-S. (1989). A kinematic analysis of the Fosbury-Flop technique of Korean male elite high jumpers. *Korean Journal of Sport Science*, 1, 51-70.
- Sung, R.-J., Chung, C.-S. and Shin, I.-S. (1990). A kinematic analysis of the Fosbury Flop technique of Korean representative high jumpers. *Korean Journal of Sport Science*, 2, 96-123.
- Taguchi, M., Kajiyama, H., Kawakami, M. and Katamine, T. (1983). The take-off motion in Fosbury-flop technique. *Japanese Journal of Sports Science*, 2(8), 614-622.
- Tansley, J. (1980). *The Flop book*. Santa Monica, California: Petersen Lithograph Corporation.
- Tidow, G. (1993). Model technique analysis sheets. Part VII: The Flop high jump. *New Studies in Athletics*, 8(1), 31-44.

- Townend, M.S. (1984). Jumping. In mathematics in sports (pp. 52-58). Chichester: Ellis Harwood Ltd.
- Tsirakos and Bartlett, R. (1995). Accuracy of cine and video digitization compared with an on-line analysis (ELITE). *Journal of Sport Sciences*, 13(5), 8-9.
- Van Gheluwe, B. (1981). A biomechanical simulation model for airborne twist in backward somersault. *Journal of Human Movement*, 7, 1-2.
- Van Gheluwe, B. and van Donnick, W. (1978). A comparative cinematographic study of the Flop and the Straddle technique in high jumping. In A. Ayalon (Ed.), *Biomechanics of Sport Games and Sport Activities* (pp. 72-79). Jerusalem: Wingate Institute for Physical Education and Sport.
- Vaughan, C.L. (1984). Computer simulation of human motion in sports biomechanics. In R.L. Terjung (Ed.), *Exercise and Sport Science Reviews*, 12 (pp. 373-416). Toronto: The Collamore Press.
- Vittori, C. (1972). Should high jumpers use the Straddle or the Fosbury Flop? In F. Wilt (ed.), *The Jumps* (pp. 33-36). Los Altos, California: Tafnews Press.
- Wagner, B. (1985). High jump (Fosbury technique). In H. Payne (Ed.), *Athletes in Action* (pp. 116-133). London: Pelham Books.
- Whitsett, C.E. (1962). Some dynamic response characteristics of weightless man. Unpublished Master Thesis, U.S. Air Force Institute of Technology, Dayton, OH: Wright-Patterson Air Force Base
- Wilson, B.D. (1977). Toppling techniques in diving. *Research Quarterly*, 48, 806-811.
- Winter, D.A. (1990). *Biomechanics and Motor control of Human Movement*. (2nd edition). Chichester: Wiley and Sons.
- Winter, D.A. , Sidwall, H.G. and Hobson, D.A. (1974). Measurement and reduction of noise in kinematics locomotion, *Journal of Biomechanics*. 7, 157- 159.
- Wood, G.A. and Marshall, R.N. (1986). The accuracy of DLT extrapolation in three-dimensional film analysis. *Journal of Biomechanics*, 19, 781-785.
- Wood, G.A. and Jennings, L.S. (1979). On the use of spline functions for data smoothing. *Journal of Biomechanics*, 12, 477-479.
- Yeadon, M.R. (1984). The mechanics of twisting somersaults. Unpublished doctoral dissertation thesis. Loughborough University.

- Yeadon, M.R. (1993). The biomechanics of twisting somersaults Part III: Aerial twist. *Journal of Sports Sciences*, **11**, 209-218.
- Yeadon, M.R., Atha, J. and Hales, F.D. (1990). The simulation of aerial movement Part VI: A computer simulation model. *Journal of Biomechanics*, **23**, 85-89.
- Yeadon, M.R. and Challis, J.H. (1994). The future of performance related sports biomechanics research. *Journal of Sports Sciences*, **12**, 3-32.
- Yeadon, M.R., Challis, J.H. and Ng, R. (1994). Personalised segmental inertial parameters. In Abstracts of the XIVth International Society for Biomechanics Congress 1993, Paris, *Journal of Biomechanics*, **27**, 6, 770.
- Zacharias, T. (1976). Higher height with the Straddle. *Track Technique*, **63**, 1976, 1995-1998.

APPENDIX A

Listing of the program APPROACH

[illegible]

c APPROACH

- c This program simulates a single segment body moving on a curve.
c It outputs time, tilt angle, tilt angular velocity, twist angle
c foot velocity, curve radius and stride distance.
c
c Prompts for different output files and input variables.
c Prompts for the different input variables like weight, average
c moment of inertia about the long axis and angular momentum about i -axis
c Also prompt for time interval of numerical integration, time at
c touchdown, midstance and takeoff.
c
c Stride distance (s) is also calculated from the mid-foot coordinates.
c Express foot contact psi angles and ground distance (SA) as
c polynomial function to calculate the radius of each contact.
c Express tilt angle as a polynomial function. and calculate
c initial angular tilt velocity.
c
c Express stride distance (foot) as quadratic function of time
c to mark the different phases for the simulation.
c and calculate foot velocity, v_f .
c
c Input the distance of the mass centre to foot at touchdown
c midstance and takeoff for each foot contact.
c Express these distances at each foot contact as a quadratic
c function of s so that the distances and their rate of change
c can be obtained from the function for tilt acceleration calculation.
c
c Input the moment of inertia about frontal axis at touchdown
c midstance and takeoff for each foot contact.
c Express these value at the each foot contact as a quadratic
c function of s so that the moment of inertia and its rate of change can be
c obtained from the function for tilt acceleration calculation.
c
c Model ground and flight phases differently.
c Recalculate radius the foot curve with radius at midpoint and the
c difference in psi angle between two contacts.
c Output simulated foot coordinates.
c Use cubic spline to fit the psi angle and s distance to get foot radius.
c Use equation of aerial phase to calculate the tilt angle in aerial phase.

100

c thed, thedf and thedav = tilt velocity (initial, final and average)
 c thedd0, theddf, thedd, = tilt acceleration (initial, final and average)
 c th1,t1 = Evaluated tilt angle from the quartic function of time and time angle
 c t, t0, tf = Instant in time of simulation, time at beginning and end of simulation
 c dt = Time interval of simulation
 c t1(nn)= Arrays of time
 c TD(nn), tt(nn), TO(nn), = Array of time at *td*, *ms* and *to*
 c tt1 = Evaluated time in quadratic function of *s* and *t*
 c vf, = foot velocity
 c V(nn)= Array of foot velocity
 c Hf(nn)= Array of forward angular momentum
 c sp(3) = Evaluated values of cubic spline, 1st and 2nd derivatives
 c ccy1(nn,4), ccy2 (nn,4) = cubic spline coefficients
 c aaa(6,5) = An array of stride distances in between foot contact
 c bbb(4)= An array of twist angles
 c Cpsi(4) = Coefficient of the cubic function (psi vs stride distance)
 c Xx, Yy= Coordinates of each point of the simulated foot curve
 c Xmx Ymy = Coordinates of simulated mass centre location
 c Xms Yms = Coordinates of the fixed foot of simulated the foot curve
 c Xm, Ym = Coordinates of the fixed foot from video
 c A, B, C = Coefficient of a quadratic function of foot velocity and time
 c Ac, Bc, Cc = Coefficient of a quadratic function of *s* and time
 c De, Ee, Fe = Coefficient of a quadratic function of *s* and *h*
 c Dg, Eg, Fg = Coefficient of a quadratic function of *s* and *I2*
 c Aa(7,6) = Array of time values
 c Ba(5) = Array of tilt angle
 c Ca = Coefficients of the quartic function of time and tilt angles

cc

double precision

* a11, c11, d11, e11, f11, g11,h11, i11,
 * psi2(nn), psi1 psi(nn), psik (nn), psik2(nn), Dpsi, Dpsif, psiA, psiD,
 *adpsi, mx(5), g, m, pi, rtd, fds, fdx, fdy,Ls.OE, Oed,
 * h, h1(nn), hm(nn), hd(nn), ho(nn), Id(nn), ,Im(nn),Io(nn)
 * ,I1, I3, I2, Isl(nn), r1, r2 Rm(nn), Rc(nn),
 * SA(nn), sAD(nn), sAM(nn), sAO(nn), SB(nn), SA1, SB1,
 * s, ss, ds, sdy(nn), sl(nn), ssD(nn),
 * the, thed, thedd, thef, thedf, theddf, thedd0, thedav, th(nn), th1,
 * t, dt, t0, tf, tt(nn), t1(nn),tt1,TD(nn),TO(nn),
 * v1, vf, V(nn), Hf(nn), sp(3), ccy1(nn,4), ccy2(nn,4),
 * aaa(6,5), bbb(4), Cpsi(4), Ls,
 * Xx, Yy, Xmx, Ymy, Xm(nn), Ym(nn), Xms(nn), Yms(nn)
 * A, B, C, , Ac, Bc, Cc, De, Ee, Fe, Dg, Eg, Fg,
 * Aa(7,6), Ba(5), Ca(5)

integer i, k, j, q

```
character output1*20
character output2*20
```

[illegible]

```
print*, 'state name of the angle and angular vel. output file'
read(*,*) output1
```

```
print*, 'state the curve coord. of foot contacts output file'
read(*,*) output2
```

```
print*, 'input inlean angles (deg.) from C6-C0'
read*, th(6), th(5), th(4), th(3), th(2), th(1)
```

```
print*, 'input horizontal forward velocity (m/s) at C4-C0'
read*, Hf(6), Hf(5), Hf(4), Hf(3), Hf(2), Hf(1)
```

```
print*, 'input dist bet m.c.& foot at C5-0 and at TD, MS, T'
read*, hd(6), hd(5), hd(4), hd(3), hd(2), hd(1)
read*, hm(6), hm(5), hm(4), hm(3), hm(2), hm(1)
read*, ho(6), ho(5), ho(4), ho(3), ho(2), ho(1)
```

```
print*, 'input I2 at C5-0 and at TD, MS, TO'
read*, Id(6), Id(5), Id(4), Id(3), Id(2), Id(1)
read*, Im(6), Im(5), Im(4), Im(3), Im(2), Im(1)
read*, Io(6), Io(5), Io(4), Io(3), Io(2), Io(1)
```

```
print*, 'Input aerial It, I2, Il of the jumper'
read*, It, I2, Il
```

```
print*, 'Input the mass (kg) of the jumper'
read*, m
```

```
print*, 'Input f.c. coords of 1st, mid, last ground contact at C5'
read*, Xm(6), Ym(6)
```

```
print*, 'Input f.c. coords of 1st, mid, last ground contact at C4'
read*, Xm(5), Ym(5)
```

```
print*, 'Input f.c. coords of 1st, mid, last ground contact at C3'
read*, Xm(4), Ym(4)
```

```
print*, 'Input f.c. coords of 1st, mid, last ground contact at C2'
read*, Xm(3), Ym(3)
```



```
t = 0
g = 9.81
pi = 3.14159265358
rtd = 180.0 / 3.14159265358
tf = TO(1)
t0 = tt(k+1)
the = th(k+1)
ccccccccccccccccccccccccccccccccccccccccccccccccccccccccccccccccc
c
c   Express tilt angles as a function of time on a 4th poly curve
c   Interpolate for the initial lean angular velocity (thed)
c   for the simulation
c
ccccccccccccccccccccccccccccccccccccccccccccccccccccccccccccccccc
C
Aa(1,1) = tt(2)**4
Aa(1,2) = tt(2)**3
Aa(1,3) = tt(2)**2
Aa(1,4) = tt(2)
Aa(1,5) = 1
Aa(2,1) = tt(3)**4
Aa(2,2) = tt(3)**3
Aa(2,3) = tt(3)**2
Aa(2,4) = tt(3)
Aa(2,5) = 1
Aa(3,1) = tt(4)**4
Aa(3,2) = tt(4)**3
Aa(3,3) = tt(4)**2
Aa(3,4) = tt(4)
Aa(3,5) = 1
Aa(4,1) = tt(5)**4
Aa(4,2) = tt(5)**3
Aa(4,3) = tt(5)**2
Aa(4,4) = tt(5)
Aa(4,5) = 1
Aa(5,1) = tt(6)**4
Aa(5,2) = tt(6)**3
Aa(5,3) = tt(6)**2
Aa(5,4) = tt(6)
Aa(5,5) = 1
Ba(1) = th(2)
Ba(2) = th(3)
Ba(3) = th(4)
Ba(4) = th(5)
Ba(5) = th(6)
```

C


```
cccccccccccccccccccccccccccccccccccccccccccccccccccccccccccccccc
```

```
c Evaluate the psi angle from the function
```

```
cccccccccccccccccccccccccccccccccccccccccccccccccccccccccccccccc
```

```
write (20,*),' Ground distance(SA) Psi angles at C0 to C4'
```

```
do 54, i = 1, 5
```

```
psi2(i) = Cpsi(1)*SA(i)**3 + Cpsi(2)*SA(i)**2+Cpsi(3)*SA(i)+Cpsi(4)
```

```
write (20,105), SA(i), ',', psi2(i)*rtd
```

```
54 continue
```

```
SB1 = 0
```

```
s = SA(k+1)
```

```
ds = (SA(1)/(TO(1)-tt(6)))*dt
```

```
q = nint(SA(1) /ds)
```

```
write (20,*),' Ground distance Psi angle from quad fn'
```

```
do 55, i = 1,q+1
```

```
psi1 = Cpsi(1)*SB1**3 + Cpsi(2)*SB1**2+Cpsi(3)*SB1+Cpsi(4)
```

```
c psi1 = Ab*((SB1)**2) + Bb*(SB1) + Cb
```

```
write (20,105), SB1, ',', psi1*rtd
```

```
SB1 = SB1 + ds
```

```
55 continue
```

```
cccccccccccccccccccccccccccccccccccccccccccccccccccccccccccccccc
```

```
c Calculate Radius of the foot curve fr poly. fn of Psi and s
```

```
cccccccccccccccccccccccccccccccccccccccccccccccccccccccccccccccc
```

```
print*,'
```

```
print*,' C Radius dist(SA) Radius
```

```
* dist(SB)'
```

```
do 60, i = 1,5
```

```
Rc(i) = abs(1/(3*Cpsi(1)*SA(i)**2 + 2*Cpsi(2)*SA(i) + Cpsi(3)))
```

```
Rm(i) = abs(1/(3*Cpsi(1)*SB(i)**2 + 2*Cpsi(2)*SB(i) + Cpsi(3)))
```

```
print*, i-1, Rc(i), SA(i), Rm(i), SB(i)
```

```
60 continue
```

```
cccccccccccccccccccccccccccccccccccccccccccccccccccccccccccccccc
```

```
c
```

```
c Adjust the stride distance so that the curve is taken into consideration
```

```
c
```

```
cccccccccccccccccccccccccccccccccccccccccccccccccccccccccccccccc
```

```
SA(6) = 0.0
```

```
SA(5) = sqrt ( (Xm(6)- Xm(5))**2 + (Ym(6) - Ym(5))**2)
```


[illegible]

c Evaluate of v_f at each foot contact

[illegible]

```

do 68, i = 1,6
  V(i) = (2*Ac*(t1(i)) + Bc)
68 continue
  print*, ' '
  print*, ' Velocity of foot curve at contact '
  print*, ' C  V(i) '
  print*, ' 5', V(6)
do 69, i = 5, 1, -1
  Va(i) = (V(i) + V(i+1))/2
  print*, i-1, V(i)
69 continue

```

[illegible]

C

c Calculate the stride distance of the different phases

C

[illegible]

```
print*, ' '
print*, 'Quad Interpolated Stride distances'
print*, ' C sAD sAM sAO'
```

do 72, i = 1,6

```

sAD(i) = Ac*(TD(i)**2) + Bc*TD(i) + Cc
sAM(i) = Ac*(tt(i)**2) + Bc*tt(i) + Cc
sAO(i) = Ac*(TO(i)**2) + Bc*TO(i) + Cc
print*, i-1, sAD(i), sAM(i), sAO(i)

```

72 continue

[illegible]

C

c Express stride distance with foot velocity on a quad curve.

c Interpolate velocities for the simulation.

c set t as the time of starting the simulation

[illegible]

```
call QUAD(A,B,C,SA(1),V(1),1,5)
```

```
s = SA(k+1)
ss = SAA(k+1)
vf = A*(s)**2 + B*(s) + C
t = t0
```

[illegible]


```
c print*, ' S          sAM          h '
   print*, 'time a11/d11 c11/d11*r1 e11/(d11*r1) g11
   * h11 i11'
```

```

r2 = r1-(h*sin(the))
hdt = (((2*De*s)+Ee)*vf)

a11 = m*g*(h*sin(the)-OE)
c11 = m*(vf**2)*h*cos(the)*r2
d11 = Is + (m*h*(h-OE*sin(the))
e11 = m*(r1-OE)*tan(Dpsi-psi2(k+1))*vf*h*thed*sin(the)
f11 = d11*r1*r1
g11 = (2*m*h*hdt -m*OE*hdt*sin(the)-m*h*OE*d*sin(the)-m*h*OE*
*cos(the)*thed)
g11 = (g11*thed)/d11
h11 = (Hf(k+1)*vf)/(d11*r1)
i11 = (((2*Dg*s)+Eg)*vf)*thed/d11

cccccccccccccccccccccccccccccccccccccccccccccccccccccccccccccccc
c
c   use simultaneous equations of a11 to i11 first
c   to calculate initial angular acceleration
c
cccccccccccccccccccccccccccccccccccccccccccccccccccccccccccccccc

    thedd0 = a11/d11 - c11/f11 - e11/(d11*r1) -g11 -h11 -i11

    print 115, t, a11/d11, c11/f11, e11/(d11*r1), g11, h11, i11
c   print*, r1, r2, vf

cccccccccccccccccccccccccccccccccccccccccccccccccccccccccccccccc
c
c   Calculate final tilt angles and angular velocities using initial
c   angles, velocity and acceleration
c
cccccccccccccccccccccccccccccccccccccccccccccccccccccccccccccccc

    thef = the + thed*dt + 0.5*thedd0*dt**2
    thedf = thed + thedd0*dt

    t = t + dt
    s = s + vf*dt

cccccccccccccccccccccccccccccccccccccccccccccccccccccccccccccccc
c
c   Printing the simulated foot placements
c
cccccccccccccccccccccccccccccccccccccccccccccccccccccccccccccccc

    fds = vf*dt
    fdy = fds*cos(Dpsi)
    Yy = Yy - fdy

```

```
Ymy = Yy + (h*sin(the)*sin(Dpsi))
fdx = fds*sin(Dpsi)
Xx = Xx + fdx
```

```
Xmx = Xx + (h*sin(the) *(cos(Dpsi)))
write(20,107) t, Xx, ',', Yy, ',', Xmx, ',', Ymy
```

[illegible]

```
CALL VALCD(sp,s,ccyl,11,ssD(1))
Dpsi = sp(1)
r1 = abs(1/sp(2))
vf = A*(s)**2 + B*(s) + C
h = De*(s)**2 + Ee*(s) + Fe
Is = Dg*(s)**2 + Eg*(s) + Fg

psiA = ATAN((Yms(k+1)-Yy) / (Xms(k+1)-Xx)) + pi/2
psiD = abs(Dpsi - psiA)
Ls = SQRT ((Yms(k+1) -Yy)**2 + (Xms(k+1) -Xx)**2)
```

[illegible]

```

r2 = r1-(h*sin(the))
hdt = (((2*De*s)+Ee)*vf)
OE = Ls*psiD
OE d = .5*vf*(Dpsi-psi2(k+1)) + 0.5*(s-SA(k+1))*vf/r1

```

```

a11 = m*g*(h*sin(theft)-OE)
c11 = m*(vf**2)*h*cos(theft)*r2
d11 = Is + (m*h*(h-OE*sin(theft)))
e11 = m*(r1-OE)*tan(Dpsi-psi2(k+1))*vf*h*thedf
* sin(theft)
f11 = (d11*r1*r1)
g11 = (2*m*h*hdt-m*OE*hdt*sin(theft)-m*h*OE*d*sin(theft)-m*h*OE*
* cos(thedf)*thedf)
g11 = (g11*thedf)/d11
h11 = (Hf(k+1)*vf)/(d11*r1)
i11 = (((2*Dg*s)+Eg)*vf)*thedf/d11

theddf = a11/d11 - c11/f11 - e11/(d11*f*r1) - g11 - h11
* -i11

```


[illegible]

```

close (20)
stop
end

```

```

C
C
C
C*****
C
C   QUAD FITS QUADRATIC FUNCTION
C
C*****
C
C   SUBROUTINE QUAD( A, B, C, T, Z, M, N )

C   PARAMETER (NN=12)

C   DOUBLE PRECISION A, B, C, T0, T1, T2, T3, T4, Z0, Z1, Z2,
C   *           NUM, DEN, T(NN), Z(NN)

C   INTEGER J, M, N

C   T0=0.0
C   T1=0.0
C   T2=0.0
C   T3=0.0
C   T4=0.0
C   Z0=0.0
C   Z1=0.0
C   Z2=0.0

C   DO 20, J=M,N

C       T0 = T0 + 1.00
C       T1 = T1 + T(J)
C       T2 = T2 + T(J)**2
C       T3 = T3 + T(J)**3
C       T4 = T4 + T(J)**4

C       Z0 = Z0 + Z(J)
C       Z1 = Z1 + Z(J)*T(J)
C       Z2 = Z2 + Z(J)*T(J)**2

C   20 CONTINUE

C   NUM = ( Z2*T1 - Z1*T2 ) * ( T3*T0 - T1*T2 )
C   NUM = NUM - ( Z2*T0 - Z0*T2 ) * ( T3*T1 - T2*T2 )

```

```
DEN = ( T4*T1 - T3*T2 ) * ( T3*T0 - T1*T2 )
DEN = DEN - ( T4*T0 - T2*T2 ) * ( T3*T1 - T2*T2 )
```

```
A = NUM / DEN
```

```
B = ( Z2*T1 - Z1*T2 ) - A * ( T4*T1 - T3*T2 )
B = B / ( T3*T1 - T2*T2 )
```

```
C = ( Z0 - A*T2 - B*T1 ) / T0
```

```
c PRINT *, ' A = ', A, ' B = ', B, ' C = ', C
```

```
DO 40, J = M, N
```

```
Z(J) = A*T(J)**2 + B*T(J) + C
```

```
40 CONTINUE
```

```
RETURN
END
```

```
C
C*****
C
C   SPLINC FITS SPLINES TO ESTIMATES X1,X2 OF THE DIGITISED
C   COORDINATE OF A JOINT CENTRE
C
C   PARAMETERS:
C       C1,C2 = SPLINE COEFFICIENTS
C       N = NUMBER OF DATA POINTS
C       T = ARRAY OF TIME VALUES
C       X1,X2 = ARRAYS OF DIGITISED DATA
C
C*****
C
C   SUBROUTINE SPLINC(C1,C2,SD0,N,T,X1,X2)
C   PARAMETER (NN=12)
C
C   DOUBLE PRECISION C1(NN,4),C2(NN,4),T(NN),X1(NN),
C   *X2(NN),ACC,D(NN),SD0,V(NN),VAR,const,
C   *S,DD(NN)
C
C   INTEGER J,N
C
C   INTRINSIC MAX,SQRT
C
C   var = 0.0
c
```



```

DO 10,J=1,N
D(J) = (X2(J) - X1(J))
D(J) = D(J) / 2.0
V(J) = 2*D(J)**2
C
IF(V(J).GT.0.04D0) V(J)=0.04
C
VAR=VAR+V(J)
c
10 CONTINUE
c
VAR=VAR/N
SD0=SQRT(VAR)
c
c SD0=0.022
c
C*****
C
C CALCULATE ERROR ESTIMATES DD FOR EACH POINT
C
C*****
C
50 DO 20,J=1,N
c
ACC = 0.003
DD(J) = SQRT(0.75*V(J)+0.25*VAR)
IF(DD(J).LT.1.0D-5) DD(J)=0.01
DD(J) = MAX(DD(J),ACC)
c
c DD(J) = 0.022
DD(J) = 0.0
c
20 CONTINUE
C
c if(n.gt.12) const = 1.0
c if(n.le.12) const = 0.6 this is something to do with impact
c
c this const = 0 gives an interpolating spline
const = 0
S=const*N
c
c PRINT *, '*'
C
CALL REINSH(C1,N,T,X1,DD,S)
CALL REINSH(C2,N,T,X2,DD,S)
C
c print*, C1(1,1), C1(1,2), C1(1,3), C1(1,4)

```

```

c  print*, C1(2,1), C1(2,2), C1(2,3), C1(2,4)
c  print*, C1(3,1), C1(3,2), C1(3,3), C1(3,4)
c  print*, C1(4,1), C1(4,2), C1(4,3), C1(4,4)
c  print*, C1(5,1), C1(5,2), C1(5,3), C1(5,4)
  RETURN
  END

C
C
C*****
C
C  VALC EVALUATES A CUBIC SPLINE
C
C*****
C
C  SUBROUTINE VALC(SP1,T,C,N,K)
C
C  DOUBLE PRECISION C(*),K(*),SP(3),SP1,T
C
C  INTEGER N
C
C  EXTERNAL VALC3
C
C  CALL VALC3(SP,T,C,N,K)
C  SP1=SP(1)
C  RETURN
C  END

C
C
C*****
C
C  VALCD EVALUATES A CUBIC SPLINE (FIRST TWO DERIVATIVES)
C
C*****
C
C  SUBROUTINE VALCD(SP,T,C,N,K)
C
C  DOUBLE PRECISION C(*),K(*),SP(3),T
C
C  INTEGER N
C
C  EXTERNAL VALC3
C
C  CALL VALC3(SP,T,C,N,K)
C  RETURN
C  END

C
C

```

```

C*****
C
C   VALC3 EVALUATES A CUBIC SPLINE AND ITS FIRST TWO
C   DERIVATIVES
C
C*****
C
C   SUBROUTINE VALC3(SP,T,CC,N,K)
C   PARAMETER (NN=12)
C   DOUBLE PRECISION A,B,C,D, e, f, CC(NN,4),
C   *H,K(NN),T,SP(3)
C
C   INTEGER I,I1,N,N1
C
C   N1=N-1
C   DO 10,I=1,N1
C     I1=I+1
C     IF(T.LE.K(1)) GO TO 20
C     IF(T.GE.K(N)) go to 30
C     IF(T.GE.K(I).AND.T.LT.K(I1)) GO TO 20
C   10 CONTINUE
C
C   30 i = n-1
C   20 A=CC(I,1)
C     B=CC(I,2)
C     C=CC(I,3)
C     D=CC(I,4)
C
C   H=T-K(I)
C   if(t.ge.k(n)) h = k(n) - k(n-1)
C   if(t.le.k(1)) h = 0.0
C
C   SP(1)=A+B*H+C*H**2+D*H**3
C
C   SP(2)=B+2.0*C*H+3.0*D*H**2
C
C   SP(3)=2.0*C+6.0*D*H
C
C   if(t.lt.k(1).or.t.gt.k(n)) then
C     if(t.gt.k(n)) h = t - k(n)
C     if(t.lt.k(1)) h = t - k(1)
C     e = sp(1)
C     f = sp(2)
C     sp(1) = e + f*h
C     sp(2) = f
C     sp(3) = 0.0
C   endif
C
C

```

RETURN
END

```

C
C*****
C
C   REINSH FITS SMOOTHEST CUBIC SPLINE
C
C   THIS SUBROUTINE IS A TRANSLATION OF THE ALGOL PROGRAM
GIVEN
C   BY CARL REINSCH 1967, NUMERISCHE MATHEMATIK, PP. 177-183.
C
C   PARAMETERS:
C       CC =SPLINE COEFFICIENTS
C       N2 = NUMBER OF DATA POINTS
C       K = ARRAY OF INDEPENDENT VARIABLE VALUES
C         = FRAME NUMBER WHEN SPLINING TIME VALUES
C       Y = ARRAY OF DEPENDENT VARIABLE
C       DY = ARRAY OF ESTIMATE OF ERROR IN Y
C       S = CONSTANT DETERMINING CLOSENESS OF FIT
C
C*****
C

```

APPENDIX B**A sample input file for a simulation**

Is01-(typical input file)

```

APPROACH << eof
os01 ( output file 1)
es01 (output file 2)
10.3 25.3 28.8 31.2 27.1 -7.8 (tilt angles C5-C0)
16.33 7.10 9.20 3.05 -3.28 0.80 (Angular momentum about i axis)
1.050 1.0510 1.0464 1.0130 1.0129 0.9102 (mass centre to foot distances at touch down)
1.0070 1.0240 1.01326 0.9967 0.9719 1.0768 (mass centre to foot distance at midstance)
1.0640 1.0140 1.03276 1.0296 0.9514 1.2252 (mass centre to foot distance at toeff)
10.428 10.830 10.635 10.958 11.301 10.62 (Moment of inertia about  $f_2$  at touch down)
10.670 11.126 10.882 10.833 11.951 11.125 (Moment of inertia about  $f_2$  at midstance)
11.002 11.235 10.660 11.1785 10.419 10.983 (Moment of inertia about  $f_2$  at midstance)
12.65 10.29 4.02(Mean moment of inertia about  $f_1$   $f_2$   $f_3$  during flight)
72.55 (Weight of the athlete)
-5.6065 9.6005 (Mid-foot coordinates from video data: C5 -C0)
-5.4415 6.8165
-4.6025 4.6785
-3.5065 3.0105
-1.8575 1.5845
0.157 1.095
0.01 (time interval for simulation)
0.48 0.87 1.19 1.45 1.71 1.89 (time at touchdown C5-C0)
0.54 0.94 1.24 1.50 1.76 2.00(time at midstance C5-C0)
0.63 1.01 1.33 1.59 1.85 2.04 (time at toeff C5-C0)
-0.5 (Adpsi- adjustment  $\psi$  between C1 and C2)
-4.6025 4.6785 (Simulated foot coordinates: C3-C0)
-3.4963 2.9915
-1.8608 1.6067
0.1789 1.0922
3 (indicate that the simulation starts at C3)
eof

```

APPENDIX C**Sample output files for a simulation**

Os01 (typical outputfile 1)

t(s)	$\theta(^{\circ})$	$\dot{\theta}(\text{rs}^{-1})$	R(m)	s(m)	$\psi(^{\circ})$	$v_f(\text{ms}^{-1})$
1.24	28.80	0.20	7.57	5.15	27.15	7.68
1.25	28.91	0.19	7.46	5.22	27.73	7.69
1.26	29.02	0.17	7.43	5.30	28.33	7.69
1.27	29.11	0.16	7.48	5.38	28.92	7.70
1.28	29.19	0.14	7.62	5.45	29.50	7.71
1.29	29.27	0.12	7.85	5.53	30.07	7.72
1.30	29.34	0.11	8.21	5.61	30.63	7.72
1.31	29.40	0.10	8.70	5.68	31.15	7.73
1.32	29.45	0.09	9.40	5.76	31.64	7.74
1.33	29.50	0.08	10.37	5.84	32.09	7.75
1.34	29.55	0.08	11.53	5.92	32.50	7.75
1.35	29.59	0.08	12.61	5.99	32.86	7.76
1.36	29.64	0.08	13.48	6.07	33.20	7.77
1.37	29.68	0.08	14.03	6.15	33.53	7.78
1.38	29.73	0.08	14.15	6.23	33.84	7.78
1.39	29.77	0.07	13.83	6.30	34.16	7.79
1.40	29.81	0.07	13.12	6.38	34.49	7.80
1.41	29.85	0.07	12.12	6.46	34.85	7.81
1.42	29.89	0.07	10.99	6.54	35.23	7.81
1.43	29.93	0.07	9.82	6.62	35.66	7.82
1.44	29.97	0.07	8.70	6.70	36.15	7.83
1.45	30.01	0.06	7.67	6.77	36.70	7.84
1.46	30.04	0.06	6.85	6.85	37.32	7.84
1.47	30.07	0.04	6.28	6.93	38.01	7.85
1.48	30.08	0.01	5.88	7.01	38.75	7.86
1.49	30.08	-0.02	5.60	7.09	39.53	7.87
1.50	30.06	-0.06	5.41	7.17	40.35	7.87
1.51	30.01	-0.10	5.30	7.24	41.20	7.88
1.52	29.95	-0.13	5.25	7.32	42.05	7.89
1.53	29.86	-0.17	5.27	7.40	42.91	7.90
1.54	29.75	-0.21	5.36	7.48	43.77	7.90
1.55	29.62	-0.25	5.52	7.56	44.60	7.91
1.56	29.46	-0.28	5.77	7.64	45.40	7.92
1.57	29.29	-0.31	6.14	7.72	46.17	7.93
1.58	29.10	-0.34	6.65	7.80	46.88	7.93
1.59	28.90	-0.36	7.39	7.88	47.53	7.94
1.60	28.69	-0.38	8.27	7.96	48.11	7.95
1.61	28.47	-0.38	9.08	8.04	48.64	7.96
1.62	28.25	-0.38	9.70	8.12	49.12	7.97
1.63	28.03	-0.39	10.03	8.20	49.58	7.97
1.64	27.81	-0.39	9.99	8.28	50.04	7.98
1.65	27.59	-0.39	9.60	8.36	50.50	7.99
1.66	27.37	-0.39	8.93	8.43	51.00	8.00

1.67	27.14	-0.40	8.09	8.51	51.53	8.00
1.68	26.91	-0.40	7.20	8.59	52.13	8.01
1.69	26.68	-0.40	6.33	8.68	52.81	8.02
1.70	26.45	-0.41	5.53	8.76	53.59	8.03
1.71	26.21	-0.42	4.82	8.84	54.48	8.03
1.72	25.97	-0.43	4.27	8.92	55.50	8.04
1.73	25.71	-0.51	3.90	9.00	56.63	8.05
1.74	25.39	-0.60	3.65	9.08	57.86	8.06
1.75	25.02	-0.69	3.48	9.16	59.15	8.06
1.76	24.59	-0.80	3.37	9.24	60.51	8.07
1.77	24.11	-0.91	3.32	9.32	61.89	8.08
1.78	23.55	-1.02	3.32	9.40	63.29	8.09
1.79	22.94	-1.14	3.37	9.48	64.67	8.09
1.80	22.25	-1.25	3.47	9.56	66.03	8.10
1.81	21.50	-1.36	3.63	9.64	67.34	8.11
1.82	20.69	-1.48	3.88	9.72	68.58	8.12
1.83	19.81	-1.58	4.25	9.80	69.73	8.12
1.84	18.88	-1.67	4.79	9.89	70.77	8.13
1.85	17.90	-1.76	5.63	9.97	71.67	8.14
1.86	16.87	-1.83	6.63	10.05	72.43	8.15
1.87	15.83	-1.83	7.21	10.13	73.10	8.15
1.88	14.78	-1.83	7.09	10.21	73.74	8.16
1.89	13.73	-1.83	6.32	10.29	74.44	8.17
1.90	12.67	-1.84	5.48	10.37	75.24	8.18
1.91	11.59	-1.95	4.88	10.46	76.14	8.18
1.92	10.44	-2.05	4.42	10.54	77.16	8.19
1.93	9.24	-2.15	4.08	10.62	78.26	8.20
1.94	7.98	-2.25	3.80	10.70	79.46	8.21
1.95	6.66	-2.34	3.58	10.78	80.73	8.21
1.96	5.30	-2.42	3.41	10.87	82.08	8.22
1.97	3.89	-2.49	3.27	10.95	83.49	8.23
1.98	2.45	-2.55	3.15	11.03	84.96	8.24
1.99	0.97	-2.60	3.06	11.11	86.48	8.24
2.00	-0.52	-2.63	2.99	11.20	88.04	8.25
2.01	-2.04	-2.66	2.94	11.28	89.64	8.26
2.02	-3.57	-2.67	2.90	11.36	91.26	8.27
2.03	-5.10	-2.68	2.88	11.44	92.89	8.27

Es01 (typical outputfile2)

This section of the output file evaluates

1. Tilt angles from the polynomial function of the time and tilt angle (θ).
2. Twist angles from the cubic function of stride distance and twist angle (ψ).
3. Stride distance from the quadratic function of time and stride distance (s).

This section also prints the time history of the simulated foot and mass centre coordinates.

Evaluating tilt angle from the polynomial function

time	θ°
0.54	10.30
0.55	11.09
0.56	11.85
0.57	12.58
0.58	13.28
0.59	13.95
0.60	14.59
0.61	15.20
0.62	15.78
0.63	16.34
0.64	16.87
0.65	17.38
0.66	17.87
0.67	18.34
0.68	18.78
0.69	19.20
0.70	19.61
0.71	19.99
0.72	20.36
0.73	20.71
0.74	21.04
0.75	21.36
0.76	21.66
0.77	21.95
0.78	22.23
0.79	22.49
0.80	22.74
0.81	22.98
0.82	23.20
0.83	23.42
0.84	23.63
0.85	23.83
0.86	24.02
0.87	24.20
0.88	24.38
0.89	24.55
0.90	24.71
0.91	24.86
0.92	25.01
0.93	25.16
0.94	25.30
0.95	25.44
0.96	25.57
0.97	25.70
0.98	25.83

0.99	25.95
1.00	26.07
1.01	26.19
1.02	26.31
1.03	26.42
1.04	26.54
1.05	26.65
1.06	26.76
1.07	26.87
1.08	26.99
1.09	27.10
1.10	27.21
1.11	27.32
1.12	27.43
1.13	27.54
1.14	27.66
1.15	27.77
1.16	27.88
1.17	27.99
1.18	28.11
1.19	28.22
1.20	28.34
1.21	28.45
1.22	28.57
1.23	28.68
1.24	28.80
1.25	28.92
1.26	29.03
1.27	29.15
1.28	29.26
1.29	29.38
1.30	29.49
1.31	29.61
1.32	29.72
1.33	29.83
1.34	29.94
1.35	30.05
1.36	30.16
1.37	30.26
1.38	30.36
1.39	30.46
1.40	30.55
1.41	30.64
1.42	30.72
1.43	30.81
1.44	30.88
1.45	30.95
1.46	31.01

1.47	31.07
1.48	31.12
1.49	31.17
1.50	31.20
1.51	31.23
1.52	31.24
1.53	31.25
1.54	31.25
1.55	31.23
1.56	31.21
1.57	31.17
1.58	31.12
1.59	31.05
1.60	30.97
1.61	30.88
1.62	30.77
1.63	30.64
1.64	30.49
1.65	30.33
1.66	30.15
1.67	29.95
1.68	29.73
1.69	29.48
1.70	29.22
1.71	28.93
1.72	28.61
1.73	28.28
1.74	27.91
1.75	27.52
1.76	27.10
1.77	26.65
1.78	26.17
1.79	25.66
1.80	25.12
1.81	24.55
1.82	23.94
1.83	23.29
1.84	22.61
1.85	21.89
1.86	21.13
1.87	20.34
1.88	19.50
1.89	18.62
1.90	17.69
1.91	16.72
1.92	15.71
1.93	14.64
1.94	13.53

1.95	12.37
1.96	11.16
1.97	9.89
1.98	8.58
1.99	7.20
2.00	5.77
2.01	4.28
2.02	2.73
2.03	1.12
2.04	-0.55

Stride distance(s) and psi angles at Cm0 to Cm4
(at points midway between foot contacts)

s	ψ
10.30	76.34
8.17	49.15
6.08	33.31
3.94	21.43
1.39	3.39

Stride distance(s) and psi angles at C0 to C4

s	ψ
11.33	94.60
9.26	61.74
7.08	40.22
5.09	27.49
2.79	15.26

Evaluating psi angle from quadratic function of s and ψ

s	ψ
0.00	-5.29
0.08	-4.56
0.15	-3.84
0.23	-3.13
0.30	-2.43
0.38	-1.75
0.45	-1.08
0.53	-0.41
0.60	0.24
0.68	0.87

0.76	1.50
0.83	2.12
0.91	2.73
0.98	3.33
1.06	3.91
1.13	4.49
1.21	5.06
1.28	5.62
1.36	6.17
1.44	6.71
1.51	7.25
1.59	7.78
1.66	8.29
1.74	8.81
1.81	9.31
1.89	9.81
1.96	10.30
2.04	10.78
2.12	11.26
2.19	11.73
2.27	12.19
2.34	12.65
2.42	13.10
2.49	13.55
2.57	13.99
2.64	14.43
2.72	14.87
2.80	15.30
2.87	15.72
2.95	16.14
3.02	16.56
3.10	16.98
3.17	17.39
3.25	17.80
3.32	18.20
3.40	18.61
3.48	19.01
3.55	19.41
3.63	19.81
3.70	20.20
3.78	20.60
3.85	20.99
3.93	21.39
4.00	21.78
4.08	22.17
4.16	22.56
4.23	22.96
4.31	23.35

4.38	23.74
4.46	24.14
4.53	24.54
4.61	24.93
4.69	25.33
4.76	25.73
4.84	26.14
4.91	26.54
4.99	26.95
5.06	27.36
5.14	27.78
5.21	28.19
5.29	28.61
5.37	29.04
5.44	29.47
5.52	29.90
5.59	30.34
5.67	30.78
5.74	31.23
5.82	31.68
5.89	32.14
5.97	32.60
6.05	33.07
6.12	33.54
6.20	34.02
6.27	34.51
6.35	35.01
6.42	35.51
6.50	36.02
6.57	36.53
6.65	37.06
6.73	37.59
6.80	38.13
6.88	38.68
6.95	39.24
7.03	39.81
7.10	40.38
7.18	40.97
7.25	41.56
7.33	42.17
7.41	42.78
7.48	43.41
7.56	44.05
7.63	44.69
7.71	45.35
7.78	46.02
7.86	46.70
7.93	47.39

8.01	48.10
8.09	48.82
8.16	49.55
8.24	50.29
8.31	51.04
8.39	51.81
8.46	52.59
8.54	53.39
8.61	54.20
8.69	55.02
8.77	55.86
8.84	56.71
8.92	57.58
8.99	58.46
9.07	59.36
9.14	60.27
9.22	61.20
9.29	62.15
9.37	63.11
9.45	64.09
9.52	65.08
9.60	66.10
9.67	67.13
9.75	68.17
9.82	69.24
9.90	70.32
9.97	71.42
10.05	72.54
10.13	73.68
10.20	74.83
10.28	76.01
10.35	77.20
10.43	78.42
10.50	79.65
10.58	80.90
10.65	82.18
10.73	83.47
10.81	84.79
10.88	86.13
10.96	87.49
11.03	88.87
11.11	90.27
11.18	91.69
11.26	93.14
11.33	94.60

Time	Adjusted s (C5-C))
2.04	11.45

1.76	9.37
1.50	7.16
1.24	5.14
0.94	2.79
0.54	0.00

time s distance (Evaluating s)

0.54	-0.04
0.55	0.03
0.56	0.10
0.57	0.17
0.58	0.24
0.59	0.31
0.60	0.39
0.61	0.46
0.62	0.53
0.63	0.60
0.64	0.67
0.65	0.75
0.66	0.82
0.67	0.89
0.68	0.96
0.69	1.04
0.70	1.11
0.71	1.18
0.72	1.25
0.73	1.33
0.74	1.40
0.75	1.47
0.76	1.55
0.77	1.62
0.78	1.69
0.79	1.77
0.80	1.84
0.81	1.91
0.82	1.99
0.83	2.06
0.84	2.13
0.85	2.21
0.86	2.28
0.87	2.36
0.88	2.43
0.89	2.50
0.90	2.58
0.91	2.65
0.92	2.73
0.93	2.80
0.94	2.88

0.95	2.95
0.96	3.02
0.97	3.10
0.98	3.17
0.99	3.25
1.00	3.32
1.01	3.40
1.02	3.47
1.03	3.55
1.04	3.62
1.05	3.70
1.06	3.78
1.07	3.85
1.08	3.93
1.09	4.00
1.10	4.08
1.11	4.15
1.12	4.23
1.13	4.31
1.14	4.38
1.15	4.46
1.16	4.53
1.17	4.61
1.18	4.69
1.19	4.76
1.20	4.84
1.21	4.92
1.22	4.99
1.23	5.07
1.24	5.15
1.25	5.22
1.26	5.30
1.27	5.38
1.28	5.45
1.29	5.53
1.30	5.61
1.31	5.68
1.32	5.76
1.33	5.84
1.34	5.92
1.35	5.99
1.36	6.07
1.37	6.15
1.38	6.23
1.39	6.31
1.40	6.38
1.41	6.46
1.42	6.54

1.43	6.62
1.44	6.70
1.45	6.77
1.46	6.85
1.47	6.93
1.48	7.01
1.49	7.09
1.50	7.17
1.51	7.25
1.52	7.32
1.53	7.40
1.54	7.48
1.55	7.56
1.56	7.64
1.57	7.72
1.58	7.80
1.59	7.88
1.60	7.96
1.61	8.04
1.62	8.12
1.63	8.20
1.64	8.28
1.65	8.36
1.66	8.44
1.67	8.52
1.68	8.60
1.69	8.68
1.70	8.76
1.71	8.84
1.72	8.92
1.73	9.00
1.74	9.08
1.75	9.16
1.76	9.24
1.77	9.32
1.78	9.40
1.79	9.48
1.80	9.56
1.81	9.64
1.82	9.73
1.83	9.81
1.84	9.89
1.85	9.97
1.86	10.05
1.87	10.13
1.88	10.21
1.89	10.30
1.90	10.38

1.91	10.46
1.92	10.54
1.93	10.62
1.94	10.70
1.95	10.79
1.96	10.87
1.97	10.95
1.98	11.03
1.99	11.12
2.00	11.20
2.01	11.28
2.02	11.36
2.03	11.45
2.04	11.53

Mid-foot coordinates of foot contact from video data

Xm	Ym
0.1570	1.0950
-1.8575	1.5845
-3.5065	3.0105
-4.6025	4.6785
-5.4415	6.8165
-5.6065	9.6005

Simulated Foot and mass centre coordinates

Time	x	y	x	y
1.25	-4.5675	4.6102	-4.1331	4.8329
1.26	-4.5317	4.5422	-4.0993	4.7695
1.27	-4.4952	4.4744	-4.0645	4.7066
1.28	-4.4580	4.407	-4.0286	4.6442
1.29	-4.4200	4.3399	-3.9916	4.5824
1.3	-4.3813	4.2732	-3.9534	4.5210
1.31	-4.342	4.2067	-3.9142	4.4600
1.32	-4.302	4.1405	-3.8737	4.3994

1.33	-4.2614	4.0747	-3.8322	4.3392
1.34	-4.2203	4.009	-3.7894	4.2792

←Aerial phase

1.47	-3.6439	3.1754	-3.2426	3.4813
1.48	-3.5955	3.1135	-3.1993	3.4231
1.49	-3.5463	3.0522	-3.1553	3.366
1.5	-3.4963	2.9915	-3.1105	3.3099
1.51	-3.4453	2.9315	-3.0649	3.2548
1.52	-3.3934	2.8722	-3.0184	3.2005
1.53	-3.3405	2.8136	-2.9710	3.1470
1.54	-3.2868	2.7558	-2.9226	3.0943
1.55	-3.2321	2.6987	-2.8733	3.0424
1.56	-3.1765	2.6424	-2.8229	2.9911
1.57	-3.1201	2.5868	-2.7715	2.9404
1.58	-3.0629	2.5319	-2.7189	2.8902
1.59	-3.0050	2.4776	-2.6653	2.8404
1.6	-2.9464	2.424	-2.6105	2.7910

←Aerial phase

1.73	-2.1357	1.7749	1.8868	2.1370
1.74	-2.0685	1.7306	-1.8313	2.0908
1.75	-2.0003	1.6877	-1.7753	2.0457
1.76	-1.9310	1.6464	-1.7188	2.0018
1.77	-1.8608	1.6067	-1.6616	1.9588
1.78	-1.7895	1.5686	-1.6036	1.9167
1.79	-1.7173	1.5323	-1.5446	1.8755
1.8	-1.6442	1.4976	-1.4845	1.8349
1.81	-1.5701	1.4647	-1.4233	1.795
1.82	-1.4953	1.4335	-1.3609	1.7555

1.83	-1.4197	1.4039	-1.2971	1.7165
1.84	-1.3435	1.3757	-1.2320	1.6778
1.85	-1.2668	1.3489	-1.1655	1.6393
1.86	-1.1895	1.3233	-1.0975	1.6009

←Aerial phase

1.91	-0.7977	1.2094	-0.7471	1.4017
1.92	-0.7183	1.1898	-0.6747	1.3665
1.93	-0.6384	1.1716	-0.6018	1.3323
1.94	-0.5581	1.1549	-0.5282	1.299
1.95	-0.4775	1.1399	-0.4539	1.2664
1.96	-0.3964	1.1267	-0.3788	1.2346
1.97	-0.3150	1.1154	-0.3027	1.2033
1.98	-0.2332	1.106	-0.2256	1.1724
1.99	-0.1511	1.0988	-0.1474	1.1418
2.00	-0.0689	1.0938	-0.0678	1.1114
2.01	0.01360	1.0909	0.0133	1.0811
2.02	0.09620	1.0904	0.0959	1.0507
2.03	0.17880	1.0922	0.1804	1.0203

Outs01(typical outputfile3)

(Prompts for the input values)

state name of the angle and angular vel. output file
 state name of the simulated foot coordinate output file
 input tilt angles (deg.) from C5-C0
 input forward angular momentum (kgmm/s) at C5-C0
 input distance bet mass centre& foot at TD, MS,TO for C5-C0
 input moment of inertia I2 at TD, MS,TO for C5-C0
 Input aerial I1, I2, I3 of the jumper
 Input the mass (kg) of the jumper
 Input foot coords of TD, MS, TO ground contact at C5
 Input foot coords of TD, MS, TO ground contact at C4
 Input foot coords of TD, MS, TO ground contact at C3
 Input foot coords of TD, MS, TO ground contact at C2
 Input foot coords of TD, MS, TO ground contact at C1
 Input foot coords of TD, MS, TO ground contact at C0
 time increment for each integration in simulation (s)
 input TD time (s) from C5-C0
 input MS time (s) from C5-C0
 input TO time (s) from C4-C0
 input adjustment to twist angle between C1-C2
 input simulated foot coord at MS for C3-C0
 Begin the simulation at C _

The radius and the stride distances at each foot contact (SA)
 and points at midway of foot contacts (SB)

C	Radius	distance (SA)	Radius	distance (SB)
0	2.926	11.334	3.636	10.298
1	4.574	9.261	5.869	8.171
2	7.489	7.081	9.112	6.083
3	10.474	5.085	11.007	3.937
4	10.118	2.788	7.970	1.394

Velocity of foot curve at each contact

C	V(i)
5	7.149
4	7.451
3	7.678
2	7.874
1	8.070
0	8.282

Stride distances at touchdown (sAD), midstance (sAM) and takeoff (sAO)
(These values are obtained from the evaluation of the quadratic function
of time and stride distance)

C	sAD	sAM	sAO
0	10.295	11.198	11.529
1	8.837	9.239	9.969
2	6.774	7.167	7.878
3	4.762	5.145	5.839
4	2.355	2.875	3.399
5	-0.472	-0.044	0.601

The 6 terms of $\ddot{\theta}$ equations are:

Term1: $mg(h\sin\theta - d)/(I_2 + mh(h-d\sin\theta))$

Term2: $-(m\,v f^2\,r\,h\cos\theta)/R^2(I_2 + mh(h-d\sin\theta))$

Term3 $-(m\,f\,h\,v f\dot{\theta}\sin\theta)/R(I_2 + mh(h-d\sin\theta))$

Term4

$$-\frac{[2mh\dot{h}\dot{\theta} - m\dot{h}d\sin\theta - m\dot{h}d\sin\theta - m\dot{h}\dot{\theta}d\cos\theta]\dot{\theta}}{(I_2 + mh(h - d\sin\theta))}$$

Term5 $-(L\dot{v} f)/R(I_2 + mh(h-d\sin\theta))$

Term6 $-(\dot{I}_2\,\dot{\theta})/(I_2 + mh(h-d\sin\theta))$

time	Term1	Term2	Term3	Term4	Term5	Term6
1.24	4.07	5.50	0.00	-0.12	0.11	0.01
1.25	4.08	5.59	0.01	-0.08	0.11	0.00
1.25	4.08	5.59	0.01	-0.08	0.11	0.00
1.26	4.09	5.63	0.01	-0.04	0.11	0.00
1.26	4.09	5.63	0.01	-0.04	0.11	0.00
1.27	4.09	5.60	0.02	-0.01	0.11	0.00
1.27	4.09	5.60	0.02	-0.01	0.11	0.00
1.28	4.08	5.52	0.02	0.02	0.11	0.00
1.28	4.08	5.52	0.02	0.02	0.11	0.00
1.29	4.05	5.37	0.02	0.04	0.11	0.00
1.29	4.05	5.37	0.02	0.04	0.11	0.00
1.30	4.03	5.16	0.02	0.06	0.10	-0.01
1.30	4.03	5.16	0.02	0.06	0.10	-0.01
1.31	3.99	4.88	0.02	0.07	0.10	-0.01
1.31	3.99	4.88	0.02	0.07	0.10	-0.01
1.32	3.95	4.54	0.02	0.08	0.09	-0.01
1.32	3.95	4.54	0.02	0.08	0.09	-0.01

1.33	3.90	4.13	0.02	0.09	0.08	-0.01
1.33	3.90	4.13	0.02	0.09	0.08	-0.01
1.34	3.85	3.73	0.02	0.10	0.07	-0.01

←Aerial phase

1.46	4.20	6.24	-0.01	-0.04	0.04	0.00
1.47	4.24	6.78	-0.01	-0.02	0.05	0.00
1.47	4.24	6.78	-0.01	-0.02	0.05	0.00
1.48	4.27	7.23	0.00	0.00	0.05	0.00
1.48	4.27	7.23	0.00	0.00	0.05	0.00
1.49	4.28	7.59	0.00	0.01	0.05	0.00
1.49	4.28	7.59	0.00	0.01	0.05	0.00
1.50	4.28	7.86	0.00	0.01	0.05	0.00
1.50	4.28	7.86	0.00	0.01	0.05	0.00
1.51	4.27	8.03	0.00	0.00	0.05	0.00
1.51	4.27	8.03	0.00	0.00	0.05	0.00
1.52	4.24	8.12	-0.01	-0.01	0.06	0.00
1.52	4.24	8.12	-0.01	-0.01	0.06	0.00
1.53	4.20	8.11	-0.03	-0.04	0.06	-0.01
1.53	4.20	8.11	-0.03	-0.04	0.06	-0.01
1.54	4.14	8.01	-0.04	-0.07	0.05	-0.01
1.54	4.14	8.01	-0.04	-0.07	0.05	-0.01
1.55	4.08	7.82	-0.06	-0.12	0.05	-0.01
1.55	4.08	7.82	-0.06	-0.12	0.05	-0.01
1.56	4.00	7.53	-0.08	-0.17	0.05	-0.02
1.56	4.00	7.53	-0.08	-0.17	0.05	-0.02
1.57	3.91	7.14	-0.11	-0.24	0.05	-0.02
1.57	3.91	7.14	-0.11	-0.23	0.05	-0.02
1.58	3.81	6.64	-0.13	-0.31	0.04	-0.03
1.58	3.81	6.64	-0.13	-0.30	0.04	-0.03
1.59	3.71	6.03	-0.15	-0.38	0.04	-0.03
1.59	3.71	6.03	-0.15	-0.38	0.04	-0.03
1.60	3.60	5.43	-0.17	-0.45	0.03	-0.04

←Aerial phase

1.72	3.57	10.58	0.11	0.59	-0.07	-0.10
1.73	3.60	11.56	0.10	0.65	-0.08	-0.09
1.73	3.60	11.56	0.10	0.66	-0.08	-0.09
1.74	3.61	12.37	0.08	0.72	-0.09	-0.08
1.74	3.61	12.37	0.08	0.73	-0.09	-0.08
1.75	3.60	13.03	0.05	0.79	-0.09	-0.06
1.75	3.60	13.03	0.05	0.79	-0.09	-0.06
1.76	3.57	13.54	0.00	0.85	-0.10	-0.02
1.76	3.57	13.54	0.00	0.85	-0.10	-0.02
1.77	3.52	13.91	-0.06	0.90	-0.10	0.02
1.77	3.52	13.91	-0.06	0.90	-0.10	0.02
1.78	3.44	14.12	-0.14	0.93	-0.10	0.08
1.78	3.44	14.12	-0.14	0.94	-0.10	0.08
1.79	3.34	14.16	-0.23	0.94	-0.10	0.15
1.79	3.34	14.16	-0.23	0.94	-0.10	0.15

1.80	3.21	14.02	-0.33	0.92	-0.10	0.24
1.80	3.21	14.02	-0.33	0.92	-0.10	0.24
1.81	3.05	13.68	-0.43	0.85	-0.10	0.34
1.81	3.05	13.68	-0.43	0.85	-0.10	0.34
1.82	2.87	13.12	-0.54	0.73	-0.09	0.45
1.82	2.87	13.12	-0.54	0.73	-0.09	0.45
1.83	2.67	12.30	-0.64	0.55	-0.08	0.58
1.83	2.67	12.30	-0.64	0.54	-0.08	0.58
1.84	2.46	11.20	-0.72	0.30	-0.07	0.72
1.84	2.46	11.20	-0.72	0.30	-0.07	0.71
1.85	2.23	9.78	-0.79	-0.01	-0.06	0.86
1.85	2.23	9.78	-0.79	-0.01	-0.06	0.86
1.86	1.99	8.50	-0.84	-0.36	-0.05	1.00

←Aerial phase

1.90	0.65	11.04	1.09	-0.45	0.02	-0.25
1.91	0.64	12.39	1.00	-1.77	0.02	-0.24
1.91	0.64	12.39	1.00	-1.77	0.02	-0.24
1.92	0.62	13.61	0.89	-3.20	0.02	-0.22
1.92	0.62	13.61	0.89	-3.20	0.02	-0.22
1.93	0.59	14.71	0.76	-4.72	0.02	-0.19
1.93	0.59	14.71	0.76	-4.72	0.02	-0.19
1.94	0.54	15.68	0.63	-6.31	0.02	-0.16
1.94	0.54	15.68	0.63	-6.30	0.02	-0.16
1.95	0.48	16.53	0.49	-7.95	0.02	-0.13
1.95	0.48	16.53	0.49	-7.94	0.02	-0.13
1.96	0.40	17.23	0.36	-9.60	0.02	-0.09
1.96	0.40	17.23	0.36	-9.58	0.02	-0.09
1.97	0.30	17.81	0.24	-11.25	0.02	-0.06
1.97	0.30	17.81	0.24	-11.22	0.02	-0.06
1.98	0.17	18.25	0.13	-12.85	0.02	-0.03
1.98	0.17	18.25	0.13	-12.83	0.02	-0.03
1.99	0.03	18.56	0.04	-14.40	0.02	0.01
1.99	0.03	18.56	0.04	-14.37	0.02	0.01
2.00	-0.13	18.73	-0.02	-15.85	0.02	0.04
2.00	-0.13	18.73	-0.02	-15.82	0.02	0.04
2.01	-0.30	18.77	-0.05	-17.20	0.02	0.06
2.01	-0.30	18.77	-0.05	-17.16	0.02	0.06
2.02	-0.47	18.68	-0.06	-18.42	0.02	0.09
2.02	-0.47	18.68	-0.06	-18.38	0.02	0.09
2.03	-0.66	18.46	-0.04	-19.49	0.02	0.11
2.03	-0.66	18.46	-0.04	-19.45	0.02	0.11
2.04	-0.84	18.11	0.00	-20.40	0.02	0.12

APPENDIX D**Anthropometric measurements of the subjects**

ANTHROPOMETRIC MEASUREMENTS FOR SEGMENTAL INERTIA PARAMETERS

NAME AGE HEIGHT DATE

MEASURER WEIGHT

All measurements in millimetres

TORSO

level	hip	umbilicus	ribcage	nipple	shoulder	neck		nose	ear	top
length	0	162	229	394	518	568	0	144	209	353
perimeter	925	780	788	936		374		456	550	
width	319	284	278	310	373					
depth					156					

LEFT ARM

level	shoulder	midarm	elbow	forearm	wrist	thumb	knuckle	nails	
length	0		360	427	630	0	67	96	200
perimeter	327	270	272	264	179		249	204	110
width					61		99	80	47

RIGHT ARM

level	shoulder	midarm	elbow	forearm	wrist		thumb	knuckle	nails
length	0		351	422	640	0	71	103	214
perimeter	325	269	280	280	184		264	216	117
width					62		105	85	50

LEFT LEG

level	hip	crotch	midthigh	knee	calf	ankle	heel	arch	ball	nails	
length	0	93		534	700	985	0	18		157	230
perimeter		570	534	398	375	243		344	265	256	152
width										98	62
depth							130				

RIGHT LEG

level	hip	crotch	midthigh	knee	calf	ankle	heel	arch	ball	nails	
length	0	96		550	716	1000	0	18		157	230
perimeter		577	541	400	380	244		346	266	257	153
width										99	62
depth							131				

ANTHROPOMETRIC MEASUREMENTS FOR SEGMENTAL INERTIA PARAMETERS

NAME	S. SMITH	AGE		HEIGHT	1.86	DATE	
------	----------	-----	--	--------	------	------	--

MEASURER WEIGHT 73 kg

All measurements in millimetres

TORSO

[illegible]

LEFT ARM

[illegible]

RIGHT ARM

[illegible]

LEFT LEG

[illegible]

RIGHT LEG

[illegible]

APPENDIX E

Record of competition performances

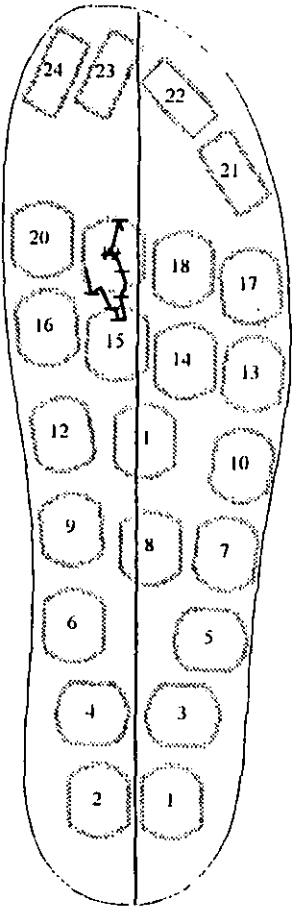
Jump	Attempt	Height	Clearance
B01	1 st	2.20	failed
B02	2 nd	2.20	cleared
B03	1 st	2.20	failed
B04	2 nd	2.20	failed
B05	3 rd	2.20	failed
S01	1 st	2.10	cleared
S02	1 st	2.20	cleared
S03	1 st	2.27	failed
S04	2 nd	2.27	failed
S05	3 rd	2.27	cleared
S06	1 st	2.31	failed
S07	2 nd	2.31	cleared
S08	1 st	2.36	failed
S09	2 nd	2.36	failed
S10	3 rd	2.36	failed

* B01-B05 Jumps attempted by B. Reilly on 11 June 95 at Loughborough Stadium.

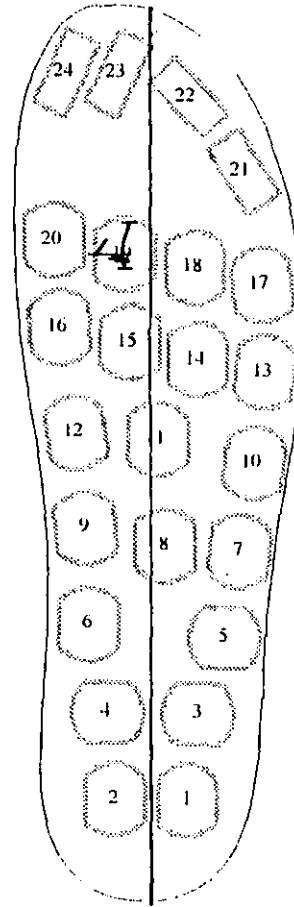
*S01-S1 Jumps attempted by S. Smith on 16 June 96 at Alexander Stadium.

APPENDIX F

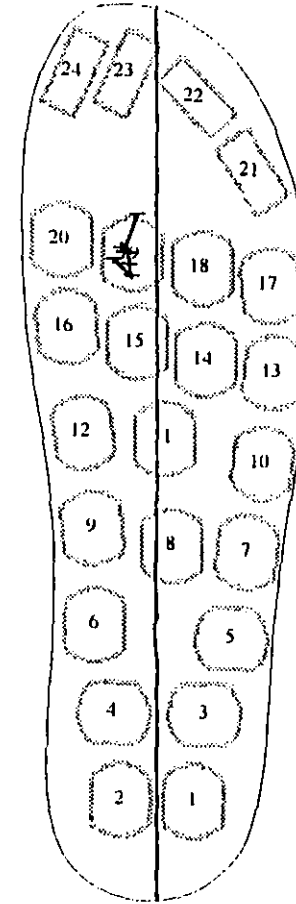
CENTRE OF PRESSURE PATTERNS FOR CURVE RUNNING



Trial 1

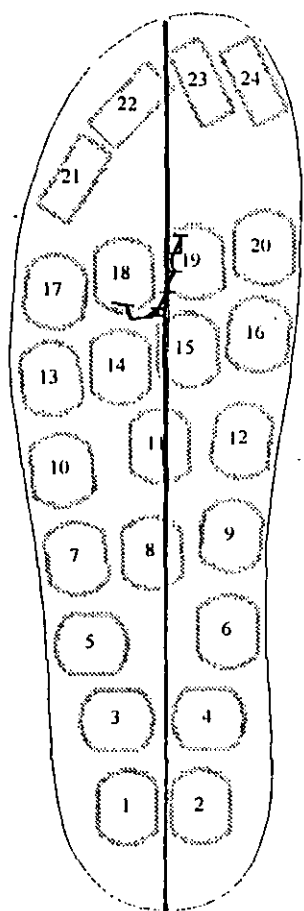


Trial 2

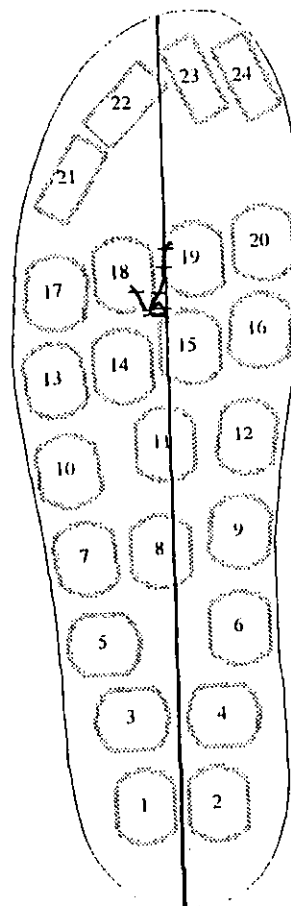


Trial 3

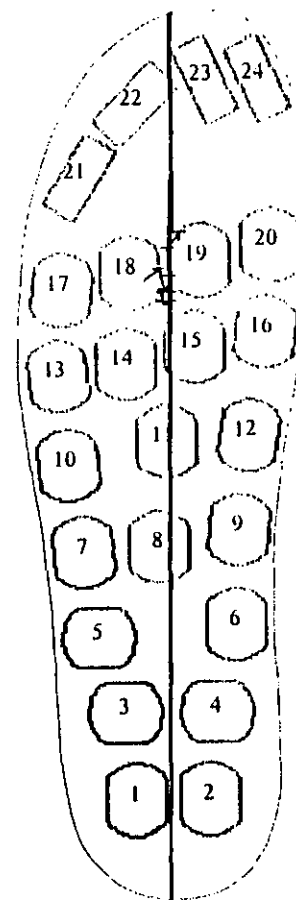
Centre of pressure location during (outer) foot contact (C3) of the approach.



Trial 1



Trial 2



Trial 3

Centre of pressure location during (inner) foot contact (C2) of the approach.

